A biotechnological perspective on groundwater sand filtration

Corbera Rubio, F.

DOI
10.4233/uuid:43146d99-7ac2-43fe-8b93-5bfdb410c825

Publication date
2024

Document Version
Final published version

Citation (APA)
Corbera Rubio, F. (2024). *A biotechnological perspective on groundwater sand filtration*. [Dissertation (TU Delft), Delft University of Technology]. https://doi.org/10.4233/uuid:43146d99-7ac2-43fe-8b93-5bfdb410c825

Important note
To cite this publication, please use the final published version (if applicable).
Please check the document version above.

A BIOTECHNOLOGICAL PERSPECTIVE ON GROUNDWATER SAND FILTRATION

FRANCESC CORBERA RUBIO

A biotechnological perspective on groundwater sand filtration

Dissertation

for the purpose of obtaining the degree of doctor

at Delft University of Technology

by the authority of the Rector Magnificus prof. dr. ir. T.H.J.J. van der Hagen,

chair of the Board for Doctorates

to be defended publicly on

Friday 6 December 2024 at 10:00 o'clock

by

Francesc CORBERA RUBIO

Master of Science in Life Science & Technology

Delft University of Technology, the Netherlands

born in Montornes del Valles, Barcelona, Spain

This dissertation has been approved by the promotors

prof. dr. ir. D. van Halem
prof. dr. ir. M.C.M. van Loosdrecht
dr. M. Laureni

Composition of the doctoral committee:

Rector Magnificus	chairperson
prof. dr. ir. D. van Halem	Delft University of Technology, the Netherlands, promotor
prof. dr. ir. M.C.M. van Loosdrecht	Delft University of Technology, the Netherlands, co-promotor
dr. M. Laureni	Delft University of Technology, the Netherlands, co-promotor

Independent members:

prof. dr. C.U. Welte	Radboud Univerity, the Netherlands
prof. dr. L. Villanueva	NIOZ Royal Institute for Sea Research, the Netherlands
dr. ir. L. Ramsay	VIA University College, Denmark
prof. dr. ir. L.C. Rietveld	Delft University of Technology, the Netherlands
prof. Dr. H. Schmitt	Delft University of Technology, the Netherlands - *reserve*

The research presented in this thesis was performed at the Environmental Biotechnology Section, Department of Biotechnology, Faculty of Applied Sciences, Delft University of Technology, The Netherlands. This work was financed by the NWO partnership program 'Dunea–Vitens: Sand Filtration' (project 17830) of the Dutch Research Council (NWO) and the drinking water companies Vitens NV and Dunea Duin & Water

Keywords: Sand Filtration; Metagenomics, Iron, Ammonia, Manganese, Groundwater; Drinking water

Printed by: Proefschriftspecialist

Cover design by: Francesc Corbera Rubio

ISBN: 978-94-6366-965-8

An electronic version of this dissertation is available at http://repository.tudelft.nl/

Printing of this thesis was financially supported by the Netherlands Society of Medical Microbiology (NVMM) and the Royal Netherlands Society for Microbiology (KNVM).

A la mama. A totes les mares.

CONTENTS

The supplementary material of all chapters can be found in the online versions of the associated publications.

SUMMARY

Drinking water production works well, but we can do better.

Anaerobic groundwater is an excellent drinking water source. It presents several advantages over its counterpart, surface water, such as constant quality and temperature, and it is considered to be microbiologically safe. The main contamination sources of anaerobic groundwater are the decomposition of natural organic matter and the dissolution of soil minerals. The first one produces compounds such as ammonia, while the second introduces manganese, iron, and trace metals. Iron, ammonia and manganese must be removed from groundwater to produce drinking water. For this purpose, humans have been using rapid sand filtration - preceded by an aeration step - for over a century.

The purpose of aeration is to strip out undesired gases and to introduce oxygen up to saturation levels. At this oxidation-reduction potential, iron, ammonia and manganese are oxidized by different physical-chemical and biological processes in the subsequent rapid sand filter. As a result, most contaminants precipitate, forming solids that are captured by the filter, and clean water is produced. Although widely used and robust, solid understanding of the intricacies of rapid sand filters is still missing. A high degree of complexity is hidden behind their seemingly simple working principles.

The main reason underneath this extraordinary complexity is the high oxygen load introduced during the aeration step. The saturation of anaerobic groundwater with oxygen onsets a series of simultaneous, interwoven and uncontrolled reactions whose nature and contribution to the overall process remains unknown and generally unpredictable. This process convolution precludes understanding and optimization of rapid sand filtration.

The overarching goal of this thesis is to gain knowledge to advance towards the design of high-flow, resource-efficient sand filters. To do so, we must be able to understand the mechanisms that govern which reactions take place, in which order they occur, and how they affect each other, which will ultimately allow us to predict and control *i)* microbial community assembly and performance and *ii)* the interplay between chemical and biological reactions. In the first part of this thesis, we focused on gaining mechanistic understanding of how current sand filters work using laboratory, pilot, and

full-scale experiments. In the second one, we used this freshly acquired knowledge to design and test novel systems.

In **Chapter 2** we evaluated the state-of-the-art of groundwater sand filtration, focusing on the latest and most successful cases of innovation. We summarized the critical bottlenecks and unknowns for the removal of iron, ammonia, manganese and arsenic, pointed out the direction that the upcoming research should take and, most importantly, presented evidence to praise for novel filtration concepts that prioritize biological over physical-chemical reactions, putting the sand filter microbiome at the forefront.

Deepening our understanding on microbial community assembly and fitness strategies is precisely what we did in **Chapter 3**. We employed a combination of full-scale sampling, laboratory experiments and metagenomics-resolved metaproteomics to characterize filters from two full-scale drinking water treatment plants. The homogeneity of the media coating and genome-based microbial composition in each filter compartment highlighted the effect of backwashing on filter media mixing. In stark contrast, intra-compartment contaminant removal was highly stratified following decreasing substrate availability along the filter height. This apparent and long-standing conflict was resolved by quantifying the expressed proteome at different filter heights, revealing a consistent stratification of proteins catalyzing ammonia oxidation and protein-based relative abundances of nitrifying genera. Our findings imply that microorganisms adapt their protein pool to the available nutrient load at a faster rate than the backwash mixing frequency.

Most often, nitrification starts only upon complete Fe oxidation in sand filters. In **Chapter 5** we aimed at unmasking the root cause of this spatial delay, which inevitably forces engineers to over-dimension sand filters. We proved that dissolved Fe^{2+} and reactive oxygen species have no detrimental effect on ammonia oxidation, and saw that the Fe oxide coating embedding sand grains seems to aid ammonia oxidation, likely by easing the establishment of a biofilm. Through laboratory-scale columns, we showed that Fe^{3+} flocs severely decrease the ammonia removal capacity of (the biofilm on) sand grains, and a combination of modeling and full-scale sampling indicated the the inhibition is reversible and seems to be some sort of contact-based interaction.

The findings of **Chapter 3** and **Chapter 4** clearly set a target to optimize sand filtration: avoiding Fe^{3+} floc formation. In a work (not included in this thesis) led by my colleague and friend Simon Müller, we proved that running filters at low oxygen concentrations (<5 mg O_2/L) and low pH (<7) stirred Fe oxidation towards purely adsorptive-biological

reactions, avoiding Fe^{3+} floc formation and allowing filters to run at >3x higher flow rates. Following the same principle, in **Chapter 4** we run a pilot-scale sand filter in the absence of oxygen. We used nitrate, commonly present in groundwater, as the electron acceptor for Fe oxidation. Our novel filter concept was driven by a newly found nitrate-reducing iron oxidizer, which we baptized as "*Candidatus* Siderophilus nitratireducens". Although it still warrants further research, the lack of Fe^{3+} floc formation makes us confident that the filter can be run at significantly higher flow rates than conventional rapid sand filters.

Our last work focused on decreasing the carbon footprint of groundwater treatment. It is common practice to remove methane by stripping it to the atmosphere through aeration. An extremely efficient method, although hardly sustainable considering that methane has a global warming potential 25 times higher than carbon dioxide. In **Chapter 6** we fed methane-rich anaerobic groundwater directly into a trickling filter to evaluate whether methane could be biologically oxidized. It worked. Methane emissions decreased by half, and the effluent water quality remained excellent. Interestingly, the presence of methane-oxidizing bacteria inhibited the growth of the autochthonous sand filter microorganisms. Ammonia and manganese removal were minimal in the trickling filter and were displaced to the post-filters, while Fe oxidation switched from (at least partially) biological to chemical.

In **Chapter 7** I collected the main findings of the thesis, put them in context with the literature, and provided an outlook for future research lines.

SAMENVATTING

Drinkwaterproductie werkt goed, maar het kan beter.

Anaeroob grondwater is een uitstekende bron voor drinkwater. Het biedt verschillende voordelen ten opzichte van oppervlaktewater, zoals een constante kwaliteit en temperatuur, en het wordt als microbiologisch veilig beschouwd. De belangrijkste verontreinigingsbronnen van anaeroob grondwater zijn de afbraak van natuurlijk organisch materiaal, die verbindingen zoals ammonium produceert, en de oplossing van bodemmineralen, wat leidt tot mangaan, ijzer en sporenelementen in het grondwater. IJzer, ammonium en mangaan moeten uit het grondwater worden verwijderd om drinkwater te produceren. Hiervoor wordt al meer dan een eeuw snelfiltratie gebruikt, voorafgegaan door een beluchtingsstap.

De beluchting verwijdert ongewenste gassen en introduceert zuurstof tot verzadigingsniveaus. Bij dit redoxpotentiaal oxideren ijzer, ammonium en mangaan door verschillende fysisch-chemische en biologische processen in het daaropvolgende snelfilter. Hierdoor slaan de meeste verontreinigingen neer en vormen ze vaste stoffen die door het zandfilter worden afgevangen, waardoor schoon water wordt geproduceerd. Hoewel snelfiltratie op grote schaal wordt toegepast en als robuust beschouwd wordt, ontbreekt nog steeds een diepgaand begrip van de werking van deze filters. Achter de schijnbaar eenvoudige werkingsprincipes schuilt een hoge mate van complexiteit.

De voornaamste reden voor deze complexiteit is de hoge zuurstofintroductie tijdens de beluchtingsstap. De verzadiging van anaeroob grondwater met zuurstof initieert een reeks van gelijktijdige, verweven en ongecontroleerde reacties waarvan de aard en bijdrage aan het totale proces onbekend en vaak onvoorspelbaar blijven. Deze complexiteit belemmert het begrip en de optimalisatie van snelfiltratie.

Het overkoepelende doel van dit proefschrift is om kennis te verwerven die bijdraagt aan het ontwerpen van efficiënte zandfilters met een hoge stroomsnelheid. Hiervoor moeten we de mechanismen begrijpen die bepalen welke reacties plaatsvinden, in welke volgorde ze optreden en hoe ze elkaar beïnvloeden. Dit maakt het mogelijk om i) de samenstelling en prestaties van microbiële gemeenschappen te voorspellen en te

beheersen, en ii) de wisselwerking tussen chemische en biologische reacties te reguleren. In het eerste deel van dit proefschrift hebben we ons gericht op het verkrijgen van een mechanistisch begrip van hoe huidige zandfilters werken door middel van experimenten op lab- en pilotschaal, maar ook met fullscale experimenten. In het tweede deel hebben we deze verworven kennis gebruikt om nieuwe systemen te ontwerpen en te testen.

In **Hoofdstuk 2** hebben we de stand van zaken van grondwaterzandfiltratie geëvalueerd, met de focus op de nieuwste en meest succesvolle innovaties. We hebben de knelpunten en onbekendheden samengevat voor de verwijdering van ijzer, ammonium, mangaan en arseen, een aanbeveling gegeven voor toekomstig onderzoek en, het belangrijkst, laten zien dat het nuttig is om in het ontwerp van nieuwe filters de voorkeur te geven aan biologische reacties in plaats van fysisch-chemische reacties, waarmee het microbioom van zandfilters op de voorgrond geplaatst wordt.

Het verdiepen van ons begrip van de samenstelling en overlevingsstrategieën van microbiële gemeenschappen is wat we in **Hoofdstuk 3** hebben gedaan. We combineerden het bemonsteren van snelfilters, laboratoriumexperimenten en metagenomics-gebaseerde metaproteomics om filters van twee drinkwaterzuiveringsinstallaties te karakteriseren. De homogeniteit van de coating van het filtermedium en de op het genoom gebaseerde microbiële samenstelling in elk filtercompartiment benadrukten het effect van terugspoelen op de menging van het filtermedium. In de verwijdering van de verontreinigen werd echter juist een duidelijke stratificatie waargenomen als gevolg van een afnemende substraatbeschikbaarheid over de filterhoogte. Deze schijnbare tegenstrijdigheid werd opgelost door het kwantificeren van het tot expressie gebrachte proteoom op verschillende filterhoogten, waarbij een consistente stratificatie van eiwitten die ammoniumoxidatie katalyseren en de relatieve aanwezigheid van nitrificerende soorten werden aangetoond. Onze bevindingen impliceren dat micro-organismen hun eiwitpool in een sneller tempo aanpassen aan de beschikbare nutriëntenbelasting dan de frequentie van terugspoelen.

Meestal begint nitrificatie pas na volledige oxidatie van ijzer in zandfilters. In **Hoofdstuk 5** was ons doel om de oorzaak van deze vertraging te achterhalen, aangezien dit ingenieurs er toe dwingt zandfilters hoger te ontwerpen dan nodig. We hebben aangetoond dat opgelost Fe^{2+} en radicalen geen nadelig effect hebben op ammoniumoxidatie, en dat de ijzeroxidecoating op zandkorrels waarschijnlijk de ammoniumoxidatie bevordert, vermoedelijk doordat een biofilm zich gemakkelijk aan de coating kan hechten.. Door middel van kolomexperimenten in het laboratorium

hebben we aangetoond dat Fe^{3+}-vlokken de ammoniumverwijderingscapaciteit van (de biofilm op de) zandkorrels sterk verminderen, en een combinatie van modellering en het bemonsteren van een fullscale zandfilter liet zien dat de remming omkeerbaar is en gebaseerd is op een soort contact-gebaseerde interactie.

De bevindingen van **Hoofdstuk 3** en **Hoofdstuk 4** geven duidelijk aan dat het optimaliseren van zandfiltratie gericht moet zijn op het vermijden van Fe3+-vlokvorming. In een onderzoek, geleid door mijn collega en vriend Simon Müller (niet opgenomen in dit proefschrift), hebben we aangetoond dat bij lage zuurstofconcentraties (<5 mg O_2/L) en lage pH (<7) de ijzeroxidatie puur adsorptief-biologisch is, waardoor Fe^{3+}-vlokvorming werd vermeden en filters met >3x hogere debieten konden draaien. In **Hoofdstuk 4** hebben we een pilotschaal zandfilter gedraaid zonder zuurstofinbreng. Nitraat, dat vaak aanwezig is in grondwater, werd gebruikt als elektronenacceptor voor ijzeroxidatie. Dit innovatieve filter werd aangedreven door een nieuw ontdekte nitraat reducerende ijzeroxidator, die we hebben gedoopt als “Candidatus Siderophilus nitratireducens”. Verder onderzoek is nog nodig, maar wij zijn overtuigd dat het vermijden van Fe^{3+}-flocculatie het mogelijk maakt om het filter op hogere debieten te draaien dan gebruikelijk.

Ons laatste onderzoek richtte zich op het verminderen van de CO_2-voetafdruk van grondwaterbehandeling. In de praktijk is het gebruikelijk om methaan uit het grondwater te verwijderen met de beluchtingsstap. Hoewel dit een efficiënte methode is, is het niet duurzaam. Het vrijgekomen methaan, met een 25 keer hogere opwarmingspotentieel dan CO_2, komt namelijk in de atmosfeer terecht. In **Hoofdstuk 6** onderzochten we of methaan biologisch geoxideerd kon worden, door methaanrijk anaeroob grondwater rechtstreeks in een droogfilter te leiden. Dit werkte; methaanemissies namen met de helft af en het geproduceerde water bleef van uitstekende kwaliteit. Een interessante bevinding was dat de aanwezigheid van methaan-oxiderende bacteriën de groei van autochtone zandfiltermicro-organismen remde. Ammonium- en mangaanverwijdering waren minimaal in het druppelfilter en schoven op naar de nafilters, terwijl ijzeroxidatie overschakelde van (gedeeltelijk) biologisch naar chemisch. In **Hoofdstuk 7** heb ik de belangrijkste bevindingen van het proefschrift verzameld, ze in context geplaatst met de literatuur, en een perspectief gegeven voor toekomstig onderzoek.

RESUM

La producció d'aigua potable funciona, però podem fer-ho millor.

De totes les fonts d'aigua potable, l'aigua anaeròbia subterrània es probablement la millor. Te moltes avantatges respecta la competidora, l'aigua superficial, com nivells constants de contaminants i temperatura estable, a mes de ser considera lliure de patògens. Les principals fonts de contaminació de l'aigua subterrània son la descomposició de matèria orgànica i la dissolució de metalls del sòl. La primera produeix compostos com l'amoni, i la darrera allibera elements com al manganès i el ferro, entre d'altres. Disminuir la concentració de ferro, amoni i manganès es fonamental per generar aigua potable partint d'aigua subterrània. Durant mes d'un segle, els humans hem fet servir filtres de sorra - precedits per un pas d'aeració – per aquesta tasca.

L'objectiu de l'aeració es eliminar gasos indesitjables i introduir oxigen. La introducció de l'oxigen augment el potencial d'oxidació-reducció de l'aigua fins a nivells en els que el ferro, l'amoni i el manganès són oxidats en diverses reaccions d'origen tant fisicoquímic com biològic en el filtre de sorra posterior. El resultat d'aquests processes es que la majoria dels contaminants precipiten, formats sòlids que es queden atrapats al filtre i per tant generant aigua potable. Malgrat els filtres de sorres s'utilitzen freqüentment i son considerats aparells molt robusts, hi ha una manca evidentment de coneixement sobre el seu funcionament. Els filtres de sorra amaguen un alt grau de complexitat que s'oculta darrera un funcionament aparentment senzill.

El gran culpable d'aquest alt nivell de complexitat es la introducció d'altíssimes dosis d'oxigen durant el pas d'aeració. La saturació d'oxigen de l'aigua subterrània anaeròbia desencadena una conjunt de reaccions simultànies, entortolligades i incontrolables de les quals no podem traçar ni l'origen ni la contribució en el procés global. Aquest manca de control, i de coneixement en general, dificulta enormement no nomes la operació, sinó també, evidentment, la optimització dels filtres de sorra.

L'objectiu d'aquest tesi doctoral es adquirir coneixement que ens permeti avançar cap al disseny de filtres amb cabals superior i mes sostenibles. Per aconseguir-ho, hem de ser capaços d'entendre els mecanismes que dicten quines reaccions ocorren, en quin

ordre ho fan i quin efecte tenen les unes sobre les altres. La nostra tesi es que si ho aconseguim, serem capaços de predir i controlar *i)* la formació i el funcionament de les comunitats microbianes i *ii)* les interaccions entre les reaccions fisicoquímiques i biològiques. A la primera part de la tesi ens centrem en entendre en profunditat com funcionen els filtres a escala laboratori, pilot i industrial. A la segona, col·leccionem el coneixement adquirit per dissenyar, testejar i implementar nous dissenys de filtres de sorra.

Al **Capítol 2** avaluem l'estat de l'art en filtració de sorra d'aigua subterrània, posant èmfasi en els darrers casos d'innovació de mes èxit. Resumim quins son els colls d'ampolla i les incògnites realment mes rellevants per l'eliminació de ferro, amoni, manganès i arsènic. A més, indiquem la direcció en la que creiem hauria d'anar la recerca d'ara en endavant i, sobre tot, presentem evidencies per encoratjar la comunitat a tirar endavant nous dissenys de filtració que prioritzin les reaccions biològiques, posant les comunitats microbianes en el focus d'atenció.

Augmentar el grau de coneixement sobre la formació i el funcionament de les comunitats microbianes es precisament el que férem al **Capítol 3**. Mitjançant una combinació de mostreig, un segui d'experiments al laboratori i metaproteomica, vàrem caracteritzar dos filtres d'escala industrial. La homogeneïtat del recobriment dels grans de sorra i de la composició de la comunitat basada en metagenomica en els compartiments dels filtres exemplifica l'efecte de barreja que te el *backwashing*. Oposadament, la capacitat per eliminar contaminants en cada compartiment estava clarament estratificada, seguint la disminució de la concentració de substrat al llarg del filtre. Vam resoldre l'atzucac quantificant les proteïnes dels microorganismes al llarg del filtre. Els resultats van de la ma dels de la capacitat de degradació dels contaminants: clarament estratificats.

Sovint, l'oxidació d'amoni als filtres de sorra nomes comença un cop el ferro ha estat totalment oxidat. L'objectiu del **Capítol 5** es entendre la raó darrera aquest retràs espacial, que inevitablement obliga els enginyers a sobredimensionar els filtres. Mitjançant assajos al laboratori demostrem que el Fe^{2+} dissolt i les especies reactives d'oxigen tenen un efecte marginal sobre l'oxidació d'amoni. A mes, observarem que els oxides de ferro que recobreixen els grans de sorra semblen tenir un efecte positiu en l'oxidació d'amoni, probablement perquè les rugositats de la seva superfície facilita la colonització del gra per part dels microorganismes. Fent servir filtres de sorra a escala laboratori, presentem proves irrefutables per demostrar que els flocs de Fe^{3+} disminueixen la capacitat per oxidar amoni dels biofilms que viuen sobre els grans de sorra. Finalment, amb una combinació de de mostreig a escala i industrial i un model

computacional observarem que la inhibició sembla estar basada en un contacte directe entre els flocs i les bactèries que oxiden amoni.

Les troballes del **Capítol 3** i del **Capítol 4** vàrem deixar en evidencia que, si volíem optimitzar els filtres, havíem d'evitar de totes, totes la formació de Fe^{3+} flocs. En un projecte (que no forma part d'aquest tesi), liderat pel meu company i bon amic Simon Muller, vàrem demostrar que operar els filtres a baixes concentracions d'oxigen (<5 mg O_2/L) i baix pH (<7) estimula la oxidació de Fe cap a reaccions adsorvatives-biologiques, evitant la formació de Fe^{3+} flocs i permetent operar al filtre a, com a mínim, el triple de cabal. Seguint el mateix principi, al **Capítol 5** vàrem operar un filtre de sorra a escala pilot sense dosificar oxigen. En aquest cas, l'acceptor d'electrons era el nitrat, un component present en bona part de l'aigua subterrània. Aquest nou disseny de filtre es basa en la feina d'un microorganisme que vàrem descobrir i que vàrem batejar com a "*Candidatus* Siderophilus nitratireducens". Malgrat encara queda feina, la manca de Fe^{3+} flocs ens fa creure que aquest filtre també el podrem fer anar cabals molt mes altres que els filtres convencionals.

Abans de tancar el projecte, tenia ganes de treballar per mirar de minimitzar les emissions de gasos d'efecte hivernacle dels filtres de sorra. El model mes habitual (potser fins i tot m'atreviria a dir únic) d'eliminació de meta es aeració i emissió directa a l'atmosfera. Malgrat el procés funciona, es evident que l'impacte ambiental es altíssim degut a l'alt índex d'escalfament global del meta, que es 25 vegades el del diòxid de carboni. Al **Capítol 6** vàrem introduir aigua subterrània amb altes concentracions de meta directament en un filtre sorra, sense aeració prèvia, per intentar eliminar el metà biològicament. El concepte fou tot un exit: les emissions de meta varen reduir-se en un 50%, i la qualitat de l'aigua potable produïda no va veure's afectada.

La tesi la tanca el **Capítol 7**, on recopilo les troballes mes importants de la tesi, tot contextualitzant-les amb la literatura i indicant quines línies d'investigació son les mes rellevants per acabar d'entendre, ben be, com funcionen els filtres de sorra.

PREFACE

Done is better than *Well* Done

Luca is 6. He just received the grades for his first-ever exam in school. It's a 10 out of 10, the best of his class. Luca does not quite understand what this means. He simply remembered what the teacher explained and was able to repeat it accurately. *Luca is told he is very smart*. *Luca is thrilled*.

Luca is 12. He just finished his first year of high school, and he nailed it. He excelled everywhere. Luca barely studies, he just remembers and repeats. *Luca starts to believe he is very smart*. *Luca is happy*.

Luca is now 17. He got the highest grades in his promotion. Listen, memorize, repeat. He will attend the best university in the country. *Luca is convinced he is a genius*. *Luca is content*.

Luca is now 20. Luca invests more time studying now. Listen, memorize, memorize, memorize, memorize, repeat. A 10. *Luca is relieved people did not discover he actually is not that smart*.

Luca is 24. He just started his PhD. There is nothing to memorize now. Luca has to *create*. Luca has to *explore*. Luca has to *draft*. Luca panics. Luca never learned how to *create, explore, or draft*. Luca procrastinates. He is afraid of sending the first version of his article to his supervisor. He does not dare to ask what he does not understand. He avoids thinking out loud. *Luca wonders how he managed to fool his supervisor into hiring him*.

I was Luca, and know many of them. And so do you. In fact, you may very well be one. We were not born as a Luca, but *became* him. And we are not responsible for it. But we can change it. *Create, explore, draft*. *Make mistakes. Try new things. Fear nothing. Set yourself free, so that Luca can go*.

Great doubt, great enlightenment;

Small doubt, small enlightenment;

No doubt, no enlightenment.

Zen saying

INTRODUCTION

1

1.1. WHICH WAS YOUR FAVORITE DINOSAUR?

Mine was Ankylosaurus. Which 5-year-old can say no to a massive reptile with a back full of spikes and a swinging, ball-ended tail strong enough to fracture bones? (Figure 1). Dinosaurs were incredible creatures. There is no debate here. But why? Why are so many 5-year-olds around the globe fascinated by dinosaurs? Some may argue it is due to their impressive build or fierceness. I think it is because of their diversity: they came in different sizes and shapes and were able to live underwater, on earth, and in the sky, not to mention the myriad of actions for which they specialized: velociraptors are best at speeding, while triceratops shine at warfare and anyone knows that Pterosaurs are your go-to choice for a good panoramic view. This seemingly endless variability spoon-feeds the curiosity of kids. *Click*. Triggered. Engine on. System in motion. The pursuit of knowledge starts, and it is not meant to stop.

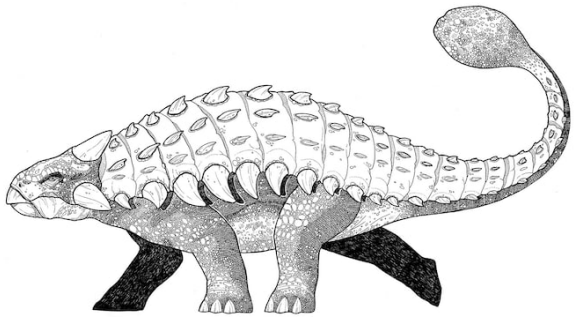

Figure 1. Ankylosaurus. Courtesy of Annabel Grant.

One cannot simply choose *not to learn*. The quest is perennial. But it needs fuel. Eventually, the vast spectrum of shapes and sizes of dinosaurs is not that vast anymore. There is no more diversity to explore, and the fascination of that 5-year-old fades as quickly as it rose. But there is hope. Quickly, one discovers how diverse the *Pokémon* world is, how many different types of troops fought for the Roman, Greek, and Egyptian Empires, or the variety of powers held by superheroes in the Marvel Universe. The thirst for knowledge awakes again, and Hollywood knows it. Yet, that fuel does not last long either. 1025 different *Pokémon* and 750 superheroes sound like a lot but don't taste like much when you are truly fascinated. And then what? It took The Pokémon Company 27 years to design those 1025 distinct creatures. 27 years of painstaking work, and yet

kids catch them all in a few weeks. As humans, our ability to create cannot keep up with our desire to discover. There is, however, a creator whose work we will never be able to digest. The original designer. The almighty 0.0000000001% error rate in DNA replication. Fasten your seatbelts, big numbers are coming.

1.2 million. This is how many different species exist. In the eukaryotic world. That we know of. Current estimates report that there are about 8.7 million different species of eukaryotes [1]. If we include prokaryotes, the number becomes something between 10 million [2] and 1 billion [31]. Those are *a lot* of different species. So much we are incapable of comprehending the magnitude of it. So let's accept it for now – a lot. But how much diversity is there? Well, also a lot. Superman bends iron? *Gallionella ferruginea* eats it for breakfast and builds Gaudi-like structures with the leftovers (Figure 2). Pikachu attacks with thunder? *Geobacter sulfurreducens* grows a tail to shoot and absorb electrons (Figure 2). Dragons spit fire? *Strain 121* replicates at 121°C and it does not even need oxygen to breathe. And you know what the best part is? These organisms actually exist. We share our planet with them. A group of *Gallionella ferruginea* are sharing an entrée of iron while you read these lines. And do you know what is even better than that? These microorganisms belong to the <3% of prokaryotes we know, which means that over 97% of them are still to be discovered [4]. Hypnotizing, isn't it? Humans are unable to understand the vertiginous diversity of the microbial world, but we excel at harnessing it.

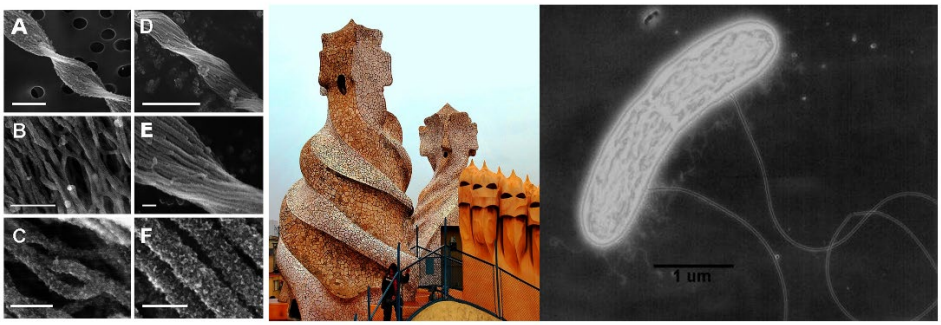

Figure 2. Left – Twisted iron stalks produced by bacterium Gallionella ferruginea. Courtesy of Tomoko Suzuki and colleagues [5]. Center – Central towers at the top of La Pedrera in Barcelona, designed by Antoni Gaudi and of remarkable resemblance with

[1] Robert May, one of the most prolific academics of the modern era, claimed that if aliens came to Earth and asked *How many distinct life forms – species – does your planet have?,* he would be *embarrassed* to admit how little we know about it and how inaccurate our estimates are. [39]

Gallionella's staks. Courtesy of Javier1949 (Flickr). Right – Pili (tail) that Geobacter sulfurreducens uses to shoot and absorb electrons from other microorganisms or inert materials.

1.2. (UN)FRIENDLY CREATURES

If the reader is still here, there is no need to convince her about the pivotal role microorganisms play in our society. From food preservation to drug production, human idiosyncrasy simply cannot be understood without taking into account the action of our little friends. The first (unconscious) use of microorganisms is beverage fermentation from rice, which started almost ten thousand years ago [6]. The *unconscious* component of that practise is crucial here. First, to grasp how microorganisms behave: if the conditions are favourable, they will grow, even if we don't actively try to foster that. This rather trivial idea holds tremendous power, and it sets the fundaments not only of this book, but of biotechnology as a discipline[2]. In fact, preventing microbial growth costs the pharmaceutical industry a lot of money [7]. Second, because the idea that *tiny animals*[3] existed was not conceived until the 17th century, when Robbert Hooke depicted the first microfungus and Antoni van Leeuwenhoek saw bacteria for the first time [8].

Following that event, microorganisms were basically ignored during the next 200 years. Until 1854, when John Snow (Figure 3), the father of epidemiology, found out that the epicentre of the cholera outbreak that killed hundreds of Londoners was a public fountain, that the disease was spreading via the faecal-oral route, and that what was causing cholera *must necessarily have some sort of structure, most likely that of a cell* [9]. His work led to the discovery of the bacteria *Vibrio cholerae* as the causing agent by Robert Koch thirty years later [10], and from that point on everything went downhill for microorganisms: tuberculosis, diphtheria, tetanus, plague or syphilis, among many others, were found to be caused by pathogenic microorganisms. In the late 19th century microorganisms

[2] This idea stems from the seminal *Everything is everywhere, but the environment selects* from Baas Becking.

[3] Antoni van Leeuwenhoek wrote "*among these streaks there were besides very many little animalcules … And the motion of most of these animalcules in the water was so swift, and so various upwards, downwards and round about that 'twas wonderful to see: and I judged that some of these little creatures were above a thousand times smaller than the smallest ones I have ever yet seen"* in a letter to the Royal Society in London upon seeing bacteria for the first time [40] .

were not exactly worshiped. Then serendipity came into play, and Alexander Fleming showed the world that microbes can produce valuable chemicals. On his workbench, the fungus *Penicillum notatum* excreted something that inhibited the growth of all bacteria around it. He named that substance penicillin, and changed medicine forever[4].

Figure 3. John Snow, father of epidemiology, and the public fountain through which cholera was spreading in London. The pump has been preserved and can still be visited. Image from ARTIS-Micropia.

With Fleming, microorganisms became cattle: living forms that we could grow to obtain goods. The discovery of penicillin was quickly followed by that of many others. Probably the most notorious one is streptomycin, from bacteria of the genus *Streptomyces*. The industrial production of streptomycin and penicillin kept the death toll of World War II much lower than it would have been otherwise [11]. With time, we mastered the art of harvesting chemicals from microbes, and reached the climax in 1982, when human insulin was produced by a genetically modified bacterium. Suddenly, we were not restricted to compounds naturally produced by microorganisms, but we could synthesize virtually *anything*[5]. And that is not all. Stirring the 'behaviour' (metabolism) of microorganisms allows us to do more than *produce* compounds, we can also *degrade* them. Microbes are not peaky commensals. On the contrary, they enjoy savouring nasty stuff: wood

[4] *When I woke up just after dawn on September 28, 1928, I certainly didn't plan to revolutionize all medicine by discovering the world's first antibiotic, or bacteria killer.* Alexander Fleming [41].
[5] I learnt this at 16 in high school, and it is the ultimate reason why I am writing these lines right now.

[12], plastic [13], crude oil [14], you name it. We can get this done in the laboratory, but it is not easy at large scale. The problem? Economics, of course. You will not even check the price tag of a drug you need to save your life[6], but who wants to pay a fortune to clean soil or water? No one. We needed an affordable alternative, and we found it.

1.3. SUMMONING MICROORGANISMS

Jean-Baptiste Lamarck was a brilliant man but was fooled by giraffes[7]. He posited the first theory of evolution, that can be unfairly summarized as 'giraffes grew larger necks to reach the leaves at the top of trees'. Charles Darwin improved it afterward to something like 'all organisms of a species harbour random mutations in their genetic material that will gift them different attributes. Some of the mutations will provide an advantage given a specific situation, and will allow those organisms to survive, while the rest will perish'. In the giraffe context, this means that randomly one of the giraffes will have a longer neck, which will allow it to eat, survive and thus generate offspring. The main difference between the Lamarckian and Darwinian theories is the *randomness*. Giraffes did not actively try to grow larger necks, it just *randomly* happened due to genetic variability - i.e. the 0.0000000001% error rate in DNA replication –, and the environment selected who survived (the one that could reach the food).

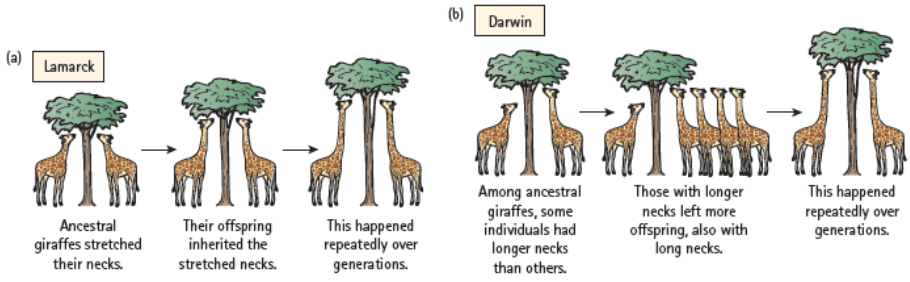

Figure 4. Sketch comparing the evolution theories of Lamarck and Darwin.

[6] No one should need to, at least.
[7] And so would you and me.

As you can imagine, if this happened to giraffes, it also happens to microorganisms. Stay with me here: if we set a specific set of conditions, like providing only compound Y as food, microorganisms will eventually get a random mutation in their DNA that will allow them to eat compound Y. This sounds like magic, but it is not. This happens. Well, can happen. It took thousands of years of evolution for giraffes to look the way they look now. And we do not have thousands of years to wait for our microorganisms to evolve. And here the beauty of microbial diversity comes back. The microbial world is so (and I cannot stress how much) diverse, that virtually any trait you can think of probably already exists. Marvellous, right? But there is a catch. In most cases, this only holds if an environment that selects for that specific trait existed for long enough. For example, ammonia is a natural compound that has been on earth for longer than we have. Thus, there are microorganisms that are able to consume it. On the contrary, tennessine is a man-made element which was only crafted in 2010 [15], and thus no microorganism can degrade it. This principle generally sets the boundaries for what we can achieve using microorganisms[8]. But since microbial diversity is practically limitless, the framework we are left with is ridiculously wide. Basically, all we have to do is properly set an environment in which organisms with the functionality that we want can thrive, and they will thrive. Simple, isn't it? Not really, no. Setting the proper environment requires deep understanding of microbiology and chemistry, thorough experimental design, meticulous work, endless trouble-shooting and lots of creativity. It is, basically, art.

During the last 6 years, I have been fortunate to study and work in one of the Mechas of this art: TU Delft. Plenty of *artists* worked here before me, and granted the world magnificent examples of how to set proper environments. One of my favourites is *Survival of the fattest*, where Peter R. Mooij selected for microalgae with the highest capacity to remove organic contaminants from water based on its ability to produce fat [16]. Some other beautiful examples are the work of Katja Johnson, who managed to select for organisms with the highest bioplastic production [17] or that of Gertjan Smolders, who maximized phosphate removal [18]. These successful examples have one thing in common: they aim at maximizing the capacity to metabolize one single compound - fat for Peter,

[8] These boundaries can be expanded with genetic engineering, but let's ignore that for now.

bioplastic for Katja, phosphate for Gertjan. What if we need to target more than one compound at the same time?

Sometimes we are lucky, and there is an organism that can carry out the job. In wastewater treatment, for instance, denitrifying organisms consume nitrogen and carbon simultaneously, and thus the focus is on setting an environment for them to thrive. Occasionally, however, luck is not on our side, and there is no such microorganism. Take, for instance, groundwater treatment, where ammonia, iron and manganese must be removed. The simplest, rudimentary solution is to set three different environments. This will likely work, but of course be far from an optimal solution: three different environments require three different bioreactors with high capital and operational expenditures. The better solution is to set an environment where all the microbes – ammonium degraders, iron degraders, and manganese degraders – can co-exist. As you probably already guessed, this exponentially increases the complexity of the challenge. Microorganisms interact with each other directly, i.e. by producing antibiotics, but especially indirectly by modifying the environment (that you previously tried to meticulously design and set-up). Dealing with such complexity is what me and my colleagues did during the last four years. Here, you'll read what we found.

1.4. THE BETTER WATER SOURCE

Most drinking water in the world is produced from surface water or groundwater. Surface water includes all the water we see, such as rivers, lakes or artificial reservoirs. Due to its constant exposure to air, surface water gets contaminated. Among others, pesticides and microplastics floating in the air reach these water bodies, and so do microorganisms and other potentially pathogenic small creatures. On top of that, rivers receive streams from polluting industries and wastewater treatment plans, creating a cocktail of rather unpleasant ingredients. Converting this source into drinking water is a challenging task that requires the combination of several technologies and that is forced to constantly evolve due to the appearance of emerging contaminants. The alternative to surface water is groundwater, which is water stored underground.

Groundwater is divided into several categories depending on its depth and reduction-oxidation potential, but here we will focus only on deep, anaerobic[9] groundwater. Unlike surface water, anaerobic groundwater has constant quality and temperature, is (generally) confined and thus free of new contaminants, and is considered to be microbiologically safe due to its decades-long underground storage. Groundwater is clearly the better choice for drinking water production, and many countries use it as its preferred drinking water source. The Danes drink exclusively groundwater [19], and 60% of Dutch drinking water originates from groundwater [20] (and it would be 100% if they could). And there is more: not only is groundwater less polluted than surface water, but its pollutants are also easier to degrade. Let's explore them.

The two main sources of contamination of groundwater are the decomposition of natural organic matter and the dissolution of soil mineral [21]. The first one produces ammonia and methane, while the second one introduces manganese, iron, and trace metals such as arsenic. Ammonia and methane are not toxic at the concentrations present in groundwater, but their degradation ensures microbial stability during transportation – this means, microorganisms will not grow in the pipes of the reader's house. Similarly, iron is not dangerous at groundwater concentrations, but it gives unpleasant organoleptic properties to water – taste, odour, aspect – and it stains clothes. On the contrary, manganese and arsenic are toxic to humans at groundwater concentrations. Health concerns associated with the presence of manganese are mostly related to neurologic symptoms [22]. Arsenic is extremely poisonous, and its long-term intake results in arsenicosis, which englobes several fatal diseases [23]. Out of these five, only iron, ammonia and manganese are present at concerning concentrations in the majority of deep, anaerobic groundwater wells in the Netherlands, and their removal is a crucial step and the focus of most drinking water treatment plants. Such a heavy burden lies on the shoulders of sand filters.

[9] In the field of microbiology, the terms 'aerobic' and 'anaerobic' are used to refer to microbial metabolisms, whereas 'oxic' and 'anoxic' are used to describe systems or conditions. These definitions disregard the presence of alternative electron acceptors such as nitrate and nitrite, which play a crucial in the drinking water field. Therefore, in this thesis we adhere to the water engineering nomenclature, and use the terms 'aerobic' to refer to systems with oxygen, 'anoxic' to systems without oxygen but with alternative oxygenated electron acceptors such as nitrate or nitrite, and 'anaerobic' to systems where oxygenated electron acceptors are not present.

1.5. A QUICK GUIDE ON SAND FILTRATION

In essence, sand filters are vessels filled with tiny rocks. Simple. Their working principle is simple as well: dirty water flows through a bed of sand, and clean water leaves the filter. *How* this happens is not that simple, though. In fact, nowadays, 150 years after the first industrial application of sand filters, we do not fully understand it yet.

1.5.1. Removal mechanisms of iron, manganese and ammonia

Iron

Sand filters were originally designed to remove iron from anaerobic groundwater. Since the water is anaerobic, the iron it contains is in its reduced form (Fe^{2+}), which is soluble. Oxidizing the water matrix – introducing oxygen by aeration – onsets the chemical oxidation of Fe^{2+} to Fe^{3+} (eq. 1). This reaction takes places solely in one phase (water), and is thus known as homogeneous iron oxidation. The product are solid hydrous ferric oxide flocs (Fe^{3+} flocs, Fig. 5) [24]. Upon injecting the water into the sand filter, Fe^{3+} flocs are entrapped within the bed, and clean water leaves the filter. It works.

$$Fe^{2+} + \frac{1}{4}O_2 + 2\frac{1}{2}\,H_2O \rightarrow Fe(OH)_3 \downarrow + 2\,H^+ \qquad \text{eq. 1}$$

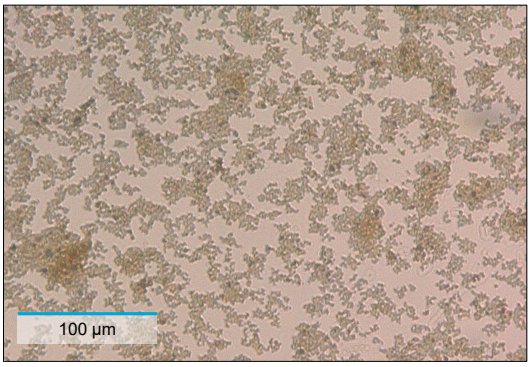

Figure 5 . Fe^{3+} flocs formed in the water phase, suspended in the supernatant prior to injection into the filter bed.

However, a quick iron mass balance shows that not all Fe^{2+} ends up as Fe^{3+} flocs. A fraction of Fe^{2+} is adsorbed onto the sand grains, which are covered by a layer of metal oxides. Among them, Fe^{3+} oxides are usually the most common ones. Fe^{2+} - Fe^{3+} complex formation is followed by the oxidation of Fe^{2+} to Fe^{3+} and subsequent hydrolysis, producing compact, brown hydrous ferric oxides that become part of the coating and contribute to sand grain growth (eq. 2, Fig. 6) [24]. This biphasic reaction (Fe^{2+} dissolved in water, Fe^{3+} as solid) is called heterogeneous iron oxidation.

$$Fe^{3+} - OH + Fe^{2+} + \frac{1}{4}\, O_2 + 1\frac{1}{2} H_2O \rightarrow\ Fe^{3+} - OFe(III)(OH)_2 + 2\, H^+ \qquad \text{eq. 2}$$

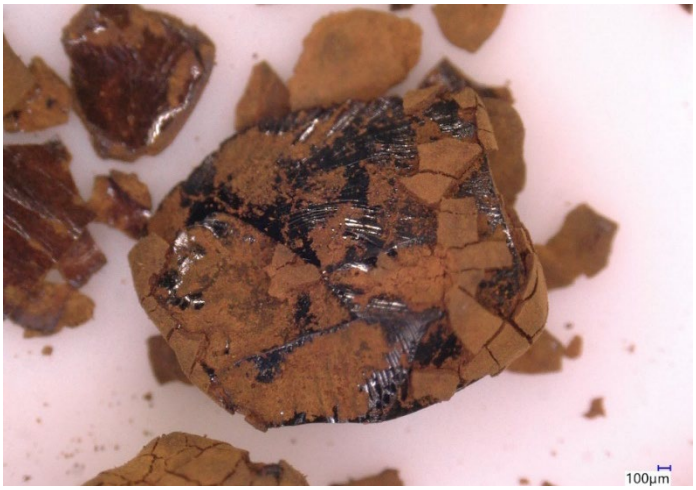

Figure 6. Sand grains (black) partially covered in iron oxides (brown) from drinking water treatment plant Druten (Vitens N.V.).

And that is not all. The combination of oxygen and Fe^{2+} sets the perfect environment for iron oxidizing bacteria (FeOB) to grow, and so they do. As we saw before, FeOB like *Gallionella ferruginea* oxidize Fe^{2+} and excrete Fe^{3+} stalk-like structures (eq. 3) [25] :

$$Fe^{2+} + \frac{1}{4} O_2 + 2\frac{1}{4}\, H_2O\ \rightarrow Fe(OH)_3 \downarrow\ + 2\, H^+ + FeOB - biomass \qquad \text{eq. 3}$$

The oxidation of Fe^{2+} can take place via three different pathways, both chemically and biologically, all yielding different products.

Manganese

Homogeneous manganese oxidation is unfeasible in groundwater, so we are left with heterogeneous and biological oxidation. The mechanisms are the same as for iron, with the exception that oxidized manganese can be present both as Mn^{3+} and Mn^{4+}. Heterogeneous oxidation occurs when soluble Mn^{2+} is complexed by a $Mn^{3+/4+}$ oxide at the surface of sand grains. Mn^{2+} is subsequently oxidized and hydrolyzed, producing black Mn oxides that contribute to sand grain growth (eq. 4, Fig. 7) [26]:

$$MnOx + Mn^{2+} + O_2 + xH_2O \rightarrow 2\ MnOx + xH^+ \qquad \text{eq. 4}$$

Figure 7. Sand grains covered in manganese oxides (black) from drinking water treatment plant Holten (Vitens N.V). Picture courtesy of Simon Muller.

Groundwater conditions are also appealing for manganese oxidizing bacteria (MnOB). The stoichiometry of that reaction or the nature of the products remain

unclear, but it definitely entails the oxidation of Mn^{2+} to $Mn^{3+/4+}$ and the catalytic activity of bacterial enzymes [27].

As for Fe^{2+}, the oxidation of Mn^{2+} can be both chemically or biologically driven, and those reactions produce different types of solids. The picture changes for ammonia.

Ammonia

Ammonia oxidation is carried out exclusively by microorganisms. Traditionally, and for the sake of simplicity, complete ammonia oxidation is considered to be a two-step reaction. First, ammonia is oxidized to nitrite, and then nitrite oxidation to nitrate follows. Both bacterial and archaeal species are known to perform these reactions, but bacteria are generally considered to be the main contributors in sand filters[28]. We call the group of bacteria that perform the first reaction (eq. 5) ammonia-oxidizing bacteria (AOB), and the second ones (eq. 6) nitrite-oxidizing bacteria (NOB). Organisms that perform both of them are referred to as complete ammonia oxidizers (comammox) (eq. 7) [29].

$$NH_4^+ + 1.5\ O_2 \rightarrow NO_2^- + 2\ H^+ + H_2O \qquad \text{eq. 5}$$

$$NO_2^- + 0.5\ O_2 \rightarrow NO_3^- \qquad \text{eq. 6}$$

$$NH_4^+ + 2\ O_2 \rightarrow NO_3^- + H_2O + 2\ H^+ \qquad \text{eq. 7}$$

Ammonia oxidation is relatively simple compared to iron and manganese, but relying only on microorganisms also has its downsides.

1.5.2. Sources of complexity

Abundance and nature of the oxidizing agent

As we have just seen, multiple reactions can oxidize each of the main groundwater contaminants. On the one hand, sand filtration tremendously benefits from their existence, as it widens the window of operational conditions in which all compounds can be removed simultaneously. On the other hand, this simultaneity is also the source of most headaches for practitioners and most enigmas for researchers. To understand why, we need to dive deeper.

The first step to remove iron, manganese and ammonia from anaerobic groundwater is incorporating an oxidizing agent. In Northern Europe, oxygen is the preferred option. There are several reasons as to why oxygen is a better choice compared to the other main oxidizing agents, namely chlorine and permanganate. It is safer to handle, it has a much higher end-of-the-pipe biological stability than permanganate, no disinfection by-products are formed - typical in chlorination -, and its accessibility protects the drinking water companies from supply chain problems. Oxygen is dosed to saturation levels using spray or tower aerators (Figure 8). On top of introducing oxygen, aeration also strips out undesired gases from groundwater such as methane, hydrogen sulfide, and carbon dioxide. Carbon dioxide and one of its dissolved counterparts, bicarbonate, dictate the pH of the water. As a result of aerating, we are left with oxygenated water (*ca*. 10 mg O_2/L) at high(er) pH (7.5 to 8.5).

At these conditions, virtually any of the aforementioned conversions is possible. Thus, excessive aeration onsets a convoluted network of simultaneous, interconnected, and uncontrolled chemical and biological reactions. Although generally effective, this convolution deprives us of understanding, let alone deciding, what happens in the filter, which effectively becomes a *black box*. As a result, troubleshooting and optimization demand titanic efforts and often become unattainable.

Figure 8. Spray aeration on top of the sand filter is one of the standard methods to introduce oxygen into anaerobic groundwater. Picture taken from drinking water treatment plant Leidsche Rijn (Vitens N.V.).

Direct and indirect interactions and futile cycles

Although far from deliberate, the removals of iron, manganese and ammonia tend to naturally stratify along the filter height. Iron is always removed at the top, followed first by ammonia and then by manganese (Fig. 9). The overlap between the removal processes seems to be filter-specific. In some sites there is hardly any, and manganese oxidation only starts upon complete ammonia removal, which only onsets after all Fe^{2+} is gone [30]. In other cases, the separation is not obvious, and some reactions occur simultaneously [31]. The literature is full of full-scale examples of these differences, but the underlying reasons why the removal process (do not) stratify remain largely unexplored [32]. What is certain is that a direct consequence of stratification is that the products of the first reactions will interfere with the conversions taking place further down the filter.

Three main problems arise when products of upstream reactions come into contact with downstream conversions: direct inhibition, indirect inhibition, and futile cycles. Let's dissect them one by one, using Fe^{2+} oxidation as an example.

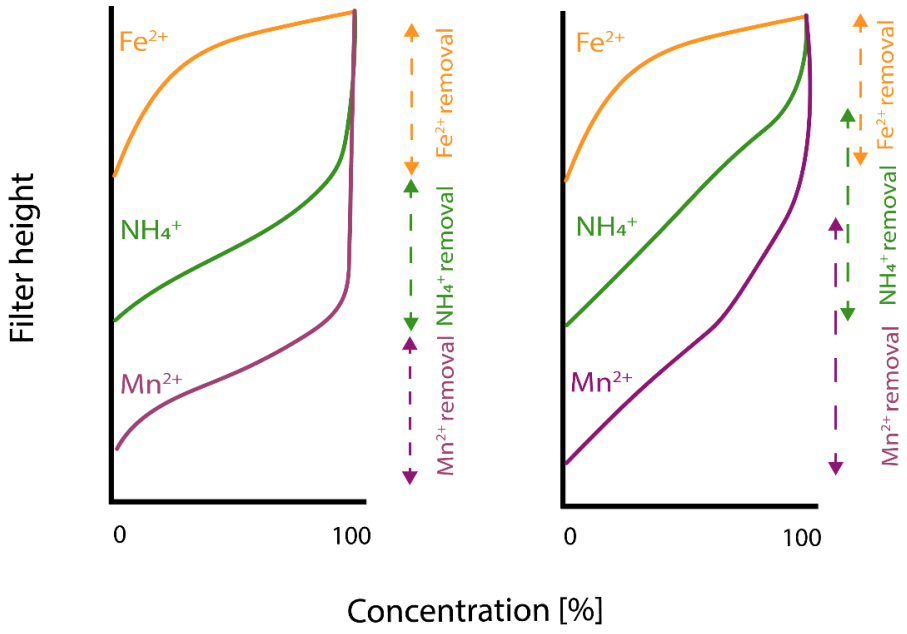

Figure 9. Schematic representation of the removal of iron, ammonia and manganese along the height of sand filters. In some cases (left), the removal is sequential, while in others (right) some of the reactions overlap.

The oxidation of iron may be dominated by either homogeneous, heterogeneous or biological oxidation depending on the process conditions [33], but the first one is always present to a bigger or lesser extent. Fe^{3+} flocs are the main reaction product of homogeneous iron oxidation, and reactive oxygen species are generated as by-products via Fenton chemistry. Both compounds have been shown to negatively impact ammonia oxidation by directly inhibiting cellular activity or by promoting cell death [34,35].

A good example of indirect interaction is phosphate limitation. Phosphorus is an essential nutrient for cellular growth that bacteria need to uptake from their surroundings. Groundwater naturally contains phosphorous at sufficient concentrations to promote and sustain microbial networks in sand filters. Yet, there are many mouths to feed, and iron oxides are very hungry. During the oxidation of Fe^{2+} to Fe^{3+} flocs, phosphate is incorporated [36] or adsorbed [37] into the formed Fe^{3+} floc, potentially limiting P bioavailability and thus compromising the growth of all bacteria and indirectly inhibiting ammonia oxidation [38].

Before we leave direct and indirect interaction behind, there is an additional category that deserves special attention. It entails microbial competition and is hard to place in either of the two previous categories due to the uncertainty in its working mechanisms. As previously mentioned, methane is stripped from groundwater in the aeration step, and thus it hardly ever reaches the filter. But what happens if it does? Methane-oxidizing bacteria have been found to occupy the first section of the filter, displacing ammonia-oxidizing bacteria further down [30]. Practically, this translates into a loss of ammonia removal capacity.

The last category of problems is futile cycles. Manganese undergoes oxidation from its reduced state Mn^{2+} to an oxidized one (Mn^{3+} or Mn^{4+}) and precipitates as a solid manganese oxide. Manganese oxides are not only a reaction product but also a potent oxidizing agent, which means they can also promote the oxidation of other compounds. One of these compounds is Fe^{2+}, which can be oxidized to Fe^{3+} by Mn oxides, which in turn are reduced back to its original state Mn^{2+}. If we zoom out, the result is that manganese enters the filter as Mn^{2+} and leaves as Mn^{2+} as well, while undergoing a set of reactions that cancel each other out (a futile cycle). Out of the three types of problems (direct and indirect interaction and futile cycles), futile cycles are by far the least studied in filters.

Backwashing

The general working principle of sand filtration encompasses two steps: *i)* oxidation and precipitation of the reduced groundwater contaminants and *ii)* its subsequent entrapment within the filter bed. The oxidation of all compounds leaves solids behind, either as flocs (Fe), grain coating (Fe, Mn), or biomass (mainly NH_4^+, but also Fe and Mn). Among them, Fe^{3+} flocs are the most troublesome for sand filter operation. Fe^{3+} flocs accumulate in the pore space – the free space between sand grains through which water flows. The longer the operation runs, the more flocs accumulate. Eventually, the filter would clog completely, so before that happens sand filters are stopped and backwashed to remove most of the Fe^{3+} flocs. During backwashing, sand grains move across the three dimensions of the bed, which means that they never start two

consecutive operational cycles in the same position. This has crucial implications for microorganisms, which are exposed to different environments every time. Imagine, let's say, a grain that lays at the middle section of the filter, where ammonia is usually oxidized. The microbial community of the grain is exposed to ammonia, so ammonia-oxidizing bacteria can thrive. The filter is now backwashed, and the grain moves, let's say, downwards. There is no ammonia, so AOB will starve. What if it moved upwards, to the top? There is ammonia there, but lots of Fe^{3+} flocs and other inhibiting Fe-derived compounds as well. A steady state, which is the microbial *zen*, is never reached, and microorganisms are forced to constantly adapt. How do they do it? The eco-physiological tricks that microorganisms use to handle the dynamic conditions in sand filters must be truly exceptional, and as of today, we know close to nothing about them.

1.5.3. And now what?

We have seen that setting a proper environment to deliberately promote the growth of several types of microorganisms simultaneously is an arduous task. Microorganisms tend to compete for limited resources, but with a masterful command of environmental biotechnology, one may succeed. Sand filters bring the challenge one step further by adding chemical reactions and their products into the equation. However, they still work. Sand filters are robust and effective systems that have been producing drinking water for over 150 years. How does it happen? Can we improve them? And most importantly, what can we learn from sand filters? The complexity behind their seemingly simple working principles remains poorly understood, and I believe it holds the secrets not only for optimization but also for designing the next generation of efficient and sustainable groundwater-based drinking water production systems.

1.6. SCOPE OF THIS THESIS

Research aim

The overarching goal of this thesis is to gain knowledge to advance towards the design of high-flow, resource-efficient sand filters. To do so, we must be able to

understand the mechanisms that govern which reactions take place, in which order they occur, and how they affect each other, which will ultimately allow us to predict and control *i)* microbial community assembly and performance and *ii)* the interplay between chemical and biological reactions. Our working hypothesis is that the fate of these two phenomena is mainly dictated by *i)* the abundance and identity of the oxidizing agent, *ii)* direct and indirect interactions and futile cycles between removal processes and *iii)* backwashing.

In the first part of this thesis, we focused on gaining mechanistic understanding of how current sand filters work using laboratory, pilot, and full-scale. In the second one, we used this freshly acquired knowledge to design and test novel systems.

Outline

Chapter 2 is an opinion article where we evaluate the state-of-the-art of sand filtration, compiling the most recent advances on the field and highlighting which are the crucial bottlenecks that should be addressed by the scientific community. Specifically, we focus on the new insights and research gaps that we envision will lead to more efficient and sustainable designs.

The goal of Chapter 3 is to understand how the microbial community adapts to the dynamic conditions imposed by backwashing. To do so, we evaluate the distribution of iron, ammonia, and manganese removal mechanisms along the heights of full-scale sand filters from two drinking water treatment plants.

In Chapter 4 we systematically and quantitatively assess how Fe and its oxidation (by)products impact ammonia oxidation. We use laboratory-scale columns to isolate the effect of the compounds generally considered to inhibit ammonia oxidizing bacteria and combine them with full-scale observations and a model.

Chapter 5 covers the role of the oxidizing agent. We switched oxygen for nitrate, moving away from conventional aerobic sand filtration to an anaerobic process. Iron does not react chemically with nitrate, which leaves biological iron and nitrate co-removal as the only iron oxidation mechanism in the filter.

In Chapter 6 we test whether biological methane oxidation is feasible in full-scale sand filters, and evaluate how its presence affects the microbial community structure and the oxidation pathways for iron, ammonia, and manganese removal.

This book just includes part of the findings of the project. Part of the findings are in the publications of my colleague and friend Simon Müller. Together, we worked on several other projects, like the exclusive biological/absorptive iron removal [31].

To wrap up, Chapter 7 includes first a compilation and integration of the key scientific findings of the thesis and then a technical summary of their industrial relevance and applicability.

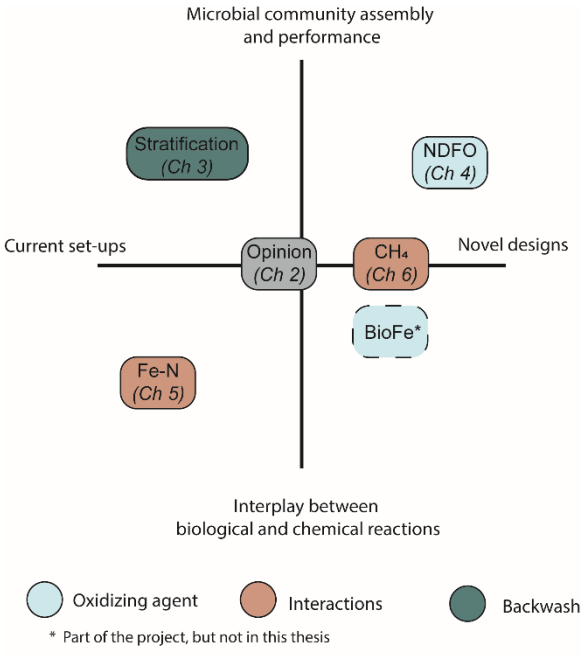

Figure 10. Distribution of the focus of chapters between understanding microbial community assembly and the interplay between biological and chemical reactions across current and novel sand filtration designs.

REFERENCES

1. Mora, C., Tittensor, D. P., Adl, S., Simpson, A. G. B. & Worm, B. How many species are there on earth and in the ocean? *PLoS Biol*. **9**, 1–8 (2011).

2. Louca, S., Mazel, F., Doebeli, M. & Parfrey, L. W. A census-based estimate of earth's bacterial and archaeal diversity. *PLoS Biol*. **17**, e3000106 (2019).

3. Locey, K. J. & Lennon, J. T. Scaling laws predict global microbial diversity. *Proc. Natl. Acad. Sci. U. S. A.* **113**, 5970–5975 (2016).

4. Zhang, Z., Wang, J., Wang, J., Wang, J. & Li, Y. Estimate of the sequenced proportion of the global prokaryotic genome. *Microbiome* **8**, 1–9 (2020).

5. Suzuki, T. *et al*. Two types of morphologically distinct fibers comprising gallionella ferruginea twisted stalks. *Microbes Environ*. **27**, 338–341 (2012).

6. McGovern, P. E. *et al*. Fermented beverages of pre- and proto-historic China. *Proc. Natl. Acad. Sci. U. S. A.* **101**, 17593–17598 (2004).

7. Tidswell, E. The Cost of Microbial Control. 3–5 (2017).

8. Gest, H. The discovery of microorganisms by Robert Hooke and Antoni Van Leeuwenhoek, fellows of the Royal Society. *Notes Rec. R. Soc. Lond*. **58**, 187–201 (2004).

9. Paneth, N. & Fine, P. The art of medicine: The singular science of John Snow. *The Lancet* vol. 381 1267–1268 (2013).

10. Lippi, D. & Gotuzzo, E. The greatest steps towards the discovery of Vibrio cholerae. *Clin. Microbiol. Infect*. **20**, 191–195 (2014).

11. Vergun, D. Medical Improvements Saved Many Lives During World War II. https://www.defense.gov/News/Feature-Stories/story/Article/2115192/medical-improvements-saved-many-lives-during-world-war-ii/ (2020).

12. Cragg, S. M. *et al*. Lignocellulose degradation mechanisms across the Tree of Life. *Curr. Opin. Chem. Biol*. **29**, 108–119 (2015).

13. Urbanek, A. K., Rymowicz, W. & Mirończuk, A. M. Degradation of plastics and plastic-degrading bacteria in cold marine habitats. *Appl. Microbiol. Biotechnol*. **102**, 7669–7678 (2018).

14. Rahman, K. S. M., Thahira-Rahman, J., Lakshmanaperumalsamy, P. & Banat, I. M. Towards efficient crude oil degradation by a mixed bacterial consortium. *Bioresour. Technol*. **85**, 257–

261 (2002).

15. Hamilton, J. H. *et al.* Synthesis of the new element with Z=117. in *Journal of Physics: Conference Series* vol. 312 142502 (American Physical Society, 2011).

16. Mooij, P. R. *On the use of selective environments in microalgal cultivation*. (2016).

17. Johnson, K. *PHA production in aerobic mixed microbial cultures*. (2010).

18. Smolders, G. J. F., van der Meij, J., van Loosdrecht, M. C. M. & Heijnen, J. J. Model of the anaerobic metabolism of the biological phosphorus removal process: Stoichiometry and pH influence. *Biotechnol. Bioeng.* **43**, 461–470 (1994).

19. Skraem, D. *Sustainable Groundwater Management in Lucknow City*. https://iwa-network.org/sustainable-groundwater-management-in-denmark/ (2021).

20. Rijksoverheid. Drinking water | Environmental Health Atlas. https://www.atlasleefomgeving.nl/en/node/1071.

21. de Vet, W., Van Genuchten, C. C. A., Van Loosdrecht, M. C. M. & Van Dijk, J. C. Water quality and treatment of river bank filtrate. *Drink. Water Eng. Sci.* **3**, 79–90 (2010).

22. Santamaria, A. B. & Sulsky, S. I. Risk assessment of an essential element: manganese. *J. Toxicol. Environ. Health. A* **73**, 128–155 (2010).

23. WHO. Guidelines for Drinking-Water Quality. (2006) doi:10.1248/jhs1956.35.307.

24. Van Beek, C. G. E. M. *et al.* Homogeneous, heterogeneous and biological oxidation of iron(II) in rapid sand filtration. *J. Water Supply Res. Technol. - AQUA* **61**, 1–13 (2012).

25. Chan, C. S., Fakra, S. C., Edwards, D. C., Emerson, D. & Banfield, J. F. Iron oxyhydroxide mineralization on microbial extracellular polysaccharides. *Geochim. Cosmochim. Acta* **73**, 3807–3818 (2009).

26. Tekerlekopoulou, A. G., Pavlou, S. & Vayenas, D. V. Removal of ammonium, iron and manganese from potable water in biofiltration units: A review. *J. Chem. Technol. Biotechnol.* **88**, 751–773 (2013).

27. Geszvain, K., McCarthy, J. K. & Tebo, B. M. Elimination of manganese(II, III) oxidation in pseudomonas putida GB-1 by a double knockout of two putative multicopper oxidase genes. *Appl. Environ. Microbiol.* **79**, 357–366 (2013).

28. Ma, B., LaPara, T. M., Kim, T. & Hozalski, R. M. Multi-scale Investigation of Ammonia-Oxidizing Microorganisms in Biofilters Used for Drinking Water Treatment. *Environ. Sci. Technol.* **57**, 3833–3842 (2023).

29. Soler-Jofra, A., Pérez, J. & van Loosdrecht, M. C. M. Hydroxylamine and the nitrogen cycle: A review. *Water Research* vol. 190 116723 (2021).

30. Corbera-Rubio, F. *et al*. Biological methane removal in groundwater trickling biofiltration for emissions reduction. *Manuscr. Submitt. Publ*. (2024).

31. Müller, S. *et al*. Shifting to biology promotes highly efficient iron removal in groundwater filters. *bioRxiv* 2024.02.14.580244 (2024) doi:10.1101/2024.02.14.580244.

32. Corbera-Rubio, F., Goedhart, R., Laureni, M., van Loosdrecht, M. C. M. & van Halem, D. A Biotechnological Perspective on Sand Filtration for Drinking Water Production. *Manuscr. Submitt. Publ*. (2024).

33. Van Beek, C. G. E. M. *et al*. Contributions of homogeneous, heterogeneous and biological iron(II) oxidation in aeration and rapid sand filtration (RSF) in field sites. *J. Water Supply Res. Technol. - AQUA* **65**, 195–207 (2016).

34. Swanner, E. D. *et al*. Modulation of oxygen production in Archaean oceans by episodes of Fe(II) toxicity. *Nat. Geosci.* **8**, 126–130 (2015).

35. Tong, M. *et al*. Fe(II) oxygenation inhibits bacterial Mn(II) oxidation by P. putida MnB1 in groundwater under O2-perturbed conditions. *J. Hazard. Mater.* **435**, 128972 (2022).

36. Gunnars, A., Blomqvist, S., Johansson, P. & Andersson, C. Formation of Fe(III) oxyhydroxide colloids in freshwater and brackish seawater, with incorporation of phosphate and calcium. *Geochim. Cosmochim. Acta* **66**, 745–758 (2002).

37. Saeed, H. *et al*. Regulation of phosphorus bioavailability by iron nanoparticles in a monomictic lake. *Sci. Reports 2018 81* **8**, 1–14 (2018).

38. de Vet, W., Van Loosdrecht, M. C. M. & Rietveld, L. C. Phosphorus limitation in nitrifying groundwater filters. *Water Res.* **46**, 1061–1069 (2012).

39. May, R. M. Tropical Arthropod Species , More or Less ? Downsizing the Hydrated. *Science (80-.).* **329**, 41–42 (2010).

40. Lane, N. The unseen world: reflections on Leeuwenhoek (1677) 'Concerning little animals'. *Philos. Trans. R. Soc. B Biol. Sci.* **370**, 20140344 (2015).

41. Tan, S. Y. & Tatsumura, Y. Alexander Fleming (1881–1955): Discoverer of penicillin. *Singapore Med. J.* **56**, 366 (2015).

The truth – that love is the ultimate and the highest goal to which man can aspire…the salvation of man is through love and in love

Viktor E. Frankl, in *Man's search for meaning*

A BIOTECHNOLOGICAL PERSPECTIVE ON SAND FILTRATION FOR DRINKING WATER PRODUCTION

2

ABSTRACT

Gravity-driven sand filters are the dominant groundwater treatment technology for drinking water production. In the past, physicochemical reactions were often assumed to play the main role in the removal of contaminants, but recent breakthroughs showcase the vital role of microorganisms. In this Current Opinion, we thoroughly assess the current understanding of biology in sand filters and explore the potential benefits of shifting towards designs aimed at promoting biological reactions. We highlight the main bottlenecks and propose key areas to be explored towards the next generation of sustainable, resource-efficient groundwater biofilters.

HIGHLIGHTS

- Recent microbial insights shed light into groundwater filters *black box*
- Promoting biological iron oxidation significantly improves process performance
- Contribution of biological manganese and arsenic oxidation is likely underestimated
- Nitrification problems often arise from (by)products of iron and manganese oxidation
- Biological processes are key towards resource-efficient groundwater treatment

Published as:

Corbera-Rubio, F., Goedhart, R., Laureni, M., van Loosdrecht, M. C. M. & van Halem, D. (in press) A Biotechnological Perspective on Sand Filtration for Drinking Water Production. *Current Opinion in Biotechnology* (2024).

2.1. THE COMPLEXITY BEHIND SEEMINGLY SIMPLE GROUNDWATER BIOFILTERS

The sequence of aeration followed by gravity-driven filtration[1] has been the dominant groundwater treatment technology for centuries. Relatively simple designs and operational conditions yield reliable and robust systems for the removal of the main anaerobic groundwater contaminants, namely iron, ammonia, manganese and arsenic. However, behind its seemingly trivial working principles, sand filters harbour a high degree of complexity. The introduction of oxygen to saturation levels into anaerobic groundwater onsets a sophisticated network of simultaneous, interconnected and uncontrolled physicochemical and biological reactions (Figure 1). Additionally, the continuous accumulation of iron and manganese deposits within the sand filter forces practitioners to backwash the sand filter, perturbating its steady-state and creating a dynamic system. This inherent complexity makes both research and process optimization challenging. As a result, sand filters have traditionally been considered as a *black box*.

During the last decade, the implementation of new molecular tools, in particular metagenomics [1] and metaproteomics [2], substantially increased our understanding of sand filters. The central role of microorganisms has been recognized, and sand filters are now commonly referred to as *biofilters*. However, research is often limited by the difficulty to access the biofilm, intricately entangled with metal oxides. This makes not only the extraction of DNA and proteins challenging but also prevents the application of sensitive techniques such as flow cytometry or isotope labelling which find application in sand filters treating metal-free surface waters [3,4]. Despite these hurdles, attention towards groundwater biofilters continues to increase, particularly on the biological front. Leveraging this growing momentum, we challenge the field

[1] Groundwater filtration is most often performed with granular media, known as granular filtration. Several types of matrices such as quartz sand, anthracite or pumice are used in granular filtration. Among them, sand quartz is the one used in the vast majority of cases in full-scale filters, thus the most commonly used in research. As a result, *sand filtration* is the term commonly used to refer to all types of granular filtration. For consistency, we use the term *(sand) filtration* throughout this opinion article, but refer to all types of granular filtration.

by discussing whether a more ecologically-informed control over the microbiome is the key to designing, operating and controlling the next generation of groundwater biofilters. To do so, we highlight the current bottlenecks, present the latest innovations in this and adjacent fields and, most importantly, critically assess whether ongoing research aligns with the practical needs for drinking water production. We identify nine key focus areas and research questions (RQ).

This *Current Opinion* focuses on the four main ionic groundwater contaminants, namely iron, ammonia, manganese and arsenic. We excluded gaseous compounds commonly present in groundwater, such as hydrogen sulfide and methane, as they are currently most often stripped during pre-aeration. However, methane oxidizing bacteria are commonly found in sand filters [5], and the interest in biological methane removal to decrease the greenhouse emissions from drinking water production is increasing [5]. Future opinion papers on sand filtration may consider including methane as the fifth main groundwater contaminant.

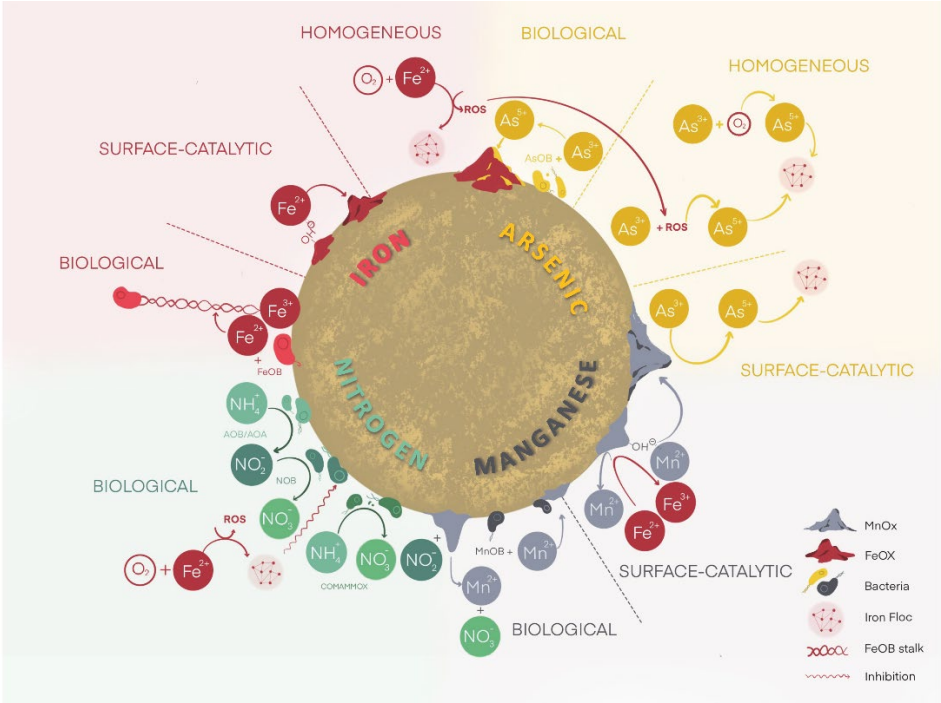

Figure 1. Biological and physicochemical reactions involved in the transformation of the main groundwater contaminants, namely iron, arsenic, manganese and nitrogen. Oxidation processes are divided in chemical (homogeneous, surface-catalytic) and biological. Homogeneous reactions take place when both reactants are in the same phase, in this case the water phase, and is especially relevant for iron (with O_2) and As (with ROS that are generated from iron oxidation and, to a lesser extent, with O_2). Surface-catalytic reactions take place when the reactants are in two different phases, in this case water and solid. Surface-catalytic oxidation is relevant for iron (catalyzed by Fe oxides), manganese (commonly known as autocatalytic, by Mn oxides) and arsenic (by Mn oxides). Biological reactions are driven by microorganisms. Nitrogen transformations are exclusively biological, either as the canonical two-step nitrification carried out by AOB and NOB, or as the one-step comammox. The (by)products of all these simultaneous reactions interact with each other, and these interactions play a critical role in determining the fate of each contaminant. Our current understanding is that ROS produced during homogeneous iron oxidation oxidize As(III), while iron flocs and iron oxides adsorb As(V) and As(III). Iron flocs inhibit nitrifying bacteria, and Fe(II) oxidizes to Fe(III) while Mn oxides are reduced. Mn oxides are also reduced by nitrite, which is oxidized to nitrate. All the depicted reactions are feasible and proved to occur in sand filters. The inhibition of nitrifying bacteria by iron flocs and the chemical oxidation of nitrite couple of reduction of Mn oxides are the only exceptions still awaiting experimental confirmation in full-scale filters.. Abbreviations: MnOx, manganese oxides; FeOx, iron oxides; ROS, reactive oxygen species; AOB, ammonia-oxidizing bacteria; AOA, ammonia-oxidizing archaea; comammox, complete ammonia-oxidizing (bacteria);NOB, nitrite-oxidizing bacteria; FeOB, iron-oxidizing bacteria, MnOB, manganese-oxidizing bacteria; AsOB, arsenic oxidizing bacteria.

2.2. IRON: HARNESSING THE WEALTH OF INFORMATION ON IRON-OXIDIZING BACTERIA

Iron is always the first dissolved contaminant to be removed, regardless of process conditions. Three different mechanisms contribute to iron removal [6] (Figure 1, red section). Homogeneous (flocculent) oxidation is the chemical reaction between dissolved iron (Fe(II)) and dissolved oxygen resulting in the production of iron flocs (Fe(III)). Surface-catalytic (adsorptive) oxidation is the two-step chemical reaction where dissolved iron binds to an iron oxide on the surface of a filter-medium grain and is subsequently oxidized to Fe(III) [6]. The product is a compact iron oxide that becomes part of the grain coating. Last, Fe(II) can be oxidized by iron-oxidizing bacteria (FeOB), yielding relatively compact iron oxide solids as well [7]. Biofilters were, and still are, designed to promote flocculent iron oxidation, a fast, simple and effective method. However, iron flocs are fluffy, loosely bound structures with high water content, making them prone to clog biofilters. Among others, iron floc accumulation forces frequent backwashing [6] and delays the removal of other groundwater contaminants [2].

Muller et al. [7] designed and operated a groundwater biofilter capable of exclusive adsorptive/biological iron removal at low pH and oxygen concentrations. The absence of iron flocs allowed for a three-fold higher flowrate, longer runtimes and a 75% reduction in energy/water losses, showcasing the benefits of the adsorptive/biological route over conventional flocculent iron oxidation. Interestingly, the morphology of filter-medium grain coating was different to those of conventional biofiltration systems, representing a novel FeOB biosignature. Another recent example of biosignature are the as-of-yet unidentified peaks detected by gas chromatography – mass spectrometry which result from low-molecular-weight molecules unique to all known iron-oxidizing bacteria [8]. These findings allow for a simple, fast identification of biological iron removal even in the absence of detectable organisms and potentially beyond those forming the classic twisted stalks, hollow sheaths or dreads [9,10].

Fast, simple methods to identify and characterize FeOB are essential to promote and control biological iron oxidation. Unfortunately, FeOB have

historically been particularly challenging to identify. Yet, the recent rapid advance of the field has made the task considerably easier. First, information about FeOB phylogenetic distribution has always been scarce, hindering their taxonomic identification. The pangenomic analysis of the *Zetaproteobacteria* class [9] and *Gallionelllaceae* family [11], encompassing most known iron oxidizers, has resolved the FeOB phylogeny. Second, iron oxidation genes had only been identified as *candidates* in neutrophilic organisms. Moreover, the available information was limited to iron oxidases, while the other genes involved in the pathway were unknown. As a result, FeOB identification via marker genes has also been challenging. Now, the iron oxidation function of cytochrome Cyc2, the most commonly found iron oxidase, has been experimentally validated [12]. Its presence, along with other iron oxidases and additional genes of the iron oxidation pathway, has been detected at metagenomic [13,14], metaproteomic [2] and metatranscriptomic [15,16] level in both natural and engineered settings. Moreover, candidate genes for other functions in the iron metabolism, such as electron transfer [17] and twisted stalk formation [18], have been recently proposed, and iron genome mining is now possible thanks to FeGenie, an annotation tool for iron-related genes in (meta)genomes [19]. Leveraging exclusive adsorptive/biological iron oxidation is crucial to bring groundwater biofiltration to the next level, and the recent blossom of information about FeOB is an essential first step. Ahead of us lies the next challenge:

> ***RQ1***. *How do we translate the newly generated knowledge on biological iron oxidation into guidelines to design the next generation of groundwater biofilters?*

2.3. AMMONIA: BRIDGING THE GAP BETWEEN ACADEMIA AND PRACTICE

The nitrogen cycle is pivotal in bioremediation, *e.g.*, during wastewater treatment, and as such widely studied. However, the unique conditions in groundwater treatment for drinking water production, *i.e.*, low temperatures and oligotrophy, make direct translation of this vast knowledge challenging. The drinking water biofiltration field focused on unravelling the taxonomy of the core

nitrification microbiome. While in constant evolution [20], the current understanding is that ammonia oxidation is carried out primarily by ammonia-oxidizing and comammox bacteria [21], with minor contributions from ammonia-oxidizing archaea [22] (Figure 1, green section) . Significant efforts are also being devoted to resolving the effect of biofilters operational parameters on microbial community composition and nitrification capacity, such as reported for surface water in terms of backwashing and filter-medium type [23], temperature [24], and flow configuration [25]. Yet, the newly generated insights did not translate into new filter designs or performance improvements.

Central challenges in groundwater biofiltration remain the fact that nitrification often onsets only after full iron removal, and that not all influent ammonium is removed, or nitrification stops at nitrite. Usually tightly connected, these problems have been tackled only recently and nitrification remains unpredictable. Several studies demonstrate that sorption of essential nutrients onto the surface of iron oxides is a common cause for incomplete nitrification [26–28]. Wagner et al. [26] proved this principle for copper, and achieved a significant increase in nitrification via external copper dosing. The same strategy has also been successfully applied in a full-scale biofilter treating anoxic groundwater [27], and the work of Zheng and colleagues [28] proved that also phosphate can become limiting. In some cases, nitrification problems are associated to specific compounds, although the inhibition mechanism is unknown. For example, iron flocs seem to delay the start of nitrification until Fe^{2+} is completely depleted [29]. In other cases, operation fails but the root cause cannot be traced back [30]. These are common observations in practice, yet they receive little to no attention in the scientific literature. To bridge the gap between the focuses of academia and the needs of practice, we identified three crucial areas and research questions that need to be addressed.

RQ2. Reactive oxygen species formed during iron oxidation are known to inhibit ammonia oxidation at nanomolar concentrations [31], dissolved iron has been reported to cause oxidative stress [32] and manganese oxides alter nitrification [33]. *What is the direct effect of iron and manganese oxidation (by)products on ammonia-oxidizing organisms, and to which extent does this occur in biofilters?*

RQ3. Nitrite, free nitrous acid and hydroxylamine potentially accumulate during (de)nitrification. These intermediates hamper ammonia oxidation directly [34], and potentially also indirectly by reducing the already formed Fe or Mn oxides and generating products that subsequently interact with ammonia oxidizers. *What is the impact of reactive intermediate nitrogen species on key biofilter processes, and what is their implication for process stability?*

RQ4. The effect of operational conditions on biofilter microbiome composition is being explored, yet what remains largely unknown is how taxonomic changes reflect in biofilter performance. *Does taxonomy matter, and is it a good indicator for process performance?*

2.4. MANGANESE: OPENING THE BLACK BOX

Manganese removal can be of chemical and biological origin (Figure 1, grey section). Surface-catalytic (autocatalytic) manganese oxidation is a chemical reaction in which dissolved manganese (Mn(II)) adsorbs onto manganese oxide coating on the surface of filter-medium grains. Once adsorbed, manganese is subsequently oxidized to Mn(III) or Mn(IV) and forms a compact oxide that is incorporated in the coating. Biological manganese oxidation is catalysed by manganese-oxidizing bacteria (MnOB), and results in compact manganese oxides as well. The morphology and properties of biological and chemical oxides differ (32, and references therein), yet both harbour the ability to catalyse surface-catalytic manganese oxidation.

In newly established groundwater biofilters, manganese removal is always the last to meet water quality standards. Consequently, substantial efforts have been put into shortening filters start-up times. The current understanding is that MnOB initiate manganese oxidation, and chemical reactions dominate in mature filters [36]. A plethora of successful strategies have been developed based on this principle, focusing either on promoting the growth of MnOB [28] or on the addition of mature sand coated with manganese oxides [37]. The biggest challenge for Mn removal remains ensuring long-term stable operation [38]. The complexity

stems from the fact that manganese removal takes place in the downstream sections of a biofilter, where filter media is exposed to both residual groundwater contaminants and their (by)products from upstream reactions. High iron [39] loads have been reported to negatively influence manganese removal. Nitrogen species are also expected to impact Mn removal, as observed for ammonia [40] and nitrite [41] in surface water filters. Additionally, oxygen depletion in the low sections of biofilters treating groundwater with high contaminant concentrations may occur. Under anoxic conditions, manganese oxides become the strongest oxidant in the biofilter environment, and catalyse the oxidation of Fe(II), nitrite and As(III). Even small fluctuations in the performance of the upper filter sections may induce the downstream reduction of manganese oxides back to dissolved Mn^{2+} [42], and ultimately manganese release in the effluent. The emerging oxidation-reduction cycles cannot be fully explained with currently available snapshot-based studies. In the pursuit of long-term, stable manganese removal, two main questions are identified.

RQ5. *Which groundwater components or reaction (by)products impact manganese (a)biotic removal the most?*

RQ6. *What are the underlying mechanisms controlling manganese oxidation-reduction cycles in biofilters, and can they be prevented?*

Recent studies challenge also the rationale of MnOB role being limited to the filter start-up phase [39]. The lack of consensus originates from the inherent challenge of identifying the organisms responsible for manganese oxidation. The ability to oxidize manganese is taxonomically more widespread than iron and ammonium oxidation, requiring sequencing at strain level resolution, and is not necessarily associated with energy conservation [43]. Several enzymes have been proven to catalyse manganese oxidation, with multicopper oxidases being the most common. However, the known substrate promiscuity of multicopper oxidases hinders their use as marker gene to univocally infer manganese oxidation potential in complex communities [44]. Elucidating the *in-situ* contribution of biology to manganese removal during groundwater filtration remains an extremely challenging task. Deepening our understanding of manganese oxidizing organisms, and developing fast analytical methods for their rapid identification is crucial to control and optimize manganese removal in biofilters. The central open fronts are summarized in one question.

RQ7. *To what extent is Mn biologically removed in biofilters, and what are the responsible organisms?*

2.5. ARSENIC: PROMOTING REMOVAL THROUGH BIOLOGICAL OXIDATION

Arsenic removal in biofilters primarily relies on adsorption to iron oxides. In anaerobic groundwater, the oxyanion arsenite (As(III), H_3AsO_3) is the dominant arsenic species. However, iron oxides have a higher adsorption affinity for its oxidized, negatively charged counterpart arsenate (As(V), $H_2AsO_4^-$, $HAsO_4^{2-}$) [45]. This emphasizes the importance of As(III) oxidation to As(V) to ensure efficient removal. Since homogeneous As(III) oxidation with dissolved oxygen is slow (days), surface-catalytic As(III) oxidation by Mn oxides [46] and homogeneous oxidation by reactive oxygen species [47] have long been claimed to be the dominant As(III)-oxidizing mechanisms (Figure 1, yellow section). Yet, several researchers have indicated that microorganisms also play a role in arsenic oxidation [48–51], achieving a higher oxidation rate than abiotic process alone [52]. However, experimental proof in sand filters is missing.

Biological As(III) oxidation is carried out by chemolithoautotrophic organisms for energy conservation as well as by heterotrophs as detoxification strategy, using oxygen or nitrate as electron acceptor [53]. Arsenic-oxidizing bacteria (AsOB) have been widely detected in aquifers [50] and lab-scale biofilters [48,49] either by PCR-based methods targeting As(III) oxidase *aio*, or with metagenomic-based approaches [51,54]. However, both methods share a major limitation that compromise the reliable detection of AsOB. The low concentration of AsOB in biofilters resulting from micromolar arsenic concentrations in groundwater (2-3 orders of magnitude below ammonia), and the suboptimal DNA extraction yields from metal-coated sand grains make AsOB identification challenging, often practically impossible. Ultimately, to develop filter designs targeting also arsenic removal, a paramount requirement in areas where arsenic exposure via drinking water remains a major health risk, we identified two areas and questions of outmost interest.

RQ8. The lack of established methods to detect AsOB and differentiate between biological and chemical As oxidation processes prevents further understanding of the dominant As oxidation mechanisms in biofilters, let alone identifying which one should be promoted to improve filter performance. *How could biological As oxidation and chemical oxidation with Mn oxides be differentiated?*

RQ9. While As uptake by abiotically-formed Fe oxides is a well-known process, the as-of-yet answered question is: *what is the uptake of arsenic during biological Fe oxidation?*

2.6. PERSPECTIVE

Groundwater biofiltration research is rapidly growing. Complex and multidisciplinary challenges are being solved, and our vision of biofilters is evolving from *black* towards *white box*. Besides the long established knowledge on the underlying physicochemical processes, the prominent role of the biofilter microbiome in process robustness is emerging and sets the foundations for new design opportunities. Promoting adsorptive/biological iron removal seems to be a superior strategy compared to the decades-old conventional homogeneous iron oxidation. By preventing loose iron flocs formation, adsorptive/biological iron removal extends filter runtime, and prevents the potential inhibition of the downstream ammonia and manganese removal. The importance of iron oxidation (by)products on ammonia-oxidizing organisms is also being recognized, and more research is needed to understand the causes of often reported nitrification failures. The discharge of nitrification intermediates, such as nitrite, impacts water quality both directly and indirectly, as it may promote the largely-overlooked reduction and re-dissolution of previously precipitated manganese. The contribution of biotic reactions to manganese removal remain to date unclear, and we encourage the scientific community to concentrate efforts to gain a deeper understanding of the differences in filter performance and (by)products of biological and chemical manganese oxidation. In contrast, the paradigm is changing for arsenic, and

evidence is growing for biological oxidation to be its dominant removal mechanism. Efforts should focus on confirming the biotic nature of arsenic removal, and on optimizing filter design to promote the growth of arsenic-oxidizing bacteria. Within this framework, metagenomic and metaproteomic approaches provide unprecedented possibilities to resolve the microbial metabolic network in biofilters. Research should target the optimization of protocols to extract DNA and proteins from a biomass enmeshed with solid precipitates. The rapid progress in understanding the controls of biofilters microbiomes undoubtedly provides a new operational dimension to design and operate the next generation of groundwater biofilters. However, scientific insights into removal mechanisms remain detached from operational practice, hindering the implementation of the new understandings to improve filters performance. Combining the efforts of microbiologists, biotechnologists and bioprocess engineers with applied research is now critical to bridge the gap between individual removal mechanisms and full-scale sand filters complexity.

REFERENCES

1. Poghosyan, L., Koch, H., Frank, J., van Kessel, M. A. H. J., Cremers, G., van Alen, T., Jetten, M. S. M., Op den Camp, H. J. M. & Lücker, S. Metagenomic profiling of ammonia- and methane-oxidizing microorganisms in two sequential rapid sand filters. *Water Res.* **185**, 116288 (2020).

2. Corbera-Rubio, F., Laureni, M., Koudijs, N., Müller, S., van Alen, T., Schoonenberg, F., Lücker, S., Pabst, M., van Loosdrecht, M. C. M. & van Halem, D. Meta-omics profiling of full-scale groundwater rapid sand filters explains stratification of iron, ammonium and manganese removals. *Water Res.* **233**, 119805 (2023).

3. Haig, S. J., Schirmer, M., D'Amore, R., Gibbs, J., Davies, R. L., Collins, G. & Quince, C. Stable-isotope probing and metagenomics reveal predation by protozoa drives E. Coli removal in slow sand filters. *ISME J.* **9**, 797–808 (2015).

4. Vignola, M., Werner, D., Hammes, F., King, L. C. & Davenport, R. J. Flow-cytometric quantification of microbial cells on sand from water biofilters. *Water Res.* **143**, 66–76 (2018).

5. Corbera-Rubio, F., Boersma, A. S., de Vet, W. W. J. M., Pabst, M., van der Wielen, P. W. J. J., Kessel, M. A. H. J. Van, van Loosdrecht, M. C. M., van Halem, D., Lücker, S. & Laureni, M. Biological methane removal in groundwater trickling biofiltration for emissions reduction. *Manuscr. Submitt. Publ.* (2024).

6. Van Beek, C. G. E. M., Hiemstra, T., Hofs, B., Nederlof, M. M., Van Paassen, J. A. M. & Reijnen, G. K. Homogeneous, heterogeneous and biological oxidation of iron(II) in rapid sand filtration. *J. Water Supply Res. Technol. - AQUA* **61**, 1–13 (2012).

7. Müller, S., Corbera-Rubio, F., Schoonenberg-Kegel, F., Laureni, M., Van Loosdrecht, M. C. M., Van Halem, D., Loosdrecht, M. C. M. van & Halem, D. van. Shifting to biology promotes highly efficient iron removal in groundwater filters. *bioRxiv* 2024.02.14.580244 (2024).

8. Floyd, M. A. M., Williams, A. J., Grubisic, A. & Emerson, D. Metabolic Processes Preserved as Biosignatures in Iron-Oxidizing Microorganisms: Implications for Biosignature Detection on Mars. *Astrobiology* **19**, 40–52 (2019).

9. McAllister, S. M., Moore, R. M., Gartman, A., Luther, G. W., Emerson, D. & Chan, C. S. The Fe(II)-oxidizing Zetaproteobacteria: historical, ecological and genomic

perspectives. *FEMS Microbiol. Ecol.* **95**, (2019).

10. Gülay, A., Çekiç, Y., Musovic, S., Albrechtsen, H. J. & Smets, B. F. Diversity of Iron Oxidizers in Groundwater-Fed Rapid Sand Filters: Evidence of Fe(II)-Dependent Growth by Curvibacter and Undibacterium spp. *Front. Microbiol.* **9**, 2808 (2018).

11. Hoover, R. L., Keffer, J. L., Polson, S. W. & Chan, C. S. Gallionellaceae pangenomic analysis reveals insight into phylogeny, metabolic flexibility, and iron oxidation mechanisms. *bioRxiv* 2023.01.26.525709 (2023).

12. Keffer, J. L., McAllister, S. M., Garber, A. I., Hallahan, B. J., Sutherland, M. C., Rozovsky, S. & Chan, C. S. Iron oxidation by a fused cytochrome-porin common to diverse iron-oxidizing bacteria. *MBio* **12**, (2021).

13. Hribovšek, P., Denny, E. O., Dahle, H., Mall, A., Viflot, T. Ø., Boonnawa, C., Reeves, E. P., Steen, I. H. & Stokke, R. Novel hydrogen- and iron-oxidizing sheath-producing Zetaproteobacteria thrive at the Fåvne deep-sea hydrothermal vent field. *bioRxiv* **0**, 2023.06.20.545787 (2023).

14. Corbera-Rubio, F., Stouten, G. R., Bruins, J., Dost, S. F., Merkel, A. Y., Müller, S., van Loosdrecht, M. C. M., van Halem, D. & Laureni, M. "Candidatus Siderophilus nitratireducens": a putative nap-dependent nitrate-reducing iron oxidizer within the new order Siderophiliales. *ISME Commun.* (2024).

15. Zhou, N., Keffler, J. L., Polson, S. W. & Chan, C. S. Unraveling Fe (II) -Oxidizing Mechanisms in a Facultative Fe (II). **88**, 1–16 (2022).

16. Zhou, N., Kupper, R. J., Catalano, J. G., Thompson, A. & Chan, C. S. Biological Oxidation of Fe(II)-Bearing Smectite by Microaerophilic Iron Oxidizer Sideroxydans lithotrophicus Using Dual Mto and Cyc2 Iron Oxidation Pathways. *Environ. Sci. Technol.* **56**, 17443–17453 (2022).

17. Ullrich, S. R., Fuchs, H. & Schlömann, M. Shedding light on the electron transfer chain of a moderately acidophilic iron oxidizer: Characterization of recombinant HiPIP-41, CytC-18 and CytC-78 derived from Ferrovum sp. PN-J47-F6. *Res. Microbiol.* 104088 (2023).

18. Koeksoy, E., Bezuidt, O. M., Bayer, T., Chan, C. S. & Emerson, D. Zetaproteobacteria Pan-Genome Reveals Candidate Gene Cluster for Twisted Stalk Biosynthesis and Export. *Front. Microbiol.* **12**, 1–14 (2021).

19. Garber, A. I., Nealson, K. H.,

Okamoto, A., McAllister, S. M., Chan, C. S., Barco, R. A. & Merino, N. FeGenie: A Comprehensive Tool for the Identification of Iron Genes and Iron Gene Neighborhoods in Genome and Metagenome Assemblies. *Front. Microbiol.* **11**, 37 (2020).

20. Luo, X., Shen, T., Guan, C., Li, N. & Jiang, J. Ammonia-oxidizing microbes and biological ammonia removal in drinking water treatment. *Environ. Sci. Water Res. Technol.* **8**, 1152–1172 (2022).

21. Palomo, A., Jane Fowler, S., Gülay, A., Rasmussen, S., Sicheritz-Ponten, T. & Smets, B. F. Metagenomic analysis of rapid gravity sand filter microbial communities suggests novel physiology of Nitrospira spp. *ISME J.* **10**, 2569–2581 (2016).

22. Fowler, S. J., Palomo, A., Dechesne, A., Mines, P. D. & Smets, B. F. Comammox Nitrospira are abundant ammonia oxidizers in diverse groundwater-fed rapid sand filter communities. *Environ. Microbiol.* **20**, 1002–1015 (2018).

23. Ma, B., Lapara, T. M. & Hozalski, R. M. Microbiome of Drinking Water Biofilters is Influenced by Environmental Factors and Engineering Decisions but has Little Influence on the Microbiome of the Filtrate. *Environ. Sci. Technol.* **54**, 11526–11535 (2020).

24. Jantarakasem, C., Kasuga, I., Kurisu, F. & Furumai, H. Temperature-Dependent Ammonium Removal Capacity of Biological Activated Carbon Used in a Full-Scale Drinking Water Treatment Plant. *Environ. Sci. Technol.* **54**, 13257–13263 (2020).

25. Rui, M., Chen, H., Ye, Y., Deng, H. & Wang, H. Effect of Flow Configuration on Nitrifiers in Biological Activated Carbon Filters for Potable Water Production. *Environ. Sci. Technol.* **54**, 14646–14655 (2020).

26. Wagner, F. B., Diwan, V., Dechesne, A., Fowler, S. J., Smets, B. F. & Albrechtsen, H. J. Copper-Induced Stimulation of Nitrification in Biological Rapid Sand Filters for Drinking Water Production by Proliferation of Nitrosomonas spp. *Environ. Sci. Technol.* **53**, 12433–12441 (2019).

27. Koike, K., Smith, G. J., Yamamoto-Ikemoto, R., Lücker, S. & Matsuura, N. Distinct comammox Nitrospira catalyze ammonia oxidation in a full-scale groundwater treatment bioreactor under copper limited conditions. *Water Res.* **210**, 117986 (2022).

28. Zheng, J., Li, D., Zeng, H., Yang, S., Zhu, Y. & Zhang, J. Rapid start-up of the biofilter for simultaneous manganese and

ammonia removal at low temperature: Effects of phosphate and copper. *J. Clean. Prod.* **430**, 139721 (2023).

29. Corbera-Rubio, F., Kruisdijk, E., Malheiro, S., Leblond, M., Verschoor, L., van Loosdrecht, M. C. M., Laureni, M. & van Halem, D. A difficult coexistence: resolving the iron-induced nitrification delay in groundwater filters. *Water Res.* 121923 (2024).

30. de Vet, W., Rietveld, L. C. & Van Loosdrecht, M. C. M. Influence of iron on nitrification in full-scale drinking water trickling filters. *J. Water Supply Res. Technol. - AQUA* **58.4**, 247–256 (2009).

31. Wang, H., Li, P., Liu, X., Zhang, J., Stein, L. Y. & Gu, J. D. An overlooked influence of reactive oxygen species on ammonia-oxidizing microbial communities in redox-fluctuating aquifers. *Water Res.* **233**, 119734 (2023).

32. Shcolnick, S., Summerfield, T. C., Reytman, L., Sherman, L. A. & Keren, N. The mechanism of iron homeostasis in the Unicellular Cyanobacterium Synechocystis sp. PCC 6803 and Its relationship to oxidative stress. *Plant Physiol.* **150**, 2045–2056 (2009).

33. Xin, X., Jiang, X., Su, J., Yan, X., Ni, J., Faeflen, S. J., Huang, X. & Wright, A. L. Manganese oxide affects nitrification and ammonia oxidizers in subtropical and temperate acid forest soils. *Catena* **137**, 24–30 (2016).

34. Soler-Jofra, A., Pérez, J. & van Loosdrecht, M. C. M. Hydroxylamine and the nitrogen cycle: A review. *Water Research* vol. 190 116723 at https://doi.org/10.1016/j.watres.2020.116723 (2021).

35. Namgung, S., Chon, C. M. & Lee, G. Formation of diverse Mn oxides: a review of bio/geochemical processes of Mn oxidation. *Geosci. J.* **22**, 373–381 (2018).

36. Breda, I. L., Søborg, D. A., Ramsay, L. & Roslev, P. Manganese removal processes during start-up of inoculated and non-inoculated drinking water biofilters. *Water Qual. Res. J.* **54**, 47–56 (2019).

37. Yang, H., Bai, L., Yu, H., Shu, X., Tang, X., Du, X., Qu, F., Rong, H., Li, G. & Liang, H. Acceleration of sand filtration start-up for manganese-containing groundwater treatment: microbial-mediated autocatalytic oxidation of manganese oxides. *Environ. Sci. Water Res. Technol.* **9**, 2631–2642 (2023).

38. Haukelidsaeter, S. *et al.* Influence of filter age on Fe, Mn and NH4+ removal in dual media rapid sand filters used for drinking water production.

Water Res. **242**, 120184 (2023).

39. Zheng, J., Li, D., Zeng, H., Yang, S., Zhang, Z. & Zhang, J. Effect of Fe(II) on manganese removal in biofilters: Microbial community, formation of manganese oxide and related mechanisms. *J. Water Process Eng.* **56**, 104519 (2023).

40. Tian, X., Zhang, R., Huang, T. & Wen, G. The simultaneous removal of ammonium and manganese from surface water by MeOx: Side effect of ammonium presence on manganese removal. *J. Environ. Sci. (China)* **77**, 346–353 (2019).

41. Cheng, Q., Nengzi, L., Xu, D., Guo, J. & Yu, J. Influence of nitrite on the removal of Mn(II) using pilot-scale biofilters. *J. Water Reuse Desalin.* **7**, 264–271 (2017).

42. Le, A. Van, Muehe, E. M., Bone, S., Drabesch, S., Fischer, S. & Kappler, A. Field and Laboratory Evidence for Manganese Redox Cycling Controlling Iron and Arsenic Retention in Household Sand Filters. *ACS ES T Water* (2023).

43. Zhou, H. & Fu, C. Manganese-oxidizing microbes and biogenic manganese oxides: characterization, Mn(II) oxidation mechanism and environmental relevance. *Rev. Environ. Sci. Biotechnol.* **19**, 489–507 (2020).

44. Brouwers, G. J., Vijgenboom, E., Corstjens, P. L. A. M., De Vrind, J. P. M. & De Vrind-De Jong, E. W. Bacterial Mn2+ oxidizing systems and multicopper oxidases: An overview of mechanisms and functions. *Geomicrobiol. J.* **17**, 1–24 (2000).

45. Ahmad, A. & van Genuchten, C. M. Deep-dive into iron-based co-precipitation of arsenic: A review of mechanisms derived from synchrotron techniques and implications for groundwater treatment. *Water Res.* **249**, 120970 (2024).

46. Gude, J. C. J., Rietveld, L. C. & van Halem, D. As(III) oxidation by MnO2 during groundwater treatment. *Water Res.* **111**, 41–51 (2017).

47. Hug, S. J. & Leupin, O. Iron-catalyzed oxidation of Arsenic(III) by oxygen and by hydrogen peroxide: pH-dependent formation of oxidants in the Fenton reaction. *Environ. Sci. Technol.* **37**, 2734–2742 (2003).

48. Crognale, S., Casentini, B., Amalfitano, S., Fazi, S., Petruccioli, M. & Rossetti, S. Biological As(III) oxidation in biofilters by using native groundwater microorganisms. *Sci. Total Environ.* **651**, 93–102 (2019).

49. Gude, J. C. J., Rietveld, L. C. & van Halem, D. Biological As(III) oxidation in rapid sand filters. *J. Water Process Eng.* **21**, 107–115 (2018).

50. Diba, F., Hoque, M. N., Rahman, M. S., Haque, F., Rahman, K. M. J., Moniruzzaman, M., Khan, M., Hossain, M. A. & Sultana, M. Metagenomic and culture-dependent approaches unveil active microbial community and novel functional genes involved in arsenic mobilization and detoxification in groundwater. *BMC Microbiol.* **23**, 241 (2023).

51. Cavalca, L., Corsini, A., Zaccheo, P., Andreoni, V. & Muyzer, G. Microbial transformations of arsenic: Perspectives for biological removal of arsenic from water. *Future Microbiol.* **8**, 753–768 (2013).

52. Katsoyiannis, I. A., Zouboulis, A. I. & Jekel, M. Kinetics of Bacterial As(III) Oxidation and Subsequent As(V) Removal by Sorption onto Biogenic Manganese Oxides during Groundwater Treatment. *Ind. Eng. Chem. Res.* **43**, 486–493 (2004).

53. Hassan, Z., Sultana, M., Khan, S. I., Braster, M. & Röling, W. F. M. Ample Arsenite Bio-Oxidation Activity in Bangladesh Drinking Water Wells : A Bonanza for Bioremediation ? *Microorg. 2019, Vol. 7, Page 246*.

54. Andres, J. & Bertin, P. N. The microbial genomics of arsenic. *FEMS Microbiol. Rev.* **40**, 299–322 (2016).

Si nosaltres, com a catalanoparlants a Catalunya, no parlem català, qui el parlarà?

Which somehow translates to

If we, as Catalan speakers in Catalunya, do not speak Catalan, who will?

Òscar Andreu

META-OMICS PROFILING OF FULL-SCALE GROUNDWATER RAPID SAND FILTERS EXPLAINS STRATIFICATION OF IRON, AMMONIUM AND MANGANESE REMOVALS

3

ABSTRACT

Rapid sand filters are an established and widely applied technology for groundwater treatment. Yet, the underlying interwoven biological and physical-chemical reactions controlling the sequential removal of iron, ammonia and manganese remain poorly understood. To resolve the contribution and interactions between the individual reactions, we studied two full-scale drinking water treatment plant configurations, namely (*i*) one dual-media (anthracite and quartz sand) filter and (*ii*) two single-media (quartz sand) filters in series. In situ and ex situ activity tests were combined with mineral coating characterization and metagenome-guided metaproteomics along the depth of each filter. Both plants exhibited comparable performances and process compartmentalization, with most of ammonium and manganese removal occurring only after complete iron depletion. The homogeneity of the media coating and genome-based microbial composition within each compartment highlighted the effect of backwashing, namely the complete vertical mixing of the filter media. In stark contrast to this homogeneity, the removal of the contaminants was strongly stratified within each compartment, and decreased along the filter height. This apparent and longstanding conflict was resolved by quantifying the expressed proteome at different filter heights, revealing a consistent stratification of proteins catalysing ammonia oxidation and protein-based relative abundances of nitrifying genera (up to 2 orders of magnitude difference between top and bottom samples). This implies that microorganisms adapt their protein pool to the available nutrient load at a faster rate than the backwash mixing frequency. Ultimately, these results show the unique and complementary potential of metaproteomics to understand metabolic adaptations and interactions in highly dynamic ecosystems.

HIGHLIGHTS

- Single dual- and consecutive single-media filters are eco- and operationally equivalent.
- Both systems exhibited comparable performances and process compartmentalization.
- Media coating and genome-based composition were homogeneous in each compartment.
- Only protein abundances reflected stratification in activity.
- Backwash shapes microbial community distribution in rapid sand filters.

Published as:

Corbera-Rubio, F., Laureni, M., Koudijs, N., Müller, S., van Alen, T., Schoonenberg, F., Lücker, S., Pabst, M., van Loosdrecht, M. C. M. & van Halem, D. Meta-omics profiling of full-scale groundwater rapid sand filters explains stratification of iron, ammonium and manganese removals. *Water Res.* **233**, 119805 (2023).

3.1. INTRODUCTION

Anaerobic groundwater is an excellent drinking water source due to its microbiological safety, stable temperature and composition [1–3]. Rapid sand filters (RSFs), preceded by an aeration step, are the most commonly applied technology for groundwater treatment. In RSFs, the main groundwater contaminants – soluble iron (Fe^{2+}), ammonium (NH_4^+) and manganese (Mn^{2+}) - are sequentially removed in a series of interwoven biological and physical-chemical reactions [4]. While the latter have been the subject of decades of research, our understanding of the involved microbiology is limited. Our current understanding is that Fe^{2+} is removed both chemically and biologically[5], Mn^{2+} via chemical autocatalytic oxidation and to some extent biologically[6], and NH_4^+ exclusively biologically[7]. However, not only the impact of microbial activity on the removal processes and their stratification along the height of RSFs is largely unknown, but also the individual physiologies of the involved microorganisms remain elusive[8]. Deepening our knowledge of the underlying microbiology is paramount to improve current RSF operation and to design and implement novel, resource-efficient systems.

The first characterization of nitrifying biomass stratification in RSFs dates back to the beginning of this century [9]. In their pioneering work, Kihn and colleagues observed an uneven distribution of nitrifying activity along a full-scale RSF using *ex-situ* batch incubations. Subsequently, molecular methods, such as fluorescence *in situ* hybridization (Lydmark et al., 2006), 16S rRNA gene cloning and sequencing (Qin et al., 2007), and denaturing gradient gel electrophoresis (de Vet et al., 2009) have been used to investigate the diversity of nitrifying bacteria and to estimate the relative abundance of ammonia-oxidizing bacteria and archaea. Furthermore, quantitative polymerase chain reaction (qPCR) has been applied to determine the distribution of nitrifying and denitrifying microorganisms in RSFs [13], linking absolute microbial abundances to *in situ* ammonium removal capacity (Tatari et al., 2016; Tatari et al., 2017). Recently, shotgun metagenomics has established itself as the predominant approach for the characterization of the composition and functional potential of complex microbiomes, and led to remarkable discoveries in RSFs such as the complete oxidation of ammonia by a single organism (comammox) [16,17] or the metabolic-

coupling between methane- and ammonia-oxidizing communities (Poghosyan et al. (2020)). On the contrary, information about biological iron and manganese oxidation in RSFs is scarce, primarily due to our limited understanding of the underlying metabolic pathways [19,20]. In spite of this, the presence and importance of iron- and manganese-oxidizing organisms in RSFs has repeatedly been shown by culture-dependent [21–24] and culture-independent studies [25–28], *ex situ* batch incubations [29], and metagenomics [16,30]. However, mechanistic insights linking filter performance with actual microbial activities have not been established to date.

Recent technical advancements made the characterization of the entire pool of proteins expressed in complex communities feasible [31,32]. Proteins are the biological entities catalyzing metabolic reactions. Thus, beyond genome-based approaches, their identification and quantification allow for the simultaneous resolution of the identity and actual metabolic function of core community members [33]. Protein abundances also provide a more accurate estimation of the relative biomass contribution of different populations in a community [34,35]. Over the past decades, metaproteomics has been successfully applied to characterize microbiomes from different environments, including marine [36], soil [37], wastewater [38] and freshwater [39] ecosystems. Moreover, differential protein expression has been used to characterize microbiomes' physiological responses to rapid environmental changes [40], making metaproteomics particularly relevant to study dynamic environments such as RSF systems.

RSFs are regularly backwashed to remove particles that have been trapped during operation. As a result, biomass-colonized filter media grains are displaced along the filter height and exposed to different substrate loads at every cycle [41]. Consistently, metagenome-based studies commonly report even distributions of core taxa along filter heights [13,15], and conventional RSFs models consider them as homogeneous systems (Uhl & Gimbel, 2000). In contrast, and irrespective of the backwash, contaminant removal stratification along the filter is commonly reported [14,44]. Within this framework, we hypothesize that genetically homogeneous RSFs' microbial communities hold the ability to rapidly modify their pool of expressed proteins to metabolically respond to the environmental conditions encountered at a given filter height. To this end, we quantified the *in-situ* removal of iron, manganese, and ammonium, and resolved the taxonomy and function of the microbial communities along the

filter height of two full-scale RSF plants, one dual-media (anthracite and sand) single filter system and one comprising two single-media sand filters in series.

3.2. MATERIALS AND METHODS

3.2.1. Sample collection

Filter media and water samples were collected from two groundwater-fed drinking water treatment plants (DWTP) operated by the company Vitens. The first one, located in Druten, was a single filter (SF) with a dual media bed of 0.6 m anthracite on top and 2 m of quartz sand at the bottom. The second one, located in Hasselo, was a double filter (DF) consisting of two single-media 2 m high quartz sand filters (DF1 and DF2) connected in series. The filter media was sampled with a peat sampler at three different heights in each filter (approximately every 0.5 m), referred to as top (t), middle (m) and bottom (b) sections (Figure 1). Sampling from the bottom section of DF1 (*i.e.*, DF1_b) was technically not possible. Filter media samples were taken at the end of the operational cycle before backwashing. Influent, effluent, and filter-bed porewater samples were immediately filtered (0.45 µm), stored at 4 °C, and measured within 12 h. Samples for total iron and manganese quantification were acidified to pH < 1 with 69 % ultrapure nitric acid. pH, O_2 concentration, temperature and redox potential were measured on-site using a multimeter (Multi 3630 IDS, Xylem Analytics, Germany). Operational parameters and raw water characteristics for each filter are shown in Table 1.

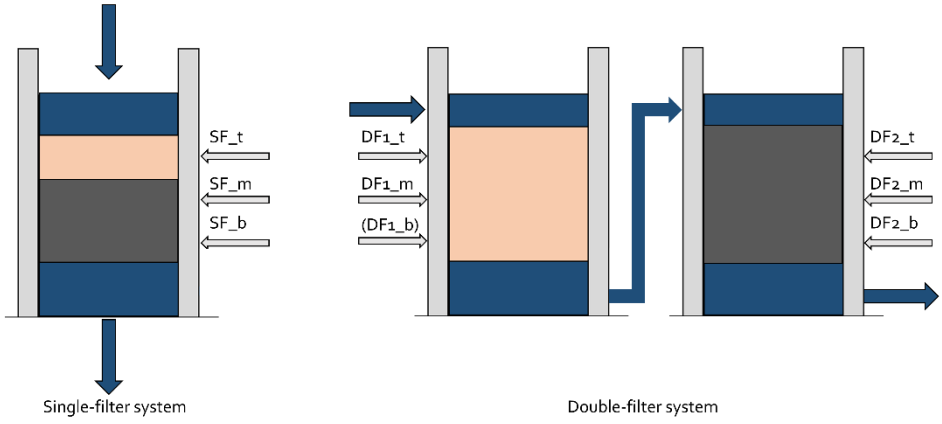

Figure 1. Schematic illustration of the two drinking water treatment plants. Each individual filter is characterized at three different heights: top (t), middle (m) and bottom (b). Colors of the filter media material reproduce the color of the coating (beige and dark grey for iron and manganese oxides, respectively), and reflect the compartmentalization of the removal processes.

Table 1. Operational parameters of the DWTPs and the characteristics of the respective groundwaters. Historical data refer to average and standard deviation of the weekly concentrations between November 2018 and July 2020. For the double filter system, data refer to the influent to the first filter.

	Units	Single filter (SF)	Double filter (DF1, DF2)
Filter height and media	m	0.6 (anthracite)	2 (quartz sand)
	m	2.0 (quartz sand)	
Height of supernatant	m	0.3-0.5	0.3 - 0.5
Age of media	years	1 (anthracite)	2.5 - 3
		5 (quartz sand)	
Filter area	m^2	28.3	15.2
Filtration rate	m/h	5.7	4.3
Run cycle time	h	50	84
Backwash cycle time	min	45	45
		Groundwater	
Online measurements			
pH		7.15	7.1
Temperature	°C	12.1	11.5
Oxidation-Reduction Potential	mV	-104.2	-128.4
O_2	mg/l	0.024	0.025
Historical data			
Fe^{2+}	mg/l	6.5 ± 0.1	5.1 ± 0.2
Mn^{2+}	mg/l	0.67 ± 0.03	0.31 ± 0.02
NH_4^+	mg N/l	0.41 ± 0.02	1.9 ± 0.1
NO_2^-	mg N/l	< 0.003	< 0.003
NO_3^-	mg N/l	< 0.2	< 0.2

3.2.2. Ex situ ammonium and manganese maximum removal rates

The maximum ammonium and manganese removal rates of the filter media were determined in batch. 4 g of wet filter media, 200 mL of tap water, and 100 µl of trace element solution (L^{-1}; 15g EDTA, 4.5g $ZnSO_4 \cdot 7H_2O$, 4.5g $CaCl_2 \cdot 2H_2O$, 3g $FeSO_4 \cdot 7H_2O$, 1g H_3BO_3, 0.84g $MnCl_2 \cdot 2H_2O$, 0.3g $CoCl_2 \cdot 6H_2O$, 0.3g $CuSO_4 \cdot 5H_2O$, 0.4g $Na_2MoO_4 \cdot 2H_2O$, 0.1g KI) were mixed in 300 mL shake flasks. After an acclimatization period of 30 min at 25 °C and 150 rpm, each flask was spiked with 3 ml of 100 mg NH_4^+-N L^{-1} NH_4Cl or 100 mg Mn^{2+} L^{-1} $MnCl_2 \cdot 4H_2O$ (Sigma Aldrich, Saint Louis, Missouri USA). Liquid samples (1 ml) were taken at different time intervals throughout the entire process. Maximum removal rates per mass (wet weight) of filter media were calculated by interpolation of the concentration profiles and converted into volumetric rates using the measured filter media densities (Supplementary Table 4). Biological ammonia oxidation was suppressed by overnight incubation at 50 °C with 0.05 g penicillin g L^{-1} (Sigma Aldrich) [25] and confirmed with ATP measurements (see below).

3.2.3. Water quality analyses

Samples for ammonium, nitrite, and nitrate quantification were immediately filtered through a 0.2 µm nanopore filter and measured within 12 h using photometric analysis (Gallery Discrete Analyzer, Thermo Fischer Scientific, Waltham, Massachusetts, USA). Samples for dissolved iron and manganese quantification were immediately filtered through a 0.2 µm nanopore filter and analysed within 12 h. Raw water samples were filtered after a minimum of 16 hours of acidification for total iron and manganese quantification. Iron and manganese were quantified by ICP-MS (Analytik Jena, Jena, Germany).

For ATP detection, 1 ml miliQ H_2O was added to 1 g wet weight of sand. The samples were sonicated for 1 min at an output power of 15 W and a frequency of 20 kHz (ultrasonic homogenizer, Qsonica sonicators, Newtown, Connecticut, USA). Samples were subsequently filtered through a 0.22 µm nanopore filter. The concentration of ATP in the liquid was determined in duplicates using an ATP analyzer as described by the manufacturer (Clean-Trace™ Luminometer NG3, 3M, Maplewood, Minnesota USA).

3.2.4. Filter-bed coating characterisation and visualization

Coating extraction was carried out in triplicate as described elsewhere [45] with minor modifications. 1.5 g of wet filter media were frozen overnight at -80 °C and freeze-dried for 48 h (Alpha 1-4 LD plus, Christ, Osterode am Harz, Germany). Samples were immersed in 40 ml citrate buffered dithionite solution for 4 h, centrifuged at 4000 rpm for 10 minutes, and filtered through a 0.45 µm pore size filter. Iron was measured using the 3500-Fe B: Phenanthroline method [46], and manganese colorimetrically (LCK 532, Hach Lange, Tiel, The Netherlands). Light microscopy images were taken with a VHX-5000 digital microscope (Keyence, Osaka, Japan) with an VH-Z20UR lens.

3.2.5. DNA extraction

Nucleic acid extraction was carried out using the MagMAX CORE Nucleic Acid Purification Kit (Applied Biosystems, Thermo Fisher Scientific). A pre-treatment step using bead beating tubes from MagMAX CORE Mechanical Lysis Module was introduced to improve DNA recovery. In duplicates, 0.25 g of sample, 350 µL lysis solution, and 10 µL proteinase K were mixed and bead-beaten for 2 × 30 seconds (Bead Mill Homogenizer, BioSpec, Bartlesville, Oklahoma, USA), and then centrifuged for 2-7 minutes at 10000 × *g* until the supernatant was clear. Next, the supernatants of two tubes were combined in a clean tube, mixed with 450 µL Bead/PK mix and vortexed for 10 min. The tubes were placed on a magnetic stand for 1 min and the supernatant was removed. The samples were washed twice by adding 500 µL of 'wash solution 1/2', and vortexed for 1 minute prior to supernatant removal on the magnetic stand. After the second washing step, samples were air-dried for 5 minutes. 90 µL elution buffer were added and samples were vortexed for 10 min. After 2 min on the magnetic stand, the supernatants were transferred to clean tubes. Afterwards, all samples were purified using the GeneJET PCR Purification kit following the manufacturer's protocol (Thermo Scientific, Thermo Fisher Scientific). DNA was quantified with a Qubit 4 Fluorometer and Qubit dsDNA HS assay kit (Invitrogen, Thermo Fisher Scientific).

3.2.6. Library preparation and sequencing

Metagenomic library preparation was performed using the Nextera XT kit (Illumina, San Diego, California U.S.A.) according to the manufacturer's instructions. Enzymatic tagmentation was performed starting with 1 ng of DNA, followed by incorporation of the indexed adapters and PCR amplification. After purification of the amplified library using AMPure XP beads (Beckman Coulter, Indianapolis, USA), the libraries were checked for quality and size distribution using an Agilent 2100 Bioanalyzer and the High sensitivity DNA kit (Agilent, San Diego, USA). Quantitation of the library was performed by Qubit using the Qubit dsDNA HS Assay Kit (Invitrogen, Thermo Fisher Scientific, USA). The libraries were pooled, denatured, and sequenced with Illumina MiSeq (San Diego, California USA). Paired end sequencing of 2 x 300 base pairs was performed using the MiSeq Reagent Kit v3 (San Diego, California USA) according to the manufacturer's instructions.

3.2.7. Assembly, functional annotation, and taxonomic classification

Raw sequencing data was quality-filtered and trimmed using Trimmomatic v0.39 (HEADCROP:16 LEADING:3 TRAILING:5 SLIDINGWINDOW:4:10 CROP:240 MINLEN:35) [47]. Sequencing data quality was analyzed using FastQC v0.11.7 before and after trimming [48]. MEGAHIT v1.2.9 was used to assemble the quality-filtered and trimmed reads into contigs with default settings (Li et al., 2015). Raw reads were mapped back to the assembled contigs using BWA-MEM2 [50]. SAMtools v1.14 was used to determine contig coverage and for indexing with default settings (Li et al., 2009). Taxonomic classification of each contig was performed using the Contig Annotation Tool (CAT) with default settings and the NCBI database [52]. Ultimately, the relative abundance of each taxa was calculated by matching the CAT results and the read mapping information (SAMtools), expressed as percentage of the sum of the trimmed reads mapping to the contigs of each taxa compared to the total number of trimmed reads [53]. Functional annotation was done with GhostKoala v2.2 [54] against the Kyota Enciclopedia of Genes and Genomes (KEGG; accessed September 2021). FeGenie [55] was used to refine the annotation of genes involved in iron metabolism using the metagenomics ('-meta') settings. Genes encoding the three subunits of the particulate methane monooxygenase (*pmoABC*) and ammonia monooxygenase (*amoABC*) were translated into

protein sequences and differentiated by constructing phylogenetic trees in MEGA11 using *MUSCLE* as alignment tool and the Neighbor-Joining method with the *WAG* substitution model [56] (Figure S2, Figure S3, Figure S4). Reference sequences were extracted from the National Center for Biotechnology Information database (2021_09), ensuring a wide representation of all beta- and gammaproteobacterial ammonia-oxidizing bacteria [57], and methanotrophs affiliated with the Alpha- and Gammaproteobacteria and *Verrumicrobia* [58] in the resulting phylogenetic trees. Nitrite oxidoreductases (*nxrAB*) and nitrate reductases (*narGH*) were manually identified based on taxonomy after their protein sequences were blasted using 'blastp' against the SwissProt database (v. 2022_02). In analogy, the nitrite reductases *nirK* and *nirS* were taxonomically assigned to nitrifying or denitrifying organisms. Twelve published Mn(II)-oxidizing genes [30] were used as reference database for manganese oxidation. Protein assemblies of each sample were aligned to the database using local blastp v2.13 with e-value < 1e-6, percentage identity > 35 % [59] and coverage > 70 % [55]. RStudio v1.4.1106 was used for data analysis and visualization (RStudio Team, 2021). Raw DNA sequences can be found on the National Center for Biotechnology Information (NCBI) website under BioProject PRJNA830362.

3.2.8. Protein extraction, proteolytic digestion, and shotgun proteomic analysis

For protein extraction, 150 mg of filter (sand) material was mixed with 125 µL of B-PER reagent (78243, Thermo Scientific) and 125 µL 1 M TEAB buffer (50 mM TEAB, 1 % w/w NaDOC, adjusted to pH 8.0). The mixture was briefly vortexed and exposed to shaking using a Mini Bead Beater 16 (BioSpec Products) for 3 min. Afterwards, the sample was exposed to one freeze/thaw cycle at -80 °C and +80 °C for 15 and 5 min, respectively. The samples were centrifuged for 10 min at 10000 rpm at 4 °C, and the supernatant was transferred into a clean LoBind tube Eppendorf tube (Eppendorf, Hamburg, Germany). Another 125 µL of B-PER reagent and 125 µL 1 M TEAB buffer was added to the sand sample, vortexed and sonicated (Branson 5510, sonication mode, at room temperature) for 5 min. The sample was then centrifuged for 10 min at 10000 rpm at 4 °C, and the supernatant was collected and pooled with the first supernatant. Extracted proteins were precipitated by adding 200 µL ice-cold acetone to the supernatant, vortexing and incubation at -20 °C for 1 h. The protein pellet was

collected by centrifugation at 14000 rpm at 4 °C for 15 min. The supernatant was carefully removed from the pellet using a pipette. The pellet was dissolved in 200 mM ammonium bicarbonate containing 6 M urea. Disulfide bonds were reduced using 10 mM DTT (dithiothreitol) and sulfhydryl groups were blocked using 20 mM IAA (iodoacetamide). The solution was diluted to below 1 M urea and digested using sequencing grade Trypsin (Promega). The proteolytic peptides were finally desalted using an Oasis HLB solid phase extraction well plate (Waters) according to the manufacturer's protocol. An aliquot corresponding to approximately 250 ng of protein digest was analyzed with a shotgun proteomics approach as described earlier [35]. Briefly, the peptides were analyzed using a nano-liquid-chromatography system consisting of an EASY nano-LC 1200, equipped with an Acclaim PepMap RSLC RP C18 separation column (50 um × 150 mm, 2 µm, 100 Å) and a QE plus Orbitrap mass spectrometer (Thermo Fisher, Germany). The flow rate was maintained at 350 nL over a linear gradient from 5 % to 30 % solvent B over 65 minutes and finally to 60 % B over 20 min. Solvent A was ultrapure H_2O containing 0.1 % v/v formic acid, and solvent B consisted of 80 % acetonitrile in H_2O and 0.1 % v/v formic acid. The Orbitrap was operated in data-dependent acquisition (DDA) mode acquiring peptide signals from 385-1250 m/z at 70K resolution. The top 10 signals were isolated at a window of 2.0 m/z and fragmented at a NCE of 28 at 17.5K resolution with an AGC target of 2e5 and a max IT 75 ms. The collected mass spectrometric raw data were analyzed combined against the metagenomics reference sequence database built from the assembled contigs using PEAKS Studio 10 (Bioinformatics Solutions, Canada) in a two-round search approach. The first-round database search using the clustered database (892436 proteins) was used to construct a focused protein sequence database, considering one missed cleavage, and carbamidomethylation as fixed modification, and allowing 15 ppm parent ion and 0.02 Da fragment ion mass error. The focused database (containing 9729 proteins) was then used in a second-round search, considering 3 missed cleavages, carbamidomethylation as fixed and methionine oxidation and N/Q deamidation as variable modifications. Peptide spectrum matches were filtered for 5 % false discovery rate (FDR) and protein identifications with at least 2 unique peptides were considered as significant. Functional annotations (KO identifiers) and taxonomic lineages were obtained by GhostKoala (https://www.kegg.jp/ghostkoala) and by Diamond [60] using the NCBI nr protein sequence reference database (Index of /blast/db/FASTA (nih.gov)). For Diamond

annotations, the lineage of the lowest common ancestor was determined from the top 10 sequence alignments.

Comparison of the relative abundance of proteins between samples was performed using "relative spectral counts" (*i.e.*, normalized spectral counts, defined as spectral counts per protein divided by the molecular weight, divided by the sum of spectral counts of all proteins of all samples). Since protein extraction was performed from filter media of equal mass (150 mg per sample), the protein abundance of sample SF_t was multiplied upfront by 0.76 to correct for the density difference between anthracite (1.3 g/cm^3) and quartz sand (1.7 g/cm^3). For sake of simplicity, further corrections for differences in nutrient loads between systems, resulting from different superficial velocities and filter volumes (Table 1), were omitted as they did not yield significantly different results. To identify the functional guilds of interest, all proteins were taxonomically classified using their best hit in the NCBI and KEGG database and subsequently grouped at genus level, and the resulting genera were manually classified based on their most probable energy source, iron, nitrogen or "others", based on the literature (Table S3). Similarly, the contribution of a specific protein was estimated by summing up the relative abundances of all proteins with the same annotation.

3.3. RESULTS

3.3.1. In situ oxidation of Fe2+, NH4+, Mn2+ display similar compartmentalisation in both configurations

The concentration profiles of ammonium, iron and manganese along the studied treatment processes are shown in Figure 2A and 2B. Iron was completely removed (< 0.04 mg Fe^{2+}/L) in the top layer of the single-filter system (*i.e.*, anthracite layer, SF_t) and in the first filter of the double-filter system (DF1). Consistently, manganese consumption only started after iron depletion in both systems, namely in SF_m and DF2_t, and was complete (< 0.002 mg Mn^{2+}/L) at the end of each treatment process. In analogy, most ammonium was removed after iron depletion, with < 30% removal in SF_t and DF1.

The observed process compartmentalization was also reflected in each filter section in the total mass of iron and manganese oxides, the end products of Fe^{2+} and Mn^{2+} oxidation [5] (Figure 2C, D). The coating in SF_t and DF1 mainly consisted

of iron (118 ± 8 mg_{Fe}/g_{media}), while the coating in SF_m, SF_b, and DF2 mainly consisted of manganese (33 ± 6 mg_{Mn}/g_{media}). In SF, anthracite and quartz sand remained clearly separated after over one year of operation despite frequent backwashing cycles. Nevertheless, trace amounts of anthracite particles were found in the lower filter sections and might explain the slightly higher iron coating content in SF_m and SF_b as compared to DF2 (Figure 2C, D).

Overall, concentration profiles and coating composition results revealed similar compartmentalization of removal processes in the two DWTPs, irrespective of dual-media single filter or single-media double filter configurations.

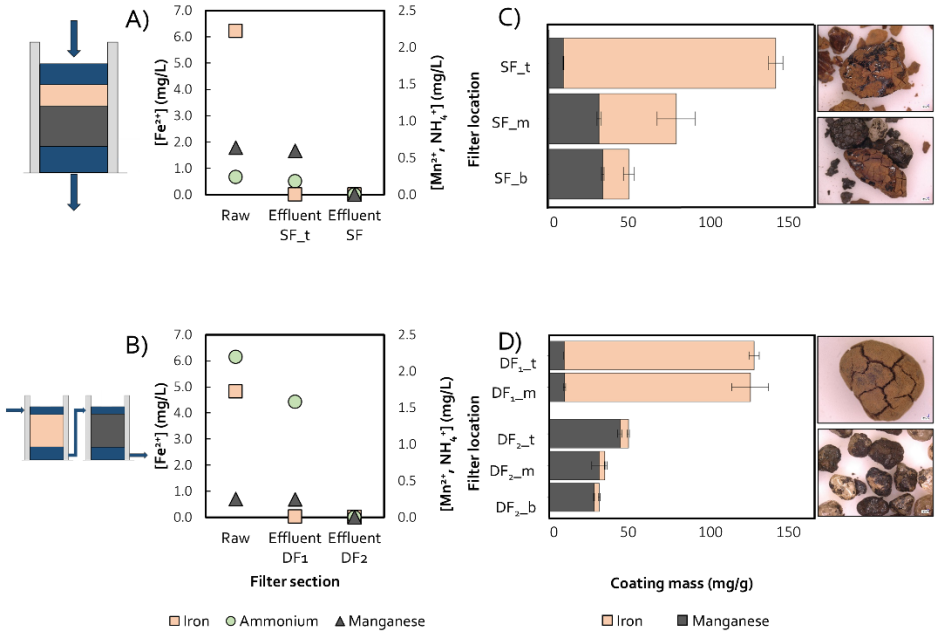

Figure 2. Concentration profiles of iron, manganese, and ammonium along the rapid sand filter heights in both the (A) single- and (B) double-filter DWTPs. Total removal is achieved at the end of the treatment. Coating composition of filter medium from the (C) single- and (D) double-filter DWTPs, with microscope images of SF_t, SF_b, DF1_t and DF2_b. Measurements were carried out in duplicates (A, B) or triplicates (C, D); error bars represent standard deviation.

3.3.2. Ex situ NH_4^+ and Mn^{2+} removal mechanisms and rates reflect in situ compartmentalization

Manganese is chemically oxidized or adsorbed depending on filter media coating

The manganese removal capacity of the filter media in the different sections was quantified in batch activity tests (Figure 3A). Complete Mn^{2+} removal was observed with manganese-coated media from the later sections of both treatments (*i.e.*, SF_m, SF_b and DF2). Contrastingly, it remained incomplete with iron-coated media from the first treatment sections (*i.e.*, SF_t and DF1). To further characterize the removal mechanism, desorption experiments were performed by submerging drained media in demineralized water. Mn^{2+} desorption was observed exclusively with iron-rich media (Figure 3B), suggesting that Mn^{2+} is adsorbed by iron oxides, while it is oxidized on manganese oxide-coated particles.

First-order oxidation rate constants were calculated for manganese-oxidizing media (Figure 4), as manganese oxidation is known to occur mainly physicochemically and to linearly depend on Mn^{2+} concentration [29,61]. Removal rate constants were similar in both systems (0.010-0.013 min^{-1} in SF_m and SF_b; 0.014-0.016 min^{-1} in DF2), consistent with the comparable total amounts of manganese oxide coating, the catalyst of manganese oxidation [29]. Moreover, the rate constants were comparable in all sections devoid of iron oxides, despite decreasing manganese concentrations along the filter height (Fig. 2). Likely, this is the result of media mixing during frequent backwash events.

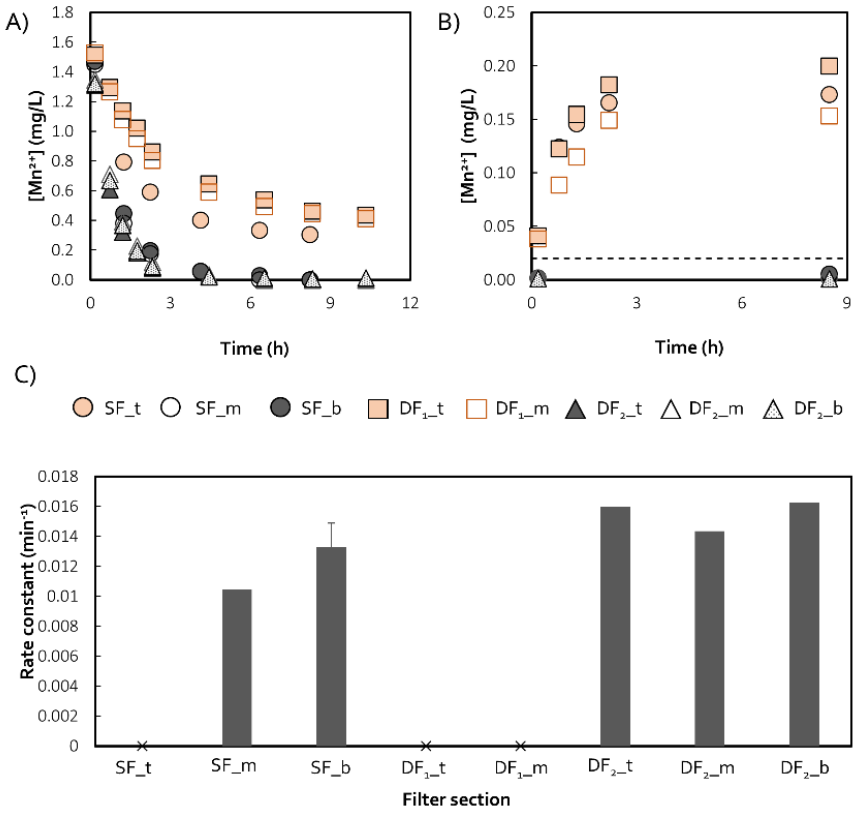

Figure 3. Manganese removal in (A) batch and (B) desorption tests. Colors correspond to the main component of the coating, grey for manganese and orange for iron. Batch tests were carried out in duplicate, error bars represent standard deviation (smaller than symbols). C) First-order manganese oxidation rate constants estimated with manganese-coated media. Tests were run in duplicates, values represent averages with error bars indicating standard deviation. No oxidation constants were calculated for iron-rich media where removal is primarily driven by adsorption (x).

Ammonia oxidation is biological, compartmentalized and stratified within each compartment

The maximum volumetric ammonia oxidation rates along the filter heights were tested *ex situ* in batch experiments (Figure 4A). The biological nature of

ammonia oxidation was validated with penicillin-amended batch tests (Figure 4B). Consistent with the measured ammonium concentration profiles along the two treatments (Figure 2A and 2B), the maximum ammonium removal rates were significantly lower in the sections where iron is present (4.5-4.7 g $NH_4^+/(m_{media}^3 \cdot h)$; SF_t, DF1_t, and DF1_m) compared to the downstream sections where iron was depleted (15-62 g $NH_4^+/(m_{media}^3 \cdot h)$; SF_m, SF_b, and throughout DF2). Moreover, in contrast to the relatively uniform chemical manganese oxidation rate constants (Figure 3C), the biological ammonium removal rates displayed a decreasing trend, likely reflecting the decreasing substrate availability along the filter height (Figure 4A).

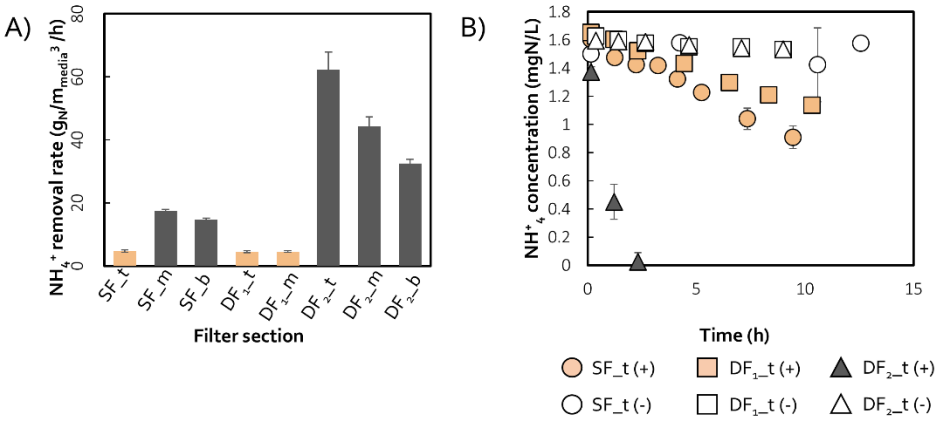

Figure 4. A) Maximum volumetric ammonium removal rates of the filter medium at each filter section. B) Ammonium concentration profiles in batch tests with fresh (full symbols) and penicillin-inactivated (empty symbols) filter media from the top section of each filter. All activities were quantified in triplicate, error bars represent standard deviation. The color of the symbols corresponds to the main component of the media coating, iron in orange and manganese in grey.

3.3.3. Taxonomic and functional analysis bridge plant operation with microbial physiology

Metagenomic-based microbial composition reflects process compartmentalization

The metagenome of the microbial community in each section was sequenced to characterize the phylum-level taxonomic profile of each RSF, and to serve as reference database for metaproteomics. After quality filtering, an average of $7{\cdot}10^6 \pm 3.1{\cdot}10^6$ paired-end reads were obtained per sample (Table S1). *De novo* assembly of trimmed reads yielded $1{\cdot}10^5 \pm 5.8{\cdot}10^4$ contigs (≥ 0.5 kb) with an average N50 of 1118 ± 215 bases. Samples from the lower sections of each treatment, namely SF_m, SF_b and DF2_b, yielded the shortest contigs with an average length < 1 kb. An average of $1.8{\cdot}10^6 \pm 1{\cdot}10^6$ coding sequences per sample were predicted on the assembled contigs.

Bacteria accounted for 91.2 ± 1.9 % of the total contigs in all samples, while *Archaea* accounted for < 1% and the remainder remained unclassified. 75.4 ± 3.7 of the bacterial contigs were classified at phylum level (Figure 5). *Proteobacteria* (45.7 ± 12.1 %) and *Nitrospirae* (18.8 ± 10.8 %) dominated all sections, followed by *Planctomycetes* and *Acidobacteria* that were present in all sections except for SF_t. *Verrucomicrobia* and *Bacteroidetes* were found in SF_t and DF1, and *Actinobacteria* only in DF1. Importantly, contigs associated with the *Nitrosomonadaceae* and *Nitrospiraceae* families (Figure S2) were more abundant in the upper parts of the filters where the actual removal of ammonium occurred. In analogy, contigs assigned to phyla or families known to contribute to iron oxidation were present in all compartments but were mainly present in the anthracite layer of SF, where iron removal occurs. Overall, the composition of the microbial communities reflected the observed activity compartmentalization (Fig. 2 and 4), and this was especially evident in the dual filter system featuring a uniform community composition within each filter (*i.e.*, DF1 and DF2). Despite the potential mixing effect of backwash, an analogous compartmentalization was also observed between the anthracite (SF_t) and sand layers (SF_m, SF_b) in SF.

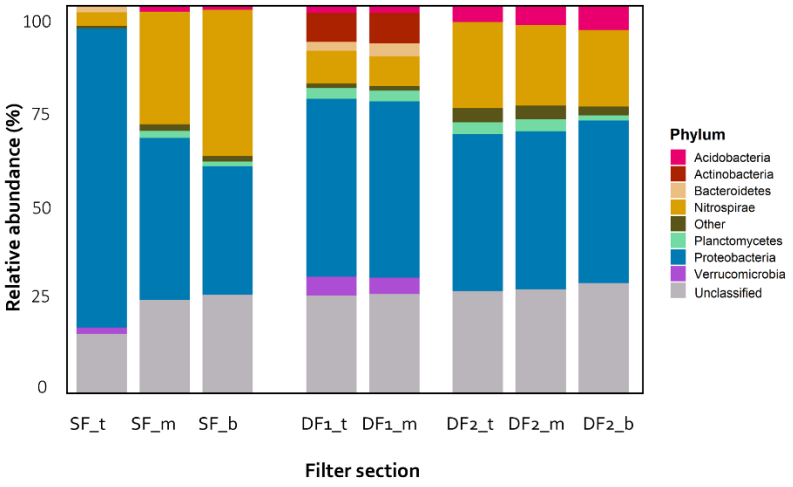

Figure 5. Phylum-level taxonomic classification and relative abundance calculated as percentage of total contigs of the most abundant (> 1 %) phyla in each filter section. The taxonomic classification of each contig was performed using the Contig Annotation Tool [52] *with standard parameters using contigs as input and the NCBI reference database.*

Differential protein abundance explains biological activity stratification

The proteome of each section was quantified to estimate the relative contribution of known nitrogen and iron metabolizing guilds to the total biomass, as well as the distribution of core nitrogen, iron and manganese transforming enzymes. Per sample, we obtained on average 176 ± 79 individual protein groups that contained at least two unique peptides and false discover rate (FDR) < 1% (Table S4). The guilds of interest were identified by taxonomically grouping all proteins at genus level, and subsequently classifying the resulting genera based on their most-probable energy source, *i.e.*, iron, nitrogen or "others" (Figure 6 and Table S3) based on the reported physiologies of the respective genus. The relative contribution of individual proteins of interest was estimated by grouping all proteins with the same KO number and summing up all the corresponding relative abundances.

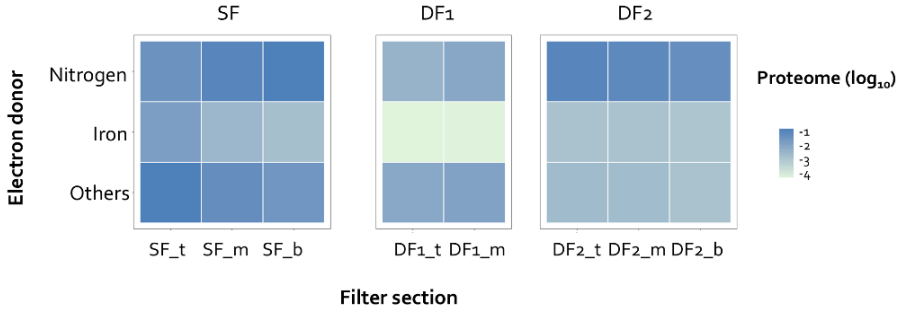

Figure 6. Relative protein-based biomass abundance expressed as relative spectral counts (i.e., protein weight normalized spectral counts divided by the sum of spectral counts of all proteins of the 8 samples together) of iron, nitrogen and 'others' cycling organisms, based on the most-probable energy source at genus level. Only genera with at least 2 different identified proteins (hits) were used. No genus directly associated with manganese oxidation was found. Detailed information can be found in Supplementary Table 3.

The protein-based quantification of nitrogen metabolizing guilds revealed a clear increase in their relative abundance in the lower sections of SF and in DF2, with a marked stratification in DF2 (Figure 6), in analogy with the *ex-situ* activities (Figure 4A). The genes of core nitrogen metabolisms - nitrification, denitrification, and dissimilatory nitrite reduction to ammonium (DNRA) - were present in all samples (Figure 7A; Table S2), and the abundance of the corresponding proteins was higher in the downstream sections of both systems. Specifically, the key proteins for nitrification, ammonia monooxygenase (AmoABC) and nitrite oxidoreductase (NxrAB), were present in all samples. Conversely, hydroxylamine dehydrogenase (Hao) was found at much lower abundances and only in some sections, while its coding gene *hao* was ubiquitously present. In terms of denitrification, nitrite reductase (NirK or NirS) was the only detected protein even if most genes, *i.e.*, nitrate reductase (*narGHI*), nitric oxide reductase (*norBC*) and nitrous oxide reductase (*nosZ*), were found in the metagenome of all sections. In analogy, DNRA genes were found in most metagenomes but none of the corresponding proteins were detected (data not shown; Table S2).

Consistent with the iron concentration profiles and the coating composition along SF (Figure 2), putative iron-oxidizers were most abundant in the first section of SF (SF_t; Figure 6). In turn, surprisingly low abundance of iron-

oxidizers was found in DF1, despite all iron being removed in this filter. This observation coincides with low overall biomass abundances in DF1_t and DF1_m, calculated as the sum of normalized spectral counts of each section divided by the sum of spectral counts of all samples combined, as compared to the other filters (Figure S3). Genes encoding for putative iron oxidizing proteins Cyc2, Cyd1, MtoABC (based on FeGenie [55]) were present in all sections, yet the corresponding proteins were only found in SF and DF2 (Figure 7B). Other putative iron-oxidizing genes, *i.e.*, *foxABC*, *foxEYZ* and *pioABC* [55], were not detected in any sample. Lastly, putative manganese-oxidizing genes were spread across all samples with no evident correlation with filter operation, but no expressed proteins were detected.

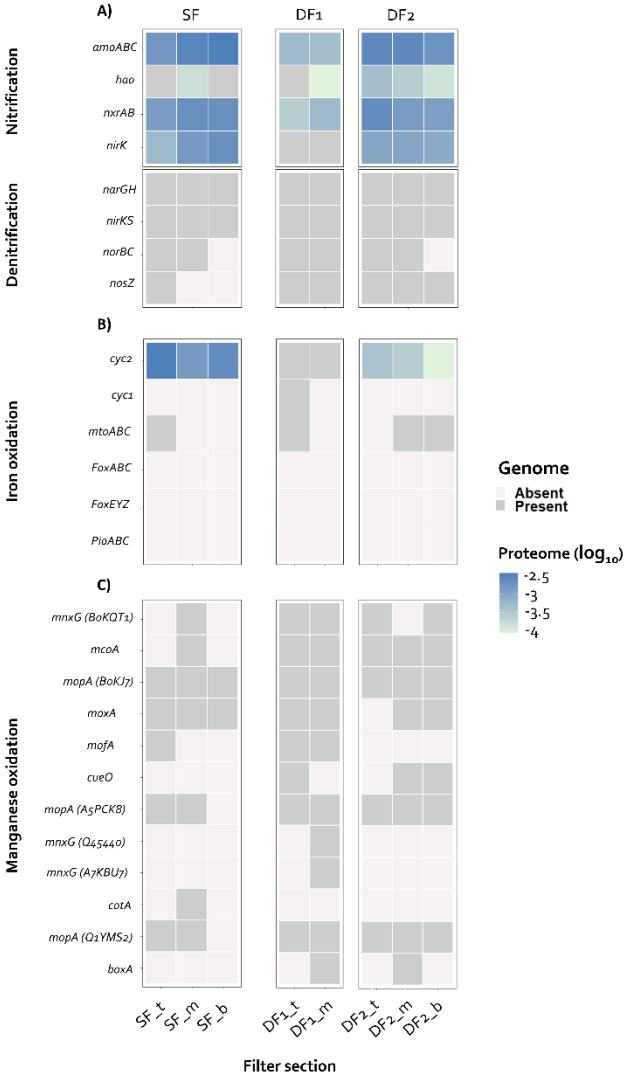

Figure 7. Relative protein abundance (protein-mass normalized spectral counts divided by the total spectral counts of the 8 samples) of the main (A) nitrogen, (B) iron and (C) manganese metabolism genes. Genes were selected based on the nitrification and denitrification pathways (#M00528, #M00529) of the (A) Kyoto Encyclopedia of Genes and Genomes, (B) FeGenie [55], and (C) a custom-made database based on [30]. Dark grey, genes found at least once in the metagenome but not in the metaproteome; light grey, genes not found in the metagenome. Detailed information about each enzyme can be found in Supplementary Table 2.

3.4. DISCUSSION

Two full-scale drinking water treatment plants were chosen to unravel the interaction between physicochemical and biological processes, and their distribution along the height of rapid sand filters (RSFs). While treating groundwater with similar compositions, the first plant employed a single-filter with an anthracite layer on top of a quartz sand core, and the second comprised a double-filter configuration containing quartz sand only. *In situ* and *ex situ* quantification of iron, manganese, and ammonium removals were combined with the characterization of the corresponding filter-media coating. Genomic and proteomic profiling along the filter height was used to compare the metabolic potential (*i.e.*, genes encoding for certain proteins) with the actual metabolism (*i.e.*, expressed proteins) of the underlying microbial communities.

3.4.1. Backwash-driven filter-media mixing results in compartments with homogeneous coating and genetic fingerprints

Both sand filtration systems exhibited highly comparable operational performances and harboured microbial communities with surprisingly similar taxonomic and functional profiles. Iron was removed in the first sections, being it the anthracite top layer in the single filter system or the first filter in the double filter configuration, while ammonium and manganese removal occurred primarily in the downstream sections (Figure 2).

Spatial separation between iron and manganese removal has often been reported in rapid sand filters [4,62], and it is commonly attributed to the different pH/oxidation-reduction potentials required for their oxidation and precipitation [63]. Also, the mineral coating composition is often used as a proxy to localize where removals occur during the lifespan of a filter [64]. Consistently, we observed the process compartmentalization clearly reflected in the coating composition of the filter media of both studied systems. Iron and manganese oxides dominated the first and the downstream sections of each system, respectively (Figure 2), with coating amounts comparable to other DWTPs (Breda et al.,

2019). Moreover, both the manganese coating mass and the removal rate constants were rather constant in all sections devoid of iron (Figure 2 and 3). As the physicochemical oxidation of manganese is directly proportional to the available concentration of manganese [29,61], manganese oxide coating was expected to decrease along the filter height. In contrast, we observed homogeneity of coating thickness within the manganese-removing compartments of both filter systems, which is likely the result of filter-media mixing during backwash [41].

The observed compartmentalization of *in situ* removal rates and metal oxide coating types was also supported by the taxonomic classification of the shotgun metagenomics-derived contigs (Figure 5), and by the distribution of genes encoding for proteins involved in the oxidation of iron, ammonium, and manganese (Figure 7). The relative abundance of families commonly associated to the oxidation of iron (*Gallionellaceae*; (Gülay et al., 2018)) and nitrogen (*Nitrosomonadaceae* and *Nitrospiraceae*; [65]) in RSFs were higher in the top and downstream sections of each DWTP, respectively (Figure S 1). Moreover, their distribution within each compartment was relatively homogeneous (Figure 5) suggesting that microbial growth on the available substrates in each section is slower compared to the frequency of backwash filter media mixing. Similar spatial separation between iron and ammonium removal (Bourgine et al., 1994; de Vet et al., 2009; Sharma et al., 2005) but low heterogeneity in genome-based microbial community compositions have been observed along the height of different filters previously (Bai et al., 2013; Tatari et al., 2017). de Vet et al., (2009) ascribed this phenomenon to the accumulation of iron hydroxide flocs in the filter media, and phosphate [68] or copper [69] limitation have also been shown to hinder nitrification in RSFs. While the direct impact of iron oxides needs further investigation, our work allows to rule out the impact of nutrient limitations in the investigated DWTPs as full nitrification was not suppressed but simply spatially delayed.

Taken together, these results provide solid evidence that irrespective of treatment configuration, being it a dual-media single filter or single-media double filter setup, processes compartmentalize along filter heights. The fact that anthracite and quartz sand remained clearly separated in the single filter after over one year of operation also proves the effectiveness of dual-media filtration in spatially separating processes, and its equivalence to two filters in series. Moreover, the homogeneity of media coating and genome-based

microbial community composition within each compartment highlights the process-wise relevance of backwashing filter media mixing.

3.4.2. 4.2. Protein abundance profiles reflect biological activity stratification and substrate gradients

In stark contrast to the clear intra-compartment homogeneity, *in situ* iron, ammonium and manganese concentration profiles (Figure 2) and *ex situ* biological ammonium oxidation rates displayed a strongly stratified profile within the different filter compartments (Figure 4). To investigate the discrepancy between the stratified activities and the homogeneous metagenome-based distribution of iron-, ammonia-, and manganese-oxidizing genes (Figure 7), we employed shotgun metaproteomics to quantify the relative abundance of the encoded proteins along the filter heights as proxy for *in situ* biological activity.

Stratification patterns in *ex situ* and *in situ* ammonia oxidation rates, similar to the ones observed in SF and DF, have been reported in sand filters treating water with[14,70] and without[71] iron, and have been attributed to the progressive decrease in ammonium concentration along the filter height[67]. We detected higher protein-based relative abundances of putative nitrifying microorganisms in the downstream sections where most ammonia oxidation occurs, and we even observed a clear stratification in DF2 where all three investigated filter sections were devoid of iron (Figure 6). Importantly, the same decreasing trend could also be observed in the abundance of the core enzymes of nitrification, *i.e.*, ammonia monooxygenase (AmoABC), nitrite oxidoreductase (NxrAB) and nitrifier-assigned nitrite reductase (NirK/NirS), used here as proxy for the actual nitrifying activity of the microbial community (Figure 7). In analogy, the protein-based relative abundance of putative iron-oxidizing bacteria was the highest in the anthracite layer of SF (Figure 6), the only section where contigs of the *Gallionellaceae* family, the most common iron-oxidizing bacteria [72], were found. In terms of specific enzymes, the only detected Fe-oxidizing protein with a proven function was the *c*-type cytochrome Cyc2[73], a protein reported to be conserved in most neutrophilic iron oxidizers[74]. No other iron-oxidizing protein was detected and, likely due to the still limited biochemical characterization of this process, only few of the known iron-oxidizing genes reviewed by Garber et

al. (2020) were found. The surprisingly low relative abundance of proteins assigned to putative iron oxidizers in DF1 (Figure 6) could in principle suggest a dominance of abiotic processes controlling iron oxidation in this filter. However, the overall protein recovery in DF1 was significantly lower than in all other sections. This could possibly be ascribed to iron oxides hindering protein extraction, as seen by Barco & Edwards (2014), yet this was not encountered in the iron-removing SF_t section. Thus, the reason for the low protein yield in DF1 as well as the extend of contribution of biological iron oxidation to overall iron removal deserve further investigation. Ultimately, the absence of proteins involved in manganese oxidation, despite the presence of the corresponding genes, suggests an abiotic-dominated process in strong agreement with the homogeneously distributed, first-order rate constants (Figure 3).

In conclusion, the quantification of expressed proteins allowed us to resolve the often reported dichotomy between, on the one hand, the intra-compartment homogeneity of the mineral coating and genome-based microbial community composition and, on the other, the marked stratification of the concentration profiles and biological activities. We hypothesize that backwashing results in mixing and homogenization of the filter media and thereby exposes the attached microorganisms to a different substrate load. In response, microorganisms adjust their metabolic fluxes by adapting their protein pool at a faster rate than the mixing frequency. Conversely, the actual microbial growth between mixing is minimal and does not result in detectable changes at the genome level. Beyond rapid sand filters, these results prove the potential of metagenome-guided metaproteomics as a powerful tool to understand metabolic interactions in highly dynamic ecosystems.

3.5. CONCLUSIONS

In this work, we compared two full-scale drinking water treatment plants to resolve the interaction between the physicochemical and biological processes controlling ammonium, iron and manganese removal. The first plant employed a dual-bed (anthracite and quartz sand) single filter, the second two single-bed quartz sand filters in series. Both plants treated groundwater with similar chemical composition. The combination of biological activity measurements,

mineral coating characterization, and multi-omics profiling led to the following conclusions:

- both systems exhibited comparable performances and clear process compartmentalization, with iron being fully removed in the first, and ammonium and manganese primarily in the downstream sections;

- the mineral composition of the media coating reflected the compartmentalization of processes, *i.e.*, iron and manganese oxides dominated the first and downstream sections of each system, respectively;

- the homogeneity of media coating and genome-based composition of the microbial communities within each compartment highlighted the process-wise relevance of backwashing filter media mixing;

- only protein abundance profiles reflected the intra-compartment removal stratification, strongly highlighting the potential of metaproteomic approaches for studying highly dynamic ecosystems;

- dual-media single filters and series of single-media filters are equivalent from an operational and ecological perspective, and anthracite and sand remain separated despite frequent backwashing.

REFERENCES

1. W.W.J.M. de Vet. Biological drinking water treatment of anaerobic groundwater in trickling filters. (TU Delft, 2011).

2. Giordano, M. Global Groundwater? Issues and Solutions. *Annu. Rev. Environ. Resour.* **34**, 153–178 (2009).

3. Katsanou, K. & Karapanagioti, H. K. Surface water and groundwater sources for drinking water. *Handb. Environ. Chem.* **67**, 1–19 (2019).

4. Bourgine, F. P., Gennery, M., Chapman, J. I., Kerai, H., Green, J. G., Rap, R. J., Ellis, S. & Gaumard, C. Biological Processes at Saints Hill Water-Treatment Plant, Kent. *Water Environ. J.* **8**, 379–391 (1994).

5. Van Beek, C. G. E. M., Hiemstra, T., Hofs, B., Nederlof, M. M., Van Paassen, J. A. M. & Reijnen, G. K. Homogeneous, heterogeneous and biological oxidation of iron(II) in rapid sand filtration. *J. Water Supply Res. Technol. - AQUA* **61**, 1–13 (2012).

6. Breda, I. L., Søborg, D. A., Ramsay, L. & Roslev, P. Manganese removal processes during start-up of inoculated and non-inoculated drinking water biofilters. *Water Qual. Res. J.* **54**, 47–56 (2019).

7. Tekerlekopoulou, A. G., Pavlou, S. & Vayenas, D. V. Removal of ammonium, iron and manganese from potable water in biofiltration units: A review. *J. Chem. Technol. Biotechnol.* **88**, 751–773 (2013).

8. Gülay, A., Musovic, S., Albrechtsen, H. J., Al-Soud, W. A., Sørensen, S. J. & Smets, B. F. Ecological patterns, diversity and core taxa of microbial communities in groundwater-fed rapid gravity filters. *ISME J.* **10**, 2209–2222 (2016).

9. Kihn, A., Laurent, P. & Servais, P. Measurement of potential activity of fixed nitrifying bacteria in biological filters used in drinking water production. 161–166 (2000).

10. Lydmark, P., Lind, M., Sörensson, F. & Hermansson, M. Vertical distribution of nitrifying populations in bacterial biofilms from a full-scale nitrifying trickling filter. *Environ. Microbiol.* **8**, 2036–2049 (2006).

11. Qin, Y. Y., Li, D. T. & Yang, H. Investigation of total bacterial and ammonia-oxidizing bacterial community composition in a full-scale aerated submerged biofilm reactor for drinking water pretreatment in China. *FEMS Microbiol. Lett.* **268**, 126–134 (2007).

12. de Vet, W., Dinkla, I. J. T., Muyzer, G., Rietveld, L. C. & van Loosdrecht, M. C. M. Molecular characterization of microbial

populations in groundwater sources and sand filters for drinking water production. *Water Res*. **43**, 182–194 (2009).

13. Bai, Y., Liu, R., Liang, J. & Qu, J. Integrated Metagenomic and Physiochemical Analyses to Evaluate the Potential Role of Microbes in the Sand Filter of a Drinking Water Treatment System. *PLoS One* **8**, (2013).

14. Tatari, K., Smets, B. F. & Albrechtsen, H. J. Depth investigation of rapid sand filters for drinking water production reveals strong stratification in nitrification biokinetic behavior. *Water Res*. **101**, 402–410 (2016).

15. Tatari, K., Musovic, S., Gülay, A., Dechesne, A., Albrechtsen, H. J. & Smets, B. F. Density and distribution of nitrifying guilds in rapid sand filters for drinking water production: Dominance of Nitrospira spp. *Water Res*. **127**, 239–248 (2017).

16. Palomo, A., Jane Fowler, S., Gülay, A., Rasmussen, S., Sicheritz-Ponten, T. & Smets, B. F. Metagenomic analysis of rapid gravity sand filter microbial communities suggests novel physiology of Nitrospira spp. *ISME J*. **10**, 2569–2581 (2016).

17. Pinto, A. J., Marcus, D. N., Ijaz, U. Z., Bautista-de lose Santos, Q. M., Dick, G. J. & Raskin, L. Metagenomic Evidence for the Presence of Comammox Nitrospira -Like Bacteria in a Drinking Water System. *mSphere* **1**, (2016).

18. Poghosyan, L., Koch, H., Frank, J., van Kessel, M. A. H. J., Cremers, G., van Alen, T., Jetten, M. S. M., Op den Camp, H. J. M. & Lücker, S. Metagenomic profiling of ammonia- and methane-oxidizing microorganisms in two sequential rapid sand filters. *Water Res*. **185**, 116288 (2020).

19. Ilbert, M. & Bonnefoy, V. Insight into the evolution of the iron oxidation pathways. *Biochim. Biophys. Acta - Bioenerg*. **1827**, 161–175 (2013).

20. Romano, C. A., Zhou, M., Song, Y., Wysocki, V. H., Dohnalkova, A. C., Kovarik, L., Paša-Tolić, L. & Tebo, B. M. Biogenic manganese oxide nanoparticle formation by a multimeric multicopper oxidase Mnx. *Nat. Commun*. **8**, 1–8 (2017).

21. Qin, S., Ma, F., Huang, P. & Yang, J. Fe (II) and Mn (II) removal from drilled well water: A case study from a biological treatment unit in Harbin. *Desalination* **245**, 183–193 (2009).

22. Burger, M. S., Krentz, C. A., Mercer, S. S. & Gagnon, G. A. Manganese removal and occurrence of manganese oxidizing bacteria in full-scale biofilters. *J. Water Supply Res. Technol. - AQUA* **57**, 351–359

(2008).

23. Yang, L., Li, X., Chu, Z., Ren, Y. & Zhang, J. Distribution and genetic diversity of the microorganisms in the biofilter for the simultaneous removal of arsenic, iron and manganese from simulated groundwater. *Bioresour. Technol.* **156**, 384–388 (2014).

24. Nitzsche, K. S., Weigold, P., Lösekann-Behrens, T., Kappler, A. & Behrens, S. Microbial community composition of a household sand filter used for arsenic, iron, and manganese removal from groundwater in Vietnam. *Chemosphere* **138**, 47–59 (2015).

25. Yang, H., Yan, Z., Du, X., Bai, L., Yu, H., Ding, A., Li, G., Liang, H. & Aminabhavi, T. M. Removal of manganese from groundwater in the ripened sand filtration: Biological oxidation versus chemical auto-catalytic oxidation. *Chem. Eng. J.* **382**, 123033 (2020).

26. Marcus, D. N., Pinto, A., Anantharaman, K., Ruberg, S. A., Kramer, E. L., Raskin, L. & Dick, G. J. Diverse manganese(II)-oxidizing bacteria are prevalent in drinking water systems. *Environ. Microbiol. Rep.* **9**, 120–128 (2017).

27. Bruins, J. H., Petrusevski, B., Slokar, Y. M., Wübbels, G. H., Huysman, K., Wullings, B. A., Joris, K., Kruithof, J. C. & Kennedy, M. D. Identification of the bacterial population in manganese removal filters. *Water Sci. Technol. Water Supply* **17**, 842–850 (2017).

28. Gülay, A., Çekiç, Y., Musovic, S., Albrechtsen, H. J. & Smets, B. F. Diversity of Iron Oxidizers in Groundwater-Fed Rapid Sand Filters: Evidence of Fe(II)-Dependent Growth by Curvibacter and Undibacterium spp. *Front. Microbiol.* **9**, 2808 (2018).

29. Breda, I. L., Ramsay, L., Søborg, D. A., Dimitrova, R. & Roslev, P. Manganese removal processes at 10 groundwater fed full-scale drinking water treatment plants. *Water Qual. Res. J. Canada* **54**, 326–337 (2019).

30. Hu, W., Liang, J., Ju, F., Wang, Q., Liu, R., Bai, Y., Liu, H. & Qu, J. Metagenomics Unravels Differential Microbiome Composition and Metabolic Potential in Rapid Sand Filters Purifying Surface Water Versus Groundwater. *Environ. Sci. Technol.* **54**, 5206 (2020).

31. Van Den Bossche, T. *et al.* Critical Assessment of MetaProteome Investigation (CAMPI): a multi-laboratory comparison of established workflows. *Nat. Commun.* **12**, (2021).

32. Wilmes, P. & Bond, P. L. The application of two-dimensional polyacrylamide gel electrophoresis and

downstream analyses to a mixed community of prokaryotic microorganisms. *Environ. Microbiol.* **6**, 911–920 (2004).

33. Kleiner, M. Metaproteomics: Much More than Measuring Gene Expression in Microbial Communities. *mSystems* **4**, (2019).

34. Kleiner, M., Thorson, E., Sharp, C. E., Dong, X., Liu, D., Li, C. & Strous, M. Assessing species biomass contributions in microbial communities via metaproteomics. *Nat. Commun. 2017 81* **8**, 1–14 (2017).

35. Kleikamp, H. B. C., Pronk, M., Tugui, C., Guedes da Silva, L., Abbas, B., Lin, Y. M., van Loosdrecht, M. C. M. & Pabst, M. Database-independent de novo metaproteomics of complex microbial communities. *Cell Syst.* **12**, 375-383.e5 (2021).

36. Stokke, R., Roalkvam, I., Lanzen, A., Haflidason, H. & Steen, I. H. Integrated metagenomic and metaproteomic analyses of an ANME-1-dominated community in marine cold seep sediments. *Environ. Microbiol.* **14**, 1333–1346 (2012).

37. Schulze, W. X., Gleixner, G., Kaiser, K., Guggenberger, G., Mann, M. & Schulze, E. D. A proteomic fingerprint of dissolved organic carbon and of soil particles. *Oecologia* **142**, 335–343 (2005).

38. Kleikamp, H. B. C., Grouzdev, D., Schaasberg, P., Valderen, R. van, Zwaan, R. van der, Wijgaart, R. van de, Lin, Y., Abbas, B., Pronk, M., Loosdrecht, M. C. M. van & Pabst, M. Comparative metaproteomics demonstrates different views on the complex granular sludge microbiome. *bioRxiv* 2022.03.07.483319 (2022).

39. Hanson, B. T. & Madsen, E. L. In situ expression of nitrite-dependent anaerobic methane oxidation proteins by Candidatus Methylomirabilis oxyfera co-occurring with expressed anammox proteins in a contaminated aquifer. *Environ. Microbiol. Rep.* **7**, 252–264 (2015).

40. Wilmes, P., Heintz-Buschart, A. & Bond, P. L. A decade of metaproteomics: Where we stand and what the future holds. *Proteomics* **15**, 3409–3417 (2015).

41. Ramsay, L., Du, F., Lund, M., He, H. & Søborg, D. A. Grain displacement during backwash of drinking water filters. *Water Sci. Technol. Water Supply* **21**, 356–367 (2021).

42. Uhl, W. & Gimbel, R. Dynamic modeling of ammonia removal at low temperatures in drinking water rapid filters. in *Water Science and Technology* vol. 41

199–206 (IWA Publishing, 2000).

43. Vries, D., Bertelkamp, C., Schoonenberg Kegel, F., Hofs, B., Dusseldorp, J., Bruins, J. H., de Vet, W. & van den Akker, B. Iron and manganese removal: Recent advances in modelling treatment efficiency by rapid sand filtration. *Water Res.* **109**, 35–45 (2017).

44. Gude, J. C. J., Rietveld, L. C. & van Halem, D. Fate of low arsenic concentrations during full-scale aeration and rapid filtration. *Water Res.* **88**, 566–574 (2016).

45. Claff, S. R., Sullivan, L. A., Burton, E. D. & Bush, R. T. A sequential extraction procedure for acid sulfate soils: Partitioning of iron. *Geoderma* **155**, 224–230 (2010).

46. APHA. 3500-Fe IRON - Standard Methods For the Examination of Water and Wastewater. https://www.standardmethods.org/doi/full/10.2105/SMWW.2882.055 (2018).

47. Bolger, A. M., Lohse, M. & Usadel, B. Trimmomatic: a flexible trimmer for Illumina sequence data. *Bioinformatics* **30**, 2114–2120 (2014).

48. Andrews, S. FastQC: A Quality Control Tool for High Throughput Sequence Data [Online]. at http://www.bioinformatics.babraham.ac.uk/projects/fastqc/ (2010).

49. Li, D., Liu, C. M., Luo, R., Sadakane, K. & Lam, T. W. MEGAHIT: An ultra-fast single-node solution for large and complex metagenomics assembly via succinct de Bruijn graph. *Bioinformatics* **31**, 1674–1676 (2015).

50. Vasimuddin, M., Misra, S., Li, H. & Aluru, S. Efficient architecture-aware acceleration of BWA-MEM for multicore systems. in *Proceedings - 2019 IEEE 33rd International Parallel and Distributed Processing Symposium, IPDPS 2019* 314–324 (Institute of Electrical and Electronics Engineers Inc., 2019).

51. Li, H., Handsaker, B., Wysoker, A., Fennell, T., Ruan, J., Homer, N., Marth, G., Abecasis, G. & Durbin, R. The Sequence Alignment/Map format and SAMtools. **25**, 2078–2079 (2009).

52. Von Meijenfeldt, F. A. B., Arkhipova, K., Cambuy, D. D., Coutinho, F. H. & Dutilh, B. E. Robust taxonomic classification of uncharted microbial sequences and bins with CAT and BAT. *Genome Biol.* **20**, 1–14 (2019).

53. Albertsen, M., Hugenholtz, P., Skarshewski, A., Nielsen, K. L., Tyson, G. W. & Nielsen, P. H. Genome sequences of rare,

uncultured bacteria obtained by differential coverage binning of multiple metagenomes. *Nat. Biotechnol.* **31**, 533–538 (2013).

54. Kanehisa, M., Sato, Y. & Morishima, K. BlastKOALA and GhostKOALA: KEGG Tools for Functional Characterization of Genome and Metagenome Sequences. *J. Mol. Biol.* **428**, 726–731 (2016).

55. Garber, A. I., Nealson, K. H., Okamoto, A., McAllister, S. M., Chan, C. S., Barco, R. A. & Merino, N. FeGenie: A Comprehensive Tool for the Identification of Iron Genes and Iron Gene Neighborhoods in Genome and Metagenome Assemblies. *Front. Microbiol.* **11**, 37 (2020).

56. Hall, B. G. Building phylogenetic trees from molecular data with MEGA. *Mol. Biol. Evol.* **30**, 1229–1235 (2013).

57. Purkhold, U., POMMERENING-ROSER, A., JURETSCHKO, S., SCHMID, M. C. & WAGNER, H.-P. K. M. Phylogeny of All Recognized Species of Ammonia Oxidizers Based on Comparative 16S rRNA and. *Society* **66**, 5368–5382 (2000).

58. Kalyuzhnaya, M. G., Gomez, O. A. & Murrell, J. C. *The Methane-Oxidizing Bacteria (Methanotrophs)*. (2019).

59. Rost, B. Twilight zone of protein sequence alignments. *Protein Eng. Des. Sel.* **12**, 85–94 (1999).

60. Buchfink, B., Xie, C. & Huson, D. H. Fast and sensitive protein alignment using DIAMOND. *Nat. Methods 2014 121* **12**, 59–60 (2014).

61. Katsoyiannis, I. A. & Zouboulis, A. I. Biological treatment of Mn(II) and Fe(II) containing groundwater: Kinetic considerations and product characterization. *Water Res.* **38**, 1922–1932 (2004).

62. Gouzinis, A., Kosmidis, N., Vayenas, D. V. & Lyberatos, G. Removal of Mn and simultaneous removal of NH3, Fe and Mn from potable water using a trickling filter. *Water Res.* **32**, 2442–2450 (1998).

63. Pacini, V. A., Ingallinella, A. M. & Sanguinetti, G. Removal of iron and manganese using biological roughing up flow filtration technology. *Water Res.* **39**, 4463–4475 (2005).

64. Gülay, A., Tatari, K., Musovic, S., Mateiu, R. V., Albrechtsen, H. J. & Smets, B. F. Internal porosity of mineral coating supports microbial activity in rapid sand filters for groundwater treatment. *Appl. Environ. Microbiol.* **80**, 7010–7020 (2014).

65. Fowler, S. J., Palomo, A., Dechesne, A., Mines, P. D. & Smets, B. F. Comammox Nitrospira are abundant ammonia oxidizers in diverse groundwater-fed rapid sand filter communities. *Environ.*

Microbiol. **20**, 1002–1015 (2018).

66. Sharma, S. K., Petrusevski, B. & Schippers, J. C. Biological iron removal from groundwater: A review. *J. Water Supply Res. Technol. - AQUA* **54**, 239–247 (2005).

67. de Vet, W., Rietveld, L. C. & Van Loosdrecht, M. C. M. Influence of iron on nitrification in full-scale drinking water trickling filters. *J. Water Supply Res. Technol. - AQUA* **58.4**, 247–256 (2009).

68. de Vet, W., Van Loosdrecht, M. C. M. & Rietveld, L. C. Phosphorus limitation in nitrifying groundwater filters. *Water Res.* **46**, 1061–1069 (2012).

69. Wagner, F. B., Nielsen, P. B., Boe-Hansen, R. & Albrechtsen, H. J. Copper deficiency can limit nitrification in biological rapid sand filters for drinking water production. *Water Res.* **95**, 280–288 (2016).

70. Tatari, K., Smets, B. F. & Albrechtsen, H. J. A novel bench-scale column assay to investigate site-specific nitrification biokinetics in biological rapid sand filters. *Water Res.* **47**, 6380–6387 (2013).

71. Lee, C. O., Boe-Hansen, R., Musovic, S., Smets, B., Albrechtsen, H. J. & Binning, P. Effects of dynamic operating conditions on nitrification in biological rapid sand filters for drinking water treatment. *Water Res.* **64**, 226–236 (2014).

72. de Vet, W., Dinkla, I. J. T., Rietveld, L. C. & van Loosdrecht, M. C. M. Biological iron oxidation by Gallionella spp. in drinking water production under fully aerated conditions. *Water Res.* **45**, 5389–5398 (2011).

73. Castelle, C., Guiral, M., Malarte, G., Ledgham, F., Leroy, G., Brugna, M. & Giudici-Orticoni, M. T. A new iron-oxidizing/O2-reducing supercomplex spanning both inner and outer membranes, isolated from the extreme acidophile Acidithiobacillus ferrooxidans. *J. Biol. Chem.* **283**, 25803–25811 (2008).

74. McAllister, S. M., Polson, S. W., Butterfield, D. A., Glazer, B. T., Sylvan, J. B. & Chan, C. S. Validating the Cyc2 Neutrophilic Iron Oxidation Pathway Using Meta-omics of Zetaproteobacteria Iron Mats at Marine Hydrothermal Vents. *mSystems* **5**, (2020).

75. Barco, R. A. & Edwards, K. J. Interactions of proteins with biogenic iron oxyhydroxides and a new culturing technique to increase biomass yields of neutrophilic, iron-oxidizing bacteria. *Front. Microbiol.* **5**, 259 (2014).

Tant de bo pogués,
veure'm a través
dels ulls dels qui m'estimen
per estimar-me una mica més

"*CANDIDATUS* SIDEROPHILUS NITRATIREDUCENS": A PUTATIVE NAP-DEPENDENT NITRATE-REDUCING IRON OXIDIZER WITHIN THE NEW ORDER SIDEROPHILIALES

4

ABSTRACT

Nitrate leaching from agricultural soils is increasingly found in groundwater, a primary source of drinking water worldwide. This nitrate influx can potentially stimulate the biological oxidation of iron in anoxic groundwater reservoirs. Nitrate-dependent iron- oxidizing (NDFO) bacteria have been extensively studied in laboratory settings, yet their ecophysiology in natural environments remains largely unknown. To this end, we established a pilot-scale filter on nitrate-rich groundwater to elucidate the structure and metabolism of nitrate-reducing iron-oxidizing microbiomes under oligotrophic conditions mimicking natural groundwaters. The enriched community stoichiometrically removed iron and nitrate consistently with the NDFO metabolism. Genome-resolved metagenomics revealed the underlying metabolic network between the dominant iron-dependent denitrifying autotrophs and the less abundant organoheterotrophs. The most abundant genome belonged to a new Candidate order, named Siderophiliales. This new species, "*Candidatus* Siderophilus nitratireducens," carries genes central genes to iron oxidation (cytochrome *c cyc2*), carbon fixation (*rbc*), and for the sole periplasmic nitrate reductase (*nap*). Using thermodynamics, we demonstrate that iron oxidation coupled to nap based dissimilatory reduction of nitrate to nitrite is energetically favorable under realistic Fe^{3+}/Fe^{2+} and NO_3^-/NO_2 – concentration ratios. Ultimately, by bridging the gap between laboratory investigations and nitrate real-world conditions, this study provides insights into the intricate interplay between nitrate and iron in groundwater ecosystems, and expands our understanding of NDFOs taxonomic diversity and ecological role.

KEYWORDS

- NDFO
- Iron
- Nitrate
- Groundwater

Published as:

Corbera-Rubio, F., Stouten, G. R., Bruins, J., Dost, S. F., Merkel, A. Y., Müller, S., van Loosdrecht, M. C. M., van Halem, D. & Laureni, M. " Candidatus Siderophilus nitratireducens": a putative nap -dependent nitrate-reducing iron oxidizer within the new order Siderophiliales. *ISME Commun.* **4**, 8 (2024).

"CANDIDATUS SIDEROPHILUS NITRATIREDUCENS": A PUTATIVE NAP-DEPENDENT NITRATE-REDUCING IRON-OXIDIZER WITHIN THE NEW ORDER SIDEROPHILIALES

4.1. INTRODUCTION

Globally, approximately one third of the nitrogen applied to agricultural soils is lost via leaching to the surrounding waterbodies [1]. This has led to elevated nitrate (NO_3^-) levels in anoxic groundwaters, a primary source of drinking water worldwide [2]. Owing to population growth and agriculture intensification, nitrate concentrations in subsurface waters are expected to continue increasing [3]. Besides its direct impact on human health [4], nitrate can significantly alter the biogeochemistry of groundwater reservoirs [5]. Nitrate promotes the oxidation of sulfide and in particular of iron (Fe) – the most prevalent groundwater contaminant – leading to the formation of oxides with high adsorption capacity and the emission of greenhouse gases [6]. Despite these implications, the consequences of nitrate-iron interactions on ecosystems and drinking water production systems remain largely unexplored. A detailed understanding of the underlying principles is paramount for anticipating and mitigating current and future challenges, as well as for exploring potential synergies and biotechnological opportunities.

Nitrate-dependent iron-oxidizing (NDFO) bacteria, also referred to as nitrate-reducing iron-oxidizers (NRFO) [7,8], couple the anoxic reduction of nitrate to the oxidation of Fe^{2+} (eq.1). Since their discovery in 1996 by Straub et al. (1996), NDFO microorganisms have been the focus of extensive research both in pure and mixed cultures (reviewed in [10]), and several complete genomes are already publicly available [11,12]. The metabolic versatility of NDFO bacteria spans from lithoautotrophic to mixotrophic growth [10], to partial denitrification using nitric oxide (NO) [13] and nitrous oxide (N_2O) [11] as terminal electron acceptors. At the same time, due to the inherently low energetic yield of iron oxidation, NDFO bacteria live close to the thermodynamic edge [14]. Their fitness is highly dependent on environmental factors such as substrate and product availability, pH and temperature [15]. Chemical reactions - such as the quasi-instantaneous precipitation of the biologically formed Fe^{3+} - can play a pivotal role by modulating iron and nitrogen concentrations [16]. However, our current understanding is largely based on laboratory settings, and does not necessarily reflect the complexity of natural and engineered ecosystems where several (a)biotic reactions occur simultaneously at temperatures significantly lower than tested to date [17].

$$10Fe^{2+} + 2NO_3^- + 24\,H_2O \rightarrow 10Fe(OH)_3 + N_2 + 18H^+ \qquad \text{eq. 1}$$

To address these knowledge gaps, we established a pilot-scale filter on anoxic groundwater containing both Fe^{2+} and NO_3^-. The emulated groundwater conditions allowed for the establishment of a microbial enrichment that simultaneously removed Fe^{2+} and NO_3^-. In depth metagenomic analysis of the steady-state community revealed a new order-level NDFO lineage, deepening our understanding of their taxonomic diversity and ecological roles. Overall, our study bridges the gap between laboratory studies and real-world conditions, and offers a nuanced view on the intricate interplay between nitrate and iron in groundwater ecosystems.

4.2. MATERIALS AND METHODS

4.2.1. Groundwater and pilot-scale filter characteristics

An iron reducing microbial community was enriched anoxically on the granular activated carbon of a 10-L pilot-scale filter in Emmen (the Netherlands) (Figure S1, Figure S2 and Table S1). The media was devoid of any previously formed biofilm. The anoxic, nitrate-rich groundwater (-75,2 ± 28.4 mV) featured constant Fe^{2+} and NO_3^- concentrations, 236 ± 4 µM and 8.1 ± 2.1 µM respectively (Table 1). Oxygen was consistently below quantification limit (3 µM). The groundwater pH and temperature were 6.7 ± 0.2 and 10.5 ± 0.1 °C, respectively. The filter was operated at a filtration flowrate of 3.8 m·h^{-1} (29.6 L·h^{-1}) during 120 days. After 75 days of steady-state operation, the influent nitrate concentration was manually increased in four steps up to 83.8 ± 0.6 µM, when the system changed from nitrate (NO_3^- < 1 µM) to iron limiting conditions (Fe^{2+} < 4 µM).

Table 1. Influent and effluent water characteristics corresponding to average and standard deviation of daily measurements of days 21-77, during the nitrate-limited steady-state. Fe^{3+} was calculated as described in the following section.

Parameter	Units	Value	Value
		Influent	*Effluent*
pH	-	6.9 ± 0.4	6.7 ± 0.1
T	˚C	10.5 ± 0.1	10.9 ± 0.6
ORP	mV	-64 ± 17	-58 ± 18
O_2	µmol·L^{-1}	<3*	<3*
NH_4^+	µmol·L^{-1}	11 ± 1.0	11 ± 8.1

NO_2^-	$\mu mol \cdot L^{-1}$	<0.2*	<0.2*
NO_3^-	$\mu mol \cdot L^{-1}$	8.1 ± 2.1	<1
Fe^{2+}	$\mu mol \cdot L^{-1}$	236 ± 4	178 ± 5
Fe^{3+}	$\mu mol \cdot L^{-1}$	$2 \cdot 10^{-12}$	-
DOC	$mg \cdot L^{-1}$	3.1 ± 0.1	2.0 ± 0.2

**Below detection limit*

4.2.2. Dissolved Fe^{3+} estimation

At pH 7, Fe^{3+} has a markedly low solubility and precipitates as iron oxyhydroxide ($Fe(OH)_3$). Thermodynamically, this phase transition favours the oxidation of Fe^{2+} to Fe^{3+}, and the resulting low Fe^{3+} concentration is the primary driving force of eq. 1 [18]. In our filter, the dissolved concentration of the Fe^{3+}, resulting from Fe^{2+} oxidation, was always below detection limit ($0.01 mg \cdot l^{-1}$). To discuss the thermodynamic feasibility of the NDFO process, we estimated the steady-state $[Fe^{3+}]/[Fe^{2+}]$ ratio following the method proposed by Gorski et al. (2016), which assumes thermodynamic equilibrium between $[Fe^{2+}]$ – $[Fe^{3+}]$ – [FeOx] phases based on the fact that the hydroxylation of dissolved Fe^{3+} is quasi-instantaneous at pH > 3 [20]. Consequently, the following equation can be used to determine the Fe^{3+} concentration as function of pH and the solid solubility constant.

$$\{Fe^{3+}_{(aq)}\}\{OH^-\}^3 = K_{sp}$$

The most abundant iron oxide in the sand filter was amorphous ferrihydrite (SI 4 and 5), with a K_{sp} of 10^{-39} [20]. Therefore:

$$\{Fe^{3+}_{aq}\} = \frac{10^{-39}}{(10^{-7.1})^3} = 2 \cdot 10^{-18}\ \mathrm{M}$$

4.2.3. Analytic procedures

Samples for ammonium, nitrite, and nitrate quantification were immediately filtered through a 0.2 µm nanopore filter and measured within 12 h using photometric analysis (Gallery Discrete Analyzer, Thermo Fischer Scientific, Waltham, Massachusetts, USA). Samples for dissolved iron were filtered through a 0.2 µm nanopore filter, acidified to pH<2 with H_2SO_4, and quantified by ICP-MS (Analytik Jena, Jena, Germany). Temperature, pH, oxidation-reduction

potential (ORP), and dissolved oxygen concentration (DO) were monitored daily using a HI9829-01042 multiparameter analyser (Hanna Instruments, Smithfield, RI, USA) in the raw water, after nitrate dosage and in the effluent.

4.2.4. Biomass sampling, DNA extraction and quality control

Immediately after the end of the experiment, the filter was emptied and the medium grains were completely mixed. A small volume of grains was used for DNA extraction. Nucleic acid extraction was carried out using DNeasy PowerSoil Pro Kit (QIAGEN, Hilden, Germnay) following manufacturer instructions. To improve DNA recovery and avoid the interference of carbon with the extraction, 25 µL of 20 $g \cdot l^{-1}$ autoclaved (20 min, 121° Celsius, 2 bar) skimmed milk solution (Sigma Aldrich, Saint Louis, MO, USA) were added to the extraction tube. After extraction, DNA was concentrated to 7.68 ng $DNA \cdot \mu l^{-1}$ using Microcon centrifugal filter units YM-100 (MilliporeSigma, Burlington, MA, USA) following the manufacturer's instructions. DNA was quantified with the Qubit 4 Fluorometer and Qubit dsDNA HS assay kit (Invitrogen, Waltham, MA, USA) following the manufacturer's instructions. DNA purity was determined using a NanoDrop One Spectrophotometer (Thermo Fisher Scientific, Waltham, MA, USA).

4.2.5. Library preparation, sequencing and reads processing

Long-read and short-read DNA sequencing were carried out independently. Long-read library preparation was carried out using the ligation sequencing kit SQK-LSK 109 (Oxford Nanopore Technologies, Oxford, UK). R.9.4.1 flowcells on a GridION were used for sequencing. Raw data was basecalled in super-accurate mode using Guppy v.5.0.16 (https://nanoporetech.com). Raw reads were quality-filtered and trimmed using Filtlong (https://github.com/rrwick/Filtlong) to remove reads below 4000 kb and mean quality score below 80. Adapters were removed using Porechop v.0.2.3 (https://github.com/rrwick/Porechop).

Short-read library preparation was performed using the Nextera XT kit (Illumina, San Diego, CA, U.S.A.) according to the manufacturer's instructions. The libraries were pooled, denatured, and sequenced with Illumina MiSeq (San Diego, CA, USA). Paired end sequencing of 2 x 300 base pairs was performed

using the MiSeq Reagent Kit v3 (San Diego, CA, USA) according to the manufacturer's instructions. Raw sequencing data was quality-filtered and trimmed using Trimmomatic v0.39 (HEADCROP:16 LEADING:3 TRAILING:5 SLIDINGWINDOW:4:10 CROP:240 MINLEN:35) [21]. Sequencing data quality was analyzed using FastQC v0.11.7 before and after trimming [22].

4.2.6. Reads assembly and binning

Reads assembly and binning were done as in [23] with minor modifications. Long-reads were assembled using Flye v. 2.9-b1768 [24] with the '–meta' setting enabled and the '–nano-hq' option. Polishing was carried out with Minimap2 v.2.17 [25], Racon v.1.3.3 [26], Medaka v.1.4.4 (two rounds) (https://github.com/nanoporetech/medaka). At the end, short-reads were incorporated in a final round of polishing with Racon. Both long- and short- raw reads were independently mapped back to the assembled contigs using BWA-MEM2 [27]. SAMtools v1.14 was used to determine contig coverage and for indexing with default settings [28] .

Automated binning was carried out with the long-reads assembly (polished with short-reads) using MetaBAT2 v. 2.12.1 [29] with '-s 500000', MaxBin2 v. 2.2.7 [30], and Vamb v. 3.0.2 [31] with '-o C–minfasta 500000'. Additionally, contig coverage from the short-reads assembly was provided as input to the three binners to improve binning. Output integration and refinement was done in DAS Tool v. 1.1.2 [32] . CoverM v. 0.6.1 (https://github.com/wwood/CoverM) was applied to calculate the bin coverage (using the '-m mean' setting) and the relative abundance ('-m relative_abundance'). Additional manual bin polishing was done in R using mmgenome (https://github.com/MadsAlbertsen/mmgenome).

4.2.7. Assembly processing and gene annotation

The completeness and contamination of the genome bins were estimated using CheckM v. 1.1.2 [33]. The bins were classified using GDTB-Tk v. 1.5.0 [34] 202 database. Barrnap v 0.9 (https://github.com/tseemann/barrnap) and structRNAfinder [35] were used to predict 23S, 16S and 5S ribosomal RNA sequences, and transfer RNA sequences were determined using tRNAscan-SE v.20 [36] with *default* search mode. Bins were classified using the Minimum

Information about a Metagenome-Assembled Genome (MIMAG) standards [37]: high-quality bins were > 90 % complete and < 5 % contaminated, and contained full-length 23S, 16S and 5S ribosomal RNA genes and ≥ 18 transfer RNA genes. Bins with completeness > 50 % and contamination < 10 % were classified as medium-quality, and bins with completeness <50% and <10% contamination as low-quality bins. The remaining ones were considered contamination. 68% of the filtered reads rendered high- and medium-quality bins, 11% low-quality bins and 21.1% were unbinned.

The open reading frames (ORF) of the 10 resulting high-quality and 3 medium-quality bins with relative abundance > 0.5 % were predicted using Prodigal v2.6.3 [38] and functionally annotated with GhostKoala v2.2 [39] (Kyota Enciclopedia of Genes and Genomes; accessed March 2022). FeGenie [40] was used to improve the annotation of the iron metabolism using the metagenomics ('-meta') settings. To refine the annotation for MAG.13 (*Candidatus* Siderophilus nitratireducens), the genome was uploaded to the National Center for Biotechnology Information (NCBI) database Prokaryotic Genome Annotation Pipeline v6.1 [41]. Additionally, manual annotation of genes potentially relevant but not automatically annotated was done by aligning a set of manually selected sequences from UniProtKB against the translated ORFs from MAG.13 with local blastp v2.13 [42]. After annotation, all the predicted genes of interest (manually and automatically annotated) were translated and aligned against the Non-redundant protein sequences (nr) database from NCBI using blastp (accessed June 2022) and accepted only if the coverage was > 70 % [40] and the identity > 35 % [43].

RStudio v1.4.1106 was used for data analysis and visualization.

4.2.8. Phylogenetic tree construction

Genome-based phylogenetic reconstruction was done by using 120 bacterial single copy conservative marker genes, as described previously [34]. The trees were built using the IQ-TREE 2 [44] with fast model selection via ModelFinder [45] and ultrafast approximation for phylogenetic bootstrap [46], as well as approximate likelihood-ratio test for branches [47]. Whole genome comparison was conducted by using two different methods: Average Nucleotide Identity (ANI), using

JSpeciesWS web server and DNA-DNA Hybridization (DDH) by the Genome-to-Genome Distance Calculator 2.1 online tool (https://ggdc.dsmz.de/ggdc.php) [48].

4.3. RESULTS

4.3.1. Nitrate-dependent iron removal irrespective of the limiting nutrient

A pilot-scale, granular activated-carbon filter was fed with nitrate-rich anoxic groundwater for 120 days. Stable anoxic nitrate and iron removals were achieved after less than three weeks of operation and maintained for over 100 days (Figure 1). With nitrate as the limiting nutrient at both groundwater (8.9 ± 2.8 µM) and nitrate-amended concentrations (13.5 ± 1.5 and 20.2 ± 2.4 µM), effluent nitrate concentrations were consistently below detection limit (1 µM). Throughout the nitrate-limiting period, NO_3^- and Fe^{2+} were consumed at a 7.1 ± 1.4 Fe^{2+}:NO_3^- molar ratio (Figure S3). Oxygen was always below the quantification limit of 3 µM, and roughly 80 µC-mol dissolved organic carbon (DOC·l^{-1}) was consistently removed from the influent, likely due to Fe^{2+}-DOC complexes formation owing to the non-biodegradable nature of organic matter in the groundwater matrix (< 1.2 µC-mol·$^{l-1}$ assimilable organic matter). Ammonia consumption was negligible (<0.1 µM). Effluent nitrite concentrations stayed below the detection limit (<0.2 µM), while other denitrification intermediates – nitric oxide and nitrous oxide – were not measured. The observed consistent stoichiometric coupling between nitrate and iron removals strongly suggests Fe^{2+} oxidation to be primarily driven by microbial nitrate-reducing iron oxidation.

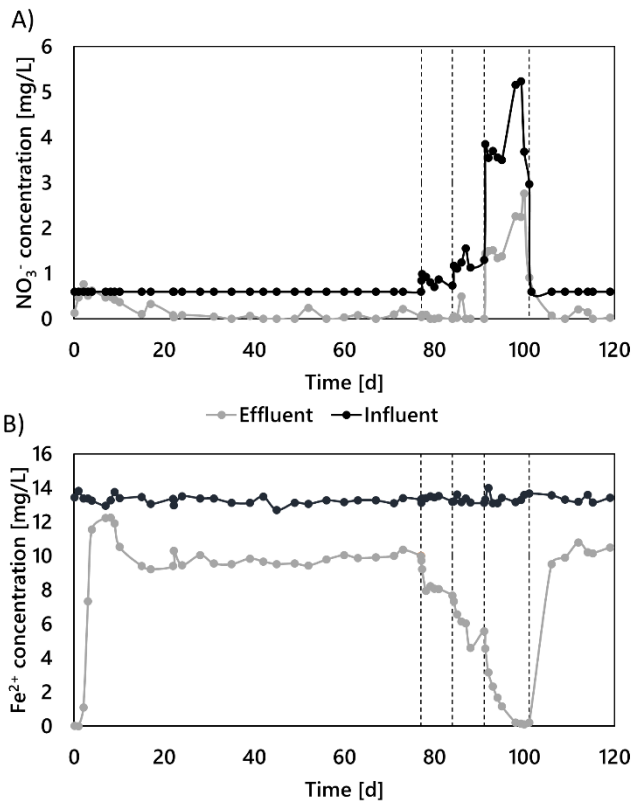

Figure 1. Simultaneous NO_3^- (A) and Fe^{2+}(B) removals in the groundwater-fed pilot-scale filter during the 120 days of continuous operation. The groundwater Fe^{2+} concentration was constant throughout the experiment (236 ± 4 µM). NO_3^- was dosed in the influent to increase the natural groundwater concentration in steps from 8.1 ± 2.1 to 20.2 ± 2.4 µM (NO_3^- limitation), and up to 83.8 ± 0.6 µM (Fe^{2+} limitation). Fe^{2+} and NO_3^- were proportionally removed throughout the whole experiment, regardless of the limiting nutrient (see Figure SI 3)

4.3.2. Microbial community dominated by iron oxidizers and denitrifiers

Metagenomic DNA sequencing yielded a total of 107,512 and 8,754,261 quality filtered short and long reads, respectively. After assembly and polishing, this resulted in 19,127 contigs with an N50 value of 15,927. Contigs binning resulted in 13 high (> 90% completeness and < 5% contamination; containing full-length 23S, 16S and 5S ribosomal RNA genes and ≥ 18 transfer RNA genes) and medium (completeness >50% and contamination <10%) quality metagenome assembled genomes (MAGs) as defined by [37] with a relative abundance exceeding 0.5% of the quality filtered long reads. Collectively, these 13 most abundant genomes accounted for 66.9% of the total quality filtered reads, and

Electron acceptor			Electron donor			Carbon fixation			Carbon metabolism		
Element	*Key genes*	*Presence*	*Element*	*Key genes*	*Presence*	*Pathway*	*Key genes*	*Presence*	*Pathway*	*Key genes*	*Presence*
Nitrogen	*nap* ABCD	+	Iron	*cyc2*	+	CBB	*rbc* LS form I	+	Gycolysis	*pfk*	-
	nar GHI	-		*cyc1*	-		*prk*	+		*gpmI*	+
	nir KS/*nor* BC/*nos* Z	-		*mto* AB	-		Carboxysome	+	TCA cycle	*cs / gltA*	+
Sulfur	*apr* AB	-	Sulfur	*sqr*	(+)					*suc* AB	+
	sox XABYZ(CD)	-		*fcc* AB	-					*fh*	-
Oxygen	*cco* NOP	+								*mdh*	+
	qox ABCD	-							Glyoxylate shunt	*glc* B	+
	cyd ABX	-								*ace* A	+

belonged to four phyla: *Proteobacteria* (51.6%), *Actinobacteria* (8.3%), *Bacteroidetes* (5.6%) and *Chloroflexi* (1.4%) (Table 2). All genomes in the community contained at least one gene encoding for a denitrifying enzyme, and five featured the genetic potential for iron oxidation. Notably, all putative iron oxidizers also possessed the genetic repertoire for carbon fixation. The most abundant MAG (MAG.13), accounting for 19.3% of the community, could only be taxonomically classified at class level (*Gammaproteobacteria*). Given its high abundance and potential metabolic elevance, the taxonomy and metabolic potential of MAG.13 was further investigated (Table S1).

Table 2. General characteristics of the MAGs recovered from the pilot-scale filter. The last three columns indicate the presence/absence of the essential genes for iron oxidation, denitrification and carbon fixation via the reductive phosphate pentose phosphate cycle. cov_il and cov_np are the coverage with Illumina short reads and Nanopore long reads, respectively.

*[1]Based on FeGenie [40]. 'Yes' if either cyc*2, *cyc*1, *fox*ABC, *fox*EYZ, *sulfocyanin*, *pio*ABC or *mto*AB *are present. [2]Based on GhostKOALA [39] and the presence of nap*AB or *nar*GHI (K02567, K02568 or K00370, K00371, K00374; $NO_3^- \rightarrow NO_2^-$), *nir*K or *nir*S (K00368, K15864; $NO_2^- \rightarrow NO$), *nor*BC (K04561, K02305; $NO \rightarrow N_2O$), *nos*Z (K00376; $N_2O \rightarrow N_2$) from denitrification (M00529). [3]*Based on GhostKOALA [39]. 'Yes' if either rbcL* (K01601) *or rbcS* (K01602) *and prk*B (K00855) *from reductive phosphate pentose phosphate cycle (Calvin Cycle) (*M00165). *** Initially classified as c_Gammaproteobacteria.*

4.3.3. "Candidatus Siderophilus nitratireducens" represents a new order within Gammaproteobacteria

Our phylogenomic analysis based on the concatenated amino acid sequences of 120 bacterial single copy conservative marker genes revealed that MAG.13 (98.6% completeness, 1.7% contamination) belongs to a bacterium forming a new order-level lineage Ga0077554 (GTDB release 08-RS214), within the class *Gammaproteobacteria,* with no known closely related pure-culture representatives (Figure 2). We propose to name the new species "*Candidatus* Siderophilus nitratireducens" gen.nov., sp.nov., a member of the *Candidate* order and family Siderophiliales and Siderophiliaceae, respectively. This lineage, along with several other MAGs from similar groundwater habitats [49], is mostly related to lineages including lithoautotrophic sulfur-ozidizing bacteria from the genera *Sulfuriflexus*, *Thioalbus* and the members of the order *Thiohalomonadales*, including *Thiohalomonas*, *Sulfurivermis* and *Thiohalophilus*. Average nucleotide identity and in-silico calculated DNA-DNA hybridization comparison between "*Ca.* Siderophilus nitratireducens" and its closest relative, a MAG from a drinking water treatment plant (GCA_001464965.1), indicated that the two organisms belong to the same genus but different species (ANI = 89%, DDH = 36.6%).

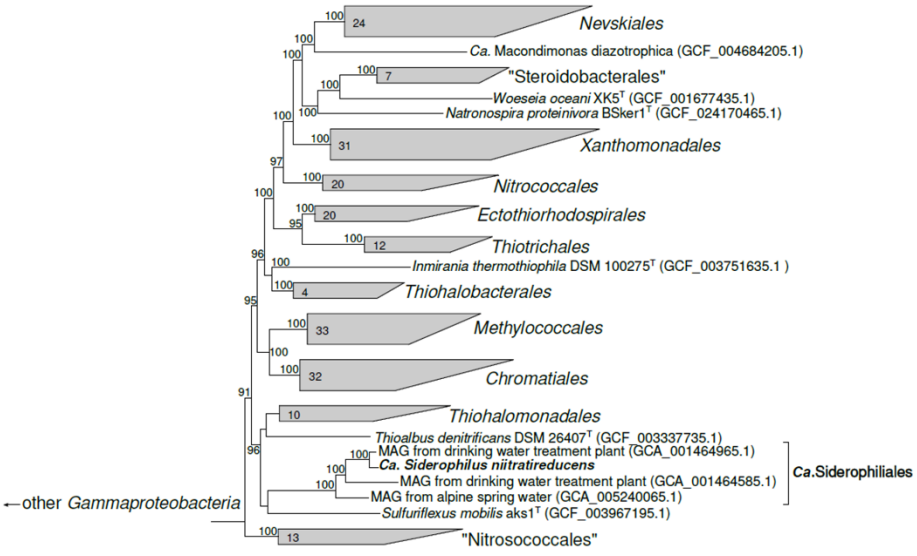

Figure 2. Phylogenetic position of the "Ca. Siderophilus nitratireducens" based on sequence analyses of concatenated alignment of 120 single-copy conserved bacterial

protein markers [50] - taxonomic designations correspond to the Genome Taxonomy DataBase 207). The trees were built using IQ-TREE2 [44] with approximate likelihood-ratio test for branches [47]. Bootstrap consensus tree is shown with values above 90% placed at the nodes. Bar, 0.10 changes per position.

4.3.4. Autotrophy in "Ca. Siderophilus nitratireducens"

To resolve the main anabolic and catabolic pathways of "*Ca*. Siderophilus nitratireducens", open reading frames (ORF) were predicted and annotated (Table 3, detailed version in Table S1). The genome contains marker genes coding for two key proteins of autotrophic CO_2 fixation via the reductive pentose phosphate (Calvin–Benson–Bassham; CBB) cycle, including the large and small subunits of the ribulose-1,5-bisphosphate carboxylase-oxygenase (*rbc*LS form I) and the phosphoribulokinase (*prk*). Genes encoding for carboxysomal shell proteins and carbonic anhydrase were also present, further supporting the inorganic carbon uptake ability of "*Ca*. Siderophilus nitratireducens". The absence of phosphofructokinase (*pfk*) indicates a modified glycolytic pathway initiating at the glyceraldehyde 3-phosphate level. All tricarboxylic acid (TCA) cycle genes were identified except for fumarate hydratase (*fh*). However, the glyoxylate shunt enzymes malate synthase (*glc*B) and isocitrate lyase (*ace*A) were present. Taken together, these findings suggest the capability for full autotrophic growth of "*Ca*. Siderophilus nitratireducens".

4.3.5. Iron oxidation in "Ca. Siderophilus nitratireducens"

The presence of a monoheme *c* cytochrome *cyc2* cluster 3, a primary iron oxidation gene, suggests that "*Ca*. Siderophilus nitratireducens" can use Fe^{2+} as an electron donor. Other common Fe^{2+} oxidases, namely the diheme *c* cytochrome cyc1 and the multiheme c cytochromes MtoA and MtoB, were not annotated. Despite the close phylogenetic proximity to lithoautotrophic sulfur-oxidizing bacteria, the genes of sulfide dehydrogenases Sqr and FccAB and sulfite dehydrogenases SorAB and SoeABC were not identified.

In terms of potential catabolic electron acceptors, the genes for a periplasmic nitrate reductase (*nap*ABCD and its membrane ferrodoxins *nap*GH) and a cbb_3-type cytochrome c oxidase (*cco*NOP) were annotated. However, genes

MAG ID	Phylogenetic affiliation	Phylum	Relative abundance (%)	Scaffolds	N50	GC (%)	Completeness (%)	Contamination (%)	cov_il	cov_np	Coding genes	MAG quality	Iron oxidation[1]	Denitrification[2]	Carbon fixation[3]
MAG.13	** *Candidatus* Siderophilus nitratireducens	Proteobac	19.3	9	1,897,007	56	98.59	1.73	298.27	300.86	3217	High	Yes	$NO_3^- \rightarrow NO_2^-$	Yes
MAG.26	f__Gallionellaceae	Proteobac	10.0	10	569,264	55	95.81	0.95	234.92	155.81	3749	High	Yes	$NO_3^- \rightarrow NO; N_2O \rightarrow N_2$	Yes
MAG.18	f__Anaeromyxobacteraceae	Proteobac	8.6	21	518,414	73	98.06	0.65	186.12	131.88	4018	High	No	$N_2O \rightarrow N_2$	No
MAG.19	g__*Devosia*	Proteobac	6.5	27	4,138,465	64	99.28	0.14	24.53	100.33	4029	High	No	$NO_2^- \rightarrow NO$	No
MAG.10	f__Chitinophagaceae	Bacteroid	5.6	4	3,646,631	40	97.54	0.9	304.83	87.01	3193	High	No	$NO \rightarrow N_2$	No
MAG.03	o__Nanopelagicales	Actinobac	4.3	11	779,605	69	99	2.37	140.41	67.49	4065	High	No	$NO_3^- \rightarrow NO$	No
MAG.27	o__Nanopelagicales	Actinobac	3.9	9	1,166,278	71	98.3	1.98	140.56	60.77	3910	High	No	$NO_3^- \rightarrow NO$	No
MAG.34	g__*Gallionella*	Proteobac	3.5	112	46,607	57	95.91	3.25	64.39	52.65	2516	High	Yes	$NO_3^- \rightarrow NO$	Yes
MAG.00	o__Anaerolineales	Chloroflex	1.4	100	114,338	55	97.27	2.91	21.93	20.04	4828	High	No	$NO_2^- \rightarrow NO$	No
MAG.08	g__*Rhodoferax*	Proteobac	1.2	121	69,171	63	88.95	2.37	33.64	17.42	3870	Medium	No	$NO_3^- \rightarrow NO$	Yes
MAG.04	f__Rhizobiaceae	Proteobac	0.9	115	80,809	60	95.12	4.1	25.97	13.93	4768	High	No	$NO_3^- \rightarrow N_2O$	No
MAG.16	f__Gallionellaceae	Proteobac	0.9	165	27,226	56	88.51	3.94	52.76	13.55	3002	Medium	Yes	$NO_3^- \rightarrow N_2O$	Yes
MAG.29	g__*Rhizobacter*	Proteobac	0.7	257	25,511	66	94.54	4.54	21.73	9.94	4225	Medium	Yes	$NO_3^+ \rightarrow NO_2^-$	Yes

encoding for other known denitrification reductases, namely membrane-bound nitrate reductase (*nar*GHI) and nitrite, nitric oxide and nitrous oxide reductases, *nir*K/*nir*S, *nor*BC and *nos*Z respectively, were not found (Table 3, detailed version in Table S1). Additionally, alternative oxidases, such as the cytochrome *bd* ubiquinol oxidase (*cyd*AB) or the *aa*$_3$-type cytochrome c oxidase (*cox*ABCD) were not identified. Also, genes of dissimilatory sulfate reduction (*apr*AB and *dsr*ABC) and the *sox* complex, responsible for sulfate reduction could not be identified. These findings suggest that "*Ca.* Siderophilus nitratireducens" relies exclusively on nitrate and oxygen as electron acceptors.

Table 3. General characteristics of the MAGs recovered from the pilot-scale filter. The last three columns indicate the presence/absence of the essential genes for iron oxidation, denitrification and carbon fixation via the reductive phosphate pentose phosphate cycle. Cov_il and cov_np are the coverage with Illumina short reads and Nanopore long reads, respectively.

[1]Based on FeGenie (61). 'Yes' if either cyc2, cyc1, foxABC, foxEYZ, sulfocyanin, pioABC or mtoAB are present

[2]Based on GhostKOALA (60) and the presence of napAB or narGHI (K02567, K02568 or K00370, K00371, K00374; $NO_3^- \rightarrow NO_2^-$), nirK or nirS (K00368, K15864; $NO_2^- \rightarrow NO$), norBC (K04561, K02305; $NO \rightarrow N_2O$), nosZ (K00376; $N_2O \rightarrow N_2$) from denitrification (M00529).

[3]Based on GhostKOALA (60). 'Yes' if either rbcL (K01601) or rbcS (K01602) and prkB (K00855) from reductive phosphate pentose phosphate cycle (Calvin Cycle) (M00165).

*** Initially classified as c_Gammaproteobacteria.*

4.3.6. On the thermodynamic feasibility of Nap-dependent nitrate-reducing iron-oxidation

Based on its genome, "*Ca.* Siderophilus nitratireducens" is potentially an autotrophic organism that obtains energy by oxidizing Fe^{2+} to Fe^{3+} while reducing NO_3^- to NO_2^-. Yet, as iron is a weak electron donor, the standard Gibbs free energy of the reaction is positive under standard biological conditions (pH 7). The process is therefore thermodynamically unfavourable:

$$Fe^{2+} + 0.5NO_3^- + H^+ \rightarrow Fe^{3+} + 0.5NO_2^- + 0.5H_2O \quad \Delta G^{01} = 35.2 \frac{kJ}{e-mol}$$

However, the exceptionally low solubility constants of iron oxides, ranging from 10^{-34} to 10^{-42} [51] result in very low Fe^{3+} concentrations. Thereby, precipitation creates the conditions for a favourable thermodynamic driving force for the oxidation of Fe^{2+} to Fe^{3+} [52]. Under the operational conditions of this study (283 K, < 1 $\mu molNO_3^- \cdot l^{-1}$, < 0.2 $\mu molNO_2^- \cdot l^{-1}$ in the effluent), the reaction becomes thermodynamically favourable owing to the calculated Fe^{3+}/Fe^{2+} ratio in the order of 10^{-16} (conservative value, see section 4.2):

$$\Delta G^1 = \Delta G_r^{01} + RTln\left[\frac{[Fe^{3+}][NO_2^-]^{\frac{1}{2}}}{[Fe^{2+}][NO_3^-]^{\frac{1}{2}}}\right] = -66.2 \frac{kJ}{e-mol}$$

A Gibbs free energy of -66 kJ/e-mol is in principle enough to transport three to four protons over the cytoplasmic membrane, considering a value of 15 $kJ \cdot mol_{H^+}^{-1}$ [53], and would yield at least one ATP. If other iron precipitation products are formed, the redox potential of Fe^{2+}/Fe^{3+} increases further. Even at more conservative Fe^{3+}/Fe^{2+} ratios and pH, due to non-equilibrium conditions and product gradients, the biological process remains favourable (Figure 3).

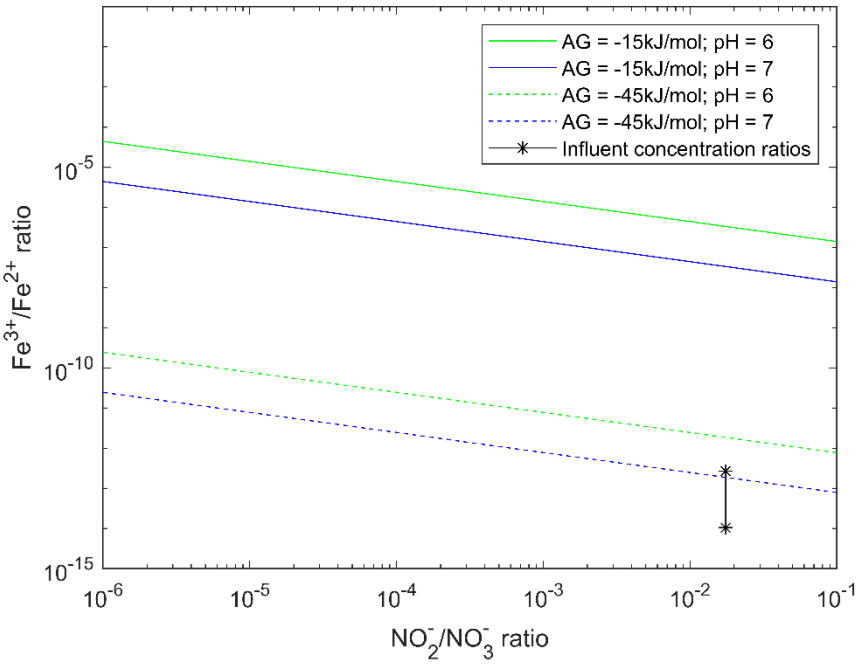

Figure 3. Gibbs energy dissipated during nitrate-reducing iron oxidation as function of the ratio of substrates and products. As reference, lines represent the ratios at which the minimum energy required to generate pmf (-15 kJ·mol^{-1}, full lines) and ATP (-45 kJ·mol^{-1}, dashed lines) is generated at intracellular pH of 6 (green) or 7 (blue) ([53]). Star dots represent the actual ratios based on measured ($NO_2^-/NO_3^-/Fe^{2+}$) and calculated (Fe^{3+}) influent reactor concentrations. Note that NO_2^- was below detection limit (< 0.2 µmol·l^{-1}), so that the actual reactor conditions were likely even more favorable, i.e. more on the left

.

4.3.7. Complete denitrification: a collaborative effort of iron-oxidizing autotrophs and organoheterotrophs

Iron oxidation genes were identified in five MAGs, namely MAG.13 ("*Ca.* Siderophilus nitratireducens*"*), MAG.29 (g_*Rhizobacter*) and MAG.26, MAG.34 and MAG.16 (f_*Gallionellaceae,* commonly associated with autotrophic iron oxidation). These MAGs also encoded for the central enzymes of the carbon dioxide fixation via the CBB cycle. While all 13 MAGs contained genes encoding

for at least one denitrification enzyme (Table 3), none of them possessed a comprehensive gene set to fully reduce nitrate to dinitrogen gas. Dissimilatory nitrate reduction to nitrite, the first denitrification step, was present in 9 MAGs, while the final step, nitrous oxide reduction to nitrogen gas, was only found in MAG.26 (g_*Rhizobacter*), MAG.18 (f_*Anaeromyxobacteraceae*) and MAG.10 (f_*Chitinophagaceae*). The five most abundant MAGs (> 5 %) alone accounted for up to 50 % of the community and covered the full denitrification (Figure 4). All putative iron oxidizers also possessed the genetic potential for aerobic respiration (*i.e.* they contained cbb_3-type terminal oxidases). Interestingly, two distinct potential niches were identified. The autotrophic iron oxidizers, *"Ca*. Siderophilus nitratireducens" and MAG.26 (f_*Gallionelleceae*), performed the initial denitrification reductions, while the lower-abundant organoheterotrophs complemented the reduction of (at least) NO to nitrous oxide possibly taking advantage of the autotrophically fixed carbon excreted by the iron oxidizers. Noticeably, due to the absence of sufficient biodegradable organic matter in the influent, a portion of the biologically generated NO was likely reduced to N_2O chemically with Fe^{2+} [54].

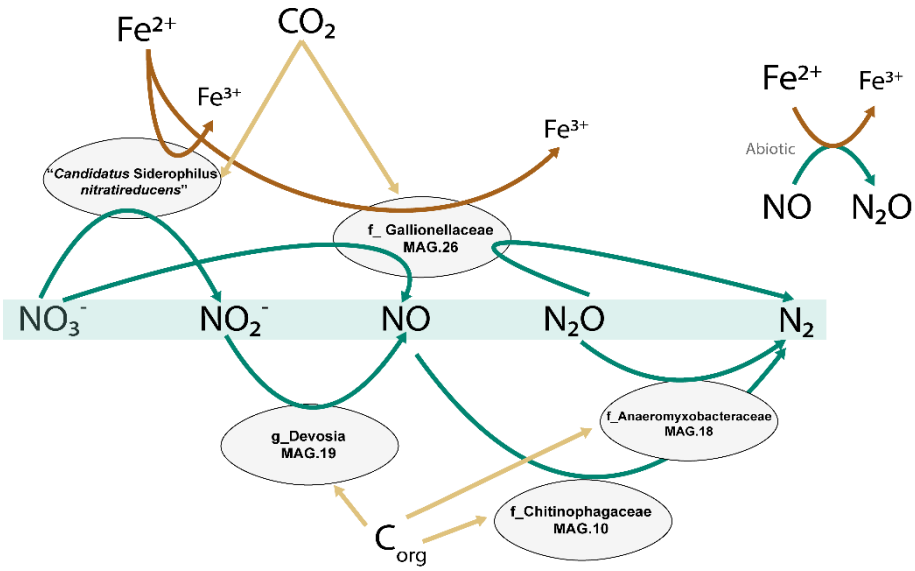

Figure 4. Genome-based conceptual model of substrates fluxes within the microbial community represented by the five most abundant MAGs. Putative autotrophic iron

oxidizers perform the upstream part of denitrification, while flanking communities reduce the toxic intermediates to innocuous dinitrogen gas. The putative autotrophic metabolism was inferred based on the presence of ribulose-1,5-biphosphate carboxylase/oxygenase (RuBisCO) and phosphofructokinase (pfk).

4.4. DISCUSSION

We established a pilot-scale filter on nitrate-rich anoxic groundwater to elucidate the structure and metabolism of nitrate-reducing iron-oxidizing microbial communities under oligotrophic conditions mimicking natural groundwater. The enriched microbial community stoichiometrically removed iron and nitrate during more than four months, and was dominated by a genome belonging to a new *Candidate* order, named Siderophiliales. The genome of this new species, "*Ca*. Siderophilus nitratireducens", encoded the genes for iron oxidation (cytochrome *c cyc2*) and, within the denitrification pathway, the periplasmic nitrate reductase (*nap*). The absence of other denitrification genes suggests a short catabolic path, which may offer a kinetic advantage in terms of higher iron oxidation rates [55] especially under nitrogen limiting conditions [56]. In contrast, the majority of NDFO genomes reported so far encode the membrane-bound nitrate reductase (*nar*) along with other downstream denitrification genes [11,57–60]. *Nar* actively translocates protons, whereas *nap* conserves energy only indirectly by accepting electrons from the quinol pool on the periplasmic side of the membrane, effectively consuming cytoplasmic protons [61]. Recently, novel Zetaproteobacteria genomes possessing *nap* have been recovered from a complex community, yet they also possessed at least another energy conserving nitrogen oxide [5,62]. The presence of a cbb_3-type cytochrome *c* oxidase suggests that "*Ca*. Siderophilus nitratireducens" may also be capable of oxygen respiration. This is consistent with the fact that all reported genomes of anaerobic iron-oxidizing bacteria contain oxygen reductases [57,60,63], including the well-studied KS [13] and AG [64] cultures. However, to the best of our knowledge, NDFO growth under (micro)aerophilic conditions has not been reported to date [11]. Although the sporadic detection of traces of oxygen (< 3 µM) in our filter does not allow to fully exclude aerobic activity, and in the absence of cultured representatives to confirm it, we posit that *nap*-driven iron oxidation was the primary catabolic route of "*Ca*. Siderophilus nitratireducens" under the *in-situ* restricted availability of alternative substrates. Furthermore, "*Ca*. Siderophilus

nitratireducens" was also identified as a putative autotroph, adding the additional challenge of energy and electrons needs for anabolic CO_2 fixation to the growth on iron, a weak electron-donor at standard conditions [15]. Thermodynamic evaluations indicate that *nap*-dependent iron oxidation can sustain growth at realistic Fe^{3+}/Fe^{2+} and NO_3^-/NO_2^- concentrations ratios. To this end, the quasi-instantaneous precipitation of the biologically formed Fe^{3+} as iron oxides under circum-neutral pH plays a central role as thermodynamic driving force [19]. The specific mechanisms by which this thermodynamic potential is harnessed for carbon fixation remain to be fully elucidated.

The subsequent reduction of the produced nitrite resulted from the concerted activity of putative autotrophic iron-oxidizers and organoheterotrophs. Within the microbial community, the second most abundant genome, MAG.26 (f_*Gallionellaceaea*), featured the genetic potential for iron oxidation and most denitrification steps, with the exception of nitrous oxide reductase (*nor*). MAG.26 also possessed the cytochrome *c* oxidase *cbb*$_3$-type *cco*NOP for aerobic respiration. Interestingly, this genome contained genes for CO_2 fixation, a trait mirrored in all other less abundant genomes with the ability to oxidize iron. This suggests that autotrophy may represent an essential trait for NDFOs in anoxic groundwaters where the dissolved organic carbon is largely non-biodegradable [65]. The three second most abundant genomes, MAG.18 (f_*Anaeromyxobacteraceae*), MAG.19 (g_*Devosia*) and MAG.10 (f_*Chitinophagaceae*) were found to lack the genes for iron oxidation and CO_2 assimilation. Yet, these genomes encompassed the full denitrification pathway starting from nitrite. Besides the likely occurrence of chemical reduction of NO to N_2O [66], we speculate that these heterotrophs complemented the NDFOs for at least the reduction of NO using autotrophically fixed organic carbon as substrate. A similar metabolic network was also recently observed in mesophilic NDFO communities [13]. Overall, the measured iron and nitrate consumption yield of 7.1 mol Fe^{2+}: mol NO_3^- is consistent with the expected 5.6, i.e. considering the theoretical catabolism (eq.1) and the recently estimated 12 % of electrons used for growth [7], but higher than the experimentally observed range of 3.8 - 4.7 [9,57,67]. At first, we hypothesized nitrate ammonification to be the reason for the slight excess in iron oxidation, yet none of the putative iron-oxidizing genomes encoded for the common *nrf* nor for the newly reported octaheme complex [68]. Also, the oxygen sporadically detected in the influent was always below the quantification limit of 3 µM, a conservative concentration that

alone would explain less than 15 % of the total iron consumption via chemical oxidation. As no Fe^{3+} was detected in the reactor effluent, all iron necessarily accumulated inside the reactor either as Fe^{2+} or Fe^{3+} precipitates. X-ray diffraction and Mössbauer spectroscopy identified over 94% of the Fe in solids as amorphous ferrihydrite, an Fe^{3+} oxide, with less than 6% of the solids attributed to magnetite, an Fe^{2+}-Fe^{3+} oxide typically formed under anaerobic conditions (SI 4 and 5). Consequently, the Fe^{2+} unaccounted for was likely continuously adsorbed onto the newly-formed Fe^{3+} oxides, a well-studied phenomenon [69], yet the extent to which this occurred was not investigated. In conclusion, pending experimental validation, we surmise that NDFO microorganisms may not only contribute to iron removal by direct oxidation but also by continuously providing newly-formed iron oxides for its adsorption.

***Description of "Ca*. Siderophilus nitratireducens" gen. nov., sp. nov.**

Siderophilus (Si.de.ro'phi.lus Gr. masc.n. *sidêros* iron; Gr. masc. adj. *philos* loving; N.L. masc. n. *Siderophilus* (loving iron).

ni.tra.ti.re.du'.cens (N.L. masc. n. *nitras (gen. nitratis)*, nitrate; L. pres. part. *reducens*, converting to a different state; N.L. part. adj. *nitratireducens*, reducing nitrate).

Autotrophic nitrate-reducing iron-oxidizing bacterium isolated from a filtration unit fed with anaerobic groundwater with iron(II) and nitrate. Harbors also the genetic potential to aerobically oxidize iron.

REFERENCES

1. Matassa, S., Batstone, D. J., Hülsen, T., Schnoor, J. & Verstraete, W. Can direct conversion of used nitrogen to new feed and protein help feed the world? *Environ. Sci. Technol.* **49**, 5247–5254 (2015).

2. Giordano, M. Global Groundwater? Issues and Solutions. *Annu. Rev. Environ. Resour.* **34**, 153–178 (2009).

3. Ward, M. H., Jones, R. R., Brender, J. D., de Kok, T. M., Weyer, P. J., Nolan, B. T., Villanueva, C. M. & van Breda, S. G. Drinking water nitrate and human health: An updated review. *International Journal of Environmental Research and Public Health* vol. 15 at https://doi.org/10.3390/ijerph15071557 (2018).

4. WHO. *Guidelines for Drinking-Water Quality*. *Resuscitation* (2010).

5. McAllister, S. M., Vandzura, R., Keffer, J. L., Polson, S. W. & Chan, C. S. Aerobic and anaerobic iron oxidizers together drive denitrification and carbon cycling at marine iron-rich hydrothermal vents. *ISME J.* **15**, 1271–1286 (2021).

6. Schaedler, F., Lockwood, C., Lueder, U., Glombitza, C., Kappler, A. & Schmidt, C. Microbially mediated coupling of Fe and N cycles by nitrate-reducing Fe(II)-oxidizing bacteria in littoral freshwater sediments. *Appl. Environ. Microbiol.* **84**, 1–14 (2018).

7. Huang, J., Mellage, A., Garcia, J. P., Glöckler, D., Mahler, S., Elsner, M., Jakus, N., Mansor, M., Jiang, H. & Kappler, A. Metabolic Performance and Fate of Electrons during Nitrate-Reducing Fe(II) Oxidation by the Autotrophic Enrichment Culture KS Grown at Different Initial Fe/N Ratios. *Appl. Environ. Microbiol.* (2023).

8. Chen, D. *et al*. Novel Insight into Microbially Mediated Nitrate-Reducing Fe(II) Oxidation by Acidovorax sp. Strain BoFeN1 Using Dual N-O Isotope Fractionation. *Environ. Sci. Technol.* **57**, 12546–12555 (2023).

9. Straub, K. L., Benz, M., Schink, B. & Widdel, F. Anaerobic, nitrate-dependent microbial oxidation of ferrous iron. *Appl. Environ. Microbiol.* **62**, 1458–1460 (1996).

10. Bryce, C. *et al*. Microbial anaerobic Fe(II) oxidation - Ecology, mechanisms and environmental implications. *Environ. Microbiol.* **20**, 3462–3483 (2018).

11. Huang, Y. M., Jakus, N., Straub, D., Konstantinidis, K. T., Blackwell, N., Kappler, A. & Kleindienst, S. 'Candidatus ferrigenium straubiae' sp. nov.,

'Candidatus ferrigenium bremense' sp. nov., 'Candidatus ferrigenium altingense' sp. nov., are autotrophic Fe(II)-oxidizing bacteria of the family Gallionellaceae. *Syst. Appl. Microbiol.* **45**, (2022).

12. Price, A., Macey, M. C., Miot, J. & Olsson-Francis, K. Draft Genome Sequences of the Nitrate-Dependent Iron-Oxidizing Proteobacteria Acidovorax sp. Strain BoFeN1 and Paracoccus pantotrophus Strain KS1. *Microbiol. Resour. Announc.* **7**, 1–2 (2018).

13. Huang, Y., Straub, D., Blackwell, N., Kappler, A. & Kleindienst, S. Meta-omics Reveal Gallionellaceae and Rhodanobacter Species as Interdependent Key Players for Fe(II) Oxidation and Nitrate Reduction in the Autotrophic Enrichment Culture KS. *Appl. Environ. Microbiol.* **87**, (2021).

14. Weber, K. A., Achenbach, L. A. & Coates, J. D. Microorganisms pumping iron: Anaerobic microbial iron oxidation and reduction. *Nat. Rev. Microbiol.* **4**, 752–764 (2006).

15. Hedrich, S., Schlömann, M. & Barrie Johnson, D. The iron-oxidizing proteobacteria. *Microbiology* vol. 157 1551–1564 at https://doi.org/10.1099/mic.0.045344-0 (2011).

16. Kleerebezem, R. & Van Loosdrecht, M. C. M. Thermodynamic and kinetic characterization using process dynamics: Acidophilic ferrous iron oxidation by Leptospirillum ferrooxidans. *Biotechnol. Bioeng.* **100**, 49–60 (2008).

17. Agudelo-Vera, C. *et al.* Drinking water temperature around the globe: Understanding, policies, challenges and opportunities. *Water (Switzerland)* **12**, (2020).

18. Jolivet, J. P., Chanéac, C. & Tronc, E. Iron oxide chemistry. From molecular clusters to extended solid networks. *Chem. Commun.* **4**, 477–483 (2004).

19. Gorski, C. A., Edwards, R., Sander, M., Hofstetter, T. B. & Stewart, S. M. Thermodynamic Characterization of Iron Oxide-Aqueous Fe2+ Redox Couples. *Environ. Sci. Technol.* **50**, 8538–8547 (2016).

20. Vlek, P. L. G., Blom, T. J. M., Beek, J. & Lindsay, W. L. Determination of the Solubility Product of Various Iron Hydroxides and Jarosite by the Chelation Method. *Soil Sci. Soc. Am. J.* **38**, 429–432 (1974).

21. Bolger, A. M., Lohse, M. & Usadel, B. Trimmomatic: a flexible trimmer for Illumina sequence data. *Bioinformatics* **30**, 2114–2120 (2014).

22. Andrews, S. FastQC: A Quality Control Tool for High Throughput Sequence Data [Online]. at

http://www.bioinformatics.babraham.ac.uk/projects/fastqc/ (2010).

23. Sereika, M., Kirkegaard, R. H., Karst, S. M., Michaelsen, T. Y., Sørensen, E. A., Wollenberg, R. D. & Albertsen, M. Oxford Nanopore R10.4 long-read sequencing enables the generation of near-finished bacterial genomes from pure cultures and metagenomes without short-read or reference polishing. *Nat. Methods 2022 197* **19**, 823–826 (2022).

24. Lin, Y., Yuan, J., Kolmogorov, M., Shen, M. W., Chaisson, M. & Pevzner, P. A. Assembly of long error-prone reads using de Bruijn graphs. *Proc. Natl. Acad. Sci. U. S. A.* **113**, E8396–E8405 (2016).

25. Li, H. Minimap2: pairwise alignment for nucleotide sequences. *Bioinformatics* **34**, 3094–3100 (2018).

26. Vaser, R., Sović, I., Nagarajan, N. & Šikić, M. Fast and accurate de novo genome assembly from long uncorrected reads. *Genome Res.* **27**, 737–746 (2017).

27. Vasimuddin, M., Misra, S., Li, H. & Aluru, S. Efficient architecture-aware acceleration of BWA-MEM for multicore systems. in *Proceedings - 2019 IEEE 33rd International Parallel and Distributed Processing Symposium, IPDPS 2019* 314–324 (Institute of Electrical and Electronics Engineers Inc., 2019).

28. Li, H., Handsaker, B., Wysoker, A., Fennell, T., Ruan, J., Homer, N., Marth, G., Abecasis, G. & Durbin, R. The Sequence Alignment/Map format and SAMtools. **25**, 2078–2079 (2009).

29. Kang, D. D., Li, F., Kirton, E., Thomas, A., Egan, R., An, H. & Wang, Z. MetaBAT 2: An adaptive binning algorithm for robust and efficient genome reconstruction from metagenome assemblies. *PeerJ* **2019**, (2019).

30. Wu, Y. W., Simmons, B. A. & Singer, S. W. MaxBin 2.0: An automated binning algorithm to recover genomes from multiple metagenomic datasets. *Bioinformatics* **32**, 605–607 (2016).

31. Nissen, J. N., Johansen, J., Allesøe, R. L., Sønderby, C. K., Armenteros, J. J. A., Grønbech, C. H., Jensen, L. J., Nielsen, H. B., Petersen, T. N., Winther, O. & Rasmussen, S. Improved metagenome binning and assembly using deep variational autoencoders. *Nat. Biotechnol.* **39**, 555–560 (2021).

32. K Sieber, C. M. *et al.* Recovery of genomes from metagenomes via a dereplication, aggregation and scoring strategy. *Nat. Microbiol. 2018 37* **3**, 836–843

(2018).

33. Parks, D. H., Imelfort, M., Skennerton, C. T., Hugenholtz, P. & Tyson, G. W. CheckM: assessing the quality of microbial genomes recovered from isolates, single cells, and metagenomes. *Genome Res.* **25**, 1043–1055 (2015).

34. Parks, D. H., Chuvochina, M., Chaumeil, P. A., Rinke, C., Mussig, A. J. & Hugenholtz, P. A complete domain-to-species taxonomy for Bacteria and Archaea. *Nat. Biotechnol.* **38**, 1079–1086 (2020).

35. Arias-Carrasco, R., Vásquez-Morán, Y., Nakaya, H. I. & Maracaja-Coutinho, V. StructRNAfinder: An automated pipeline and web server for RNA families prediction. *BMC Bioinformatics* **19**, 1–7 (2018).

36. Chan, P. P., Lin, B. Y., Mak, A. J. & Lowe, T. M. tRNAscan-SE 2.0: improved detection and functional classification of transfer RNA genes. *Nucleic Acids Res.* **49**, 9077–9096 (2021).

37. Bowers, R. M. *et al.* Minimum information about a single amplified genome (MISAG) and a metagenome-assembled genome (MIMAG) of bacteria and archaea. *Nat. Biotechnol.* **35**, 725–731 (2017).

38. Hyatt, D., Chen, G. L., LoCascio, P. F., Land, M. L., Larimer, F. W. & Hauser, L. J. Prodigal: Prokaryotic gene recognition and translation initiation site identification. *BMC Bioinformatics* **11**, 1–11 (2010).

39. Kanehisa, M., Sato, Y. & Morishima, K. BlastKOALA and GhostKOALA: KEGG Tools for Functional Characterization of Genome and Metagenome Sequences. *J. Mol. Biol.* **428**, 726–731 (2016).

40. Garber, A. I., Nealson, K. H., Okamoto, A., McAllister, S. M., Chan, C. S., Barco, R. A. & Merino, N. FeGenie: A Comprehensive Tool for the Identification of Iron Genes and Iron Gene Neighborhoods in Genome and Metagenome Assemblies. *Front. Microbiol.* **11**, 37 (2020).

41. Tatusova, T., Dicuccio, M., Badretdin, A., Chetvernin, V., Nawrocki, E. P., Zaslavsky, L., Lomsadze, A., Pruitt, K. D., Borodovsky, M. & Ostell, J. NCBI prokaryotic genome annotation pipeline. *Nucleic Acids Res.* **44**, 6614–6624 (2016).

42. Altschul, S. F., Madden, T. L., Schäffer, A. A., Zhang, J., Zhang, Z., Miller, W. & Lipman, D. J. Gapped BLAST and PSI-BLAST: a new generation of protein database search programs. *Nucleic Acids Res.* **25**, 3389–3402 (1997).

43. Rost, B. Twilight zone of protein sequence alignments. *Protein*

Eng. Des. Sel. **12**, 85–94 (1999).

44. Minh, B. Q., Schmidt, H. A., Chernomor, O., Schrempf, D., Woodhams, M. D., Von Haeseler, A., Lanfear, R. & Teeling, E. IQ-TREE 2: New Models and Efficient Methods for Phylogenetic Inference in the Genomic Era. *Mol. Biol. Evol.* **37**, 1530–1534 (2020).

45. Kalyaanamoorthy, S., Minh, B. Q., Wong, T. K. F., Von Haeseler, A. & Jermiin, L. S. ModelFinder: fast model selection for accurate phylogenetic estimates. *Nat. Methods* **14**, 587–589 (2017).

46. Thi Hoang, D., Chernomor, O., von Haeseler, A., Quang Minh, B., Sy Vinh, L. & Rosenberg, M. S. UFBoot2: Improving the Ultrafast Bootstrap Approximation. *Mol. Biol. Evol* **35**, 518–522 (2017).

47. Anisimova, M. & Gascuel, O. Approximate likelihood-ratio test for branches: A fast, accurate, and powerful alternative. *Syst. Biol.* **55**, 539–552 (2006).

48. Richter, M., Rosselló-Móra, R., Oliver Glöckner, F. & Peplies, J. JSpeciesWS: A web server for prokaryotic species circumscription based on pairwise genome comparison. *Bioinformatics* **32**, 929–931 (2016).

49. Pinto, A. J., Marcus, D. N., Ijaz, U. Z., Bautista-de lose Santos, Q. M., Dick, G. J. & Raskin, L. Metagenomic Evidence for the Presence of Comammox Nitrospira -Like Bacteria in a Drinking Water System. *mSphere* **1**, (2016).

50. Parks, D. H., Chuvochina, M., Waite, D. W., Rinke, C., Skarshewski, A., Chaumeil, P. A. & Hugenholtz, P. A standardized bacterial taxonomy based on genome phylogeny substantially revises the tree of life. *Nat. Biotechnol. 2018 3610* **36**, 996–1004 (2018).

51. Schwertmann, U., Cornell, R. M., Rao, C. N. R., Raveau, B., Jolivet, J.-P., Henry, M. & Livage, J. *The Iron Oxides*. *Synthesis* (2003).

52. H. Lees, Kwok, S. C. & Suzuki, I. The thermodynamics of iron oxidation by the ferrobacilli. 6–8 (1968).

53. Müller, V. & Hess, V. The minimum biological energy quantum. *Frontiers in Microbiology* vol. 8 2019 at https://doi.org/10.3389/fmicb.2017.02019 (2017).

54. Hayhurst, A. N. & Lawrence, A. D. The reduction of the nitrogen oxides NO and N2O to molecular nitrogen in the presence of iron, its oxides, and carbon monoxide in a hot fluidized bed. *Combust. Flame* **110**, 351–365 (1997).

55. Costa, E., Pérez, J. & Kreft, J. U. Why is metabolic labour

divided in nitrification? *Trends Microbiol.* **14**, 213–219 (2006).

56. Pessi, I. S., Viitamäki, S., Virkkala, A. M., Eronen-Rasimus, E., Delmont, T. O., Marushchak, M. E., Luoto, M. & Hultman, J. In-depth characterization of denitrifier communities across different soil ecosystems in the tundra. *Environ. Microbiomes* **17**, 1–17 (2022).

57. Huang, Y.-M., Straub, D., Kappler, A., Smith, N., Blackwell, N. & Kleindienst, S. A Novel Enrichment Culture Highlights Core Features of Microbial Networks Contributing to Autotrophic Fe(II) Oxidation Coupled to Nitrate Reduction. *Microb. Physiol.* 1–16 (2021).

58. Cheng, B., Wang, Y., Hua, Y. & Heal, K. V. The performance of nitrate-reducing Fe(II) oxidation processes under variable initial Fe/N ratios: The fate of nitrogen and iron species. *Front. Environ. Sci. Eng.* **15**, 73- (2021).

59. Jamieson, J., Prommer, H., Kaksonen, A. H., Sun, J., Siade, A. J., Yusov, A. & Bostick, B. Identifying and Quantifying the Intermediate Processes during Nitrate-Dependent Iron(II) Oxidation. (2018).

60. He, S., Tominski, C., Kappler, A., Behrens, S. & Roden, E. E. Metagenomic analyses of the autotrophic Fe(II)-oxidizing, nitrate-reducing enrichment culture KS. *Appl. Environ. Microbiol.* **82**, 2656–2668 (2016).

61. Simon, J., van Spanning, R. J. M. & Richardson, D. J. The organisation of proton motive and non-proton motive redox loops in prokaryotic respiratory systems. *Biochim. Biophys. Acta - Bioenerg.* **1777**, 1480–1490 (2008).

62. Chen, J. & Strous, M. Denitrification and aerobic respiration, hybrid electron transport chains and co-evolution. *Biochim. Biophys. Acta - Bioenerg.* **1827**, 136–144 (2013).

63. Hu, M., Chen, P., Sun, W., Li, F. & Cui, J. A novel organotrophic nitrate-reducing Fe(II)-oxidizing bacterium isolated from paddy soil and draft genome sequencing indicate its metabolic versatility. *RSC Adv.* **7**, 56611–56620 (2017).

64. Jakus, N., Blackwell, N., Straub, D., Kappler, A. & Kleindienst, S. Presence of Fe(II) and nitrate shapes aquifer-originating communities leading to an autotrophic enrichment dominated by an Fe(II)-oxidizing Gallionellaceae sp. *FEMS Microbiol. Ecol.* **97**, 1–14 (2021).

65. Caltran, I., Rietveld, L. C., Shorney-Darby, H. L. & Heijman, S. G. J. Separating

NOM from salts in ion exchange brine with ceramic nanofiltration. *Water Res.* **179**, (2020).

66. Van Cleemput, O. Subsoils: Chemo- and biological denitrification, N2O and N2 emissions. *Nutr. Cycl. Agroecosystems* **52**, 187–194 (1998).

67. Tominski, C., Heyer, H., Lösekann-Behrens, T., Behrens, S. & Kappler, A. Growth and population dynamics of the anaerobic Fe(II)-oxidizing and nitrate-reducing enrichment culture KS. *Appl. Environ. Microbiol.* **84**, 2020 (2018).

68. Sorokin, D. Y., Tikhonova, T. V, Koch, H., Berg, E. M. Van Den, Hinderks, R. S., Pabst, M., Dergousova, N. I., Soloveva, A. Y., Kuenen, G. J., Popov, V. O. & Loosdrecht, M. C. M. Van. Trichlorobacter ammonificans , a dedicated acetate-dependent ammoni fi er with a novel module for dissimilatory nitrate reduction to ammonia. 1–10 (2023).

69. Fredrickson, J. K., Zachara, J. M., Kennedy, D. W., Dong, H., Onstott, T. C., Hinman, N. W. & Li, S. M. Biogenic iron mineralization accompanying the dissimilatory reduction of hydrous ferric oxide by a groundwater bacterium. *Geochim. Cosmochim. Acta* **62**, 3239–3257 (1998).

Pain is neither unbearable nor unending, as long as you keep in mind its limits and don't magnify them in your imagination

Epikouros

A DIFFICULT COEXISTANCE: RESOLVING THE IRON-INDUCED NITRIFICATION DELAY IN GROUNDWATER FILTERS

5

ABSTRACT

Rapid sand filters (RSF) are an established and widely applied technology for the removal of dissolved iron (Fe^{2+}) and ammonium (NH_4^+) among other contaminants in groundwater treatment. Most often, biological NH_4^+ oxidation is spatially delayed and starts only upon complete Fe^{2+} depletion. However, the mechanism(s) responsible for the inhibition of NH_4^+ oxidation by Fe^{2+} or its oxidation (by)products remains elusive, hindering further process control and optimization. We used batch assays, lab-scale columns, and full-scale filter characterizations to resolve the individual impact of the main Fe^{2+} oxidizing mechanisms and the resulting products on biological NH_4^+ oxidation. Modelling of the obtained datasets allowed to quantitatively assess the hydraulic implications of Fe^{2+} oxidation. Dissolved Fe^{2+} and the reactive oxygen species formed as byproducts during Fe^{2+} oxidation had no direct effect on ammonia oxidation. The Fe^{3+} oxides on the sand grain coating, commonly assumed to be the main cause for inhibited ammonia oxidation, seemed instead to enhance it. Modelling allowed to exclude mass transfer limitations induced by accumulation of iron flocs and consequent filter clogging as the cause for delayed ammonia oxidation. We unequivocally identify the inhibition of NH_4^+oxidizing organisms by the Fe^{3+} flocs generated during Fe^{2+} oxidation as the main cause for the commonly observed spatial delay in ammonia oxidation. The addition of Fe^{3+} flocs inhibited NH_4^+ oxidation both in batch and column tests, and the removal of Fe^{3+} flocs by backwashing completely re-established the NH_4^+ removal capacity, suggesting that the inhibition is reversible. In conclusion, our findings not only identify the iron form that causes the inhibition, albeit the biological mechanism remains to be identified, but also highlight the ecological importance of iron cycling in nitrifying environments.

HIGHLIGHTS

- Dissolved Fe^{2+} and reactive oxygen species do not affect NH_4^+ oxidation
- Fe oxide coating aids sand grain colonization by NH_4^+-oxidizing bacteria
- Fe^{3+} flocs inhibit NH_4^+ oxidation by reducing the NH_4^+ oxidation capacity of NH_4^+-
  oxidizing bacteria
- Changes in transport patterns due to clogging do not play a major role in NH_4^+ oxidation
- The inhibition of NH_4^+ oxidation is reversible and reduced by backwashing

Published as:

Corbera-Rubio, F., Kruisdijk, E., Malheiro, S., Leblond, M., Verschoor, L., van Loosdrecht, M. C. M., Laureni, M. & van Halem, D. A difficult coexistence: resolving the iron-induced nitrification delay in groundwater filters. *Water Res.* **260**, 121923 (2024).

5.1. INTRODUCTION

Anaerobic groundwater is an excellent drinking water source because it is microbiologically safe and it has stable temperature, and composition [1–3]. Rapid sand filters (RSFs), preceded by an aeration step, are the most commonly applied technologies for the removal of major groundwater contaminants such as dissolved iron (Fe^{2+}) and ammonium (NH_4^+) [4]. Complete segregation of the removal processes is commonly observed in full-scale systems, where Fe^{2+} is removed at the filter top and NH_4^+ oxidation starts only upon Fe^{2+} depletion [5–7]. Despite decades of research and practice, the mechanisms governing the stratification of Fe^{2+} and NH_4^+ removal remain elusive, leading to poor process control, filter over-dimensioning, and even incomplete ammonium removal [8]. A clear understanding of this phenomenon is key to improve current RSF operation and for the design of novel resource-efficient systems.

Fe^{2+} removal in RSFs is a two-step process that consists of (i) Fe^{2+} oxidation to Fe^{3+} and (ii) subsequent entrapment of the oxidation products within the filter bed. Fe^{2+} oxidation can take place via three different oxidation mechanisms: homogeneous (flocculent), heterogeneous (surface-catalytic), and biological [9]. Homogeneous oxidation is a chemical reaction between dissolved Fe^{2+} and dissolved oxygen. Poorly crystalline, low-density hydrous ferric oxide flocs (Fe^{3+} flocs) with large specific surface area are formed [10,11], with reactive oxygen species (ROS) derived from Fenton chemistry as byproducts [12]. Fe^{3+} flocs accumulate within the pore space of RSFs during operation, clogging the filter and thus forcing backwashing. Heterogeneous oxidation occurs when Fe^{2+} adsorbed onto the surface of sand grains is oxidized. Fe^{2+}-surface complex formation is followed by the oxidation of Fe^{2+} to Fe^{3+} and subsequent hydrolysis, producing compact hydrous ferric oxides that generate a coating on the sand grains, contributing to sand grain growth [11]. Biological iron oxidation is catalyzed by iron-oxidizing bacteria (FeOB). FeOB and its Fe oxidation products form a porous coating on the sand grains, which may release stalk-like ferric oxides into the pore water. On the contrary, NH_4^+ oxidation is an exclusively biological process carried out by NH_4^+-oxidizing (AOB) and comammox bacteria, as well as NH_4^+-oxidizing archaea, with nitrite and nitrate as products [13]. During the last

decades, virtually all compounds that play a role in Fe^{2+} oxidation within RSFs have been reported to inhibit microbial activity [14–18].

Dissolved Fe^{2+} and ROS have been shown to decrease the growth rate of pure cultures [14,15]. Similar conclusions were drawn for the products of homogeneous iron oxidation, i.e. Fe^{3+} flocs [16], and heterogeneous iron oxidation, i.e. Fe oxide coating [17,18]. In a real-life industrial set-up, de Vet and colleagues (2009) concluded that the presence of Fe^{3+} flocs and Fe oxide coating reduces the nitrification capacity of full-scale sand filters. While this extensive body of knowledge certainly contributes to our understanding of the interactions that take place, it also poses a challenge in distilling the essential information - *which are the specific processes responsible for the segregation between Fe^{2+} and NH_4^+ oxidation in RSFs*. Here, we aimed at determining which compound(s) involved in Fe^{2+} oxidation have a major impact on NH_4^+ oxidation in RSFs. A systematic and quantitative evaluation of the impact of each compound on ammonia oxidation was adopted, including dissolved Fe^{2+}, Fe^{3+} flocs, ROS, and Fe oxide coating. Each Fe^{2+} oxidizing mechanism and the involved compound was separately studied using a combination of batch essays, laboratory columns, and full-scale RSFs observations, supported by modelling.

5.2. MATERIALS AND METHODS

5.2.1. Full-scale filter sampling and media collection

Fe oxide-coated filter media was collected from the top of a filter located in DWTP Hammerflier, operated by Vitens, in Den Ham (the Netherlands). The filter is fed with aerated groundwater with 2.6mg NH_4-$N^+ \cdot L^{-1}$ and 3 mg$Fe^{2+} \cdot L^{-1}$. NH_4^+ removal is completely absent at the filter top, and only starts after Fe is removed (Figure S1). Filter media was transported in water at 4 °C and added to the lab-scale column within 8h.

Full-scale sand filter experiments (Results 3.6) were performed in a groundwater-fed rapid sand filter located in DWTP Loosdrecht, operated by Vitens, in Loosdrecht (the Netherlands). The filter consisted of a 1 m top layer of anthracite (1.4-2.0 mm), and a 1 m bottom layer of sand (0.8-1.25 mm), which were slightly mixed. Water samples were taken before and after backwashing. The first round of water samples were obtained after a filter run time of about 52 hours with a flow of about 225 m^3/hour. Afterwards, the filter was backwashed

following the drinking water companies standard protocol. A second round of water samples was taken after about 2.5 hours operation.

In both cases, the filters were equipped with water taps which enabled water sampling along the filter depth of the filter bed as well as in the supernatant water. Water samples were immediately filtered (0.45 µm), stored at 4 °C, and measured within 24 h as explained below.

5.2.2. Laboratory column experiments

Six sand filter columns of 20 cm height and an inner diameter of 2.5 cm were operated continuously in down-flow mode at a superficial velocity of 1.5 $m \cdot h^{-1}$ with growth medium (L^{-1}; 2 mg NH_4-N, 17.4 mg K_2HPO_4, 60µL trace elements solution (L^{-1}; 15 g EDTA, 4.5 g $ZnSO_4 \cdot 7H_2O$, 4.5 g $CaCl_2 \cdot 2H_2O$, 3 g $FeSO_4 \cdot 7H_2O$, 1 g H_3BO_3, 0.84 g $MnCl_2 \cdot 2H_2O$, 0.3 g $CoCl_2 \cdot 6H_2O$, 0.3 g $CuSO_4 \cdot 5H_2O$, 0.4 g $Na_2MoO_4 \cdot 2H_2O$, 0.1 g KI)) at pH 7.7 ± 0.1 and ambient temperature (20°C). pH and dissolved oxygen were continuously sensed (Applikon AppliSens, the Netherlands) at the influent and effluent of the column. Three distinct sets of experiments were performed (Figure 1), focusing on (a) the effect of Fe oxide coating, (b) Fe^{2+} and (c) hydraulics. The filter medium consisted of either (*i*) 240 g of virgin quartz sand (Aqua-Techniek B.V., the Netherlands), (*ii*) 190 g of Fe oxide-coated sand from the top of a full-scale filter in DWTP Hammerflier, or (*iii*) a mixture of 120 g virgin sand and 100 g Fe oxide-coated sand to achieve a bed height of 10 cm (Figure 1).

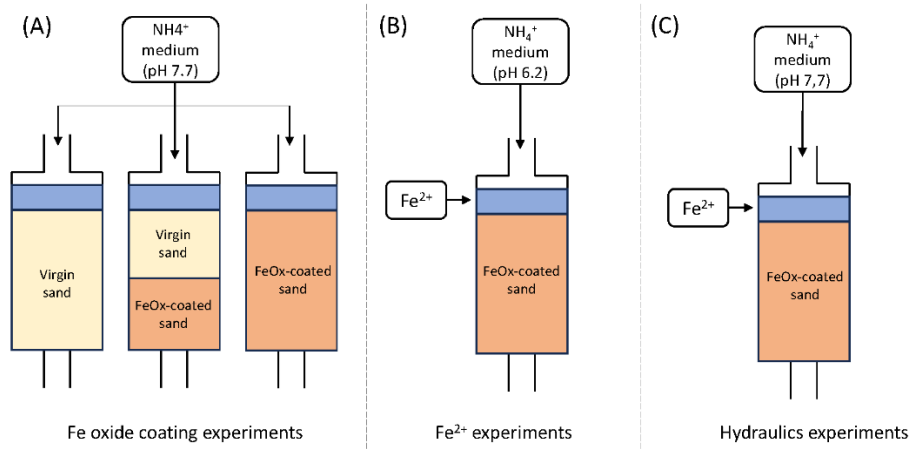

Figure 1. Schematic representation of the column experiments. A) Fe oxide coating experiments. B) Fe^{2+} experiments. C) Hydraulics experiments.

5.2.3. Fe oxide coating experiments

To evaluate the effect of the Fe oxide coating experiments on ammonia oxidation (Results 3.1), filter media from a full-scale filter with ammonia oxidation capacity was used to inoculate the columns as previously reported [20]. In short, 0.5 g of sand was vortexed with 10 mL tap water for 1.5 minutes. A total of 100 g of sand were processed. The resulting solution was amended with ammonium to reach a concentration of 10 mgN-$NH_4^+ \cdot L^{-1}$, divided in three, and recirculated through each of the three columns in a closed-circuit mode for 25 days. 250 mL of nitrifying sludge (4.6g VSS·L^{-1}) were added to the system on days 10th (and 20th for the virgin sand column), as done in previous research [21]. Before switching to standard operation (*i.e.* not recirculating), all columns were backwashed with 13.6L·h^{-1} tap water for 9 min to remove suspended particles.

5.2.4. Fe^{2+} experiments

The goal of this set of experiments was to evaluate the effect of dissolved Fe^{2+} on ammonia oxidation (Results 3.3). To properly evaluate the effect of Fe^{2+}, Fe^{2+} needs to flow through the column without being immediately oxidized to Fe^{3+} via homogeneous oxidation, which takes place in seconds at pH > 7.5. Homogeneous iron oxidation is slower at lower pHs. We chose pH 6.2 as our target, as ammonia oxidation by AOB is still physiologically feasible, and the majority of Fe^{2+} will not be chemical oxidation. The microbial community of a column filled with 190 g of Fe oxide-coated sand from the top of a full-scale filter in DWTP Hammerflier was adapted to pH 6.2 by step-wise decreasing the influent pH throughout a period of 2 months. Afterwards, a Fe^{2+} solution (0.5 g $FeCl_2 \cdot 4H_2O \cdot L^{-1}$) was fed from one of the lateral valves, directly into the supernatant, to reach a concentration of 1.5 mg$Fe^{2+} \cdot L^{-1}$.

5.2.5. Hydraulics experiments

In order to evaluate the effect of hydraulics on ammonia oxidation (Results 3.4), a column filled with 190g of Fe oxide-coated sand from the top of a full-scale filter in DWTP Hammerflier was operated at pH 7.7 throughout a period of 2 months to reach complete, stable NH_4^+ removal. Afterwards, a Fe^{2+} solution (0.5

g $FeCl_2 \cdot 4H_2O \cdot L^{-1}$) was fed from one of the lateral valves, directly into the supernatant, to reach a concentration of 1.5 mg$Fe^{2+} \cdot L^{-1}$.

5.2.6. Batch experiments

The maximum NH_4^+ removal rates of the filter media were determined in batch. 4 g of wet filter media, 50 mL of tap water, 100 µL of trace element solution (L^{-1}; 15 g EDTA, 4.5 g $ZnSO_4 \cdot 7H_2O$, 4.5 g $CaCl_2 \cdot 2H_2O$, 3 g $FeSO_4 \cdot 7H_2O$, 1 g H_3BO_3, 0.84 g $MnCl_2 \cdot 2H_2O$, 0.3 g $CoCl_2 \cdot 6H_2O$, 0.3 g $CuSO_4 \cdot 5H_2O$, 0.4 g $Na_2MoO_4 \cdot 2H_2O$, 0.1 g KI) and 500 µL of 100 nM K-phosphate buffer solution (1.37 g $KH_2PO_4 \cdot L^{-1}$, 1.75 g $K_2HPO_4 \cdot L^{-1}$, pH 7.7) were mixed in 300mL shake flasks. After an acclimatization period of 30 min at 25 °C and 100 rpm, each flask was spiked with 1 mL of feed (100 mg$N \cdot L^{-1}$ NH_4Cl and 87mg $K_2HPO_4 \cdot L^{-1}$) (Sigma Aldrich, Saint Louis, Missouri USA). Liquid samples (1 mL) were taken at different time intervals throughout the entire process. Maximum removal rates per mass (wet weight) of filter media were calculated by fitting the concentration profiles to a first-order kinetic rate equation. To study the effect of ROS, the batch tests were amended with 75 µL of ultrapure water (control), 4 g $Fe^{2+} \cdot L^{-1}$ (Fe^{2+}) or 4 g Fe^{3+}- flocs$\cdot L^{-1}$ (Fe^{3+}) and 254 µL of 4 g$\cdot L^{-1}$ TEMPOL, 215 g$\cdot L^{-1}$ mannitol, 0.4 g$\cdot L^{-1}$ catalase (3000 U$\cdot mg^{-1}$), 32 g$\cdot L^{-1}$ methanol or ultrapure water every 30 min during 3 h, mimicking the continuous operation of full-scale rapid sand filters. TEMPOL was added at a 1:1 TEMPOL:Fe^{2+} molar ratio [22], methanol at 200:1, in the range tested by Tong et al. (2022), and mannitol and catalase to reach a final concentration of 360 U$\cdot mL^{-1}$ and 30 mM, similar to the approach of Brinkman et al. (2016). Similarly, to test the effect of Fe^{3+} flocs 75 µL of 4/8/12/16 g Fe^{3+}- flocs$\cdot L^{-1}$ (Fe^{3+}) were added every 30 min during 2.5h.

The Fe^{2+} solution was prepared anaerobically in a vinyl PVC anaerobic chamber (Coy Laboratory Products, Grass Lake, Michigan, USA) at pH 2 to avoid Fe^{2+} oxidation. To prepare the Fe^{3+} floc solution, a concentrated solution of Fe^{2+} was slowly added into a recipient vessel with ultrapure water vigorously agitated to ensure direct Fe^{3+} floc formation.

5.2.7. Analytical procedures and data analysis

Samples for ammonium, nitrite, and nitrate quantification were immediately filtered through a 0.2 µm nanopore filter and measured within 12 h using photometric analysis (Gallery Discrete Analyzer, Thermo Fischer Scientific, Waltham, Massachusetts, USA). Samples for iron were analysed within 12 h by spectrophotometry (DR3900, Hach Company, Ames, Iowa, USA) using the LCK320 kit (Hach Company, Ames, Iowa, USA). Mn was analysed using inductively coupled plasma mass spectrometry (ICP-MS, Analytikal Jena PlasmaQuant MS). Water pressure along the column height was measured with a GMH 3100 manometer (Greisinger, Germany).

Batch test data were plotted and statistically analysed with GraphPad Prism software (Dotmatics, UK), which uses a statistical method equivalent to ANCOVA (Analysis of Covariance) to determine if the slopes between two linear regressions are significantly different. A significant difference was considered when $p\text{-value} < 0.05$.

Hydraulic retention time was measured using salt as a tracer. 10 mL of 1 g/L NaCl were spiked to the supernatant of the column. The increase in electric conductivity in the water effluent was measured using a flow-through cell connected to an electrical conductivity sensor (WTW, Xylem Analytics, Weilheim, Germany).

The residence time of groundwater in the filter was estimated to assess oxidation over time in the filter and to obtain kinetic rate constants of the reactants. The height of the sampling location was converted to a residence time by calculating the volume of water within the supernatant and filter bed based on the height and an assumed porosity of 0.4 and dividing the volume of water by the flow to obtain the residence time. First-order rate constants were estimated by fitting a first-order rate equation to the observed concentrations over residence time in the supernatant and filter bed. This was done using a least-squares routine in Python (v. 3.6.4).

5.3. RESULTS

5.3.1. Fe oxide coating does not inhibit NH_4^+ oxidation

Fe oxide-coated media contain reactive surfaces that might hamper the colonization, growth, or NH_4^+ oxidation capacity of NH_4^+-oxidizing organisms. To test this hypothesis, three lab-scale columns with either (i) virgin sand, (ii) Fe oxide-coated sand or (iii) 50% virgin – 50% Fe oxide-coated sand were inoculated and run in continuous mode for 45 days after a 25-day inoculation in 100% recirculation mode (Figure 2A). The two columns with Fe oxide-coated sand started consuming NH_4^+ immediately after inoculation and achieved complete removal after 10 (Fe oxide-coated sand) and 26 days (mixed sand). On the contrary, NH_4^+ conversion was absent in the virgin sand column at the beginning of the experiment, and a second inoculation with nitrifying activated sludge (day 10) did not yield better results. Therefore, on day 20, the effluent of the Fe oxide-coated sand filter was connected to the influent of the virgin sand column. Complete NH_4^+ removal was achieved within 5 days, presumably due to suspended cells carried from the Fe oxide-coated sand filter. Once the effluent of the Fe oxide-coated sand filter was disconnected (day 25), NH_4^+ consumption decreased rapidly and stabilized at 12 ± 3%. Microscopic visualization of the media showed that the onset of NH_4^+ consumption coincided with the appearance of brown patches that resemble Fe oxides (Figure 2C) on the previously virgin sand (Figure 2B).

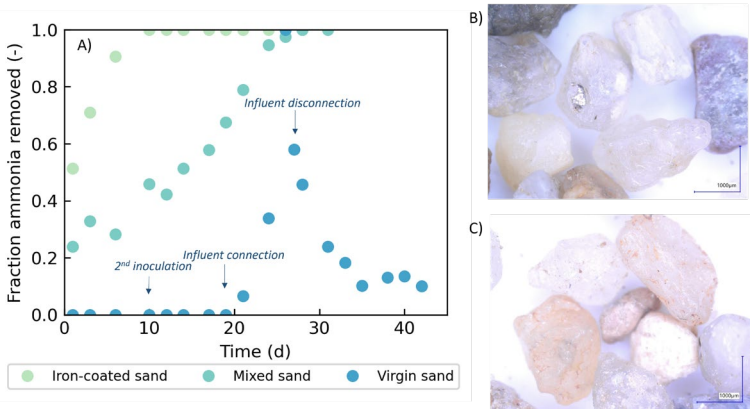

Figure 2. A) Fraction of NH_4^+ removed in the effluent of the three lab-scale sand filters during continuous operation. Blue arrows indicate the second inoculation (day 10) and the connection and disconnection of the influent of the virgin sand filter to the effluent of the Fe-oxide coated filter (days 20 and 25). B) Microscopic image of the virgin sand on day 10. C) Microscopic image of the virgin sand on day 35, slightly covered with brown patches that resemble Fe oxides.

5.3.2. Fe^{2+}-derived ROS do not inhibit NH_4^+ oxidation

Reactive oxygen species (ROS) are formed as by-products of homogeneous Fe oxidation [24]. The potential inhibition of NH_4^+ oxidation by ROS was tested in batch tests with Fe oxide-coated sand with NH_4^+-oxidizing activity amended with ROS-quenchers/scavengers TEMPOL, mannitol, catalase, and methanol. Negative control experiments showed that ROS quenchers/scavengers do not diminish the rate of NH_4^+ oxidation (light green). On the contrary, Fe^{2+} addition (which quickly oxidized to Fe^{3+}, dark green) significantly decreased the rate, regardless of the addition of ROS-quenchers/scavengers (-24.8 ± 1.8% on average). Adding Fe^{3+} flocs instead of Fe^{2+} resulted in a similar level of inhibition (-30%, blue).

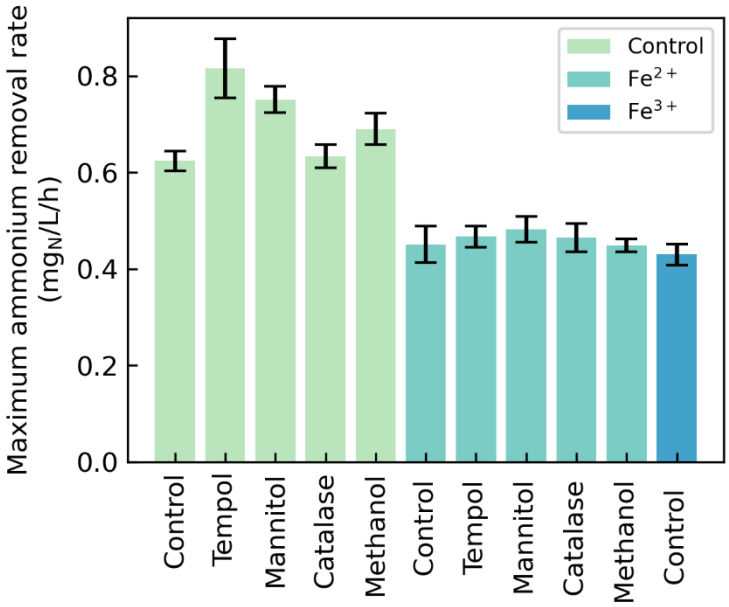

Figure 3. Maximum NH_4^+ removal rates of the sand grains in the absence (light green), or presence of Fe^{2+} (dark green) or Fe^{3+} flocs (blue). Control tests contain no ROS quenchers/scavengers (TEMPOL, mannitol, catalase, and methanol). All tests were performed aerobically to ensure quasi-instantaneous Fe^{2+} oxidation and concomitant ROS formation, mimicking the conditions of full-scale sand filter supernatants. Activities were quantified in triplicates, error bars represent standard deviation.

5.3.3. Fe^{2+} presence does not interfere with NH_4^+ oxidation

Dissolved Fe^{2+} is the Fe form that enters full-scale sand filters. To evaluate its effect on NH_4^+ oxidation, a lab-scale column filled with Fe oxide-coated sand was continuously fed with NH_4^+-amended tap water at pH 6.2. Complete NH_4^+ removal was obtained after 2 months, after which Fe^{2+} addition into the supernatant started. The low pH allowed Fe^{2+} to penetrate deep into the bed without oxidizing (Figure 4A), as both homogeneous and heterogeneous oxidation rates substantially decrease with decreasing pH [25,26]. In accordance, Fe^{3+} was barely observed throughout the filter (Figure 4B), leaving adsorption as the only cause of Fe^{2+} removal. The NH_4^+ concentration profile along the filter depth remained relatively stable during the course of the experiment (Figure 4C), demonstrating that the presence of (adsorbed) Fe^{2+} cannot explain the inhibition of NH_4^+ removal observed at the top section of full-scale sand filters.

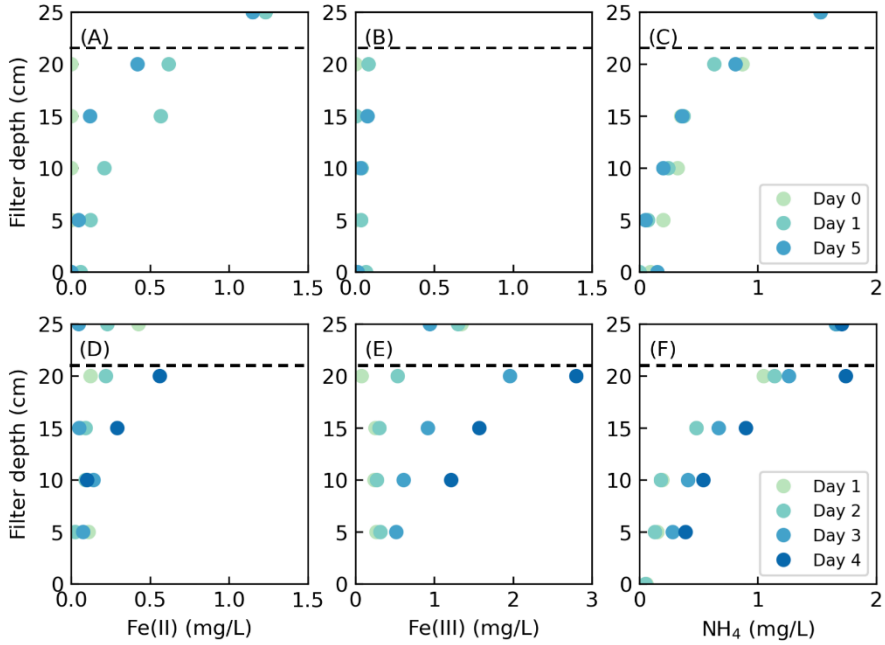

Figure 4. Fe^{2+} (A, D), Fe^{3+} (B, E), and NH_4^+(C, F) removal profiles along the depth of a lab-scale sand filter during continuous dosing of Fe^{2+} at pH 6.2 (A, B, C) and 7.7 (D, E, F), respectively. The initial Fe^{2+} concentration is 1.5 mg/L. Data points represent single measurements. Dashed horizontal line indicates supernatant position.

5.3.4. Fe^{3+} flocs spatially delay NH_4^+ oxidation

Similarly to section 3.3, a lab-scale sand filter filled with Fe oxide-coated sand was continuously fed with tap water amended with NH_4^+ but now at higher pH (pH=7.7). Full NH_4^+ removal was obtained after 2 months of acclimation, after which Fe^{2+} addition into the supernatant started. Fe^{2+} was consistently oxidized at the filter top, with >75% removal in the first 5 cm (Figure 4D). Homogeneous Fe oxidation was the main Fe removing mechanism in the system, and most flocs accumulated at the top (Figure 4E). The accumulation of Fe^{3+} flocs throughout the experiment resulted in filter clogging in the top of the column, which changed the hydraulic conditions of the filter (see SI 8.2) and spatially delayed the removal of NH_4^+ (Figure 4F). At the end of the experiment, NH_4^+ oxidation was completely absent in the first 5 cm of the filter bed (Figure 5), and the estimated first-order rate constants (k) decreased in the downstream sections (from 0.022 to 0.015 s^{-1}). These results show that Fe^{3+} floc accumulation is directly responsible for the loss of ammonia oxidation activity in sand filters, supporting the findings of Figure 3. In addition, they indicate that the loss in ammonia oxidation activity is more prominent in zones where more Fe^{3+} flocs accumulate, with total loss of activity at high floc content. The following sections aim at understanding the inhibiting mechanism.

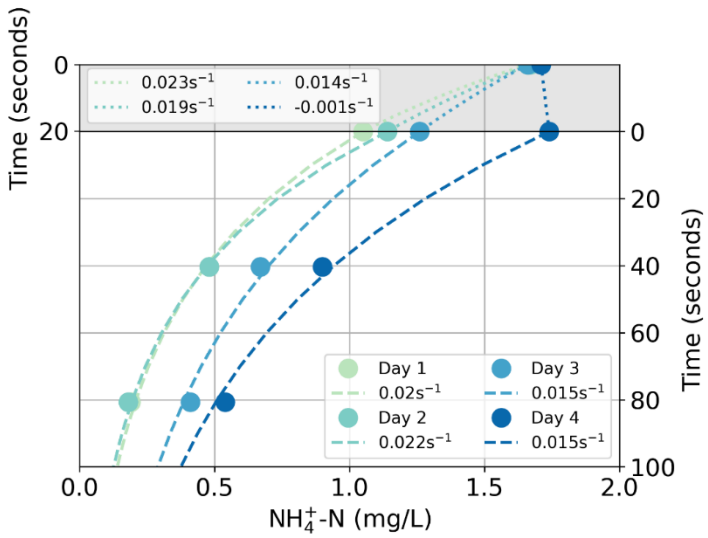

Figure 5: NH_4 oxidation rate constants (k) estimated for the top 5 cm of the filter bed (gray background) and the downstream sections (white background. Dots show the observed concentration, and dashed lines show the fits used to estimate k values. $R^2 > 0.996$ for all datasets.

5.3.5. Increasing pore velocities due to clogging alone cannot explain the spatial delay in NH_4^+ oxidation

Changing transport patterns in the filter bed due to Fe^{3+} floc accumulation may affect NH_4^+ oxidation. Since the sand filter was operated at constant flow, Fe^{3+} floc accumulation (*i.e.*, increase in filter bed resistance) directly translated into (local) increases in water pore velocity. Consequently, contact times between AOB and NH_4^+ are shorter, which could theoretically push NH_4^+ oxidation deeper into the filter bed. To evaluate the contribution of increased pore water velocities to the spatial delay of NH_4^+ oxidation, we estimated the average pore water velocity needed to explain the four observed NH_4^+ concentration profiles in Figure 5 assuming that Fe^{3+} flocs do not inhibit AOB *i.e.* maintaining a constant k of $0.02 s^{-1}$ for the top 5cm of the filter bed. A local average increase in pore water velocity changes the hydraulic retention time (HRT) in the filter, and can be estimated using the equation below:

$$C_{depth=5cm} = C_{depth=0cm} \times e^{-(k*t)} \quad \text{eq.1}$$

where t is the travel time between the two depths (s), $C_{depth\ =\ i\ cm}$ is the NH_4-N concentration ($mg \cdot L^{-1}$) at a depth *I, and k* is the NH_4^+ oxidation rate constant (s^{-1}).

Simulating the results for the top 5 cm of filter bed for each day yields theoretical HRTs of 23, 19, 14, and ~0 seconds for day 1, 2, 3, and 4, respectively. This means that a 1.2, 1.7, and infinite fold-increase in the water pore velocity are needed to explain the decrease in NH_4^+ oxidation solely by changes in HRT (Table 1), which is proportional to a loss in pore space of 17%, 41%, and ~100%, for Days 2, 3, and 4, respectively. These percentages are substantially higher than the maximum percentage of pore space that could be filled up with the theoretical amount of Fe^{3+} flocs formed during the experiment (1%). We deem it, therefore, unlikely that changes in hydraulic conditions in the clogged column alone can explain the spatial delay in NH_4^+ oxidation.

Table 1. Estimated hydraulic retention time and fold increase in pore water velocity are needed to explain the spatial delay in NH_4^+ removal in the lab-scale sand filter solely due to changes in transport phenomena.

	Day 1	Day 2	Day 3	Day 4
Hydraulic retention time (s)	23	19	14	~ 0
Pore water velocity fold-increase (-)	-	1.2	1.7	∞
Loss of pore space (%)	0	17	41	~100

5.3.6. Fe^{3+} flocs reduce the activity of NH_4^+-oxidizing bacteria (AOB)

The potential direct impact of Fe^{3+} flocs on AOB – *i.e.*, reducing their ammonia oxidation capacity - was tested in batch tests. Sand grains from the same NH_4^+ oxidising full-scale sand filter as for the column study were incubated with 0, 30, 60, 90, and 120 mgFe^{3+}flocs·L^{-1}. Sand grains are continuously mixed and thus clogging and transport limitations do not play a role. Figure 6 shows that higher floc content yielded proportionally lower maximum NH_4^+ removal rates, demonstrating that Fe^{3+} flocs inhibit AOB.

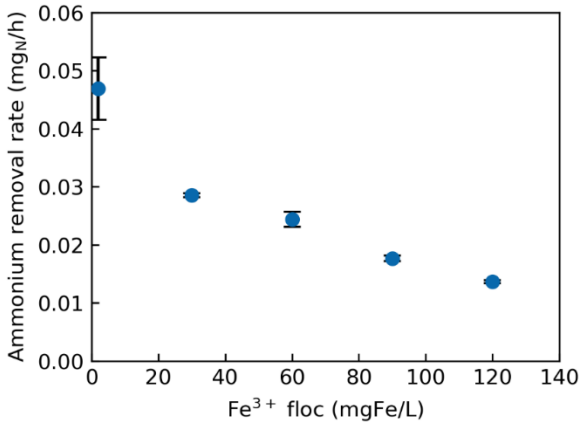

Figure 6. Maximum NH_4^+ removal rates of the sand grains with increasing amounts of Fe^{3+} flocs in the medium. Fe^{3+} flocs were added every 30 min during a period of 3h, mimicking the conditions of full-scale sand filter supernatants. X-axis indicates the concentration of Fe^{3+} at the end of the experiment. Activities were quantified in triplicates, error bars represent standard deviation between them. All data points included in Figure S4.

Comparing the amount of Fe^{3+} flocs accumulated in this experiment and the lab-scale sand filter (Figure 5) allows to estimate the likelihood of Fe^{3+} flocs contributing to the spatial delay in NH_4^+ in the sand filter. About 100 mg of Fe^{3+} flocs were produced during the sand filter experiment, which corresponds to a floc content of >2000 mg Fe/L assuming a homogeneous distribution across all pores in the column and total floc retention. A more realistic assumption is that all flocs were entrapped within the first 5 cm of the filter bed (Figure 5e), which yields a Fe^{3+} floc content of >15,000 mg Fe/L. In both cases, the floc content is 1 to 2 orders of magnitude higher than the maximum content of flocs in the batch experiments (~120 mg/L) (Figure 6), which was enough to reduce the NH_4^+ removal capacity of the sand grains by 50%. Therefore, we conclude that AOB inhibition by Fe^{3+} flocs is likely the main mechanism inhibiting NH_4^+ removal at the top of sand filters.

5.3.7. Reversible inhibition of NH_4^+ and Mn^{2+} oxidation by Fe^{3+} flocs

The reversibility of the spatial delay in NH_4^+ removal caused by Fe^{3+} flocs was evaluated by assessing the NH_4^+ concentration profiles along the filter depth of a full-scale filter before and after backwashing (Figure 7A). NH_4^+ removal was almost absent at the filter top at the end of a filter run, *i.e.* before backwashing. Backwashing moved the NH_4^+ removal to the filter top, even though dissolved – Fe^{2+} - and particulate – Fe^{3+} flocs - Fe were not completely removed (see Figure S3).

The effect of backwashing was also evaluated for Mn^{2+}, to explore putative parallelisms between the inhibiting effects of Fe^{3+} flocs (Figure 7B and 7C). Similarly, while Mn^{2+} was barely removed at the filter top before backwashing, removing the Fe^{3+} flocs moved its removal to the filter top, resulting in a similar 2.68 and 2.08 fold-increase in the first-order oxidation rate constants for NH_4^+, and Mn^{2+}, respectively. Note that, contrary to NH_4^+, the removal of Mn^{2+} does not exclusively rely on microorganisms, and can be chemically catalyzed. Interestingly, the trends are nonetheless similar, which may indicate that Fe^{3+} flocs affect the removal of both contaminants in a similar, yet undescribed fashion.

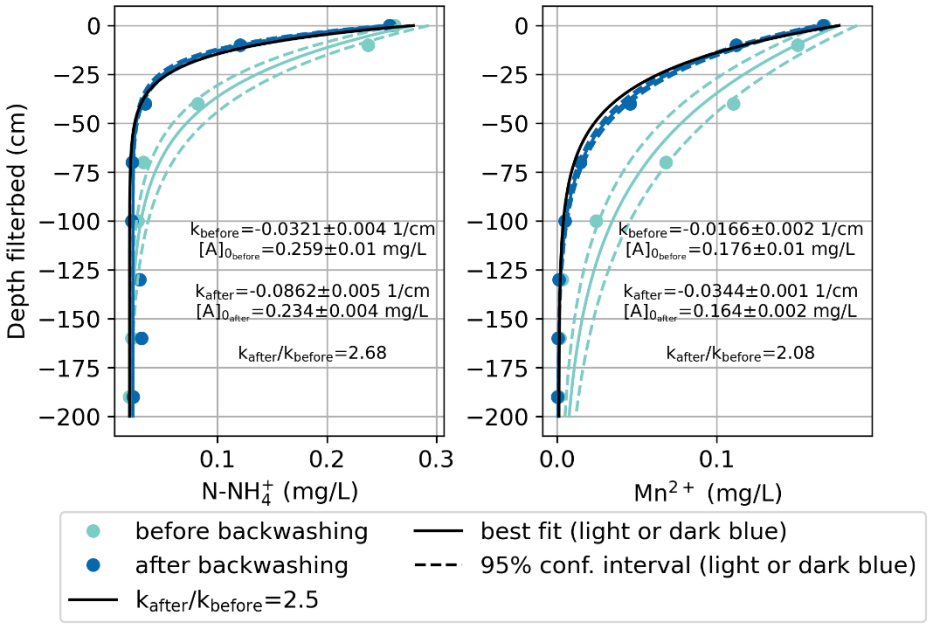

Figure 7. NH_4^+ and Mn^{2+} concentration profiles along the depth of a full-scale sand filter before (green) and after (red) backwashing. Lines indicate the fitting of the curves to first-order removal processes (full), and the 95% confidence interval of the fitting (dashed).

5.4. Discussion

5.4.1. Dissolved Fe^{2+}, reactive oxygen species, and Fe oxide coating do not decrease the NH_4^+ removal capacity of sand filters

We evaluated the influence of dissolved Fe^{2+}, reactive oxygen species, and Fe oxide coating on NH_4^+ oxidation in sand filters and found no major inhibitory effects (Figures 2, 3, and 4C). Bacteria exposure to Fe^{2+} and ROS have often been associated with detrimental physiological effects. Swanner et al., (2015) showed that Fe^{2+} addition to a cyanobacteria culture decreased growth rate and attributed it to the intracellular accumulation of ROS. In another example, Zhang et al., (2020) found that exposing *Shewanella oneidensis* strain MR-1 to Fe^{2+}

minerals and oxygen decreased cell viability and associated it with ROS production as well. Fe^{2+} concentrations, a proxy for ROS concentration under aerobic conditions, were much higher in our batch tests than in those studies (70 mM vs 5 mM and 80 µM, respectively). However, our results clearly show no immediate decrease in the NH_4^+ removal rate, and effects on cell viability are likely marginal because NH_4^+ removal capacity in full-scale sand filters recovers immediately after backwashing (Figure 7), proving inhibition to be reversible. We hypothesize that ROS exert selective pressure on the sand filter ecosystem, and as a result, only organisms able to tolerate ROS thrive. An example of adaptation is the increase in catalase activity and upregulation of several antioxidant genes in AOB *Nitrosomonas oligotropha PLL12* upon exposure to ROS observed by Wang et al., (2023).

In a similar fashion, several studies on both pure and mixed cultures pointed out the toxic effects of Fe oxides. Growth inhibition by several Fe oxides – including ferrihydrite, the most common Fe oxide in sand filters [28] – was observed by Du et al., (2019), and decreases in cell viability upon exposure to Fe oxide nanoparticles [29] and Fe oxide-containing clay minerals [18] are also commonly reported. Our nitritation experiments (Figure 2) not only indicate that Fe oxides do not impede the growth of AOB on sand grains, but also that their presence even accelerates their establishment. In addition, Fe oxide coatings have high specific surface areas [30], which seem to be a critical factor for biofilm growth [31]. One of the limitations of our study is that the experiments were carried out on a stable Fe oxide layer, *i.e.* no Fe^{2+} was fed into the system, so no new Fe oxides were generated. In contrast, the Fe oxide coating of sand grains of full-scale sand filters continuously grows during operation as a result of heterogeneous Fe^{2+} oxidation. One can argue that this dynamic situation may force AOB to match the growth rate of Fe oxides to ensure nutrient availability and avoid cell encrustation. However, Gülay et al., (2014) observed a positive correlation between cell abundance and mass mineral coating in full-scale sand filter grains, suggesting that the Fe oxide coating enhances, rather than hinders, the NH_4^+ removal capacity of full-scale sand filters. Another limitation of our work is that the experiments were run at 20°C and using artificial media, which does not mimic natural groundwater. Further research at conditions closer to that of drinking water treatment plants will improve our understanding of Fe chemistry of ammonia oxidation. Overall, we show that dissolved Fe^{2+}, reactive oxygen species, and Fe oxide coating do not have a major detrimental effect on

ammonia-oxidizing activity, contrary to what is commonly reported in literature. Beyond groundwater filtration, these results showcase the limitations of extrapolating results from pure culture studies into complex microbial communities.

5.4.2. Direct inhibition of AOB by Fe^{3+} flocs likely explains the spatial delay of NH_4^+ removal in full-scale sand filters

Fe^{3+} flocs are the main inhibitor of NH_4^+ oxidation in sand filters. We observed this phenomenon at laboratory- (Figure 5) and full-scale (Figure 7), and our results support the pioneering work of de Vet et al., (2009), which concluded that microbial nitrification in trickling filters might decline due to the irreversible accumulation of iron deposits. Likewise, the detailed molecular study of Tong et al., (2022) reported that Fe^{3+} flocs formed via homogeneous Fe^{2+} oxidation attach to the cell surface of *Pseudomonas putida*, severely decreasing its Mn^{2+} removal capacity. Ammonia oxidation kinetics in our lab-scale sand filter columns were fitted to a first-order rate equation and gave NH_4^+ oxidation rate constants (54-80 h^{-1}) slightly above those found by Lopato et al (2013) (8-16 h^{-1}) and references therein (9-17 h^{-1}) in full-scale systems, likely due to the loss of efficiency ascribed to flow pattern heterogeneity at bigger scales [33]. After 4 days of Fe^{2+} dosing, NH_4^+ removal capacity completely stopped at the filter top (NH_4^+ removal rate constant ~ 0) (Figure 5). Our experiments do not allow us to rule out completely the contribution of mass transfer limitations to the spatial delay in NH_4^+ removal in full-scale sand filters as a consequence of filter clogging but suggest that they do not play a major role (Table 1). On the contrary, Fe^{3+} floc contents in the batch test experiments were 1 to 2 orders of magnitude below the ones in lab-scale (Figure 4E) and full-scale filters (Figure S3), but were still high enough to decrease the maximum NH_4^+ removal capacity of AOB on sand grains by half (Figure 6). Taken together, these results provide solid evidence that (i) Fe^{3+} flocs inhibit the NH_4^+ oxidizing capacity of AOB and that (ii) this mechanism is likely the main responsible for the spatial delay of NH_4^+ removal in full-scale sand filters. The exact physiological mechanisms remain to be elucidated.

5.4.3. Ecological and industrial implications

Ammonium diffusion into the biofilm - *i.e.* mass transfer - has traditionally been considered to limit the nitrification capacity of sand filters fed with iron-free water [34,35]. Yet, the latest evidence indicates that NH_4^+ removal is limited by biokinetics, the product of AOB abundance and its maximum specific NH_4^+ removal rate [36]. In this work, we show that the presence of Fe^{3+} flocs inhibits the maximum NH_4^+ removal rate of AOB. Combined, these findings suggest that Fe^{3+} flocs effectively reduce the ammonia oxidation capacity of sand filters, and set avoiding Fe^{3+} floc formation as a clear optimization target. Strategies to segregate the removal of Fe and NH_4^+ have already been proposed and tested, and often encompass controlling the oxidation-reduction potential to avoid homogeneous Fe oxidation. Recent successful examples are anaerobic Fe^{2+} precipitation as vivianite [37], anoxic biological nitrate and Fe^{2+} co-removal [38] and aerobic biological Fe^{2+} oxidation at low oxygen concentration [39]. Nitrification problems caused by Fe^{3+} flocs are currently bypassed because sand filters are usually over dimensioned [40]. Nonetheless, finding solutions to directly tackle or avoid Fe^{3+} floc inhibition of ammonia oxidation is fundamental for the transition move towards resource-efficient, environmentally-friendly groundwater treatment. Beyond drinking water treatment, this work sheds light on the interplay between Fe and NH_4^+, two widespread and central compounds in many ecosystems across the planet.

5.5. CONCLUSIONS

In this work, we systematically and quantitatively evaluated the individual impact of the main Fe^{2+} oxidizing mechanisms and the resulting products on biological NH_4^+ oxidation in groundwater filters. Using a combination of batch essays, lab-scale columns experiments, full-scale column characterization and modelling, we conclude that:

- Dissolved Fe^{2+} and reactive oxygen species do not affect NH_4^+ oxidation
- Fe oxide coating aids NH_4^+-oxidizing activity on sand filter media grains
- Fe^{3+} flocs inhibit NH_4^+ oxidation by reducing the ammonia oxidation capacity of the microorganisms on the sand grains

- Changes in transport patterns due to clogging do not play a major role in NH_4^+ oxidation
- The inhibition of NH_4^+ oxidation is reversible and reduced by backwashing

Overall, our work sets finding solutions to directly tackle or avoid Fe^{3+} floc inhibition of ammonia oxidation as a priority to optimize groundwater treatment and transition towards the next generation of sustainable and efficient sand filters.

REFERENCES

1. Giordano, M. Global Groundwater? Issues and Solutions. *Annu. Rev. Environ. Resour.* **34**, 153–178 (2009).

2. Katsanou, K. & Karapanagioti, H. K. Surface water and groundwater sources for drinking water. *Handb. Environ. Chem.* **67**, 1–19 (2019).

3. de Vet, W., Dinkla, I. J. T., Rietveld, L. C. & van Loosdrecht, M. C. M. Biological iron oxidation by Gallionella spp. in drinking water production under fully aerated conditions. *Water Res.* **45**, 5389–5398 (2011).

4. Bourgine, F. P., Gennery, M., Chapman, J. I., Kerai, H., Green, J. G., Rap, R. J., Ellis, S. & Gaumard, C. Biological Processes at Saints Hill Water-Treatment Plant, Kent. *Water Environ. J.* **8**, 379–391 (1994).

5. Corbera-Rubio, F., Laureni, M., Koudijs, N., Müller, S., van Alen, T., Schoonenberg, F., Lücker, S., Pabst, M., van Loosdrecht, M. C. M. & van Halem, D. Meta-omics profiling of full-scale groundwater rapid sand filters explains stratification of iron, ammonium and manganese removals. *Water Res.* **233**, 119805 (2023).

6. Ramsay, L., Breda, I. L. & Søborg, D. A. Comprehensive analysis of the start-up period of a full-scale drinking water biofilter provides guidance for optimization. *Drink. Water Eng. Sci.* **11**, 87–100 (2018).

7. Gouzinis, A., Kosmidis, N., Vayenas, D. V. & Lyberatos, G. Removal of Mn and simultaneous removal of NH3, Fe and Mn from potable water using a trickling filter. *Water Res.* **32**, 2442–2450 (1998).

8. de Vet, W., Rietveld, L. C. & Van Loosdrecht, M. C. M. Influence of iron on nitrification in full-scale drinking water trickling filters. *J. Water Supply Res. Technol. - AQUA* **58.4**, 247–256 (2009).

9. Van Beek, C. G. E. M., Dusseldorp, J., Joris, K., Huysman, K., Leijssen, H., Schoonenberg Kegel, F., De Vet, W. W. J. M., Van De Wetering, S. & Hofs, B. Contributions of homogeneous, heterogeneous and biological iron(II) oxidation in aeration and rapid sand filtration (RSF) in field sites. *J. Water Supply Res. Technol. - AQUA* **65**, 195–207 (2016).

10. Janney, D. E., Cowley, J. M. & Buseck, P. R. Transmission electron microscopy of synthetic 2- and 6-line ferrihydrite. *Clays Clay Miner.* **48**, 111–119 (2000).

11. Van Beek, C. G. E. M., Hiemstra, T., Hofs, B., Nederlof, M. M., Van Paassen, J. A. M. & Reijnen, G. K. Homogeneous, heterogeneous

and biological oxidation of iron(II) in rapid sand filtration. *J. Water Supply Res. Technol. - AQUA* **61**, 1–13 (2012).

12. Hall, S. J. & Silver, W. L. Iron oxidation stimulates organic matter decomposition in humid tropical forest soils. *Glob. Chang. Biol.* **19**, 2804–2813 (2013).

13. Van Kessel, M. A. H. J., Speth, D. R., Albertsen, M., Nielsen, P. H., Op Den Camp, H. J. M., Kartal, B., Jetten, M. S. M. & Lücker, S. Complete nitrification by a single microorganism. *Nat. 2015 5287583* **528**, 555–559 (2015).

14. Swanner, E. D., Mloszewska, A. M., Cirpka, O. A., Schoenberg, R., Konhauser, K. O. & Kappler, A. Modulation of oxygen production in Archaean oceans by episodes of Fe(II) toxicity. *Nat. Geosci.* **8**, 126–130 (2015).

15. Zhang, Y., Tong, M., Yuan, S., Qian, A. & Liu, H. Interplay between iron species transformation and hydroxyl radicals production in soils and sediments during anoxic-oxic cycles. *Geoderma* **370**, 114351 (2020).

16. Tong, M., Zhao, Y., Sun, Q., Li, P., Liu, H. & Yuan, S. Fe(II) oxygenation inhibits bacterial Mn(II) oxidation by P. putida MnB1 in groundwater under O2-perturbed conditions. *J. Hazard. Mater.* **435**, 128972 (2022).

17. Du, H. Y., Yu, G. H., Sun, F. S., Usman, M., Goodman, B. A., Ran, W. & Shen, Q. R. Iron minerals inhibit the growth of Pseudomonas brassicacearum J12 via a free-radical mechanism: Implications for soil carbon storage. *Biogeosciences* **16**, 1433–1445 (2019).

18. Wang, X., Dong, H., Zeng, Q., Xia, Q., Zhang, L. & Zhou, Z. Reduced Iron-Containing Clay Minerals as Antibacterial Agents. *Environ. Sci. Technol.* **51**, 7639–7647 (2017).

19. Soler-Jofra, A., Picioreanu, C., Yu, R., Chandran, K., van Loosdrecht, M. C. M. & Pérez, J. Importance of hydroxylamine in abiotic N2O production during transient anoxia in planktonic axenic Nitrosomonas cultures. *Chem. Eng. J.* **335**, 756–762 (2018).

20. Wakelin, S. A., Page, D. W., Pavelic, P., Gregg, A. L. & Dillon, P. J. Rich microbial communities inhabit water treatment biofilters and are differentially affected by filter type and sampling depth. *Water Supply* **10**, 145–156 (2010).

21. Cai, Y., Li, D., Liang, Y., Luo, Y., Zeng, H. & Zhang, J. Effective start-up biofiltration method for Fe, Mn, and ammonia removal and bacterial community analysis. *Bioresour. Technol.* **176**, 149–155 (2015).

22. Bicudo, B., Medema, G. & van Halem, D. Inactivation of Escherichia coli and somatic coliphage ΦX174 by oxidation of electrochemically produced Fe2+. *J. Water Process Eng.* **47**, 102683 (2022).

23. Brinkman, C. L., Schmidt-Malan, S. M., Karau, M. J., Greenwood-Quaintance, K., Hassett, D. J., Mandrekar, J. N. & Patel, R. Exposure of bacterial biofilms to electrical current leads to cell death mediated in part by reactive oxygen species. *PLoS One* **11**, 1–23 (2016).

24. Hug, S. J. & Leupin, O. Iron-catalyzed oxidation of Arsenic(III) by oxygen and by hydrogen peroxide: pH-dependent formation of oxidants in the Fenton reaction. *Environ. Sci. Technol.* **37**, 2734–2742 (2003).

25. Tamura, H., Goto, K. & Nagayama, M. The effect of ferric hydroxide on the oxygenation of ferrous ions in neutral solutions. *Corros. Sci.* **16**, 197–207 (1976).

26. Singer, P. C. & Stumm, W. Acidic Mine Drainage: The Rate-Determining Step. *Science (80-.).* **167**, 1121–1123 (1970).

27. Wang, H., Li, P., Liu, X., Zhang, J., Stein, L. Y. & Gu, J. D. An overlooked influence of reactive oxygen species on ammonia-oxidizing microbial communities in redox-fluctuating aquifers. *Water Res.* **233**, 119734 (2023).

28. Haukelidsaeter, S. *et al.* Efficient chemical and microbial removal of iron and manganese in a rapid sand filter and impact of regular backwash. *Appl. Geochemistry* **162**, 105904 (2024).

29. Arakha, M., Pal, S., Samantarrai, D., Panigrahi, T. K., Mallick, B. C., Pramanik, K., Mallick, B. & Jha, S. Antimicrobial activity of iron oxide nanoparticle upon modulation of nanoparticle-bacteria interface. *Sci. Rep.* **5**, 1–12 (2015).

30. Haukelidsaeter, S. *et al.* Influence of filter age on Fe, Mn and NH4+ removal in dual media rapid sand filters used for drinking water production. *Water Res.* **242**, 120184 (2023).

31. Kostka, J. E., Dalton, D. D., Skelton, H., Dollhopf, S. & Stucki, J. W. Growth of iron (III)-reducing bacteria on clay minerals as the sole electron acceptor and comparison of growth yields on a variety of oxidized iron forms. *Appl. Environ. Microbiol.* **68**, 6256–6262 (2002).

32. Gülay, A., Tatari, K., Musovic, S., Mateiu, R. V., Albrechtsen, H. J. & Smets, B. F. Internal porosity of mineral coating supports microbial activity in rapid sand filters for groundwater treatment. *Appl.*

Environ. Microbiol. **80**, 7010–7020 (2014).

33. Lopato, L., Galaj, Z., Delpont, S., Binning, P. J. & Arvin, E. Heterogeneity of Rapid Sand Filters and Its Effect on Contaminant Transport and Nitrification Performance. *J. Environ. Eng.* **137**, 248–257 (2011).

34. Lopato, L., Röttgers, N., Philip, ;, Binning, J. & Arvin, E. Heterogeneous Nitrification in a Full-Scale Rapid Sand Filter Treating Groundwater. *J. Environ. Eng.* **139**, 375–384 (2013).

35. van den Akker, B., Holmes, M., Cromar, N. & Fallowfield, H. Application of high rate nitrifying trickling filters for potable water treatment. *Water Res.* **42**, 4514–4524 (2008).

36. Lee, C. O., Boe-Hansen, R., Musovic, S., Smets, B., Albrechtsen, H. J. & Binning, P. Effects of dynamic operating conditions on nitrification in biological rapid and filters for drinking water treatment. *Water Res.* **64**, 226–236 (2014).

37. Goedhart, R., Müller, S., van Loosdrecht, M. C. M. & van Halem, D. Vivianite precipitation for iron recovery from anaerobic groundwater. *Water Res.* **217**, 118345 (2022).

38. Corbera-Rubio, F., Stouten, G. R., Bruins, J., Dost, S. F., Merkel, A. Y., Müller, S., van Loosdrecht, M. C. M., van Halem, D. & Laureni, M. "Candidatus Siderophilus nitratireducens": a putative nap-dependent nitrate-reducing iron oxidizer within the new order Siderophiliales. *ISME Commun.* (2024).

39. Müller, S., Corbera-Rubio, F., Schoonenberg-Kegel, F., Laureni, M., Van Loosdrecht, M. C. M., Van Halem, D., Loosdrecht, M. C. M. van & Halem, D. van. Shifting to biology promotes highly efficient iron removal in groundwater filters. *bioRxiv* 2024.02.14.580244 (2024).

40. Tatari, K., Smets, B. F. & Albrechtsen, H. J. Depth investigation of rapid sand filters for drinking water production reveals strong stratification in nitrification biokinetic behavior. *Water Res.* **101**, 402–410 (2016).

Nature is merciful [...], live dangerously, takes things as they come, dread naught, all will be well.

W. Churchill

BIOLOGICAL METHANE REMOVAL BY GROUNDWATER TRICKLING BIOFILTRATION FOR EMISSIONS REDUCTION

6

ABSTRACT

Methane removal is an essential step for drinking water production from methane-rich groundwaters. Stripping with aeration, the most commonly applied technology, results in direct methane emissions accounting for up to a third of the total carbon footprint of a treatment plant. We designed and operated a full-scale trickling filter to oxidize methane biologically prior to a submerged sand filter, and compared its performance to a conventional aeration – submerged sand filtration set-up. Full-scale data was combined with *ex-situ* batch essays and metagenome-resolved metaproteomics to quantify the individual contribution of the main (a)biotic processes and characterize the enriched microbial communities. Both treatment schemes fully removed methane, iron, ammonium and manganese, yet the underlying mechanisms differed significantly. Methane was completely removed in the trickling filter, and biological oxidation accounted for half of the removal, and thus halving its overall emissions. Methane-oxidizing bacteria not only outcompeted nitrifiers in the trickling filter, but also likely contributed directly to ammonia oxidation. With respect to iron, in contrast to the submerged filter preceeded by methane stripping, signatures of biological iron oxidation were almost completely absent in the trickling filter suggesting that methane promotes chemical iron oxidation. All systems had similar *ex-situ* manganese oxidation capacities, yet removals occurred only in the submerged filter following the trickling filter. Ultimately, our results demonstrate that trickling filtration is effective in promoting biological methane oxidation at overall fully comparable effluent qualities. The proven potential for significant reductions in methane emission showcases the opportunities towards more sustainable drinking water production.

HIGHLIGHTS

- Trickling biofiltration effectively removed methane via biological oxidation
- Biological oxidation halved overall methane emissions at comparable effluent quality
- Methane oxidizers outcompeted ammonia oxidizers and directly contributed to ammonia removal
- Methane increased oxygen demand and shifted iron removal from (partially) biotic to abiotic

Submitted as:

Corbera-Rubio, F., Boersma, A. S., de Vet, W. W. J. M., Pabst, M., van der Wielen, P. W. J. J., van Kessel, M. A. H. J., van Loosdrecht, M. C. M., van Halem, D., Lücker, S. & Laureni, M. Biological methane removal in groundwater trickling biofiltration for emissions reduction [*Manuscript submitted for publicatiom]* (2024).

6.1. INTRODUCTION

Aeration with subsequent submerged sand filtration is the most applied technology for groundwater treatment for drinking water production. Groundwater is commonly pre-aerated to remove undesired gases like methane (CH_4), hydrogen sulfide (H_2S), and carbon dioxide (CO_2) and to introduce oxygen (O_2). The introduction of O_2 to saturation levels onsets the oxidation of the main groundwater contaminants – soluble iron (Fe^{2+}), ammonium (NH_4^+), and manganese (Mn^{2+}) – in the sand filter[1]. This treatment scheme has proven efficient and robust, and provides an eco-friendly, chemical-free alternative to chlorine- and ozone-based technologies. However, methane stripping during aeration is of environmental concern due to the direct emission of this greenhouse gas to the atmosphere, and may account for over a third of the carbon footprint of a drinking water treatment plant (DWTP)[2]. Reducing methane emissions is thus paramount to the transition towards sustainable, resource-efficient groundwater treatment systems.

Biological methane oxidation is a promising alternative to decrease direct methane emissions from DWTPs[3]. Under aerobic conditions, methane oxidation to CO_2 is performed by methane-oxidizing bacteria (MOB)[4]. Aerobic MOB conserve energy from the step-wise oxidation of CH_4 to CO_2. The first step of the reaction - the transfer of one oxygen atom from O_2 to CH_4 to form methanol (CH_3OH) - is carried out by either a soluble (sMMO) or a particulate methane monooxygenase (pMMO)[5]. The pMMO belongs to a protein family known as copper membrane monooxygenases (CuMMO), which also includes the ammonia monooxygenase (AMO). Amo catalyzes the oxidation of ammonia to hydroxylamine and is encoded by canonical ammonia-oxidizing bacteria (AOB) and archaea (AOA), and complete ammonia oxidizers (comammox) [5–7]. As methane and ammonia are structurally similar molecules, pMMO and AMO can catalize the oxidation of the other enzyme's primary substrate[5]. Recently, MOB have even been suggested to play an important role in the nitrogen cycle in environments with high ammonium concentrations[8].

Since methane removal is never complete during aeration, MOB are regularly found in rapid sand filters [9–11]. Yet their role is poorly understood and their presence is considered undesirable [12]. The reluctance to promote the growth of MOB within sand filters stems from three distinct challenges: (*i*) High methane

concentrations can lead to large biomass accumulations due to MOB large biomass growth yields[13] and extracellular polymeric substances (EPS) production[14],. This accelerates filter clogging, shortening cycle runtimes and forcing frequent backwashing. (*ii*) The complete oxidation of 1 mol CH_4 to CO_2 requires 2 mol O_2. Sand filters often already operate close to oxygen limitation, as groundwater ammonia concentrations may reach 2 mg L^{-1}. Incorporating biological methane removal could potentially not only hinder the full oxidation of some contaminants but also lead to anaerobic zone formation in the lower filter sections. Anaerobic zones may promote the reduction and solubilization of previously oxidized contaminants such as manganese [15]. (*iii*) Sand filters are oligotrophic systems. Phosphate[16] and copper[17] limitation are well-known problems hindering optimal filter performance. Incorporating MOB would increase the competition for these and other (micro)nutrients, potentially compromising ammonia oxidation and biological iron and manganese removals (see [18] for an overview of the reactions taking place in sand filters).

In this work, we hypothesize that the implementation of trickling filters as pre-treatment allows the promotion of biological methane oxidation without compromising the quality of the produced drinking water. Trickling filters have proven efficient in treating substrate-rich groundwaters, i.e., featuring ammonium concentrations as high as 4.5 mg NH_4^+-N L^{-1} [19], and minimize potential oxygen limitation problems by operating at higher air-to-water ratios. To this end, we compare at full-scale the performance of a novel configuration consisting of a trickling filter followed by a submerged filter with a conventional system, comprising two submerged filters in series preceded by an aeration step. We assess filter performance by quantifying the removal of the main groundwater contaminants methane, iron, ammonium, and manganese. *Ex-situ* batch incubations are used to estimate the maximum removal rates of ammonium and manganese, and to assess the direct impact of methane on nitrification. Analyses of conversion kinetics are complemented with metagenome-resolved metaproteomics to profile the taxonomy and metabolism of the underlying microbial communities along the filters' depths.

6.2. MATERIALS AND METHODS

6.2.1. Operational characterization and sample collection

Filter media, water, and gas samples were collected from two groundwater-fed treatment lanes in the Breehei drinking water treatment plant (DWTP) located in Leunen, The Netherlands, and operated by NV Waterleiding Maatschappij Limburg (WML) (Figure 1, Table 1). The first system consists of a tower aerator followed by parallel submerged filters (SF), a subsequent tower aerator, and a second set of submerged sand filters (after submerged filter; ASF). The second system does not include a tower aerator. Instead, the water is sprayed directly onto a trickling filter (TF) and air is forced in a co-current through the filter bed. Subsequently, the water passes through a tower aerator and a submerged sand filter (after tricking filter; ATF). The filter bed in each filter had a depth of 2 m and media was sampled with a peat sampler at 15, 90, and 190 cm from the filter top, referred to as top (t), middle (m), and bottom (b), respectively (Figure 1). Filter media samples were taken at the end of the operational cycle just before backwashing. Influent, effluent, and filter bed porewater samples were immediately filtered using 0.45 µm Millex PVDF filters (Sigma Aldrich, Saint Louis, Missouri USA), stored at 4 °C, and measured within 12 h. Porewater sampling from the trickling filter was technically not possible. Samples for total iron and manganese quantification were acidified to pH < 1 with 69 % ultrapure nitric acid. pH, dissolved O_2 concentration, temperature, and redox potential were measured on-site using a multimeter (Multi 3630 IDS, Xylem Analytics, Germany). Gas flow was measured with a pressure transmitter SITRANS P320 (Siemens, Germany). Methane concentrations in the gas phase were measured with a gas chromatograph with a flame ionization detector (Agilent Intuvo 9000, Agilent Technologies, United States). The concentration in the water phase was calculated using the water/headspace ratio and the equilibrium constant between phases of 0.0014 mol kg^{-1} bar^{-1} [20]. The biological methane consumption [g h^{-1}] was calculated as:

$$R_{CH_4} = (Q_{G,in} * C_{CH4_{G,in}} + Q_{W,in} * C_{CH4_{W\,in}}) - (Q_{G,out} * C_{CH4_{G,out}} + Q_{W,out} * C_{CH4_{W,out}})$$

where Q = flow of gas (G) or water (W) [m^3 h^{-1}] and C_{CH4} = methane concentration [g m^{-3}]. Data can be found in Table S1.

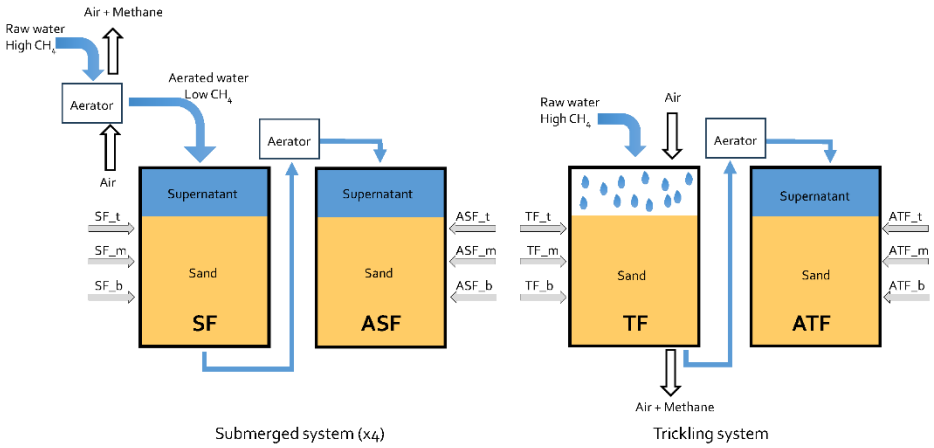

Figure 1. Schematic illustration of the two groundwater treatment lanes. Groundwater fed into the submerged system is pre-aerated in a tower aerator, removing methane and carbon dioxide and introducing oxygen. The trickling system has no tower aerator and dissolved methane directly enters the filter. Aeration is achieved by spraying the water onto the trickling filter and forcing air in co-current through the filter bed. Each filter was characterized at three different depths: top (t), middle (m), and bottom (b) at 15 cm, 90 cm, and 190 cm from the filter top, respectively. SF, submerged filter; ASF, after submerged filter; TF, trickling filter; ATF, after trickling filter. The submerged systems consist of four parallel pre-filters and after-filters. For some of the analysis in this work, we sampled both parallel pre-filters, denoted as SF1 and SF2. Unless explicitly mentioned, SF refers to SF1.

Table 1. Operational parameters of the DWTP and the characteristics of the raw groundwater and the submerged (SF, ASF) and trickling (TF, ATF) filter lanes. Groundwater characteristics indicate the average and standard deviation of the measurements taken between January 2020 and April 2023. Oxidation-Reduction Potential (ORP) was measured only once.

	Units	Submerged filters	Trickling filter
Filter depth	m	2	2
Height of supernatant	m	0.3	-
Age of media (sampling day)	years	<1	<1
Filter area	m^2	9.1	
Filtration rate	m h^{-1}	5.1	
Air-water ratio (vol./vol.)	-	-	5
Run cycle capacity	m^3	1800	2500
		Groundwater	
pH		6.93 ± 0.04	
Temperature	°C	11.2 ± 0.4	
ORP	mV	-250	

6.2.2. Ex-situ ammonium and manganese maximum removal rates

The maximum ammonium and manganese removal rates of the filter media were determined *ex-situ* in batch. 4 g of wet filter media, 200 mL of tap water, and 100 µl of trace element solution (L^{-1}; 15g EDTA, 4.5g $ZnSO_4 \cdot 7H_2O$, 4.5g $CaCl_2 \cdot 2H_2O$, 3g $FeSO_4 \cdot 7H_2O$, 1g H_3BO_3, 0.84g $MnCl_2 \cdot 2H_2O$, 0.3g $CoCl_2 \cdot 6H_2O$, 0.3g $CuSO_4 \cdot 5H_2O$, 0.4g $Na_2MoO_4 \cdot 2H_2O$, 0.1g KI) were mixed in 300 mL shake flasks. After an acclimatization period of 30 min at 25 °C and 150 rpm, each flask was spiked with 3 ml of 100 mg NH_4^+-N L^{-1} NH_4Cl or 100 mg Mn^{2+} L^{-1} $MnCl_2 \cdot 4H_2O$ to reach a concentration of 1.5 mg L^{-1} (Sigma Aldrich, Saint Louis, Missouri USA). Liquid samples (1 ml) were taken at different time intervals throughout the incubation experiment. Maximum removal rates per mass (wet weight) of filter media were calculated by interpolation of the concentration profiles and converted into volumetric rates using the measured filter media densities (2 g cm^{-3}). For the tests with methane, 1 g of wet filter media, 50 mL of tap water, and 25 µL of trace element solution were added to 110 mL sealed flasks. 5, 10, or 15 mL of methane gas (>99% purity; Linde, Dublin, Ireland) were introduced before the addition of ammonium.

6.2.3. Water quality analyses

Samples for ammonium, nitrite, nitrate, and dissolved iron and manganese quantification were immediately filtered through a 0.2 µm nanopore cellulose filter (Sigma Aldrich, Saint Louis, Missouri USA) and measured within 12 h. Raw water samples were filtered after minimally 16 hours of acidification for total iron and manganese quantification. Ammonium, nitrite, and nitrate were measured using a photometric analyzer (Gallery Discrete Analyzer, Thermo Fischer Scientific, Waltham, Massachusetts, USA). Iron and manganese were quantified by ICP-MS (Analytik Jena, Jena, Germany).

For ATP detection, 1 ml miliQ H_2O was added to 1 g wet weight of sand. The samples were sonicated for 1 min at an output power of 15 W and a frequency of 20 kHz (ultrasonic homogenizer, Qsonica sonicators, Newtown, Connecticut, USA). Samples were subsequently filtered through a 0.22 µm nanopore cellulose filter. The concentration of ATP in the liquid was determined in

duplicates using an ATP analyzer following the manufacturer's instructions (Clean-Trace™ Luminometer NG3, 3M, Maplewood, Minnesota USA).

6.2.4. DNA extraction and sequencing

DNA was isolated from 0.5 g of filter sand (wet weight) using the DNeasy Powersoil DNA isolation kit (QIAGEN, Hilden, Germany). Cell lysis was performed by bead beating at 50 Hz for 1 min using a TissueLyser LT (QIAGEN, Hilden, Germany). When this approach yielded insufficient quantities of DNA, duplicates of 0.5 g filter sand were used and pooled on one GeneJet Spin Column. All sequencing was performed by Macrogen Inc. (Seoul, South Korea) using the Illumina MiSeq platform for 16S rRNA gene amplicon sequencing and the HiSeq platform for metagenomic sequencing. Primers used for bacterial 16S rRNA gene amplification were 341F (5'-CCTACGGGNGGCWGCAG-3' [21]) and 806R (5'-GGACTACHVGGGTWTCTAAT-3' [22]). Paired-end libraries were constructed using the Herculase II Fusion DNA Polymerase Nextera XT Index Kit V2 (Illumina, San Diego, USA) with the 16S Metagenomic Sequencing Library Preparation Part # 15044223 Rev. B protocol, yielding 74,000-125,000 paired-end reads per sample. For metagenomic sequencing, paired-end libraries were constructed using the Nextera XT DNA Library Preparation Kit (Illumina, San Diego, USA) with the Nextera XT DNA Library Prep Kit Reference Guide (15031942 v03), yielding approximately 80,000,000 reads per sample.

6.2.5. 16S rRNA gene amplicon sequencing analysis

The 16S rRNA gene amplicon sequencing data was processed in R v3.5.1 using the DADA2 pipeline v1.8 [23]. The 16S rRNA gene-based taxonomy was obtained using the SILVA database v138.1 [24]. The relative abundances as calculated using DADA2 were analyzed using the R package Phyloseq v1.30.0 [25].

6.2.6. Metagenome assembly

Using BBDuk in BBTools v37.76 (https://jgi.doe.gov/data-and-tools/software-tools/bbtools/), metagenomic paired-end reads with a minimal length of 75

base pairs (bp) were filtered for quality and contamination, and adapters were removed. Trimmed reads from each sample were then assembled separately using metaSPAdes v3.15.4 [26], except for reads from SF1 and SF2, which were co-assembled. K-mer sizes of 21, 33, 55, 77, and 99 were used for assembly. Only contigs ≥ 1000 base pairs (bp) were retained for subsequent analyses.

6.2.7. Metagenome binning

Reads of each sample were mapped to every assembly using BBmap (BBTools v37.76; https://jgi.doe.gov/data-and-tools/software-tools/bbtools/) to generate differential coverage data. This data was converted from sequence alignment map (SAM) files to binary alignment map (BAM) files using SAMtools v1.8 [27]. Differential coverage binning was then performed using BinSanity v0.2.6.3 [28], CONCOCT v0.4.1 [29], MaxBin2 v2.2.7 [30], and MetaBat2 v2.12.1 [31], after which Das Tool v1.1.1 [32] was used for consensus binning. Bins were dereplicated using dRep (Olm et al., 2017), using an average nucleotide identity (ANI) of 99% for clustering. Dereplicated bins were manually refined in the Anvi'o interactive environment v7.1 [33]. The completeness and contamination of bins were estimated using CheckM2 v0.1.3 [34], and bins were defined as medium quality (≥ 70% completeness and ≤ 10% redundancy) or high quality (≥ 90% completeness, ≤ 5% redundancy, presence of 5S, 16S, and 23S rRNA genes, and at least 18 tRNAs) according to MIMAG standards [35]. The taxonomy of MAGs was computed using GTDBtk v2.1.1 [36]. Relative abundance data of bins was generated with CoverM v0.4.0 (https://github.com/wwood/CoverM).

6.2.8. Gene annotation

Gene annotation was performed using DRAM v1.2.3 [37]. Iron cycling genes were predicted using FeGenie [38]. The open reading frame (ORF) predictions from the DRAM pipeline, which are generated by Prodigal [39], were additionally mined for nitrogen cycling genes with hidden Markov models (HMMs) built for Metascan [40]. This was done to identify additional *nxrA* genes, which are poorly annotated by DRAM. Coverage data of genes was calculated with CoverM v0.4.0 (https://github.com/wwood/CoverM). Reads per kbp per million mapped reads (RPKM) were used to normalize for gene size and sequencing depth.

6.2.9. Phylogenetic analysis

To infer the phylogeny of the *Nitrospira* bins, the up-to-date bacterial core gene (UBCG) pipeline was used to extract, align, and concatenate 92 single-copy core genes [41]. This was done for the identified *Nitrospira* bins and a reference dataset containing 260 *Nitrospira* genomes. From this alignment, a maximum-likelihood tree was calculated with FastTree v2.1.10 using the GTR+CAT model [42] using 1000 bootstrap iterations. Amino acid sequences of AmoA/PmoA were aligned using MUSCLE [43]. A maximum-likelihood tree was constructed using W-IQ-TREE [44] with the GTR+F+I+G4 model as the determined best-fit model and using 1000 ultrafast bootstrap iterations. To distinguish between NxrA and NarG, an alignment was made using ARB v5.5 [45] of 67 amino acid sequences identified as described above, as well as a reference dataset of 416 NxrA and NarG sequences [10]. A maximum-likelihood tree was constructed from this alignment using IQ-TREE v2.1.4 [46], with the Q.pfam+I+G4 model as the determined best-fit model, and using 1000 ultrafast bootstrap iterations. All trees were visualized using iTOL [47].

6.2.10. Protein extraction, proteolytic digestion, and shotgun proteomic analysis

For protein extraction, 150 mg of filter (sand) material was mixed with 125 µL of B-PER reagent (78243, Thermo Scientific) and 125 µL 1 M TEAB buffer (50 mM TEAB, 1 % w:w NaDOC, adjusted to pH 8.0). The mixture was briefly vortexed and exposed to shaking using a Mini Bead Beater 16 (BioSpec Products) for 3 min. Afterwards, the sample was exposed to one freeze/thaw cycle at -80 °C and +80 °C for 15 and 5 min, respectively. The samples were centrifuged for 10 min at 10,000 rpm at 4 °C, and the supernatant was transferred into a clean LoBind Eppendorf tube (Eppendorf, Hamburg, Germany). Another 125 µL of B-PER reagent and 125 µL 1 M TEAB buffer were added to the sand sample, vortexed, and sonicated (Branson 5510, sonication mode, at room temperature) for 5 min. The sample was then centrifuged for 10 min at 10,000 rpm and 4 °C, and the supernatant was collected and pooled with the first supernatant. Extracted proteins were precipitated by adding 200 µL ice-cold acetone to the supernatant, vortexing, and incubation at -20 °C for 1 h. The protein pellet was collected by centrifugation at 14,000 rpm and 4 °C for 15 min. The supernatant

was carefully removed from the pellet using a pipette. The pellet was dissolved in 100 µL 200 mM ammonium bicarbonate containing 6 M urea. Disulfide bonds were reduced using 10 mM DTT (dithiothreitol) and sulfhydryl groups were blocked using 20 mM IAA (iodoacetamide). The solution was diluted to below 1 M urea and digested using sequencing-grade Trypsin (Promega). The proteolytic peptides were finally desalted using an Oasis HLB solid phase extraction well plate (Waters) according to the manufacturer's protocol. An aliquot corresponding to approximately 250 ng of protein digest was analyzed with a shotgun proteomics approach as described earlier [48,49]. Briefly, the peptides were analyzed using a nano-liquid-chromatography system consisting of an EASY nano-LC 1200, equipped with an Acclaim PepMap RSLC RP C18 separation column (50 um × 150 mm, 2 µm, 100 Å) and a QE plus Orbitrap mass spectrometer (Thermo Fisher, Germany). The flow rate was maintained at 350 nL over a linear gradient from 5 % to 30 % solvent B over 65 minutes and finally to 60 % B over 20 min. Solvent A was ultrapure H_2O containing 0.1 % v:v formic acid, and solvent B consisted of 80 % acetonitrile in H_2O and 0.1 % v:v formic acid. The Orbitrap was operated in data-dependent acquisition (DDA) mode acquiring peptide signals from 385-1250 m/z at 70K resolution. The top 10 signals were isolated at a window of 2.0 m/z and fragmented at a NCE of 28 at 17.5K resolution with an AGC target of 2e5 and a max IT 75 ms. The collected mass spectrometric raw data were analyzed combined against the metagenomics reference sequence database built from the assembled contigs using PEAKS Studio 10 (Bioinformatics Solutions, Canada) in a two-round search approach. The first-round database search using the clustered database (892,436 proteins) was used to construct a focused protein sequence database, considering one missed cleavage, and carbamidomethylation as fixed modification, and allowing 15 ppm parent ion and 0.02 Da fragment ion mass error. The focused database (containing 9729 proteins) was then used in a second-round search, considering 3 missed cleavages, carbamidomethylation as fixed, and methionine oxidation and N/Q deamidation as variable modifications. Peptide spectrum matches were filtered for a 5 % false discovery rate (FDR) and protein identifications with at least 2 unique peptides were considered significant. Functional annotations (KO identifiers) and taxonomic lineages were obtained by GhostKoala (https://www.kegg.jp/ghostkoala) and by Diamond [50] using the NCBI nr protein sequence reference database (Index of /blast/db/FASTA (nih.gov)). For Diamond annotations, the lineage of the lowest

common ancestor was determined from the top 10 sequence alignments. Data is attached in Table S2.

Comparison of the relative abundance of proteins between samples was performed using "relative spectral counts" (*i.e.*, normalized spectral counts, defined as spectral counts per protein divided by the molecular weight of the specific protein, and normalized by the sum of mass-normalized spectral counts of all proteins of all samples). The contribution of a specific protein was estimated by summing up the relative abundances of all proteins with the same functional annotation. For proteins with more than one subunit, only the catalytic one was considered: AmoB for ammonia monooxygenase AMO, MmoX for soluble methane monooxygenase sMMO, PmoB for particulate methane monooxygenase pMMO; NarG for nitrate reductase NAR, NxrA for nitrite oxidoreductase NXR, NorB for nitric oxide reductase NOR, MtoA for iron oxidase MTO. For the putative particulate methane monooxygenase pXMO, subunit A (PxmA) was used as it was the only one present in the metaproteome.

6.3. RESULTS

6.3.1. Complete methane and iron removal at the expense of incomplete ammonia and manganese oxidation in trickling filter

The concentration profiles of methane, iron, ammonium, and manganese differed among the two studied treatment processes (Figure 2). In the submerged system, all (>99.9%) methane was removed after aeration (AA) before reaching the first submerged filter (SF). Ammonia, iron, and manganese were completely removed in the SF, with effluent concentrations of < 0.1 mg Fe^{2+} L^{-1}, < 0.05 mg NH_4 L^{-1}, and < 0.5 µg Mn L^{-1}. In the trickling system, anaerobic groundwater is directly fed to the trickling filter (TF) together with an air stream. Methane was completely removed in the TF (> 99.5%). Based on the influent and effluent gaseous and dissolved methane concentrations (Table S1), it was estimated that approximately 47% was biologically oxidized, with the remaining methane being stripped. Iron was completely depleted in the trickling filter as well (effluent < 0.05 mg Fe^{2+} L^{-1}), while the oxidation of ammonium and manganese was only partial (26% and 19%, respectively). Total ammonium and

manganese removal was achieved at the effluent of the submerged after-trickling filter (ATF; effluent < 0.05 mg NH_4 L^{-1} ; < 0.5 µg Mn L^{-1}).

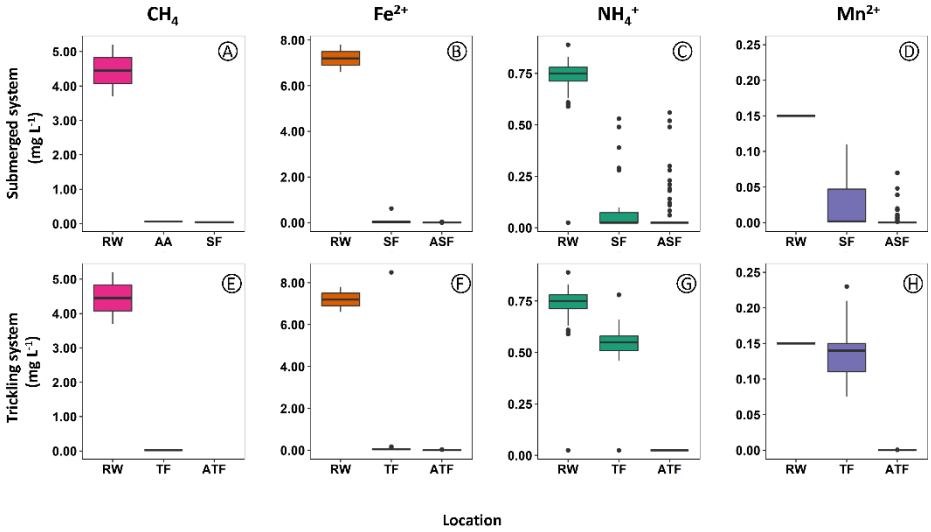

Figure 2. Concentration profiles of methane (A,E), iron (B,F), ammonium (C,G), and manganese (D,H) along the submerged (top) and trickling systems (bottom) in DWTP Breehei. Complete removal is achieved at the end of both systems. Groundwater is aerated before reaching the submerged system, where methane is removed but the other contaminants are not. Values and error bars represent the mean and standard deviation of measurements taken between January and July 2020. Lower and upper box boundaries represent the 25th and 75th percentiles, the line inside the box is the median. Lower and upper error lines indicate 10th and 90th percentiles. Individual points show outliers, which belong to the start-up phase. RW, raw water; AA, after aeration; SF, submerged filter; ASF, after-submerged filter; TF, trickling filter; ATF, after-trickling filter.

6.3.2. Methane controls nitrification and manganese oxidation rates in both systems

Ammonia and manganese removal rates

The maximum ammonium and manganese removal capacities of the filter media along the depth of all filters were quantified *ex-situ* in batch activity tests (Figure 3). Ammonium removal was comparable in the two studied parallel submerged filters (SF1 and SF2), with a subtle top-to-bottom decreasing profile following the decrease in ammonium concentrations. Consistently with the low ammonium consumption in TF (Figure 2A), the removal capacity at the top of TF

(TF_t) was 7 times lower than in SF1_t, namely 0.26 and 1.82 gNH_4^+-N m_{media}^{-3} h^{-1}, respectively. The ammonia removal increased slightly in the lower TF sections. The subsequent submerged filter (ATF) showed the highest and most stratified ammonium removal capacity with 3.49 gNH_4^+-N m_{media}^{-3} h^{-1} at the top and 0.94 at the bottom.

Ex-situ manganese removal capacities were also comparable for SF1 and SF2, with comparable rates across both filters (0.117 ± 0.007 h^{-1} for SF1 and 0.107 ± 0.007 h^{-1} for SF2). In analogy to ammonium, the manganese removal capacity increased towards the bottom of TF (from 0.103 ± 0.071 h^{-1} at TF_t to 0.133 ± 0.000 h^{-1} at TF_b). Surprisingly, the values were similar to those in SF1 and SF2, despite the fact that less than 25% of manganese is removed in the TF while complete oxidation is observed in SF1 and SF2. Again, the highest and most stratified rates were found in the ATF, likely due to the absence of methane and iron.

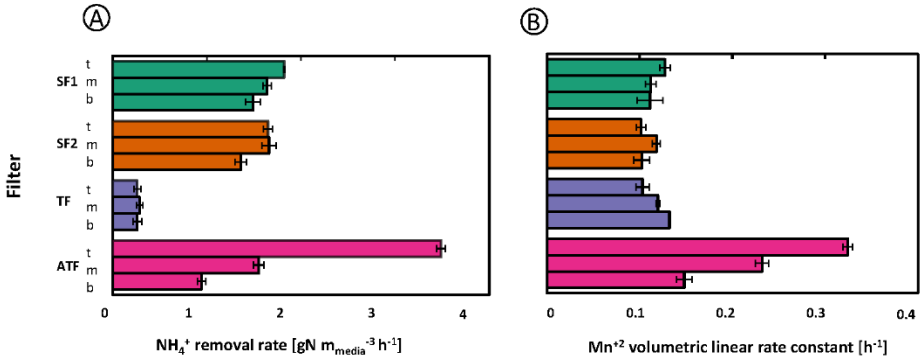

Figure 3. Maximum volumetric ex-situ ammonium (a) and manganese (b) removal rates in the top (t), middle (m), and bottom (b) sections of SF1, SF2, TF, and ATF. Batch tests were carried out in duplicate, error bars represent the standard deviation.

Methane-oxidizing bacteria (MOB) potential contribution to ammonia oxidation

To explore the impact of methane on ammonium removal, nitrification batch tests were carried out under methane-rich atmospheres using media from the top of each filter (Figure 4A). The presence of methane decreased the maximum ammonium removal rate of the media from the filters that do not receive

methane, with reductions of 65% in SF1, 73% in SF2, and 60% in ATF. In contrast, ammonium removal was 173% higher in the presence of methane for TF media.

To further characterize the mechanisms behind this effect, we exposed sand from SF1_t and TF_t to increasing concentrations of methane (gas) using 0, 8, 14, and 20% (v:v) methane atmospheres at a constant ammonium concentration (Figure 4B). For the sand from the SF, higher methane concentrations resulted in proportionally lower ammonium removal rates, with a reduction from 1.14 to 0.26 gNH_4^+-N m_{media}^{-3} h^{-1} when methane increased from 0 to 20%, respectively. Ammonium removal was accompanied by nitrite and nitrate production, consistent with full nitrification. In contrast, with TF medium, ammonium removal was the lowest at 0% methane (0.26 gNH_4^+-N m_{media}^{-3} h^{-1}), and at comparable higher rates in the presence of 8, 14, and 20% methane (0.96, 0.89, and 0.95 gNH_4^+-N m_{media}^{-3} h^{-1}, respectively). Nitrite production was detected at all methane concentrations, while no nitrate was produced. On the contrary, nitrate initially present in the vials was consumed in all TF tests, presumably due to denitrification. This resulted in nitrogen mass balance closing at most at 80%.

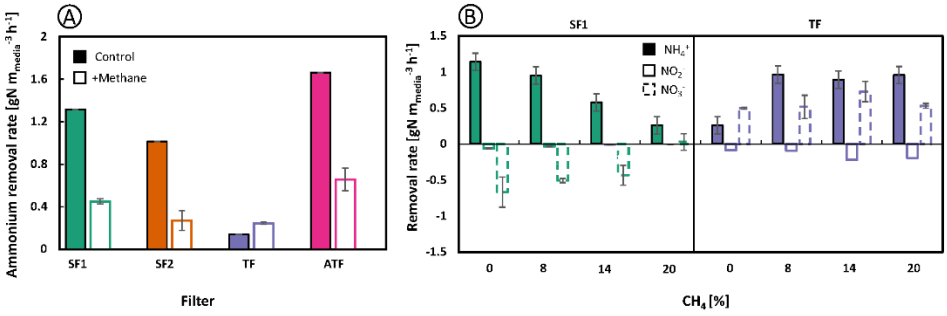

Figure 4. Maximum volumetric ex-situ ammonium removal rates. A) Ammonium removal in the top section of SF1, SF2, TF, and ATF in the presence (full) or absence (empty) of a 20% (v:v) methane atmosphere. B) Maximum volumetric ex-situ ammonium consumption (full), and nitrite (empty) and nitrate (empty, dotted) production rates in the top section of SF1 and TF in the presence of 0, 8, 14, and 20% (v:v) methane atmospheres. The other gas fraction was air. Batch tests were carried out in duplicate, error bars represent the standard deviation (in some cases smaller than symbols).

6.3.3. Microbial community composition and genome-based functional potential

Nitrifying and iron-oxidizing guilds govern the SF, while methanotrophs dominate the TF

The microbial community composition, elucidated through 16S rRNA gene amplicon sequencing, showed distinct differences between the submerged and trickling treatment systems (Figure 5). In SF1 and the identically operated parallel SF2 filter where methane is removed by pre-aeration, the genera *Gallionella* (3-27%) and *Nitrospira* (8-18%) dominated the microbial communities. The communities at the middle and bottom of SF1 and SF2 were similar. Samples from the top showed greater dissimilarity (Figure S1), primarily due to the higher prevalence of *Gallionella* in SF1 compared to SF2. In stark contrast, MOB of the genera *Methylovulum* (9-32%) and *Crenothrix* (7-11%), and methylotrophic bacteria of the genus *Methylotenera* (16-29%) dominated the TF, which directly receives methane-rich groundwater. The relative abundance of *Methylotenera* decreased from top to bottom while *Methylovulum* displayed an opposite profile (Figure 5).

The microbial community of ASF, receiving water containing minimal residual levels of ammonium, iron and manganese, featured a much lower abundance of taxa involved in their removal compared to the other filters (Figure 5). The dominant ASF bacteria belonged to the genera *Vicinamibacteraceae* (10%) and *Gallionella* (6%). Contrastingly, the influent water of the ATF still contained high levels of ammonium and manganese, and *Candidatus* Nitrotoga (4-22%), *Nitrospira* (4-8%), and *Nitrosomonas* (1-6%) were the predominant genera, particularly in the top layer.

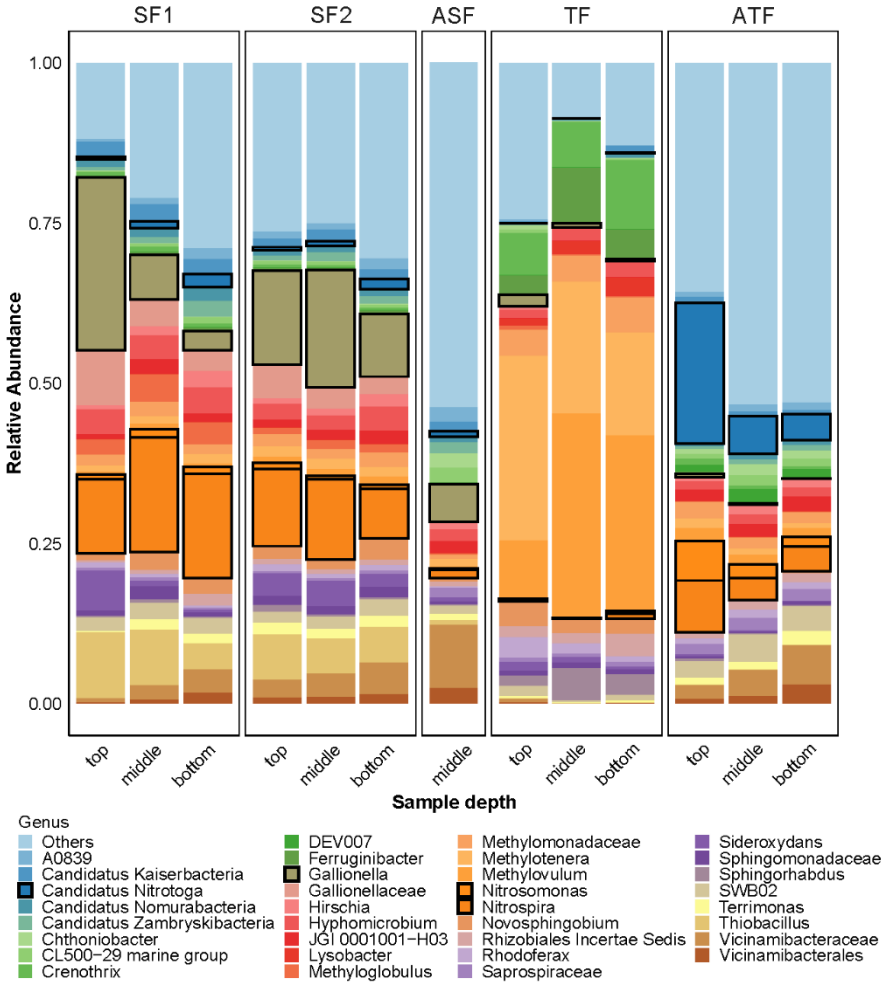

Figure 5. Relative microbial community composition based on 16S rRNA gene amplicon sequencing. All genera constituting ≥ 2% of the total microbial community in at least one of the samples are shown for every sample. All other taxa are grouped in 'Others'. The genera Candidatus Nitrotoga, Gallionella, Nitrosomonas, and Nitrospira are highlighted. SF1 and SF2, parallel submerged filters; ASF, after-submerged filter; TF, trickling filter; ATF, after-trickling filter.

The submerged and trickling lines harbor distinct functional guilds

The microbial community metagenome of each filter was sequenced to characterize the metabolic potential of the most abundant organisms.

Sequencing yielded 79-85 million paired-end raw reads and 69-77 million trimmed reads per sample (Table S3). Of the trimmed reads, 49-85% could be assembled into contigs, 55-83% of which were binned into metagenome-assembled genomes (MAGs). After dereplication at strain level, 14 high and 108 medium-quality MAGs were obtained (Table S4).

The MAGs of interest were identified based on the presence of genes involved in methane, manganese, and iron oxidation, as well as nitrification and denitrification (Figure 6). In the parallel filters SF1 and SF2, the most abundant MAGs belonged to the genera *Gallionella* and *Nitrospira*, in accordance with the 16S rRNA gene amplicon sequencing. The *Gallionella* MAGs contained one or two copies of the iron oxidation gene *cyc2*, showcasing their involvement in biological iron removal. The most abundant *Nitrospira* MAGs, ATF_7 and SF2_8, did not contain the ammonium monooxygenase subunit A (*amoA)* or hydroxylamine dehydrogenase (*hao*) genes, indicating that they are canonical (nitrite-oxidizing only) *Nitrospira*. Contrastingly, *Nitrospira* MAGs ATF_8 and SF2_2 contained both *amoA and hao*, hence representing complete ammonia-oxidizing (comammox) species. The gene encoding the nitrite oxidoreductase subunit alpha (*nxrA*) was only found in ATF 7, ATF_8, and ATF_24. However, as *nxr* is part of the core genome of all *Nitrospira* species [51], its absence in SF2_2 (as well as in SF1_2, SF2_10, and SF2_8) is attributed to MAG incompleteness.

To account for additional *amoA* copies possibly missed in the binning process resulting in *Nitrospira* MAG misclassification, the phylogeny of all *Nitrospira* MAGs and a reference dataset of 260 *Nitrospira* genomes was determined using a concatenated alignment of 92 single-copy core genes (Figure S2). All recovered *Nitrospira* MAGs belonged to lineage II, and most of them clustered with canonical nitrite-oxidizers. The phylogenetic analysis confirmed that ATF_8 and SF2_2 represented the only comammox species, belonging to comammox clade A. When comparing filters, comammox *Nitrospira* were more abundant in the parallel submerged systems (1.7% in SF1 and 1.6% SF2) than in the trickling system (0.5% in ATF). Instead, *Candidatus* Nitrotoga (ATF_9 and ATF_1) and *Nitrosomonas* (ATF_16 and ATF_2) MAGs follow the opposite trend, constituting 0.18 and 0.32%, and 0.33 and 0.45% in SF1 and SF2, and 9.7% and 2.6% in ATF, respectively. In the ASF, the MAGs involved in methane, iron, manganese, or ammonium removal were present in low abundances.

The methanotrophic *Methyloglobulus* MAG TF_26 (15.7%) and the methylotrophic *Methylotenera* MAG TF_25 (11.7%) were the most abundant MAGs in the TF. TF_26 encoded *pxmA* but lacked *pmoA*. Given that *pmoA* is a critical component of the core metabolism of all aerobic methanotrophic bacteria [52], its absence is likely due to incomplete binning. Eight less abundant methanotrophic MAGs were also found, all of which harbored *pmoA*, complemented by *pxmA* in TF_5, TF_1, and TF_21, and by the soluble methane monooxygenase (*mmoX*) in TF_4 and TF_1.

The genetic potential for manganese oxidation, as determined by the presence of *moxA*, *mnxG*, and *cotA*, was widespread across all samples and not limited to any particular group of bacteria.

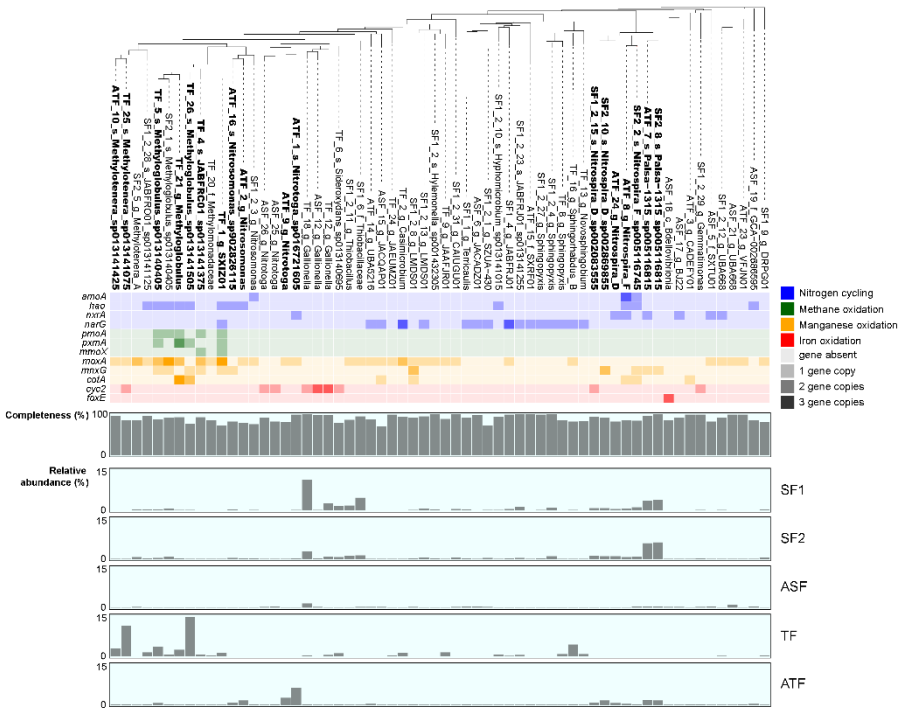

Figure 6. Overview of phylogeny, genetic potential, completeness, and distribution of 62 dereplicated high and medium-quality MAGs. These MAGs were selected out of the total 122 MAGs by the presence of genes involved in nitrogen cycling, methane, manganese, or iron oxidation. The order of the MAGs is based on the phylogeny of all 122 medium and high-quality MAGs, as determined by a maximum-likelihood tree calculated with

FastTree using the GTR+CAT model, based on the alignment of 92 single core copy genes by UBCG. Copy numbers of genes involved in nitrogen cycling, methane, manganese, and methane oxidation are shown as a heat map. Bar plots show the completeness of the MAGs (middle) and their relative abundance in the different filters (bottom).

Gene-centric analysis supports bin-centric functional distribution

While bin-centric analysis is a powerful approach to studying microbial community composition, it does not take into account unbinned genes, which may represent a significant fraction of the metagenome. Therefore, a gene-centric analysis was performed to examine the full methane and ammonia oxidation potential of the community. A phylogenetic tree of all translated copper-containing membrane monooxygenases (Cu-MMO) subunit A genes showed that the Cu-MMOs in our metagenomes cluster within five distinct groups (Figure 7A): *i)* comammox *Nitrospira* clade A AmoA, *ii)* betaproteobacterial (*Nitrosomonadacaea*) AmoA, *iii)* ERR11-like Cu-MMO, *iv)* PxmA group, and *v)* gammaproteobacterial PmoA. Based on metagenomic read mapping, *Nitrosomonadacaea amoA* was the most abundant gene for ammonium removal across all samples, especially in ATF (Figure 7B), followed by clade A comammox *amoA,* which represented *ca*. 30% - 50% of total *amoA* in the submerged system (SF1/SF2, ASF), but only comprised a minor fraction of total *amoA* in the trickling system (TF, ATF). In the TF metagenome, no *amoA* was found, while it contained the highest abundance of methane oxidation genes, corresponding to biological methane removal being the dominant process in this filter. The most abundant gene was *pxmA* (Figure 7C), with gammaproteobacterial *pmoA* also present. Surprisingly, gammaproteobacterial *pmoA* was found in similar abundances across all filters, despite the significant differences in methane concentrations in the incoming waters. Genes encoding *mmoX* were only obtained from the TF, and at low abundance.

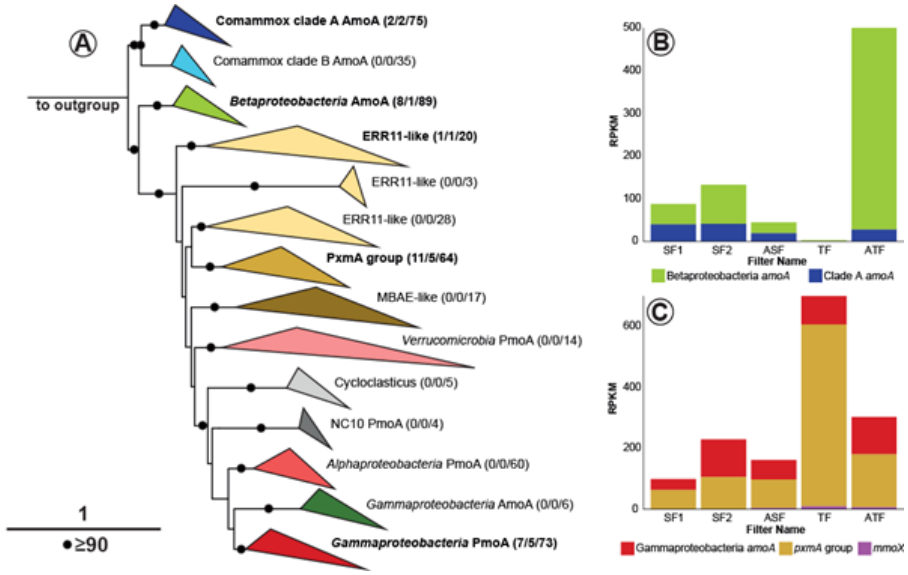

Figure 7. Diversity and abundance of genes involved in methane and ammonia oxidation. (A) The phylogenetic tree shows the diversity of Cu-MMO proteins. Clades highlighted in bold contain sequences from the rapid sand filter metagenomes of this study. The numbers in brackets represent the number of distinct sequences from the rapid sand filter metagenomes, the number of these sequences found in MAGs, and the total count of sequences in that clade, respectively. The outgroup consists of three Thaumarchaeota AmoA sequences. (B, C) Abundances of betaproteobacterial amoA and comammox Nitrospira clade A amoA (B), and gammaproteobacterial pmoA and pxmA (C) in all filters, normalized as RPKM. Although not part of the Cu-MMO family, mmoX is also included due to the role of sMMO in methane oxidation. SF1 and SF2, parallel submerged filters; ASF, after-submerged filter; TF, trickling filter; ATF, after-trickling filter.

A similar approach was followed to resolve the distribution of *nxrA* and the gene for the nitrate reductase alpha subunit (*narG*; Figure S3). In the protein-based phylogenetic analysis, these fall into four distinct groups: NarG, *Nitrospira* NxrA, *Candidatus* Nitrotoga NxrA, and putative *Nitrotoga*-like NxrA/NarG. Based on RPKM analysis, *Nitrospira nxrA* was the most abundant gene, especially in the filters where nitrification took place (SF1, SF2, and ATF).

6.3.4. Protein-centric metabolic profiles

The proteomes of the top, middle, and bottom sections of SF and TF were quantified to estimate the distribution of core nitrogen, methane, iron, and

manganese-transforming enzymes. Per sample, we obtained on average 335 ± 33 individual protein groups identified by at least two unique peptides at a false discovery rate (FDR) < 1% (Table S2). The relative contribution of individual functions of interest was estimated by grouping all proteins with the same functional annotation. Relative protein abundances were calculated as protein-mass normalized spectral counts divided by the total spectral counts of the 6 samples (Figure 8).

The catalytic subunits of the three protein complexes involved in nitrification – ammonia monooxygenase subunit B (AmoB), hydroxylamine dehydrogenase (Hao) and nitrite oxidoreductase alpha subunit (NxrA) – were present across all sections of the SF. The abundance of AmoB was clearly stratified along the filter depth, with a larger abundance in the downstream sections. In accordance, *in situ* ammonia oxidation rates in the SF were higher in the lower bed sections, subsequent to the oxidation of most Fe^{2+} (Figure S4). The distribution of Hao and NxrA did not follow a specific trend. Conversely, and in agreement with the near-absent ammonium conversion and lack of *amoA*, no nitrifying proteins were detected in the TF. Instead, proteins encoding for methane monooxygenases were abundant and displayed distinct distribution trends. PmoB and PxmA showed a decreasing top-to-bottom stratification, apparently following the direction of water flow. On the contrary, MmoX was only present at the bottom of the TF, yet at significant relative abundances.

Fingerprints of biological iron oxidation were only found in the SF, where Cyc2 was homogeneously present across all filter depths. These results are in line with the high and low abundances, respectively, of *Gallionella* in SF and TF based on 16S rRNA and iron oxidase Cyc2 genes (Figure S5). For manganese removal, genes encoding for the multicopper oxidases CotA, MnxG, and MoxA were the only putative manganese oxidation genes present in the filters, but the corresponding proteins were not detected. Lastly, genes encoding the four key enzymes in denitrification – nitrate reductase (*narG*), NO-forming nitrite reductase (*nirK* or *nirS*), nitric oxide reductase (*norB*), and nitrous oxide reductase (*nosZ*) – were present in both filters. However, NirK was the only expressed protein and exclusively found in SF, where it showed similar stratification with depth as AmoB, having an increased abundance at greater depths in the filter.

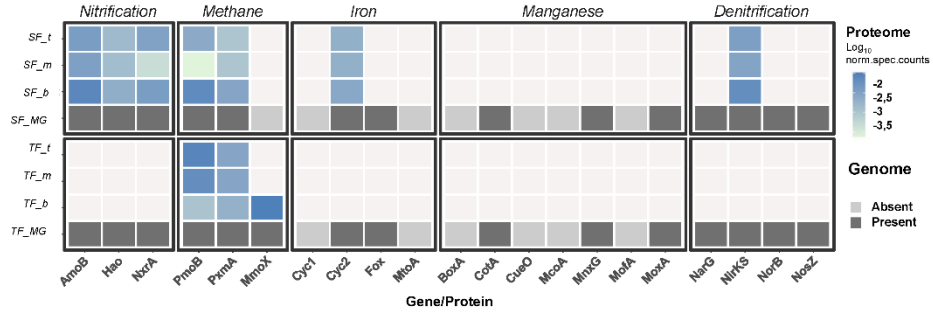

Figure 8. Distribution of the key proteins involved in methane, iron, and manganese oxidation, nitrification, and denitrification. Relative protein abundances were calculated as protein-mass normalized spectral counts divided by the total spectral counts of the 6 samples. The key proteins were selected based on the nitrification, denitrification, and methane oxidation pathways (#M00528, #M00529, #M00174) of the Kyoto Encyclopedia of Genes and Genomes, FeGenie for iron [38], and a custom-made database for manganese oxidation [53]. Dark grey: genes found at least once in the metagenome but not in the metaproteome; light grey: genes not found in the metagenome. For protein complexes, only the catalytic subunit was included. For more information, see Materials and Methods.

6.4. DISCUSSION

6.4.1. Biological methane oxidation during trickling filtration halves emissions at comparable effluent quality

Complete methane removal (>99.5%) was achieved both in the trickling and submerged systems. Most methane was stripped during aeration before reaching the filters in the conventional submerged system. In contrast, all methane was removed in the TF, with about half (47%) being biologically oxidized to carbon dioxide, and the rest of the methane being stripped. Importantly, the adoption of the new operation did not compromise the achieved effluent water quality.

Methane-oxidizing bacteria affiliated with the genus *Methylovulum* and methylotrophic bacteria of the genus *Methylotenera* dominated the microbial population across the full depth of the TF, as indicated by 16S rRNA gene abundance (Figure 5) and bin-centric analysis (Figure 6). Interestingly,

Methylotenera was the most abundant organism at the top of the TF, while the genus *Methylovulum* dominated in the downstream sections. Some *Methylotenera* species obtain energy from methylamine and methanol oxidation [54] but none have ever been reported to consume methane. Since methane oxidation to methanol does not yield energy [5], a syntrophic relationship between *Methylotenera* and MOBs based on methanol exchange is unlikely. Thus, if *Methylotenera* rely on methanol scavenging, their surprisingly high relative abundance in the first section of the TF remains at least partially unexplained. The dominant enzyme for methane oxidation also changed throughout the filter depth. While the particulate methane monooxygenase (pMMO) was the most abundant methane oxidase at the top, its soluble counterpart (sMMO) took over in the downstream section. Interestingly, the sequence-divergent particulate methane monooxygenase pXMO (Tavormina et al., 2011) was highly abundant at both gene (Figure 7C) and protein (Figure 8) level and followed the same top-to-bottom decreasing pattern as pMMO. The balance between the particulate and soluble methane monooxygenases is known to be dictated by the "copper switch" [55], with pMMO dominating at high Cu concentrations and the iron-dependent sMMO under Cu deficiency [56]. Cu limitation is known to occur in the lower sections of sand filters [17], so it is tempting to speculate that the observed distribution of MOB in the TF is dictated by Cu availability. However, while no Cu is dosed in between TF and ATF, *Nitrosomonas* dominated throughout the ATF depth over *Nitrospira*, which usually are enriched under Cu-limiting conditions [17]. Thus, further experimental evidence on the impact of Cu on MOB is warranted.

In the submerged filter, MOB and, correspondingly, the PmoB were abundant despite near-complete methane removal during the preceding aeration step (<99.9%). Proliferation of MOB in sand filters that receive aerated water supposedly devoid of methane is commonly reported [10,11,57]. Their high abundance despite the low methane concentration likely derives from their higher biomass yield (~0.7 g dry cell weight g CH_4^{-1} [13]) compared to the other main microbial community members (<0.16 g dry cell weight g NH_4^+-N^{-1} for AOB [58]; ~0.013 g dry cell weight g Fe^{-1} for FeOB [59]), but may also result from their transport from the upstream aerator without active growth.

6.4.2. MOB activity shifts Fe removal from biotic to abiotic

The oxidation of iron was complete in the first filter of both systems, *i.e.*, SF and TF, yet it was likely dominated by different processes. Strong indications of biological iron oxidation were found at genomic and proteomic levels in the SF. Bacteria of the genus *Gallionella* dominated the filter based on 16S rRNA gene amplicon sequencing (Figure 5) and bin-centric metagenomic analyses (Figure 6), and the iron oxidation protein cytochrome Cyc2 was homogeneously distributed across the filter depth (Figure 8). Contrastingly, bacteria (Figure 5 and 6) and genes (Figure S5) related to iron oxidation were found at much lower relative abundances in the TF, and iron-oxidizing proteins were below the detection limit. Since the SF and TF featured a comparable total protein abundance (a proxy for biomass concentration; Table S2) and treated the same Fe load, these results suggest that biological Fe oxidation played a comparably smaller role in the TF.

Only few studies report the application of trickling filters for drinking water production from groundwater, and biological oxidation is generally suggested to be the dominant iron removal mechanism, contributing to 35-65% of total iron removal (see [60] and references therein). In terms of dissolved oxygen concentration and pH, the two main parameters known to control the prevailing iron oxidation mechanism [60,61], the reported values of pH 7.4 – 7.5 and DO > 8 mg O_2 L^{-1} are in the same range as in our system. As both TF and SF were operated at the same filtration velocity of 5 m h^{-1}, the fact that this velocity is higher than in published systems is unlikely to explain the total suppression of biological iron removal. Instead, we hypothesize the difference to reside either in limitations in micronutrients such as Cu or in oxygen availability. While the former has already been proposed and proven for ammonia oxidizers for conventional submerged filters [17], the latter has not. The oxidation of 1 mg CH_4 demands 4 mg O_2, and groundwater contains 5 mg CH_4 L^{-1} and up to 10 mg O_2 L^{-1} after aeration. Since the diffusion coefficients of methane and oxygen are similar (see SI 8 for details), oxygen may be stoichiometrically limiting in the biofilm already for methane oxidation alone. In either case, MOB are likely outcompeting FeOB in the TF, owing to their higher biomass and energy yield per mol of oxygen. The observed full removal of iron is thus mainly ascribed to chemical reactions. Previous work on methane and iron co-removal concluded that the presence of methane itself does not interfere with overall iron removal [62,63]. Our results further confirm that complete iron removal can be attained in

the presence of methane, while also revealing the induced shift from (partially) biological to chemical processes.

6.4.3. MOB outcompete AOB, and potentially directly contribute to ammonium removal

The presence of methane affects ammonium oxidation in the trickling filter (TF). Complete ammonium removal was observed in the SF, while only partial conversion occurred in the TF (<20%). In this filter, AOB were hardly found at 16S rRNA gene level, and the ammonia monooxygenase was not detected in the metagenome (Figure 7B) or metaproteome (Figure 8). Above, we attributed the very low abundance of ammonia oxidizers, including both canonical AOB and comammox *Nitrospira*, in the TF to the competition for oxygen and micronutrients such as Cu, combined with their lower growth yield compared to MOB. In analogy, while AOB feature a similar energy yield per electron as MOB, their biomass yields remain significantly lower. Consistently, *ex-situ* batch tests revealed a very low maximum ammonia oxidation capacity of the filter medium from top section of the TF (0.26 gNH_4^+-N m_{media}^{-3} h^{-1}) compared not only to the SF medium (1.83 gNH_4^+-N m_{media}^{-3} h^{-1}), but also to methane-free filters evaluated elsewhere (1.42 [64], 4.5 [65], and 3-10 gNH_4^+-N m_{media}^{-3} h^{-1} [66]). Nevertheless, the *ex-situ* maximum ammonia oxidation rate of the TF medium increased 4-fold in the presence of CH_4 (Figure 4A), suggesting that MOB may play a primary role in ammonium removal.

The ability of MOB to oxidize ammonia has been reported for decades and is attributed to the structural similarity between methane and ammonia, and the substrate promiscuity of methane monooxygenases [67,68]. Ammonia oxidation by MOB can only yield hydroxylamine, nitric oxide, or nitrite as products [8]. Consistently, no nitrate was produced by the TF medium, while we observed nitrate production from ammonia oxidation in *ex-situ* batch tests with the nitrifiers-dominated SF medium. Growth of MOB on ammonium alone has never been reported, leading to the generally accepted assumption that MOB do not conserve energy from ammonia oxidation [69], which may partially explain the low ammonia oxidation rate by TF medium in the absence of methane. Still, the mechanism by which methane promotes ammonia oxidation by MOB warrants further research.

Ex-situ maximum ammonia oxidation rates were the highest in the ATF. The fact that filters devoid of iron have higher maximum ammonium removal capacity than filters with iron has already been observed [65] and is suggested to relate to the inhibition of AOB by Fe^{3+} flocs, a product of homogeneous Fe^{2+} oxidation [70]. Interestingly, the ATF mainly contained nitrifiers associated with the genera *Nitrosomonas* (AOB) and *Candidatus* Nitrotoga (NOB), while the SF was dominated by *Nitrospira,* the most commonly found nitrifier in rapid sand filters [10,57,71]. The observed prevalence of canonical *Nitrospira* in the SF and the higher relative abundances of NOB over AOB in all filters investigated here (Table S6) is consistent with most sand filter studies [10,53,72]. While this is generally attributed to the dominance of comammox *Nitrospira*, the most abundant *Nitrospira* MAGs obtained from the SF metagenomes (SF1 and SF2) lacked *amoA,* and were not phylogenetically affiliated with comammox *Nitrospira*. This dominance of nitrite-oxidizing bacteria over ammonia oxidizers is curious and raises the question of their metabolic flexibility in rapid sand filters.

6.4.4. MOB activity delays Mn removal despite sufficient surface catalytic potential

Manganese was fully removed in both the submerged and trickling system yet with stark differences. The SF removed > 99%, while the TF contributed less than 15% to the total removal. Interestingly, genes related to manganese oxidation were similarly distributed across all filters. Biological manganese oxidation is reported to play a minor role compared to chemical processes in mature filters [73,74], although recent work challenges this view [75]. The transition from biological to chemical-dominated manganese oxidation has been reported to occur after less than 2 months [76] to several years [77]. Both the SF and TF were run for approximately a year and the lack of detected known manganese-oxidizing proteins supports the prevalence of chemical reactions, in analogy to our previous work [65]. Surprisingly, *ex-situ* incubation tests of the filter medium grains indicated that the manganese removal potentials of the SF and TF are comparable, excluding the lack of catalytic capacity as a reason for the incomplete removal in the TF. Manganese oxidation in sand filters starts only after complete iron and ammonium removal, as was the case for the SF (Figure S4; [65]). In analogy, we hypothesize that iron (either as Fe^{2+} or Fe^{3+} flocs)

penetrated deeper into the TF than the SF and that the resulting increased oxygen demand delayed the onset of manganese oxidation. Alternatively, the delay could relate to a possible accumulation of nitrite due to ammonia oxidation by MOB instead of complete nitrification, known to interfere with manganese oxidation [78]. Still, as Mn was fully removed in the following ATF, our results show that the implementation of a trickling filter for methane removal does not hinder full Mn removal in subsequent rapid sand filtration systems.

6.5. CONCLUSIONS

The implementation of a full-scale trickling filter prior to an existing submerged sand filter halved methane emissions by promoting biological methane oxidation. The novel process scheme also fully removed iron, ammonium, and manganese, yet the underlying mechanisms differed significantly from the parallel submerged filters preceded by conventional aeration. Methane-oxidizing bacteria outcompeted ammonia oxidizers, which only proliferated in the subsequent submerged filter, and MOB likely contributed directly to ammonia removal in the trickling filter. Signatures of biological iron oxidation were much less abundant in the trickling filter, suggesting that MOB outcompeted iron oxidizers in this filter also. In contrast to the submerged filters devoid of methane, the observed complete removal of iron during trickling filtration is therefore ascribed largely to chemical reactions. The reasons for the absence of manganese removal in the trickling filter, despite similar *ex-situ* manganese oxidation capacities, remain to be elucidated. Ultimately, our results demonstrate that trickling filtration is effective in reducing methane emissions at overall fully comparable effluent qualities, and can play a pivotal role in the transition towards more sustainable, resource-efficient groundwater treatment systems.

REFERENCES

1. Bourgine, F. P., Gennery, M., Chapman, J. I., Kerai, H., Green, J. G., Rap, R. J., Ellis, S. & Gaumard, C. Biological Processes at Saints Hill Water-Treatment Plant, Kent. *Water Environ. J.* **8**, 379–391 (1994).

2. Schoonenberg, F. Personal conversation. at (2024).

3. Jiang, H., Chen, Y., Jiang, P., Zhang, C., Smith, T. J., Murrell, J. C. & Xing, X. H. Methanotrophs: Multifunctional bacteria with promising applications in environmental bioengineering. *Biochem. Eng. J.* **49**, 277–288 (2010).

4. Schmitz, R. A., Peeters, S. H., Versantvoort, W., Picone, N., Pol, A., Jetten, M. S. M. & Op Den Camp, H. J. M. Verrucomicrobial methanotrophs: Ecophysiology of metabolically versatile acidophiles. *FEMS Microbiol. Rev.* **45**, 1–20 (2021).

5. Stein, L. Y., Roy, R. & Dunfield, P. F. Aerobic Methanotrophy and Nitrification: Processes and Connections. *eLS* (2012).

6. Van Kessel, M. A. H. J., Speth, D. R., Albertsen, M., Nielsen, P. H., Op Den Camp, H. J. M., Kartal, B., Jetten, M. S. M. & Lücker, S. Complete nitrification by a single microorganism. *Nat. 2015 5287583* **528**, 555–559 (2015).

7. Daims, H. *et al.* Complete nitrification by Nitrospira bacteria. *Nat. 2015 5287583* **528**, 504–509 (2015).

8. Versantvoort, W., Pol, A., Jetten, M. S. M., van Niftrik, L., Reimann, J., Kartal, B. & Op den Camp, H. J. M. Multiheme hydroxylamine oxidoreductases produce NO during ammonia oxidation in methanotrophs. *Proc. Natl. Acad. Sci. U. S. A.* **117**, 24459–24463 (2020).

9. Haukelidsaeter, S. *et al.* Influence of filter age on Fe, Mn and NH4+ removal in dual media rapid sand filters used for drinking water production. *Water Res.* **242**, 120184 (2023).

10. Poghosyan, L., Koch, H., Frank, J., van Kessel, M. A. H. J., Cremers, G., van Alen, T., Jetten, M. S. M., Op den Camp, H. J. M. & Lücker, S. Metagenomic profiling of ammonia- and methane-oxidizing microorganisms in two sequential rapid sand filters. *Water Res.* **185**, 116288 (2020).

11. Palomo, A., Jane Fowler, S.,

Gülay, A., Rasmussen, S., Sicheritz-Ponten, T. & Smets, B. F. Metagenomic analysis of rapid gravity sand filter microbial communities suggests novel physiology of Nitrospira spp. *ISME J.* **10**, 2569–2581 (2016).

12. de Vet, W., Van Genuchten, C. C. A., Van Loosdrecht, M. C. M. & Van Dijk, J. C. Water quality and treatment of river bank filtrate. *Drink. Water Eng. Sci.* **3**, 79–90 (2010).

13. Leak, D. J. & Dalton, H. Growth yields of methanotrophs - 1. Effect of copper on the energetics of methane oxidation. *Appl. Microbiol. Biotechnol.* **23**, 470–476 (1986).

14. Malashenko, Y. R., Pirog, T. P., Romanovskaya, V. A., Sokolov, I. G. & Grinberg, T. A. Search for methanotrophic producers of exopolysaccharides. *Appl. Biochem. Microbiol.* **37**, 599–602 (2001).

15. Søborg, D. A., Breda, I. L. & Ramsay, L. Effect of oxygen deprivation on treatment processes in a full-scale drinking water biofilter. *Water Sci. Technol. Water Supply* **15**, 825–833 (2015).

16. Van der Aa, L. T. J., Kors, L. J., Wind, A. P. M., Hofman, J. A. M. H. & Rietveld, L. C. Nitrification in rapid sand filter: Phosphate limitation at low temperatures. in *Water Science and Technology: Water Supply* vol. 2 37–46 (IWA Publishing, 2002).

17. Wagner, F. B., Nielsen, P. B., Boe-Hansen, R. & Albrechtsen, H. J. Copper deficiency can limit nitrification in biological rapid sand filters for drinking water production. *Water Res.* **95**, 280–288 (2016).

18. Corbera-Rubio, F., Goedhart, R., Laureni, M., van Loosdrecht, M. C. M. & van Halem, D. A Biotechnological Perspective on Sand Filtration for Drinking Water Production. *Manuscr. Submitt. Publ.* (2024).

19. de Vet, W., Rietveld, L. C. & Van Loosdrecht, M. C. M. Influence of iron on nitrification in full-scale drinking water trickling filters. *J. Water Supply Res. Technol. - AQUA* **58.4**, 247–256 (2009).

20. Sander, R. Compilation of Henry ' s law constants for water as solvent , version. *Atmos. Chem. Phys. Discuss.*, 29615–30521 (2015).

21. Herlemann, D. P. R., Labrenz, M., Jürgens, K.,

Bertilsson, S., Waniek, J. J. & Andersson, A. F. Transitions in bacterial communities along the 2000 km salinity gradient of the Baltic Sea. *ISME J. 2011 510* **5**, 1571–1579 (2011).

22. Caporaso, J. G. *et al*. Ultra-high-throughput microbial community analysis on the Illumina HiSeq and MiSeq platforms. *ISME J. 2012 68* **6**, 1621–1624 (2012).

23. Callahan, B. J., McMurdie, P. J., Rosen, M. J., Han, A. W., Johnson, A. J. A. & Holmes, S. P. DADA2: High-resolution sample inference from Illumina amplicon data. *Nat. Methods 2016 137* **13**, 581–583 (2016).

24. Quast, C., Pruesse, E., Yilmaz, P., Gerken, J., Schweer, T., Yarza, P., Peplies, J. & Glöckner, F. O. The SILVA ribosomal RNA gene database project: improved data processing and web-based tools. *Nucleic Acids Res.* **41**, (2013).

25. McMurdie, P. J. & Holmes, S. phyloseq: An R Package for Reproducible Interactive Analysis and Graphics of Microbiome Census Data. *PLoS One* **8**, e61217 (2013).

26. Nurk, S., Meleshko, D., Korobeynikov, A. & Pevzner, P. A. MetaSPAdes: A new versatile metagenomic assembler. *Genome Res.* **27**, 824–834 (2017).

27. Li, H., Handsaker, B., Wysoker, A., Fennell, T., Ruan, J., Homer, N., Marth, G., Abecasis, G. & Durbin, R. The Sequence Alignment/Map format and SAMtools. **25**, 2078–2079 (2009).

28. Graham, E. D., Heidelberg, J. F. & Tully, B. J. Binsanity: Unsupervised clustering of environmental microbial assemblies using coverage and affinity propagation. *PeerJ* **2017**, e3035 (2017).

29. Alneberg, J., Bjarnason, B. S., de Bruijn, I., Schirmer, M., Quick, J., Ijaz, U. Z., Loman, N. J., Andersson, A. F. & Quince, C. CONCOCT: Clustering cONtigs on COverage and ComposiTion. (2013).

30. Wu, Y. W., Simmons, B. A. & Singer, S. W. MaxBin 2.0: An automated binning algorithm to recover genomes from multiple metagenomic datasets. *Bioinformatics* **32**, 605–607 (2016).

31. Kang, D. D., Li, F., Kirton, E., Thomas, A., Egan, R., An, H. & Wang, Z. MetaBAT 2: An adaptive binning algorithm for robust and efficient genome reconstruction

from metagenome assemblies. *PeerJ* **2019**, (2019).

32. Sieber, C. M. K., Probst, A. J., Sharrar, A., Thomas, B. C., Hess, M., Tringe, S. G. & Banfield, J. F. Recovery of genomes from metagenomes via a dereplication, aggregation and scoring strategy. *Nat. Microbiol. 2018 37* **3**, 836–843 (2018).

33. Eren, A. M. *et al.* Community-led, integrated, reproducible multi-omics with anvi'o. *Nat. Microbiol. 2020 61* **6**, 3–6 (2020).

34. Chklovski, A., Parks, D. H., Woodcroft, B. J. & Tyson, G. W. CheckM2: a rapid, scalable and accurate tool for assessing microbial genome quality using machine learning. *Nat. Methods 2023 208* **20**, 1203–1212 (2023).

35. Bowers, R. M. *et al.* Minimum information about a single amplified genome (MISAG) and a metagenome-assembled genome (MIMAG) of bacteria and archaea. *Nat. Biotechnol.* **35**, 725–731 (2017).

36. Chaumeil, P. A., Mussig, A. J., Hugenholtz, P. & Parks, D. H. GTDB-Tk v2: memory friendly classification with the genome taxonomy database. *Bioinformatics* **38**, 5315–5316 (2022).

37. Shaffer, M. *et al.* DRAM for distilling microbial metabolism to automate the curation of microbiome function. *Nucleic Acids Res.* **48**, 8883–8900 (2020).

38. Garber, A. I., Nealson, K. H., Okamoto, A., McAllister, S. M., Chan, C. S., Barco, R. A. & Merino, N. FeGenie: A Comprehensive Tool for the Identification of Iron Genes and Iron Gene Neighborhoods in Genome and Metagenome Assemblies. *Front. Microbiol.* **11**, 37 (2020).

39. Hyatt, D., Chen, G. L., LoCascio, P. F., Land, M. L., Larimer, F. W. & Hauser, L. J. Prodigal: Prokaryotic gene recognition and translation initiation site identification. *BMC Bioinformatics* **11**, 1–11 (2010).

40. Cremers, G., Jetten, M. S. M., Op den Camp, H. J. M. & Lücker, S. Metascan: METabolic Analysis, SCreening and ANnotation of Metagenomes. *Front. Bioinforma.* **2**, 861505 (2022).

41. Na, P. J., Yaramala, S. R., Kim, J. A., Kim, H., Goes, F. S., Zandi, P. P., Vande Voort, J. L., Sutor, B., Croarkin, P. & Bobo, W. V. The PHQ-9 Item 9 based

screening for suicide risk: a validation study of the Patient Health Questionnaire (PHQ)-9 Item 9 with the Columbia Suicide Severity Rating Scale (C-SSRS). *J. Affect. Disord.* **232**, 34–40 (2018).

42. Price, M. N., Dehal, P. S. & Arkin, A. P. FastTree 2 – Approximately Maximum-Likelihood Trees for Large Alignments. *PLoS One* **5**, e9490 (2010).

43. Edgar, R. C. MUSCLE: multiple sequence alignment with high accuracy and high throughput. *Nucleic Acids Res.* **32**, 1792 (2004).

44. Trifinopoulos, J., Nguyen, L. T., von Haeseler, A. & Minh, B. Q. W-IQ-TREE: a fast online phylogenetic tool for maximum likelihood analysis. *Nucleic Acids Res.* **44**, W232–W235 (2016).

45. Ludwig, W. *et al.* ARB: a software environment for sequence data. *Nucleic Acids Res.* **32**, 1363–1371 (2004).

46. Minh, B. Q., Schmidt, H. A., Chernomor, O., Schrempf, D., Woodhams, M. D., Von Haeseler, A., Lanfear, R. & Teeling, E. IQ-TREE 2: New Models and Efficient Methods for Phylogenetic Inference in the Genomic Era. *Mol. Biol. Evol.* **37**, 1530–1534 (2020).

47. Letunic, I. & Bork, P. Interactive Tree Of Life (iTOL) v5: an online tool for phylogenetic tree display and annotation. *Nucleic Acids Res.* **49**, W293–W296 (2021).

48. Kleikamp, H. B. C., Pronk, M., Tugui, C., Guedes da Silva, L., Abbas, B., Lin, Y. M., van Loosdrecht, M. C. M. & Pabst, M. Database-independent de novo metaproteomics of complex microbial communities. *Cell Syst.* **12**, 375-383.e5 (2021).

49. Kleikamp, H. B. C., Grouzdev, D., Schaasberg, P., van Valderen, R., van der Zwaan, R., Wijgaart, R. van de, Lin, Y., Abbas, B., Pronk, M., van Loosdrecht, M. C. M. & Pabst, M. Metaproteomics, metagenomics and 16S rRNA sequencing provide different perspectives on the aerobic granular sludge microbiome. *Water Res.* **246**, 120700 (2023).

50. Buchfink, B., Xie, C. & Huson, D. H. Fast and sensitive protein alignment using DIAMOND. *Nat. Methods 2014 121* **12**, 59–60 (2014).

51. Koch, H., van Kessel, M. A. H. J. & Lücker, S. Complete

nitrification: insights into the ecophysiology of comammox Nitrospira. *Applied Microbiology and Biotechnology* vol. 103 177–189 at https://doi.org/10.1007/s00253-018-9486-3 (2019).

52. Knief, C. Diversity and habitat preferences of cultivated and uncultivated aerobic methanotrophic bacteria evaluated based on pmoA as molecular marker. *Frontiers in Microbiology* vol. 6 170928 at https://doi.org/10.3389/fmicb.2015.01346 (2015).

53. Hu, W., Liang, J., Ju, F., Wang, Q., Liu, R., Bai, Y., Liu, H. & Qu, J. Metagenomics Unravels Differential Microbiome Composition and Metabolic Potential in Rapid Sand Filters Purifying Surface Water Versus Groundwater. *Environ. Sci. Technol.* **54**, 5206 (2020).

54. Afshin, Y., Delherbe, N. & Kalyuzhnaya, M. G. Methylotenera. in *Bergey's Manual of Systematics of Archaea and Bacteria* 1–11 (John Wiley & Sons, Ltd, 2021).

55. Stanley, S. H., Prior, S. D., Leak, D. J. & Dalton, H. Copper stress underlies the fundamental change in intracellular location of methane mono-oxygenase in methane-oxidizing organisms: Studies in batch and continuous cultures. *Biotechnol. Lett.* **5**, 487–492 (1983).

56. Murreil, J. C., Gilbert, B. & McDonald, I. R. Molecular biology and regulation of methane monooxygenase. *Arch. Microbiol.* **173**, 325–332 (2000).

57. Gülay, A., Musovic, S., Albrechtsen, H. J., Al-Soud, W. A., Sørensen, S. J. & Smets, B. F. Ecological patterns, diversity and core taxa of microbial communities in groundwater-fed rapid gravity filters. *ISME J.* **10**, 2209–2222 (2016).

58. González-Cabaleiro, R., Curtis, T. P. & Ofiţeru, I. D. Bioenergetics analysis of ammonia-oxidizing bacteria and the estimation of their maximum growth yield. *Water Res.* **154**, 238–245 (2019).

59. Neubauer, S. C., Emerson, D. & Megonigal, J. P. Life at the energetic edge: Kinetics of circumneutral iron oxidation by lithotrophic iron-oxidizing bacteria isolated from the wetland-plant rhizosphere. *Appl. Environ. Microbiol.* **68**, 3988–3995 (2002).

60. Van Beek, C. G. E. M., Dusseldorp, J., Joris, K., Huysman, K., Leijssen, H., Schoonenberg Kegel, F., De Vet, W. W. J. M., Van De Wetering, S. & Hofs, B. Contributions of homogeneous, heterogeneous and biological iron(II) oxidation in aeration and rapid sand filtration (RSF) in field sites. *J. Water Supply Res. Technol. - AQUA* **65**, 195–207 (2016).

61. Müller, S., Corbera-Rubio, F., Schoonenberg-Kegel, F., Laureni, M., Van Loosdrecht, M. C. M., Van Halem, D., Loosdrecht, M. C. M. van & Halem, D. van. Shifting to biology promotes highly efficient iron removal in groundwater filters. *bioRxiv* 2024.02.14.580244 (2024).

62. Grohmann, A., Gollasch, R. & Schuhmacher, G. Biological iron and manganese removal of a methane containing groundwater in Speyer. *GWFWasser/Abwasser* **130**, 441–446 (1989).

63. de Vet, W., Advies, H., Burger, W., Advies, H., Woerdt, D. V. A. N. D. E. R. & Advies, H. Methane load irrelevant for filter performance. *H2O* **35**, 26–29 (2002).

64. Tatari, K., Smets, B. F. & Albrechtsen, H. J. Depth investigation of rapid sand filters for drinking water production reveals strong stratification in nitrification biokinetic behavior. *Water Res.* **101**, 402–410 (2016).

65. Corbera-Rubio, F., Laureni, M., Koudijs, N., Müller, S., van Alen, T., Schoonenberg, F., Lücker, S., Pabst, M., van Loosdrecht, M. C. M. & van Halem, D. Meta-omics profiling of full-scale groundwater rapid sand filters explains stratification of iron, ammonium and manganese removals. *Water Res.* **233**, 119805 (2023).

66. Lee, C. O., Boe-Hansen, R., Musovic, S., Smets, B., Albrechtsen, H. J. & Binning, P. Effects of dynamic operating conditions on nitrification in biological rapid sand filters for drinking water treatment. *Water Res.* **64**, 226–236 (2014).

67. Bodelier, P. L. E. & Frenzel, P. Contribution of methanotrophic and nitrifying bacteria to CH4 and NH4+ oxidation in the rhizosphere of rice plants as determined by new methods of discrimination. *Appl. Environ. Microbiol.* **65**, 1826–1833 (1999).

68. Bédard, C. & Knowles, R. Physiology, biochemistry,

and specific inhibitors of CH4, NH4+, and CO oxidation by methanotrophs and nitrifiers. *Microbiol. Rev.* **53**, 68 (1989).

69. Martikainen, P. J. Heterotrophic nitrification – An eternal mystery in the nitrogen cycle. *Soil Biol. Biochem.* **168**, 108611 (2022).

70. Corbera-Rubio, F., Kruisdijk, E., Malheiro, S., Leblond, M., Verschoor, L., van Loosdrecht, M. C. M., Laureni, M. & van Halem, D. A difficult coexistence: resolving the iron-induced nitrification delay in groundwater filters. *Water Res.* 121923 (2024).

71. Albers, C. N., Ellegaard-Jensen, L., Harder, C. B., Rosendahl, S., Knudsen, B. E., Ekelund, F. & Aamand, J. Groundwater chemistry determines the prokaryotic community structure of waterworks sand filters. *Environ. Sci. Technol.* **49**, 839–846 (2015).

72. Fowler, S. J., Palomo, A., Dechesne, A., Mines, P. D. & Smets, B. F. Comammox Nitrospira are abundant ammonia oxidizers in diverse groundwater-fed rapid sand filter communities. *Environ. Microbiol.* **20**, 1002–1015 (2018).

73. Breda, I. L., Ramsay, L., Søborg, D. A., Dimitrova, R. & Roslev, P. Manganese removal processes at 10 groundwater fed full-scale drinking water treatment plants. *Water Qual. Res. J. Canada* **54**, 326–337 (2019).

74. Bruins, J. H., Petrusevski, B., Slokar, Y. M., Huysman, K., Joris, K., Kruithof, J. C. & Kennedy, M. D. Biological and physico-chemical formation of Birnessite during the ripening of manganese removal filters. *Water Res.* **69**, 154–161 (2015).

75. Haukelidsaeter, S. *et al.* Efficient chemical and microbial removal of iron and manganese in a rapid sand filter and impact of regular backwash. *Appl. Geochemistry* **162**, 105904 (2024).

76. Breda, I. L., Søborg, D. A., Ramsay, L. & Roslev, P. Manganese removal processes during start-up of inoculated and non-inoculated drinking water biofilters. *Water Qual. Res. J.* **54**, 47–56 (2019).

77. Sahabi, D. M., Takeda, M., Suzuki, I. & Koizumi, J. ichi. Removal of Mn2+ from water by 'aged' biofilter media: The role of catalytic oxides layers. *J. Biosci.*

Bioeng. **107**, 151–157 (2009).

78. Cheng, Q., Nengzi, L., Xu, D., Guo, J. & Yu, J. Influence of nitrite on the removal of Mn(II) using pilot-scale biofilters. *J. Water Reuse Desalin.* **7**, 264–271 (2017).

The maximal output of a doctoral program is not defined by the number of papers, but by the growth and acquired competences of the candidate

M.C.M. van Loosdrecht

OUTLOOK

7

The overarching goal of this thesis was to gain knowledge to advance towards the design of high-flow, resource-efficient sand filters. We started by assuming that success in designing better filters is determined by our inability to predict and control the nature, location, and interactions of the reactions. In a technology dominated by both biological and physical-chemical reactions like sand filters, this translates into predicting and controlling *i)* microbial community assembly and performance and *ii)* the interplay between physical-chemical and biological processes. In plain words: *which parameters dictate which microorganisms grow where?* and *which parameters determine which reactions take place biologically and physical-chemically and how they affect each other?*

Establishing clear cause-effect relationships in sand filters is an arduous task due to the deep convolution of the processes. Hence, the first part of the project focused on shedding light on what I call 'the three sources of complexity' of sand filtration: *i)* the oxidizing agent, *ii)* direct and indirect interactions and futile cycles between removal processes and i*ii)* backwashing. These sources either encompass a cluster of parameters that combined have a clear, rather traceable effect on the performance of the filter, e.g., oxidizing agent, or are a consequence of a cluster of parameters, e.g. futile cycles. For instance, when studying the oxidizing agent we not only considered its nature (oxygen, nitrate) but also its dose (10, 5, 0 mg L^{-1}) or injection mode. In this chapter, the key scientific insights of the thesis are integrated and contextualized with the existing sand filtration knowledge. Then, a technical summary of their industrial relevance and applicability of the projects is presented. The outlook finishes with my vision on the future of sand filtration.

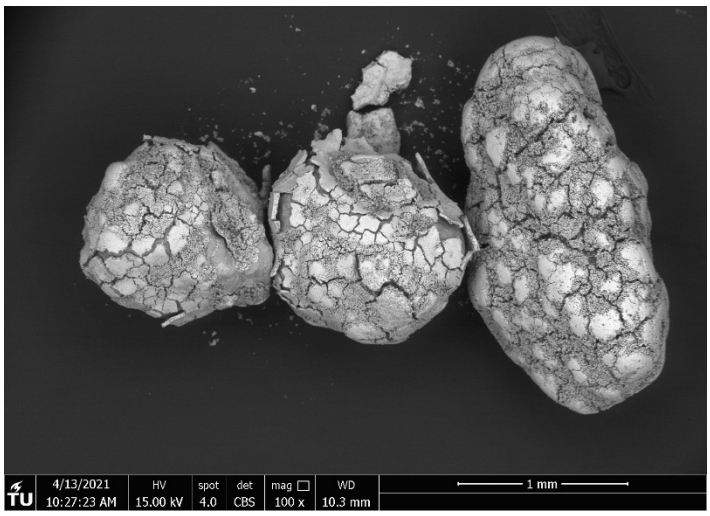

Figure 1. e-SEM picture of dry sand grains covered with oxides from a mature filter. Courtesy of Yuemei Lin.

7.1. SCIENTIFIC OUTLOOK: the three sources of complexity

7.1.1. Oxidizing agent – oxygen and beyond

It is hard – if not impossible – to find a sand filter in Northern Europe that does not use oxygen as the oxidizing agent. Introducing oxygen to saturation levels in anaerobic groundwater allows for the oxidation of the main groundwater contaminants, but it also onsets a cascade of simultaneous, uncontrolled reactions that preclude optimization. In a work led by my colleague Simon Muller [1], we operated a full-scale sand filter at <5 mgO_2 L^{-1} instead of the conventional 10 mgO_2 L^{-1}. With such a change, we shifted iron oxidation from (mainly) homogeneous to (mainly) biological-adsorptive. The result is that the filter could be operated at >3x higher flow rate, and water and energy losses decreased by >75%.

An alternative approach that follows the same rationale is to skip oxygen dosing entirely. In Chapter 5, we operated a pilot-scale sand filter using nitrate instead of oxygen as the oxidizing agent. By removing the aeration step, we managed to couple the oxidation of Fe^{2+} to Fe^{3+} to denitrification in an anoxic process known as nitrate-dependent iron oxidation (NDFO). The reaction, fully biological, was carried out by a newly found microorganism, which we baptized as "*Candidatus* Siderophilus nitratireducens". Although it warrants further research, the notorious reduction in clogging and the fact that Fe removal is biological makes us confident that this novel filtration concept will also yield higher flow rates, longer runtimes, and lower water and energy losses.

These two examples showcase the importance of the nature and dose of the oxidizing agent on shifting from chemical to biological Fe oxidation, and consequently on the performance of sand filters. In both cases, reducing the amount of effective oxidizing agent to remove only Fe^{2+} - instead of Fe^{2+}, NH_4^+ and Mn^{2+} - improves the performance of the filter. Naturally, this forces the installation of a second unit operation to oxidize ammonium and manganese, which can easily be done with a conventional aerator – sand filter module. One can, however, go even further and also split the removal of ammonium and manganese in two independent units, obtaining a 3-step process. This additional step will circumvent the commonly reported detrimental effects of

ammonium [2,3] and nitrite [4] on manganese removal, minimizing unexpected operational problems and thus making the process more predictable, robust and easy to operate.

7.1.2. Direct and indirect interactions and futile cycles

Both the biological-adsorptive iron removal and NDFO projects are based on the same principle: avoiding Fe^{3+} floc formation. The thought that Fe chemistry was somehow compromising the performance of sand filters has long been lingering in the field [5]. The literature is full of scientific articles claiming that Fe^{2+} [6], but also its oxidation products Fe^{3+} flocs [7], Fe^{3+} solids [8] and by-products like reactive oxygen species (ROS) [9] have detrimental effects on microorganisms. In Chapter 4, we present strong evidence to claim that Fe^{3+} flocs inhibit the ammonia oxidation capacity of ammonia-oxidizing bacteria. The higher flowrates and longer runtimes obtained or predicted in Fe^{3+} floc-free systems like the biological-adsorptive iron removal and NDFO filters support the claim. This finding allows us to - a priori - explain the widespread stratification of removal processes in sand filters, and changes the narrative. Until now, the common way to report such separation was 'the removal of ammonium and manganese does not start *until complete* Fe^{2+} *oxidation*', while now we should phrase it as '*in the presence of high* Fe^{3+} *floc loads*'. Still, there are many open questions that our findings cannot explain.

The most obvious one is that the stratification of processes happens often, but not always (unpublished data). Most likely the degree of inhibition/stratification depends on the load of Fe^{3+} flocs, but a quantitative evaluation would certainly erase any doubts. Another, and perhaps more intriguing one, is the suppression of ammonia removal in Fe^{3+} floc-free systems like our biological-adsorptive iron removal filter [1]. Nutrient limitation is commonly used as a justification for incomplete ammonia removal. The publications of Wagner and colleagues about copper limitation in sand filters in Denmark [10,11] remain the only example where nutrient limitation is unequivocally proven in full-scale set-ups. Similar findings have not been reported anywhere else, so it may be a problem confined to Danish groundwater or part of a network of convoluted processes. Certainly, nutrient limitation does not account for the lack of nitrification in our filter, as ammonia is completely removed in the following sand filter and there is no nutrient dosage in-between (manuscript in preparation). Another unresolved

question is how Fe^{3+} flocs interact with ammonia-oxidizing bacteria. The batch experiments and modeling in Chapter 4 indicate that there is a direct effect on the ammonium oxidation capacity of the organisms, which means that the effects go beyond growth impediments. Unpublished experiments with a free-floating culture show that ammonia-oxidizing bacteria are adsorbed on the Fe^{3+} flocs, and ammonium oxidation stops completely. This suggests a sort of contact-based interaction. Tong and colleagues [7] proposed that Fe^{3+} flocs damage the cell membrane and enter the cytoplasm. Microfluidics experiments coupled with in-line microscopic visualization may be suitable to validate this hypothesis.

Microbial competition is another kind of interaction that shapes microbial community assembly in sand filters. In Chapter 6, we explored how the appearance of methane-oxidizing bacteria drastically modified the composition of the filter community. The removals of ammonia and manganese were suppressed, and iron oxidation switched from (at least partially) biological to (almost) completely chemical. Remarkably, the operational parameters in the water phase seemed ideal at least for nitrifying organisms (10 mg O_2 L^{-1}, neutral pH, 2 mg NH_4^+N L^{-1}). We posit how either micronutrient or oxygen availability dictates which microorganisms survive and outgrow the others in a competition for space. The main conclusion of the work is that the biological oxidation of >3 mg CH_4 L^{-1} methane (which requires >10 mg O_2 L^{-1}) is unlikely to co-exist with the biological removal of any other compound, which will inevitably be displaced further down in the filter. Potentially, the same mechanism could explain why manganese oxidation tends to take place after ammonium removal in filters where manganese removal is predominantly biological. Regrettably, we cannot distinguish between chemical and biological manganese removal in filters yet. More about this in the technical summary below.

The last set of interactions that we explored are futile cycles. Bray and Olanczuk [12] and Søborg [13] investigated the effect of total oxygen deprivation in sand filters treating groundwater with iron, ammonia, and manganese. We followed up on their findings and operated a filter filled with Mn^{4+}-coated sand with an oxygen load lower than required to oxidize all ammonia (and manganese) in the incoming water (Box 1), a common situation in full-scale sand filers. As expected, and in agreement with their results, the reducing conditions derived from the lack of oxygen resulted in the reduction of Mn^{4+}-coatings to Mn^{2+}. It is tempting to hypothesize that Mn may be part of a futile cycle in filters, oxidizing

from Mn^{2+} to $Mn^{3+/4+}$ in aerobic areas – with oxygen as oxidizing agent - and reducing back to Mn^{2+} under anaerobic conditions – coupled to nitrite oxidation. This behavior raises many questions: *a) does this also happen in the bottom section or in the infamous anaerobic pockets of full-scale filters?* If so, *b) can we optimize filter performance by avoiding Mn^{4+}-Mn^{3+}-Mn^{2+} cycling? c) Does this also happen with Fe^{2+}? d) What else do the unmeasured yet crucial transient nitrite (and possible other nitrogen reactive species like hydroxylamine) peaks do in the filter?* What is clear is that these questions cannot be answered with the traditional snap-shot studies of sand filters. Sampling campaigns coupling measurements along the filter depth and through the run cycle are pivotal to understand the dynamics of sand filters.

BOX 1 – The fate of Mn in coexisting aerobic and anoxic filter zones

We operated a set of pilot-scale columns in DWTP Hammerflier (Vitens). The columns were packed with anthracite from mature sand filters, fully covered by manganese oxides. One of them was fed with the effluent of the biological-adsorptive iron removal filter, which was slightly aerated to reach: 2.2 mg NH_4^+-N L^{-1}, 0.3 mg Mn^{2+} L^{-1}, <0.1 mg Fe^{2+} L^{-1}, DO ~ 3mg O_2 L^{-1}, pH ~ 6.9. Unlike in standard sand filters, the water in our filter did not reach oxygen saturation. This situation allowed us to investigate which reactions make use of the scarce, limiting oxygen before others. The experiment had several objectives, one of them being characterizing the fate of Mn through the aerobic (top) and anoxic (bottom) zones of the column.

All available oxygen was used for ammonia oxidation. However, the oxygen load was insufficient to fully oxidize all ammonia to nitrate, which must have resulted in transient concentrations of nitrite in the filter (not measured). We observed that during interrupted cycles, i.e. without backwashing, Mn^{2+} concentration in the effluent increased steadily, reaching values higher than in the influent (Figure 1). We hypothesize that, under anoxic conditions, the Mn^{4+} coating at the bottom of the filter slowly reduced to Mn^{3+} coating, and eventually to dissolved Mn^{2+}. As far as we can see, nitrite is the only available electron donor, so Mn reduction was likely coupled to nitrite oxidation to nitrate. Interestingly, Mn^{2+} disappeared from the effluent right after backwashing, possibly because the Mn^{3+} coating was regenerated to Mn^{4+} with the oxygen present in the backwash water, reestablishing the Mn^{2+} oxidation capacity of the filter.

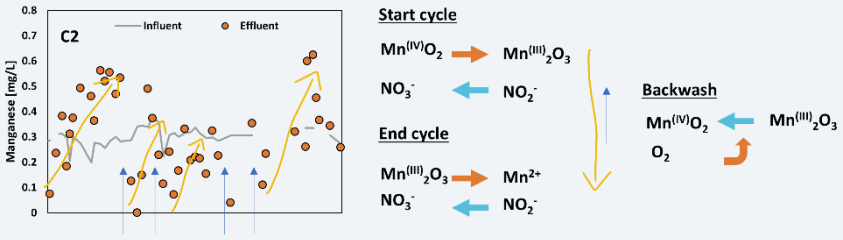

Figure 2. Dynamics of Mn oxidation and reduction during anoxic periods interrupted by backwashing events. Grey line indicates influent Mn^{2+} concentration. Orange dots are effluent Mn^{2+} concentration. Orange lines depict trends of increasing Mn^{2+} effluent concentrations through long anoxic periods without backwashing. Blue arrows indicate backwashing.

7.1.3. Backwashing

The main purpose of backwashing is removing Fe^{3+} flocs to unclog the filter, decreasing the resistance built during a run cycle. Backwashing has, however, other practical consequences for the filter. One of them is sand grain displacement. In Chapter 3 we explored how backwashing and sand grain displacement affect microbial community assembly and performance. Protein abundance and *ex-situ* ammonium removal rates showed that the ammonium removal capacity of the filter was strongly stratified along the filter depth, something we could not see with the homogeneous taxonomic composition over the bed. From these observations, we hypothesize that microbial community turnover is too slow to adapt to the constant environmental changes due to grain displacement through backwashing, meaning that the fitness of the community relies on the modulation of the protein pool. Additionally, our study suggests that taxonomic composition is not a suitable surrogate of filter activity.

After the publication of Chapter 3, two studies found stratified microbial communities in groundwater sand filters [14,15]. It is hard to pinpoint the cause underlying the differences between these studies and our Chapter 3, but I'd bet it has to do with backwashing frequency and intensity. Lower backwashing frequency and intensity will leave the community of each grain exposed to the same concentration of contaminants for longer periods, eventually longer than the time required to see changes in microbial community composition. Potentially, one could correlate backwashing frequency and intensity to the extent to which the community is stratified. If this is true, filter designers are suddenly granted a new degree of freedom. On one hand, in filters with homogeneous communities, the removal of contaminants still takes place in a specific section, which means that the filter has overcapacity. This makes the filter much more robust, able to cope with dynamic loads of contaminants. Surface water treatment may very well benefit from it. On the other hand, filters taxonomically stratified are likely to remove each contaminant in smaller filter volumes, separating the removal of each contaminant and thus avoiding interactions that slow down the process. Both approaches have benefits, so the decision-making process for every filter will have to go hand in hand with the groundwater matrix and, perhaps more importantly, the strategy of the drinking water company.

7.2. LESSONS FROM AND FOR PRACTICE

7.2.1. Which portion of the filter community do we catch?

The first time I extracted DNA from a sand grain I was shocked: <1 ng DNA/µL. There are not many sand filtration papers that examine the microbial community on the sand grains, so I am pretty sure I had read most of them. Not once did I find a single comment mentioning the difficulty in DNA extraction. This is, naturally, a consequence of a fierce publishing system that discourages not only the publication of negative results but also transparency admitting experimental and technical difficulties in successful ventures. I was immensely fortunate to supervise Nienke Koudijs, a master thesis student at that time, and together we found out that adding skimmed milk prior to cell disruption yielded at least 10 times more DNA. To this day, we still do not know exactly how it works, but I suspect that the proteins in milk bind to Fe, preventing it from attaching to DNA. This solved the problem in most cases, but it took us three long months to develop the protocol. Sometimes this was still not enough, and we had to extract DNA several times from the grains to then pull down and concentrate it before sequencing. Half a year afterward, our project partners form Radboud University encountered the same difficulties extracting DNA, and the skimmed milk method helped them as well. There are two important take-home messages in this anecdote: *i*) I hope that future researchers find our *methods* section descriptive enough and avoid that painstaking process we had to go through, and *ii*) How much can we trust the data derived from methods that require DNA or protein extraction? I do not know. I could very well be overestimating the bias, but in any case, to me it is clear that *ex-situ* activity measurements, which circumvent any sort of extraction bias, are the better approach to characterize filter activity.

7.2.2. The manganese conundrum

Manganese has historically received less attention in comparison to its counterparts iron and ammonia. This disparity can be partially attributed to the lower concentrations of Mn in groundwater relative to Fe and NH_4^+, as well as by the fact that Mn^{2+} oxidation seems to naturally occur within sand filters designed for iron removal. Nonetheless, the advancement of manganese research is also impeded by two technical bottlenecks, namely *i)* distinguishing between

chemical and biological removal and *ii)* identifying manganese-oxidizing bacteria. Let's start with the first one.

As homogeneous Mn^{2+} oxidation cannot occur in sand filters, manganese removal is shared between heterogeneous (chemical) oxidation and biological reactions. Two methods have been used to distinguish between them. The first one, proposed by Jantinus Bruins and colleagues [16], is based on the findings of Kim and colleagues [17] that electron paramagnetic resonance spectra of Mn oxides can be used to distinguish biologically- and chemically-formed Mn oxides. This method provides only indirect evidence of the origin of the oxides, and while it seems to be very successful, the only follow-up study shows opposite results [15] which means that either our knowledge about the contribution of biological Mn in mature filters is still minimal or, far worse, the method is not reliable. The other method has been used more often, and it is based on measuring the Mn^{2+}-oxidizing capacity of sand grains from a filter before and after suppressing biological activity, either in *ex-situ* batch tests [2] or directly in the filter [18]. Biological inactivation is done either by autoclaving [19] or adding biological suppressors [20]. It is well known that autoclaving changes the morphology of Mn oxides, and thus its catalytic capacity [21]. On the other side, the addition of biological suppressors like sodium azide or penicillin is usually not effective on sand grains, possibly because of the protection that the metal coating offers [20]. Additionally, and in case that the suppression of biological activity was 100% effective, chemical reactions would take over at least part of the removal that was originally biological, resulting in an underestimation of the contribution of manganese-oxidizing bacteria. Not surprisingly, works using this method tend to report that Mn removal is mainly chemical [2,20,22].

The second bottleneck is the identification of manganese-oxidizing bacteria. To date, only a single microorganism has been proven to harvest energy from Mn oxidation [23]. The ecological benefit of Mn oxidation by all the other manganese-oxidizing bacteria is yet unknown, with suggestions ranging from protection to UV radiation or ROS scavenging to keeping Mn oxides as electron acceptors for redox balancing [24]. Most of them use organic compounds as energy source, such as Pseudomonas [25] and Leptothrix [26]. Probably due to the fact that Mn oxidation is not the primary energy source, the ability to oxidize Mn^{2+} is usually not conserved between phylogenetically closely related bacteria [27], which makes taxonomic identification impossible unless species-level resolution is achieved. The alternative to phylogenetic identification is gene-centric

identification targeting Mn^{2+} oxidation genes. Two types of enzymes have been proven to oxidize Mn^{2+}: multicopper oxidases [28] and calcium-binding peroxidases [29]. Both of these enzyme types can catalyze the oxidation of several other compounds, so one cannot simply infer that an organism can oxidize Mn^{2+} because of the presence of the enzymes. Overall, resolving the contribution of biology to Mn^{2+} oxidation in sand filters is technically unattainable in the short term.

So, what do we do? I believe that continuing the old-school approach that the group of prof. Natalia Gottig started in Argentina [25] – sand grain sampling, incubation, isolation and sequencing – may be the best approach we have right now.

7.2.3. On the adoption of new technologies

A common problem in the drinking water industry is the scarcity of opportunities for the implementation of new technologies [30]. The root causes are, among others, lengthy regulatory processes, slow and difficult public and government acceptance, and humongous capital expenditures. Additionally, the responses of immature technologies to different water matrices are not always predictable, so companies willing to be early adopters of emerging technologies are scarce [31]. The implementation of the first technology here presented (biological-adsorptive iron removal) is presumably feasible short term. New equipment is not required as long as methane is not present in the water source, and the efficacy of the technology has already been tested full-scale. On the contrary, the adoption of NDFO will require much more time. Presenting these findings to water technologists, I either perceived or directly received reluctance and strong opposing opinions. If I were on their side, I would probably have reacted the same way. On top of the usual problems of new technologies, in this case there is another one – the dominant nitrogen species at the oxidation-reduction potential of anaerobic groundwater is ammonia, not nitrate.

Fortunately, Vitens organized the NWO Sand Filtration *Knowledge Day*, where I had the pleasure of presenting this thesis to an extensive group of water experts across the country. There, it was clear that several companies saw opportunities to implement NDFO in their systems. The first one is to co-feed the filter with streams from two different wells – which is already common practice – with

distinct oxidation-reduction potentials, one containing Fe^{2+}, and one with nitrate. Most likely, the main objective of this application will be decreasing the concentration of iron in iron-rich groundwater. Naturally, a conventional aerated post-filter would be required to oxidize ammonium and manganese. The second opportunity is using it to treat the concentrate stream of reverse osmosis used at the end of drinking treatment plants, which contains high concentrations of nitrate. This configuration requires a recirculation stream from the reverse osmosis unit to the NDFO sand filter at the upstream side of the plant.

Creative, collaborative sessions like the ones held during the *Knowledge Day* are of utmost importance to ensure that the drinking water sector moves as a unit. Each drinking water treatment matrix is unique, but the challenges we face are common: drought, salinity or new pollutants like PFAS are just some examples. Innovation and implementation of new technologies will only be effective and efficient if pursued as a joint venture. This requires union not only between practitioners, but also academics and regulatory agencies.

7.3. AN EYE ON THE FUTURE

Despite they have been in use for over 150 years, sand filters are still emerging across the world and there is no sign of disappearance. The Global South is slowly including sand filters in their drinking water treatment plants, and countries at the vanguard of drinking water technologies – like the Netherlands – keep choosing sand filtration as the core technology for their new plants. On top of their traditional role, the recent blossom of information about sand filtration and the emergence of new drinking water technologies broaden the scope of applications in which sand filters can be applied. Below, a quick glance at the ones I consider most promising.

1) The Membrane – Filter Hybrid

Sand filters step aside from the spotlight and become auxiliary units for anaerobic reverse osmosis membranes, the new prima donna of drinking water treatment plants. Anaerobic reverse osmosis units can cope with much higher Fe^{2+} and Mn^{2+} concentrations than sand filters as long as oxygen intrusion is completely avoided. However, at least three technical bottlenecks make them dependent on sand filters: *i)* the rejection coefficient for ammonia is <1, which means that some ammonia will pass through the membrane with the permeate,

ii) groundwater contains undesired gases like methane and hydrogen sulfide that will also pass with the permeate and *iii)* we cannot treat the concentrate stream yet. Sand filters can or will be able to solve all of these problems. For *i)* and *ii)* one can simply install an aeration – sand filtration module to treat the permeate. For *ii),* we depend on developing an efficient sand filter operation that can cope with high concentrations of Fe^{2+} and Mn^{2+}. More on this below.

2) The Bioscenario

In Chapter 2 we discuss the potential of promoting biological reactions in sand filters, showcasing the benefits for Fe, As, and nitrate removal. In the case of Fe removal, we highlight how the NDFO configuration will likely allow for higher flow rates and longer runtimes while minimizing energy and water losses. A benefit as of yet to be discussed is that the concentration of Fe2+ that can be removed is not capped by the concentration of oxygen in water, but by that of NO3-. Nitrate solubility depends on the concentration of counterions in the water matrix, but the result is that NDFO can likely treat much higher Fe2+ concentrations than conventional aerobic sand filters. Another application of NDFO may also be treating the concentrate stream of anaerobic reverse osmosis, although further research is required to cope with the high salt concentration.

3) The RedOx Project

The RedOx project was born to take control of the main conversions in the filter by being able to separate them. Although we are still far from fully understanding how to do this, we have made significant progress. We can isolate Fe removal from that of NH_4^+ and Mn, and splitting the two latter seems feasible by controlling pH and DO. The most obvious application of this knowledge is to separate the three processes in three different filters, which will likely allow us to run filters at much higher flow rates and runtimes. There is, however, much more than that to gain. Being able to dictate which reactions take place allows drinking water technologists to decide which sequence of removal processes is more beneficial given each water matrix. For instance, our groundwaters with low pH are good candidates for the application of our biological-adsorptive iron removal technology, while if the pH is high the system may benefit more from a conventional, oxygen-saturated scheme with a double bed to confine Fe^{2+} flocs.

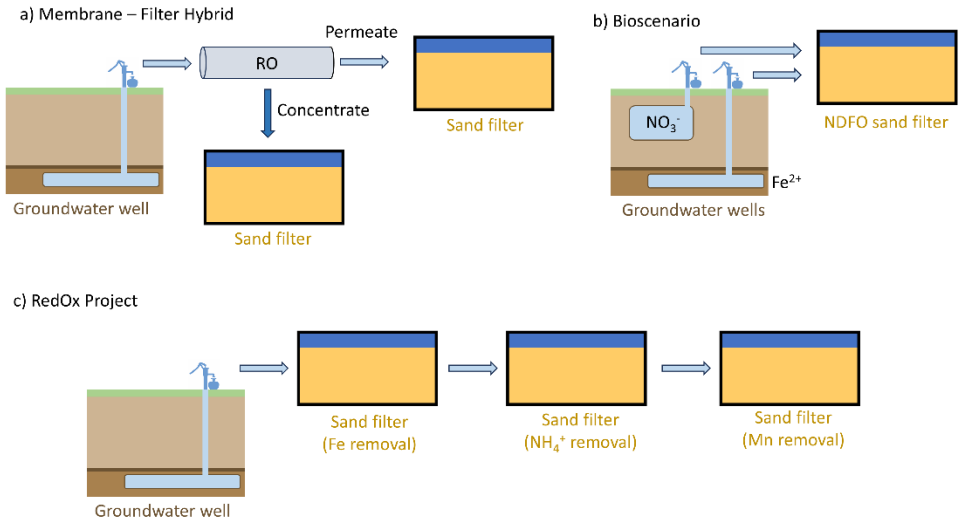

Figure 2. Three promising alternative uses of sand filters in the drinking water treatment facilities of the future.

REFERENCES

1. Müller, S., Corbera-Rubio, F., Schoonenberg-Kegel, F., Laureni, M., Van Loosdrecht, M. C. M., Van Halem, D., Loosdrecht, M. C. M. van & Halem, D. van. Shifting to biology promotes highly efficient iron removal in groundwater filters. *bioRxiv* 2024.02.14.580244 (2024).

2. Breda, I. L., Ramsay, L., Søborg, D. A., Dimitrova, R. & Roslev, P. Manganese removal processes at 10 groundwater fed full-scale drinking water treatment plants. *Water Qual. Res. J. Canada* **54**, 326–337 (2019).

3. Bruins, J. H., Vries, D., Petrusevski, B., Slokar, Y. M. & Kennedy, M. D. Assessment of manganese removal from over 100 groundwater treatment plants. *J. Water Supply Res. Technol. - AQUA* **63**, 268–280 (2014).

4. Vandenabeele, J., Vande Woestyne, M., Houwen, F., Germonpré, R., Vandesande, D. & Verstraete, W. Role of autotrophic nitrifiers in biological manganese removal from groundwater containing manganese and ammonium. *Microb. Ecol.* **29**, 83–98 (1995).

5. de Vet, W., Rietveld, L. C. & Van Loosdrecht, M. C. M. Influence of iron on nitrification in full-scale drinking water trickling filters. *J. Water Supply Res. Technol. - AQUA* **58.4**, 247–256 (2009).

6. Swanner, E. D., Mloszewska, A. M., Cirpka, O. A., Schoenberg, R., Konhauser, K. O. & Kappler, A. Modulation of oxygen production in Archaean oceans by episodes of Fe(II) toxicity. *Nat. Geosci.* **8**, 126–130 (2015).

7. Tong, M., Zhao, Y., Sun, Q., Li, P., Liu, H. & Yuan, S. Fe(II) oxygenation inhibits bacterial Mn(II) oxidation by P. putida MnB1 in groundwater under O2-perturbed conditions. *J. Hazard. Mater.* **435**, 128972 (2022).

8. Du, H. Y., Yu, G. H., Sun, F. S., Usman, M., Goodman, B. A., Ran, W. & Shen, Q. R. Iron minerals inhibit the growth of Pseudomonas brassicacearum J12 via a free-radical mechanism: Implications for soil carbon storage. *Biogeosciences* **16**, 1433–1445 (2019).

9. Zhang, Y., Tong, M., Yuan, S., Qian, A. & Liu, H. Interplay between iron species transformation and hydroxyl radicals production in soils and sediments during anoxic-

oxic cycles. *Geoderma* **370**, 114351 (2020).

10. Wagner, F. B., Diwan, V., Dechesne, A., Fowler, S. J., Smets, B. F. & Albrechtsen, H. J. Copper-Induced Stimulation of Nitrification in Biological Rapid Sand Filters for Drinking Water Production by Proliferation of Nitrosomonas spp. *Environ. Sci. Technol.* **53**, 12433–12441 (2019).

11. Wagner, F. B., Nielsen, P. B., Boe-Hansen, R. & Albrechtsen, H. J. Copper deficiency can limit nitrification in biological rapid sand filters for drinking water production. *Water Res.* **95**, 280–288 (2016).

12. Bray, R. & Olańczuk-Neyman, K. The influence of changes in groundwater composition on the efficiency of manganese and ammonia nitrogen removal on mature quartz sand filtering beds. *Water Sci. Technol. Water Supply* **1**, 91–98 (2001).

13. Søborg, D. A., Breda, I. L. & Ramsay, L. Effect of oxygen deprivation on treatment processes in a full-scale drinking water biofilter. *Water Sci. Technol. Water Supply* **15**, 825–833 (2015).

14. Haukelidsaeter, S. *et al.* Influence of filter age on Fe, Mn and NH4+ removal in dual media rapid sand filters used for drinking water production. *Water Res.* **242**, 120184 (2023).

15. Haukelidsaeter, S. *et al.* Efficient chemical and microbial removal of iron and manganese in a rapid sand filter and impact of regular backwash. *Appl. Geochemistry* **162**, 105904 (2024).

16. Bruins, J. H., Petrusevski, B., Slokar, Y. M., Huysman, K., Joris, K., Kruithof, J. C. & Kennedy, M. D. Biological and physico-chemical formation of Birnessite during the ripening of manganese removal filters. *Water Res.* **69**, 154–161 (2015).

17. Kim, S. S., Bargar, J. R., Nealson, K. H., Flood, B. E., Kirschvink, J. L., Raub, T. D., Tebo, B. M. & Villalobos, M. Searching for biosignatures using electron paramagnetic resonance (EPR) analysis of manganese oxides. *Astrobiology* **11**, 775–786 (2011).

18. Yang, H., Yan, Z., Du, X., Bai, L., Yu, H., Ding, A., Li, G., Liang, H. & Aminabhavi, T. M. Removal of manganese from groundwater in the ripened sand filtration: Biological oxidation versus chemical auto-catalytic

oxidation. *Chem. Eng. J.* **382**, 123033 (2020).

19. Sahabi, D. M., Takeda, M., Suzuki, I. & Koizumi, J. ichi. Removal of Mn2+ from water by 'aged' biofilter media: The role of catalytic oxides layers. *J. Biosci. Bioeng.* **107**, 151–157 (2009).

20. Olańczuk-Neyman, K. & Bray, R. The Role of Physico-Chemical and Biological Processes in Manganese and Ammonia Nitrogen Removal from Groundwater. *Polish J. Environ. Stud.* **9**, 91–96 (2000).

21. Otte, J. M., Blackwell, N., Soos, V., Rughöft, S., Maisch, M., Kappler, A., Kleindienst, S. & Schmidt, C. Sterilization impacts on marine sediment---Are we able to inactivate microorganisms in environmental samples? *FEMS Microbiol. Ecol.* **94**, (2018).

22. Breda, I. L., Søborg, D. A., Ramsay, L. & Roslev, P. Manganese removal processes during start-up of inoculated and non-inoculated drinking water biofilters. *Water Qual. Res. J.* **54**, 47–56 (2019).

23. Yu, H. & Leadbetter, J. R. Bacterial chemolithoautotrophy via manganese oxidation. *Nat. 2020 5837816* **583**, 453–458 (2020).

24. Tebo, B. M., Johnson, H. A., McCarthy, J. K. & Templeton, A. S. Geomicrobiology of manganese(II) oxidation. *Trends in Microbiology* vol. 13 421–428 at https://doi.org/10.1016/j.tim.2005.07.009 (2005).

25. Piazza, A., Ciancio Casalini, L., Pacini, V. A., Sanguinetti, G., Ottado, J. & Gottig, N. Environmental Bacteria Involved in Manganese(II) Oxidation and Removal From Groundwater. *Front. Microbiol.* **10**, 119 (2019).

26. Burger, M. S., Krentz, C. A., Mercer, S. S. & Gagnon, G. A. Manganese removal and occurrence of manganese oxidizing bacteria in full-scale biofilters. *J. Water Supply Res. Technol. - AQUA* **57**, 351–359 (2008).

27. Anderson, C. R., Dick, G. J., Chu, M. L., Cho, J. C., Davis, R. E., Bräuer, S. L. & Tebo, B. M. Aurantimonas manganoxydans, sp. nov. and Aurantimonas litoralis, sp. nov.: Mn(II) Oxidizing Representatives of a Globally Distributed Clade of alpha-Proteobacteria from the Order Rhizobiales. *Geomicrobiol. J.* **26**, 189–198 (2009).

28. Butterfield, C. N., Soldatova, A. V., Lee, S. W., Spiro, T. G. & Tebo, B. M. Mn(II,III) oxidation and mno2 mineralization by an expressed bacterial multicopper oxidase. *Proc. Natl. Acad. Sci. U. S. A.* **110**, 11731–11735 (2013).

29. Anderson, C. R., Johnson, H. A., Caputo, N., Davis, R. E., Torpey, J. W. & Tebo, B. M. Mn(II) oxidation is catalyzed by heme peroxidases in 'Aurantimonas manganoxydans' strain SI85-9A1 and Erythrobacter sp. strain SD-21. *Appl. Environ. Microbiol.* **75**, 4130–4138 (2009).

30. (RH-DHV), G. van H. Personal communication. at (2021).

31. Dyson, J. Water Industry Innovation, A Slow and Painful Process. *Water World* https://www.waterworld.com/water-utility-management/article/14039771/water-industry-innovation-a-slow-and-painful-process (2019)

ACKNOWLEDGEMENTS

To my wonderful supervisors, **Mark**, **Doris** and **Michele**. Your supervision styles are different, yet the three of you always prioritized my professional – and personal – development over maximizing tangible scientific output. Honestly, there is not much more a PhD candidate can ask for. A heartfelt, gigantic thanks. **Mark**, I am yet another PhD candidate who leaves EBT amused by your inability to build such a wonderful research group. Thanks for that, and even more for the encouragement to be bold and push for what I though was right, and for the security that you had my back whenever things went South. **Doris**, I have never seen anyone with your leadership skills. Thanks for making me (and everybody else in the group) feel unstoppable, for the encouragement to explore and pursue my scientific curiosity, for the trust, for accommodating your style to make this work (big, big thanks for this, really), for always, selflessly, putting me in the spotlight, and for many more things. It is only by working with you that I understood what being a 'doer' truly means. **Michele**, I would never have done a PhD if it weren't for you. I have been trying to figure out what to write here for ages cause I feel it is never good enough – I learnt that from you –, that it won't fairly summarize how grateful I feel. First of all, thanks for giving me the widest of spaces to make mistakes – designing experiments, in the lab, normalizing protein counts…but also writing, communicating, and many more –, and later on taking the time to painstakingly showing me how to improve (and in extremely rare occasions, acknowledging I was right). I honestly can't express how invaluable this has been. Second, thanks for keeping the bar so high (jeez, have I hated it). Not only for me, but also for your own work. Obtaining *Michele's certificate of excellence* has certainly been the hardest part of this journey, but also what allowed me to present our work anywhere, to anybody with all the confidence in the world. Third, thanks for showing me how to love science. Whenever I felt my work was meaningless and had no direction, your genuine interest and curiosity always inspired me not only to keep working, but also to try to do better every time. Your ability to motivate your students is a superpower. Last, thanks for showing me how to prioritize *what truly matters*. Sharing these four years with Michele The Mentor, Michele The Tyran, Michele The Mad Scientist, and Michele The Father has been an immense pleasure and an even bigger privilege.

Here, between supervisors and peers, goes my acknowledgment to **Nina,** my dearest scientific partner. What a ride, huh? Sharing 5+ years of my life in- and out- of the lab,

full of laughter and cries, of ups and downs, of happiness and sadness, and most importantly, of professional and personal growth, is an experience I am (and will probably always be) incredibly fond of. And also the one for **Simon**. I honestly do not know what I would have done without you during the first two years of the project. Thanks for being an infinite pool of kindness and wisdom. Keep going, my RedOx brother.

I have been immensely fortunate to work with many people outside TU Delft who played a pivotal role in the success of this venture. Thanks to all the drinking water experts for kindly sharing their expertise, for granting me the opportunity to work with them, and for (usually) eagerly accepting my crazy ideas. Especially to **Frank**, a scientist at heart, and also to **Melanie, Weren, Brent, Gerard, Karin** and **Jantinus**. Thanks as well to the academics with whom we joined forces: **Alje, Maartje, Sebastian, Paul**. Last but not least, thanks to Vitens, Dunea and NWO for creating the Sand Filtration program and allowing me to hop in.

Working from home should be strongly discouraged for PhD candidates – if not entirely prohibited. And I'll defend this anywhere, anytime because sharing this journey with my EBT fellas has been ~~important~~ essential for me to succeed. Yuemei, I do not know how you assigned me to what has been my desktop, but what a magnificent choice. My lovely officemates **Stefan**, **Rodoula** and **Timmy** (sorted strictly alphabetically by surname), you guys made my 9-5 (or let's be honest, my 10 – 6) the best part of the day. Thanks for our endless coffee-tea-and-lots-of-food breaks, for our office dinners, for your unconditional support, for sharing work and life experiences and miseries, and for allowing me to be myself. **Stefan**, whenever you are around, good vibes are guaranteed. You have all the goodness in the world within you. Thanks for sharing part of it with me (us). **Professor Timmy**, your habit (or need?) to share your kindness and wisdom with the whole group is extraordinary. Thousands of students will be lucky to learn from you. My dearest paranymph **Rodoufakis**, you have been the coolest, sweetest officemate anybody could ask for. Thanks for making the office feel like home. EBT harbors other unique creatures that made me want to go to the faculty every day such as my favorite model and friend-for-everything **Lemon**, my big boy **Ali**, my padel-buddy **Natalia**, cheerful **Ji,** and doctors (among others) **Diana**, **Sam**, **Max**, **Philipp, Ingrid.** Thanks to all of you, and to everybody who makes EBT wonderful every day: **Bea, Ben, Chris, Claudia, Dimitry, Dirk, Dita, Gerben, Marcelo, Jelle, Jitske, Koen, Karel, Mario, Marit, Martin, Puck, Rebeca, Robbert, Samarpita, Sebastian, Viktor, Yuemei, Zejia,** and **Zita.**

Civil also has cool people. To **Rosa**, who makes me feel so alive, and to **Emiel**. I would not have visited Civil half the times if it were not for the two of you. Although we mainly talked about life, we managed to publish together. Maybe if we did not come along that well we would have published more. Or maybe less. Who knows. I would not change an ounce of it, though. Cheers to **Bruno, Erik,** and **Silvy** as well.

To the students I had the pleasure to work with and from whom I learnt so much. First came **Nienke**, part-time my student and part-time my supervisor. Working with you is certainly one of the highlights of the PhD. Then **Marcos**, the most prolific self-learner I worked with. Fue un placer. Then **Liselotte**, a crazy and brilliant mind in- and out- of the lab and a brave soul. Keep going girl! Then **Sofia** and **Viktor**, the only ones who dared to work with the reactors I designed. It was hard, but you guys did a great job! And last **Manon**, who barely needed me. A big thanks to all of you.

One of the good things about this project and my supervisory team is that I had time to have friends outside of the lab. This may seem like a joke if you have not done a PhD. But if you have, you know it is not.

First of all, thanks to my friends from the hood: **Georg**, **Mariana, Ale** and **David**. You guys transitioned from an amalgam of 'friends-of-Sergio-who-welcome-me' to beautiful, singular souls I cherish fondly. **Georg**, you are so nice. Like, for real. Thanks for the countless hours of playing and gaming. Y por estar siempre tan cerca (sometimes physically). **Marianita,** your RBF can't be further away from your personality. Always warm and welcoming, thanks for making the Netherlands feel a little less cold. My dear **Ale**, had someone told me 4 years ago that we'd be such good, close friends, I would certainly not have believed them. You always keep my mind stimulated and my heart full. Thanks for that, and for helping me to get in touch with my cultural and artistic side. The only thing I don't like about **David** is that he has so many friends that you never know how close you actually are. Regardless, life is so much better by your side. Gracias por ser siempre el más majete, por cuidar de todos, por tu paciencia, tus jajas, tu coraje, tu tenacidad y tu querer. Thanks as well to the happy souls of **Hugo** and **Chiara**.

The most important factor to live happily abroad is to find your expat family. I found mine several years ago. It is full of artists who paint the naked canvas of my life. Thank you **Lidi, Pau**, **Zeynep, Marina, Joan, Sergio, Miguel,** and **Marc**.

El missatge de gratitud tambe l'extenc cap als de casa. Al **Pau** i la **Laura**, per fer-me sentir esperat i desitjat absolutament sempre; al **Francesc**, per aquesta amistat poc convencional i maquíssima que tenim, i al **Joan**, el **Marc** i l'**Esther**.

I també a la meva família. A tietes, tiets, cosines i cosins. Per ser-hi i no deixar d'intentar-ho. A les meves àvies, les dues persones més valentes que mai he conegut. Gràcies per moltes coses: per creure, cega i genuïnament, que sóc l'home més intel·ligent de món, per ensenyar-me a no romantitzar la pobresa, sino com se'n surt, per aferrar-vos a un model de familia que ja no existeix, i per la vostra bondat.

També al papa i a la mama, i al meu superheroi preferit, el Miquel, als qui estimo més que a ningú al món sencer.

Printing of this thesis was financially supported by the Netherlands Society of Medical Microbiology (NVMM) and the Royal Netherlands Society for Microbiology (KNVM).

SCIENTIFIC CONTRIBUTIONS

Publications included in this thesis

1. Corbera-Rubio, F., Goedhart, R., Laureni, M., van Loosdrecht, M. C. M. & van Halem, D. (in press) A Biotechnological Perspective on Sand Filtration for Drinking Water Production. *COBIOT* (2024).

2. Corbera-Rubio, F., Laureni, M., Koudijs, N., Müller, S., van Alen, T., Schoonenberg, F., Lücker, S., Pabst, M., van Loosdrecht, M. C. M. & van Halem, D. Meta-omics profiling of full-scale groundwater rapid sand filters explains stratification of iron, ammonium and manganese removals. *Water Res*. 233, 119805 (2023).

3.. Corbera-Rubio, F., Stouten, G. R., Bruins, J., Dost, S. F., Merkel, A. Y., Müller, S., van Loosdrecht, M. C. M., van Halem, D. & Laureni, M. " Candidatus Siderophilus nitratireducens": a putative nap -dependent nitrate-reducing iron oxidizer within the new order Siderophiliales. *ISME Commun*. 4, 8 (2024).

4. Corbera-Rubio, F., Kruisdijk, E., Malheiro, S., Leblond, M., Verschoor, L., van Loosdrecht, M. C. M., Laureni, M. & van Halem, D. A difficult coexistence: resolving the iron-induced nitrification delay in groundwater filters. *Water Res*. 260, 121923 (2024).

5. Corbera-Rubio, F., Boersma, A. S., de Vet, W. W. J. M., Pabst, M., van der Wielen, P. W. J. J., van Kessel, M. A. H. J., van Loosdrecht, M. C. M., van Halem, D., Lücker, S. & Laureni, M. Biological methane removal in groundwater trickling biofiltration for emissions reduction. [*Manuscript submitted for publication]* (2024).

Other publications

6. Calderón-Franco D*, Corbera-Rubio F*, Cuesta-Sanz M, Pieterse B, de Ridder D, van Loosdrecht MCM, et al. Microbiome, resistome and mobilome of chlorine-free drinking water treatment systems. *Water Res*. 235,119905 (2023). *Shared co-authorship

7. Müller S, Corbera-Rubio F, Schoonenberg-Kegel F, Laureni M, van Loosdrecht MCM, van Halem D. Shifting to biology promotes highly efficient iron removal in groundwater filters. *Water Res*. 262, 122135 (2024).

8. Laureni M, Corbera-Rubio F, Kim DD, Browne S, Roothans N, Weissbrodt DG, et al. Selective enrichment of high-affinity clade II N2O-reducers in a mixed culture. *biorXiv*. 2024.02.03.579283 (2024).

Publications in preparation

9. Kruisdijk, E*., Corbera-Rubio, F*., Schoonenberg, F., Laureni, M., van Loosdrecht, M. C. M. & van Halem, D. Complete separation of iron, ammonia and manganese removal in full-scale groundwater filters based on pH and dissolved oxygen concentration. [*Manuscript in preparation*] *Shared co-authorship.

Awards and grants

1. Kiem award, awarded by the Nederlandse Vereniging voor Medische Micriobiologie (NVMM). April 2024.

2. Bioengineering project grant, granted by the Delft Bioengineering Institute. March 2021.

Conference proceedings (oral presentations, as part of this thesis)

1. Corbera-Rubio F, Stouten G, Bruins J, Dost S, Merkel AY, Müller S, van Loosdrecht MCM, van Halem D, Laureni M (2023). *"Candidatus* Siderophilus nitratireducens": a low-temperature, nitrate-driven iron oxidizer within the new order Siderophiliales. *Microbial Ecology and Water Engineering*. International Water Association. Brisbane, Australia

2. Corbera-Rubio F, Stouten G, Bruins J, Dost S, Merkel AY, Müller S, van Loosdrecht MCM, van Halem D, Laureni M (2023). *"Candidatus* Siderophilus nitratireducens" and how to remove Fe^{2+} in the absence of oxygen. *Fe workshop*. Wetsus. Leeuwarden, the Netherlands.

3. Corbera-Rubio F, Stouten G, Bruins J, Dost S, Merkel AY, Müller S, van Loosdrecht MCM, van Halem D, Laureni M (2023). *"Candidatus* Siderophilus nitratireducens": a psychrophilic, nitrate-reducing iron oxidizer within the new order *Siderophiliales*. *KNVM Scientific Spring Meeting*. KNVM. Papendal, the Netherlands

4. Corbera-Rubio F, Helsloot V*, Bruins J, Dost S, van Loosdrecht MCM, Laureni M, van Halem D (2022). Free two birds with one key: coupling biological iron and nitrate removal in anoxic groundwater filters. *Young Water Professional Conference*. International Water Association. Delft, the Netherlands. *Speaker

5. Corbera-Rubio F, Bruins J, Dost S, van Loosdrecht MCM, Laureni M, van Halem D (2022). Free two birds with one key: coupling biological iron and nitrate removal in anoxic groundwater filters. *Leading Edge Technologies*. International Water Association. Reno, Nevada, United States of America. *Keynote speaker*.

6. Corbera-Rubio F, Laureni M, Koudijs N, Müller S, van Alen T, Lücker S, van Loosdrecht MCM, van Halem D (2022). Nitrification moves: stratification patterns in rapid sand filters for drinking water production. *25th European Nitrogen Cycle meeting*. Rome, Italy.

7. Corbera-Rubio F, Koudijs N, Müller S, van Alen T, Laureni M, van Halem D, van Loosdrecht MCM (2021). Taxonomic and functional stratification explains sequential removals in full-scale groundwater rapid sand filters. *Microbial Ecology and Water Engineering (MEWE)*. International Water Association. Delft, the Netherlands.

CURRICULUM VITAE

Francesc grew up in Vallromanes, a small town near Barcelona. He started his career there, where he undertook a BSc in Biotechnology from the Universitat Autonoma de Barcelona (UAB). During that time he was granted an *Erasmus+* scholarship to do his Bachelor thesis in Wageningen (the Netherlands) at WUR under the supervision of prof. Harry Bitter working on the *Enzymatic production of nitriles from aminoacids*, as well as an *Excellence scholarship* to work on the *Biodegradation of industrial contaminants and waste valorization in algae photobioreactors* in the group of prof. Teresa Vincent in the Chemical Engineering department of UAB.

After his BSc, Francesc worked in the department of innovation of Friselva SA, a food-tech company where he continued working on upcycling projects such as heparin extraction and production of fertilizers from waste streams from the meat industry. In 2017 he moved to Delft to pursue his MSc in Biochemical Engineering (officially, unfairly known as Life Science & Technology) at TU Delft. During this time in Delft he started to mingle with the academic life, representing his colleagues in the Board of Studies and assisting in teaching in several BSc and MSc courses. After completing his MSc thesis discovering the intricacies of nitrous oxide-reducing organisms with dr. Michele Laureni and prof. Mark van Loosdrecht, he moved to Bern (Switzerland) to work in the pharmaceutical industry at CSL Behring.

In 2020 he started his PhD journey in the drinking water world within the RedOx Filter project, a collaboration between the Nederlandse Organisatie voor Wetenschappelijk Onderzoek (NWO) and the drinking water companies Vitens and Dunea, led by prof. Doris van Halem and co-supervised by prof. Mark van Loosdrecht and dr. Michele Laureni. During his PhD, Francesc had the chance to work at lab-, pilot- and full-scale set-ups, establish and foster collaborations with industrial partners and other universities, present his research across the globe, and co-organize the Microbial Ecology and Water Engineering (MEWE) conference in Delft in 2021. In 2024 he received the KIEM award from the Koninklijke Nederlandse Vereniging voor Microbiologie (KNVM).